Dynamic Frequency-Dependent Soil-Pile-Structure Interactions in Damage-Controlled Bridge Piers with Different Foundation Systems and Their Incorporation into a Response Displacement-Based Seismic Design Framework

By:

Muhammad Mahmood Ul Hassan

A thesis submitted in partial fulfilment of the requirements for the degree of Doctor of Philosophy.

Examination Committee:

Prof. Koichi ISOBE

Prof. Takashi Matsumoto

Prof. Yasunori Miyamori

Thesis No.

Division of Field Engineering for Environment

Graduate School of Engineering, Hokkaido University

June 2026

ACKNOWLEDGEMENTS

˹He is˺ Allah! There is no god ˹worthy of worship˺ except Him, the Lord of the Mighty Throne.”

(Quran, Chapter 19, surah An-Naml, verse 26)

Unending glory to God, The Exalted, Who granted me the primary inspira-tion and stamina all along to complete this humble work. This small contribution, if just and correct, is only a drop of appreciation for His ocean of munificence.

I am extremely grateful to my supervisor, Assoc. Prof. Koichi ISOBE for his kindness, invaluable advice, persistent support, and patience. His immense knowledge and experience kept me encouraged and helped me in achieving my research objectives. I want to express my gratitude towards Japanese Government and Hokkaido University for honouring me with MEXT and then EXEX fellowship (JST SPRING, Grant Number JPMJSP2119) and making me studies smoother than my expectations. I also want to thank my lab members for their support and valuable comments during this work.

Finally, I want to express my gratitude to my parents and siblings. I am short of words, but I must say perpetual support of my parents (Sheikh Muhammad Ejaz and Shamshad Begum) and elder sister (Khadija Tul Kubra) made me believe that I can study this far. The sacrifices made by my brother Muhammad Mudassar, my sisters Bushra Fatima and Aiman Ftima in facilitating me are beyond describable limits and deserve a life-long appreciation. In this moment of pride, I also want to remember my both paternal and maternal grandmothers (Ghulam Sakina and Manzoor begum) for their kindness upon me during childhood and appreciation on my smallest of achievements. I am sure they would be happiest to know about this if they were alive. I also want to thank my friends from my school days to UET Peshawar, NUST Quetta, and here in Sapporo (Waleed Bin Khalid, Muhammad Musab, Abdul Razzaq, Muhammad Bilal, Muhammad Taimoor, Afzal Khan, Asad Jang, Faheem Shah, Sherbaz, Ali Agha, Fahad Ali, Faraz Khan, Muhammad Asif and many others). Their invaluable words and unwavering trust in my abilities has always helped me to leap harder at my dreams.

I am indebted to all of you.

This work was partially supported by JSPS KAKENHI Grant Number 16K18144. The authors also extend their gratitude to Prof. Kimura and students Mr. Mitsuyoshi, Mr. Akatsuka, and Mr. Nishii for their invaluable contributions to this research.

March 2026

Muhammad Mahmood Ul Hassan

Contents

ABSTRACT 11

PREFACE 13

CHAPTER 1. INTRODUCTION 14

CHAPTER 2: LITERATURE REVIEW 17

2.1 Damage control bridge pier structure: 17

2.2 Dynamic soil-structure-interaction 19

2.3 Post-earthquake observations of the performances of piled foundations 21

2.3.1 NHK building, 1964 Niigata earthquake 21

2.3.2 Hanshin Expressway Route 3 in Kobe, 1995 Kobe Earthquake 22

2.4 Experimental studies on the behavior of piles under seismic loading 23

2.5 Numerical methods for dynamic soil-structure interaction analysis of piled foundations 27

2.5.1 Direct method 27

2.5.2 Winkler type methods: 29

2.6 Chapter summary: 31

2.7 Objectives of study: 32

CHAPTER 3. SEISMIC PERFORMANCE EVALUATION USING THREE-DIMENSIONAL ELASTO-PLASTIC FINITE ELEMENT ANALYSIS 33

3.1 INTRODUCTION 33

3.2 OUTLINE OF SHAKING TABLE MODEL EXPERIMENT 35

3.2.1 Experiment modes 35

3.2.2 Model grounds 37

3.2.3 Excitation conditions 39

3.3 OUTLINE OF THE NUMERICAL ANALYSIS METHOD 40

3.3.1 Modelling the structures and grounds 40

3.3.2 Analysis conditions 44

3.3.3 Analysis cases 45

3.4 RESULTS OF REPRODUCTION ANALYSIS AND DISCUSSION 46

3.4.1 Dry sand ground cases 46

3.4.2 Results with L2 seismic input 53

3.4.3 Results with varying input frequencies 57

3.4.4 Liquefiable ground cases 60

3.4.5 Kinematic interaction 63

3.5 Chapter summary: 66

CHAPTER APPENDIX 67

CHAPTER 4. DYNAMIC FREQUENCY-DEPENDENT SOIL-PILE-STRUCTURE INTERACTION 70

4.1 INTRODUCTION 70

4.2 Footing type with dry sand (D-F) 70

4.2.1Time history analysis: 70

4.2.2 Pile bending moment: 71

4.2.3 Inertial vs kinematic interactions: 72

4.2.4 Parametric study on variation of input motion frequency: 77

4.3 Footingless type with dry sand (D-S) 86

4.3.1 Time history analysis: 86

4.3.2 Pile bending moment and deformations: 86

4.3.3 Quantitative comparison of inertial and kinematic interactions: 89

4.3.4 Parametric study on variation of input motion frequency: 90

4.4 Footing type with dry sand (L-F) 98

4.4.1 Time history analysis: 98

4.4.2 Pile bending moment: 98

4.4.3 Qualitative comparison of inertial and kinematic interactions:..... 100

4.4.4 Qualitative and quantitative comparison of inertial and kinematic interactions: 101

4.5 Footingless type with Liquifiable sand (L-S) 111

4.5.1 Time history analysis: 111

4.5.2 Pile bending moment and deformations: 112

4.5.3 Quantitative comparison of inertial and kinematic interactions: 114

4.5.4 Qualitative Comparison 116

4.6 Chapter summary 124

CHAPTER 5: SIMPLIFIED STATIC ANALYSIS FRAMEWORK 125

5.1 Introduction: 125

5.2 Japanese Railway Design Method (RTRI, 2012) 126

5.3 Hybrid pseudostatic analysis method 129

5.3.1 Determination of inertia force 130

5.3.2 Determination of soil displacement profile 131

5.3.3 Dry Sand Cases (D-F and D-S) 131

5.3.4 Liquifiable soil cases (L-F and L-S): 135

5.4 Chapter Summary: 141

CHAPTER 6: CONCLUSION 142

REFERENCES 145

List of Figures

Figure 1. A 3D view of damage control bridge pier structure 18

Figure 2. Smart pier structure with F- and S-types foundation 18

Figure 3. Illustration of (a) kinematic and (b) inertial interaction phenomena (Perez-Herreros, 2020) 19

Figure 4. NHK building after 1964 Niigata earthquake: a) piles damaged by lateral spreading of the foundation soil and b) correction of pile damage and site conditions (M. Hamada, 1991) 22

Figure 5. a) Hanshin Expressway bridge collapse after 1995 Kobe earthquake b) geometric characteristics and pile foundation (after Mylonakis et al. 2000. redrawn by Perez-Herreros, 2020) . 23

Figure 6. Various model configurations used in centrifuge tests (Perez-Herreros, 2020) 24

Figure 7. Soil-pile-structure model layout (Tokimatsu et. al, 2005) 25

Figure 8. Model of frame structure embedded in soft soil and arrangement of measuring points (Shutong et. al., 2020) 26

Figure 9. Finite element simulation model for pile group (Wang et al. 2017) 28

Figure 10.Combined structure-pile-soil interaction and ground response analysis model (Chiou et al. 2020) 30

Figure 11. Bridge column integrated by multiple steel pipes and multiple shear panels interconnecting the pipes for practical use 33

Figure 12. Specimens and the locations of the strain gauges in the experiment (After Isobe et al., 2016) 36

Figure 13. Model grounds along with measurement devices and their locations (After Isobe et al., 2016) 37

Figure 14. Results of the static and cyclic triaxial compression tests performed on the model ground specimens (After Isobe et al., 2016) 38

Figure 15. Modelling of the bridge pier consisting of multiple steel pipes and steel pipe piles 40

Figure 16. Conceptual diagram of the Cyclic Mobility Model (After Zhang et al., 2007) 42

Figure 17. Results of the drained static triaxial tests and simulation 42

Figure 18. Analysis mesh used in the reproduction analysis 45

Figure 19. Comparison of the experimental and simulation results for the relationship between the inertial force and the lateral displacement at the pier top 47

Figure 20. Comparison of the experimental and simulation results for the relationship between the

maximum inertia force and the maximum lateral displacement at the pier top.................................... 48
Figure 21. Relationship between the inertial force at the pier top and the shear strain in the upper shear panel 50
Figure 22. Responses of the superstructure against shear strain for elastoplastic (EP) and elastic shear panels (E) under the third excitation step 51
Figure 23. Distributions of the bending moments generated in the piles and pier when the maximum lateral displacement occurs at the pier top 52
Figure 24. Distributions of the lateral displacement of the piles and pier when the maximum lateral displacement occurs at the pier top 53
Figure 25. Level-2 input seismic motion specified in the Guidelines for Aseismic Design for Cut and Cover Tunnels published by Hanshin Expressway Co., Ltd. 54
Figure 26. Response analysis results against Level-2 seismic motion 56
Figure 27. Comparison of the results of the response analysis against the input waves with various frequencies (D-S/D-F)... 57
Figure 28. Variation in the maximum shear strain of the panels against the input frequencies 58
Figure 29. Lateral displacement profiles of the pier and piles against various frequencies of input motion 59
Figure 30. Comparison of the time histories of the excess pore water pressure ratio of the ground for the experimental and simulation results 60
Figure 31. Comparison of the experimental and simulation results for the relationship between the inertial force and the lateral displacement at the pier top for the case with liquefiable sand 61
Figure 32. Relationship between the inertial force at the pier top and the shear strain in the upper shear panel for the case with liquefiable sand 61
Figure 33. Distributions of the bending moments generated in the piles and pier when the maximum lateral displacement occurs at the pier top for the case with liquefiable sand...................................... 62
Figure 34. Distributions of the lateral displacement in the piles and pier when the maximum lateral displacement occurs at the pier top for the case with liquefiable sand... 63
Figure 35. Relationships between the inertia force and the shear force at the pile head and between the inertial force and the earth pressure for D-F (4), D-S (4), L-F and L-S 64
Figure 36. Evolution of various response parameters along the course of excitation for DF type 71

Figure 37. Pile bending moment and deformation profiles at various instances 72
Figure 38. Various analysis types conducted to determine the role of kinematic and inertial interactions 73
Figure 39. Phase difference calculation between pier top and pile, and soil and pile for DF type 75
Figure 40. A comparison of isolated pile deformation and moment of kinematic and inertial interactions against the combined response in DF 76
Figure 41. Phase difference between pier vs pile and pile vs free-field soil under various frequencies for DF-type structures .... **Error! Bookmark not defined.**
Figure 42. A comparison of pile bending from various cases (D-F, F-type and DF_{NS}) at various frequencies. 81
Figure 43. Maximum bending moment values near the pile head 82
Figure 44. Comparison of ground deformation of dry soil under various input excitations 82
Figure 45. A comparison of pile deformation from various cases (D-F, F-type and DFNS) at various frequencies. 85
Figure 46. Time evolution of various response parameters for D-S type 87
Figure 47. Bending moment and deformation envelopes of piles and ground at key instances 88
Figure 48. Phase difference calculation between pier top and pile, and soil and pile for DS type 89
Figure 49. A comparison of isolated pile deformation and moment of kinematic and inertial interactions against the combined response in DS 90
Figure 50. Phase difference between pier vs pile and pile vs free-field soil under various frequencies for DS-type structures 92
Figure 51. A comparison of pile bending from various cases (D-S, S-type and DS_{NS}) at various frequencies. 93
Figure 52. Maximum values of pile moment in S-type configuration 94
Figure 53. A comparison of pile deformation from various cases (D-S, S-type and DSNS) at various frequencies. 97
Figure 54. Evolution of various response parameters along the course of excitation for L-F type 99
Figure 55. Pile bending moment and deformation profiles at various instances 99
Figure 56. Phase difference calculation between pier top and pile, and soil and pile for L-F type 101
Figure 57. A comparison of isolated pile deformation and moment of kinematic and inertial interactions

against the combined response in L-F 102
Figure 58. Phase difference between pier vs pile and pile vs free-field soil under various frequencies for LF-type structures 103
Figure 59. A comparison of pile bending from various cases (L-F, F-type and L-F_{NS}) at various frequencies. 105
Figure 60. Maximum bending moment values near the pile head... 106
Figure 61. Comparison of ground deformation of dry soil under various input excitations 107
Figure 62.. A comparison of pile deformation from various cases (L-F, F-type and L-F_{NS}) at various frequencies. 110
Figure 63. Time evolution of various response parameters for L-S type 112
Figure 64. Bending moment and deformation envelopes of piles and ground at key instances.......... 113
Figure 65. Phase difference calculation between pier top and pile, and soil and pile for L-S type..... 114
Figure 66. A comparison of isolated pile deformation and moment of kinematic and inertial interactions against the combined response in L-S 115
Figure 67. Phase difference between pier vs pile and pile vs free-field soil under various frequencies for LS-type structures 117
Figure 68. A comparison of pile bending from various cases (L-S, S-type and LS_{NS}) at various frequencies. 119
Figure 69. Maximum values of pile moment in S-type configuration 119
Figure 70. A comparison of pile deformation from various cases (L-S, S-type and L-S_{NS}) at various frequencies. 122
Figure 71. Summarization of the direction of kinematic and inertial loadings 124
Figure 72. Pseudostatic pushover model (Redrawn after J.-S. Chiou et al. 2022) 127
Figure 73. Interaction factor for combining inertia force and kinematic loading 128
Figure 74. Comparison of conventional pseudostatic analysis modeling against FEM based hybrid pseudostatic analysis model. 130
Figure 75. Inertial and kinematic loadings for hybrid pseudostatic analysis of D-F and D-S type configurations.. 131
Figure 76. Moment and deformation profiles of pier and pile for D-F configuration....................... 133
Figure 77. Calibration of kinematic loading factor in hybrid method.. 135

Figure 78. Inertia force and ground deformation profiles for liquifiable soil cases 137
Figure 79. EPWPR at the instant of maximum pile moment 138
Figure 80. Comparison of moment and deformation profiles from hybrid pseudostatic and dynamic analysis 139
Figure 81. Comparison of kinematic factors for D-S and L-S 141

List of tables

Table 1. Properties of the structural materials 37
Table 2. Experimental cases 39
Table 3. Excitation procedure 39
Table 4. Parameters of the bridge pier specimens 41
Table 5. Soil parameters (Cyclic mobility model) 43
Table 6. Comparison of the response parameters for the F- and S-type structures under elastic and elastoplastic shear panels corresponding to the third excitation step 51
Table 7. Comparison of the response values for each member against Level-2 seismic motion 56
Table 8. Excitation characteristics of various input motions 78
Table 9. List of soil-pile phase differences for various input frequency cases 80
Table 10. List of phase difference values across various frequencies for D-S, L-F and L-S configurations 124
Table 11. List of RTRI (2012) and proposed inertial and kinematic factors for D-F and D-S configurations 134
Table 12. EPWPR at the instant of maximum pile moment for L-F configuration 138
Table 13. List of inertial and kinematic factors for L-F and L-S configurations 140

ABSTRACT

With bridge piers serving as key structural members responsible for safely transferring superstructure loads to the foundation, minimizing seismic damage is of paramount importance. This study proposes a smart bridge pier composed of four steel pipes interconnected by shear links arranged at multiple levels along the pier height. The steel pipes primarily carry vertical loads, while the shear links dissipate seismic energy through hysteretic behavior based on a damage-control design concept. Two foundation systems are considered: (i) a conventional pile group with a footing (F-type), and (ii) a directly connected steel pipe–pile system (S-type) incorporating underground beams at the pile head. Shaking table tests at a 1:20 scale were previously conducted for both systems embedded in dry (D-ground) and liquefiable (L-ground) soils, referred to as D-F, D-S, L-F, and L-S cases.

In this study, a three-dimensional elastoplastic finite element analysis is performed to reproduce the experimental results. The steel pipe columns and underground beams are modeled using bilinear beam elements, while the shear panels are represented by bilinear beam elements combined with central spring elements. Piles and their interaction with the surrounding ground are modeled using hybrid elements consisting of beam and solid components. The Cyclic Mobility model, incorporating subloading and superloading concepts, is adopted as the constitutive law for both dry and liquefiable soils, with parameters derived from triaxial and isotropic consolidation tests. A half-model is employed considering symmetry in geometry and loading, and boundary conditions are set to replicate experimental conditions before being extended for parametric analyses.

The numerical results show good agreement with experimental observations in terms of the relationship between inertial force and pier-top displacement, as well as shear panel behavior prior to yielding. Although some discrepancies appear in the post-yield range, such as wider hysteresis loops and deviations in initial stiffness, particularly for the S-type system. However, overall trends, including peak responses and deformation patterns along the piles, are well captured. Notably, at an excitation frequency of 2 Hz, the S-type system exhibits smaller responses than the F-type system, confirming its structural advantage. However, parametric analyses over a wide frequency range reveal that this advantage depends on frequency, with the S-type showing larger responses at lower frequencies due to resonance effects.

To further clarify the underlying mechanisms, the study examines soil–structure interaction by

separating inertial and kinematic components through additional analytical configurations. Specifically, the superstructure is removed to isolate pure kinematic interaction, while the soil is removed to isolate pure inertial interaction from the original D-F configuration. A phase-difference-based approach is then introduced. In this approach, the phase of the pile response in the D-F system is compared with a reference phase derived from the inertial-only configuration, defined by the relationship between pile response and superstructure inertia. Likewise, the phase relationship between pile response and soil motion is compared with that from the pure kinematic configuration. The dominant interaction mechanism is identified based on the degree of agreement between the pile response phase and each reference state. The results indicate a transition from inertial-dominated behavior at lower frequencies (around 2 Hz) to kinematic-dominated behavior at higher frequencies. Furthermore, comparison of pile-head earth pressure with inertial force reveals an increasing contribution of earth pressure with increasing input frequency, accompanied by a shift in its directional relationship—from being aligned with inertial force to opposing it—particularly in F-type configurations. Pile moment distributions also show that, although each interaction mechanism can independently generate significant demand, their combined effect may reduce the overall response due to phase differences.

Based on these findings, a simplified static analysis framework is proposed by extending the Japanese railway design method. The framework incorporates both inertial and kinematic effects through interaction factors, while accounting for phase differences and soil nonlinearity. At lower frequencies, an inertia-dominated load combination, acting in a direction consistent with kinematic effects, successfully reproduces the dynamic analysis results in terms of pile–pier deformation and bending moments. In contrast, at higher frequencies, the kinematic-dominated load combination specified in the conventional design method tends to yield overly conservative estimates. To address this issue, refined kinematic interaction factors are proposed for such cases. The framework is further extended to liquefiable soils by incorporating stiffness degradation associated with excess pore water pressure. Moreover, the method can be applied to S-type configurations through appropriate calibration of the kinematic interaction factors.

Overall, this study establishes a validated numerical simulation framework and provides new insight into soil–pile–structure interaction under dynamic loading. It also offers a rational basis for improving simplified seismic design methods for pile-supported bridge piers, particularly in capturing the coupled effects of inertial and kinematic interactions.

PREFACE

The research work, presented in this thesis was conducted at the Hokkaido University in the laboratory of Analytical Geomechanics of the Division of Field Engineering For Environment of Graduate School of Engineering during the period April 2023 to June 2026. This work was performed under the supervision of Associate Professor Koichi ISOBE. This thesis is presented in the form of a thesis by publications, based on the publications listed below.

(1) International Journals

- Hassan, M. M. U., Isobe, K., Soga, Y., Sawamura, Y., Sugiyama, H., & Shinohara, M. (2025). Seismic performance of bridge pier integrated by multiple steel pipes with directly-connected piles using soil-water coupled three-dimensional elasto-plastic finite element analysis. Soils and Foundations, 65(2), 101571. DOI: https://doi.org/10.1016/j.sandf.2025.101571

(2) International Conferences

- Hassan, M. M. U., Isobe, K., Soga, Y., Sawamura, Y., Sugiyama, H., & Shinohara, M. (2024). A Study on Soil-Structure Interaction in Smart Bridge Pier Structure Under Dynamic Excitations. Japanese Geotechnical Society Special Publication, 10(36), pp 1389-1394. DOI: https://doi.org/10.3208/jgssp.v10.OS-25-06
- Muhammad Mahmood Ul Hassan, Koichi Isobe (2026, Jan). Dynamic Soil–Structure Interaction of Smart Bridge Pier with Multiple Foundations: Identification of Inertial and Kinematic Actions and Development of a Static Design Framework, Technical Report of the Hokkaido Branch of the Geotechnical Society of Japan, No. 66 , pp. 93-102 , January 2026.
- Hassan, M. M. U., Isobe, K. (2026). Role of Kinematic and Inertial Interactions in the Response Analysis of Smart Bridge Pier Structure Under Dynamic Excitations. Proceedings of the International Conference on Computational Methods and Soil-Structure Interaction (CompDSSI 2026), Rome, Italy. (Accepted)

CHAPTER 1. INTRODUCTION

Earthquakes are among the most devastating natural hazards in terms of both loss of life and economic impact, with annual losses amounting to billions of dollars. Over the period from 1990 to 2018, earthquake-related fatalities reached approximately 925,000 worldwide, highlighting their severe societal consequences. Although the frequency of earthquake occurrences remains relatively constant from year to year, their impacts vary significantly. This variability is primarily governed by factors such as the vulnerability of constructed infrastructure and the population density of affected regions.

In recent decades, rapid urbanization and infrastructure development have led to the construction of critical facilities such as skyscrapers, bridges, ports, and lifeline systems in regions with high seismic risk. Many major cities in these regions, such as Shanghai, Bangkok, Mumbai, Kuala Lumpur, Jakarta, and Singapore, are founded on soft soil deposits, which necessitates the widespread use of pile foundations to ensure adequate load-bearing capacity and to control settlement. Under such conditions, the seismic response of pile foundations and their interaction with surrounding soil becomes a key factor governing the overall performance and safety of these structures.

Beyond supporting vertical loads, pile foundations are subjected to complex loading conditions, including transient and cyclic lateral and uplift forces induced by earthquakes, wind, waves, impacts, and machine vibrations. In seismic environments, these effects are further compounded by phenomena such as soil–structure resonance, liquefaction, and strain softening, which can significantly alter load transfer mechanisms and amplify structural demand. As a result, pile-supported structures in earthquake-prone regions often experience highly complex soil-pile-structure interaction behavior.

The design of such systems presents significant challenges for both structural and geotechnical engineers. In particular, the interaction between the superstructure and foundation is inherently coupled: loads transmitted from the superstructure induce foundation movements, which in turn influence the structural response and modify the forces acting on the foundation. This complexity is further amplified in pile groups, where interaction among piles can affect overall stiffness, load distribution, and dynamic response.

Given these challenges, there is a growing need to move beyond conventional design approaches toward more rational and performance-based frameworks. In this context, the seismic design of pile foundations should be treated as a comprehensive soil-structure interaction (SSI) problem, where the coupled response of the soil, foundation, and superstructure is explicitly considered. Such an approach enables more accurate prediction of structural performance under seismic loading, thereby improving safety while avoiding overly conservative designs.

In this study, we have investigated bridge pier structure with different types of pile foundations and studied the input motion frequency dependency of dynamic SSI mechanism which then led to introduction of a hybrid pseudostatic analysis method.

Document Outline:

In **Chapter 2**, a brief introduction to damage-controlled bridge pier structure is given along with various foundation options such as footing type (F-type) and footing-less (S-type). Then the concept of dynamic Soil-Structure Interaction (SSI) is introduced and is followed by case histories of post-earthquake observations in the literature concerning the performance of piled foundations. A review of previous experimental work dealing with deep foundations is also done in this chapter. The numerical methods available for the study of dynamic soil-structure interaction of deep foundations are also addressed briefly.

Chapter 3 describes the experimental program that consisted in a series of shaking table tests on bridge pier structure with F- and S-type configurations under sinusoidal base shakings. The characteristics of the different tests, soil profile and type of soil, applied signals, instrumentation, etc are explained. Then 3D FEM based simulation method that involves an explanation of soil-constitutive model, modeling of structural element, analysis conditions, and various analysis cases. Then, the main results are presented and analysed, especially in terms of the pier top inertia force, displacement and shear strains of panels, pier-pile deformation and moment profiles are explained for both dry and liquifiable soil configurations. The chapter concludes with a parametric study carried to study the relationship of S- and F-type structure against input excitation frequency.

Chapter 4 is aimed at studying the dynamic SSI inetraction mechanism especially in terms of kinematic and inertial interactions. It carries out additional simulation cases intended at decomposing the coupled dynamic moment and deformation of pile into individual contributions of kinematic and inertial interactions. A combination of techniques such phase difference of pier top, pile and soil along with moment and deformation profiles are used to identify the directions, role and governing component between kinematic and inertial inetraction.

Chapter 5 introduces an FEM based hybrid pseudostatic analysis method aimed at simplifying the understanding of SSI mechanism and reducing the calculation time of analysis. It assess the design combination of Japanese Design Code for railways and proposes slightly modified values of kinematic inetraction factors to increase the accuracy of introduced method.

Chapter 6 summarizes the general conclusions and future perspectives of this work.

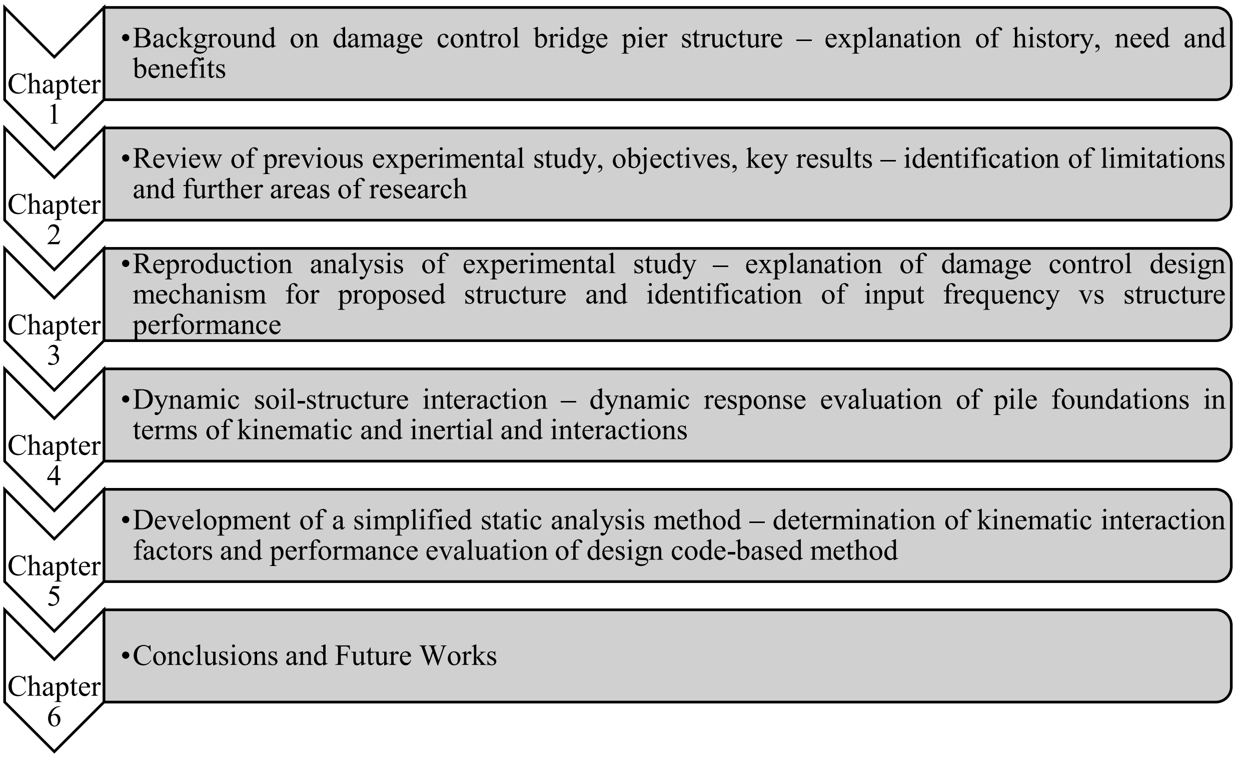

CHAPTER 2: LITERATURE REVIEW

2.1 Damage control bridge pier structure:

It is bridge pier consisting of four steel pipes interconnected by multiple shear links at various levels. All the vertical loads such as dead and live loads are carried by steel pipes whereas horizontal loads such as lateral forces arising from earthquake are combinedly supported by steel pipes and shear panels. Its design is based on damage control design concept in which damage is directed to concentrate at the shear links (panels) so that steel pipes maintain their strength. Shear panels are made of low yield strength steel and have hysteretic energy dissipation properties. Steel pipes are the main members and shear links are secondary members. Fig. 1 shows the schematics of smart bridge pier structure. Studies by (Nakamura et. al., 2014) and (Isobe et. al., 2015) confirm the energy dissipation of shear panels as they undergo most of the damage during dynamic excitations and main members still hold large strength. The replacement of shear panels restores the full-strength bridge pier, therefore, maintenance cost due to earthquake are also reduced. Based on the validity of the damage control design and the superiority over the conventional steel piers, the steel pipe combined pier has already been put into practical use (Shinohara et. al., 2012).

This bridge pier could be supported by a conventional pile group foundation or by directly connecting steel piles without footing as shown in Fig. 2. The structure on left and right in Fig. 2 would be called as F-type and S-type respectively. In S-type, an underground beam connects the piles all around at the pile head level. Advantages of S-type include the reduction in amount of load on piles due to absence of footing, removal of stress concentration point at joint of pile and footing by eliminating the stiffness contrast pier and foundation and cost reduction etc. (Shinohara et al., 2013) proposed S-type structure and conducted its performance comparison against F-type smart bridge pier and a conventional steel bridge pier with caisson foundation. Under same ground motion, the maximum tensile and compressive strain at the base of the columns for S-type is $0.73\varepsilon y$ and $0.66\varepsilon y$ respectively against the F-type structure. It was shown that construction cost and time for S type structure reduced by 59% and 35% respectively, against a conventional steel bridge pier with pile foundation. (Isobe et. al., 2015) reported that S-type structure has high seismic performance because the main members such as columns and piles hold large residual strength even after yielding of the shear panels. He also showed lower strain of columns near pier base for S-type as compared to F-type.

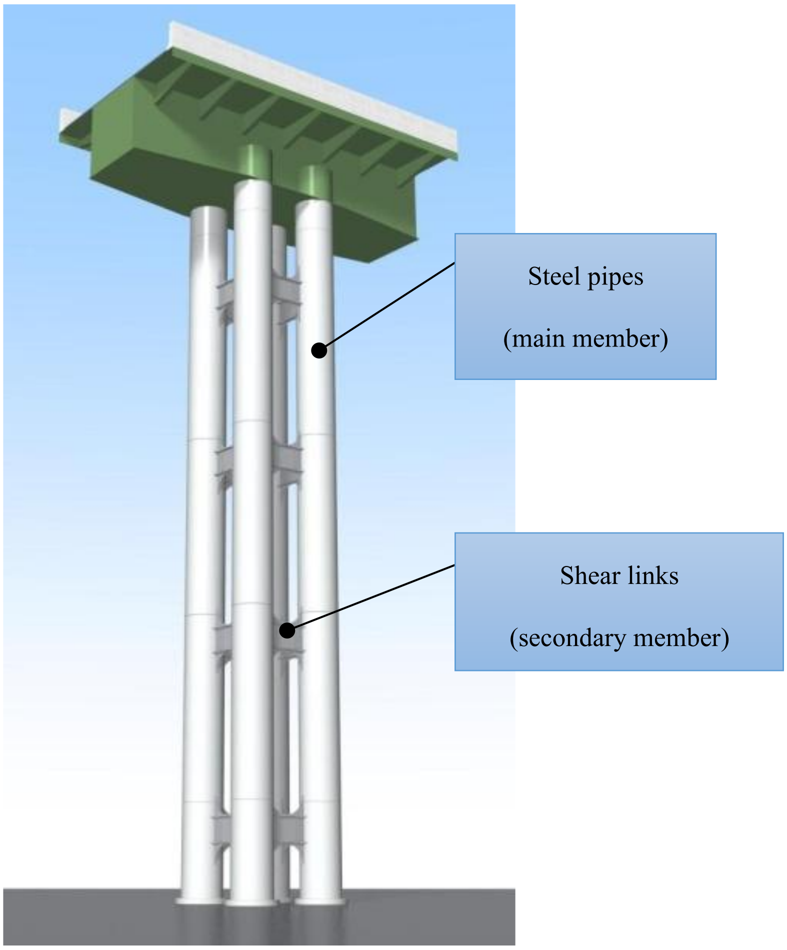

Figure 1. A 3D view of damage control bridge pier structure

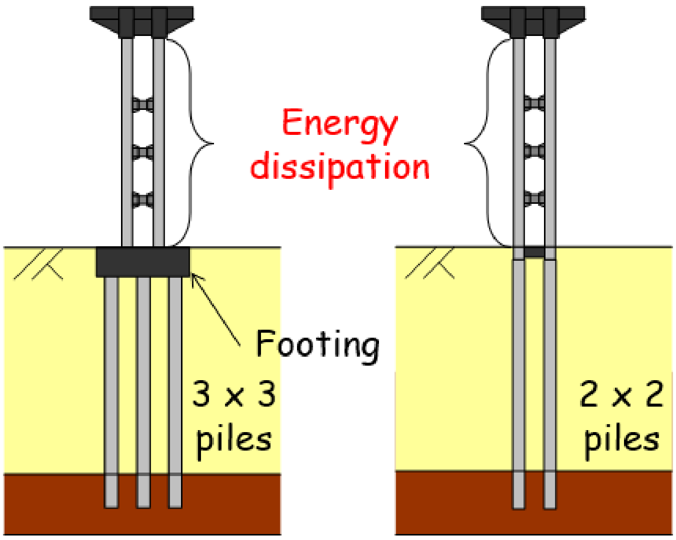

Figure 2. Smart pier structure with F- and S-types foundation

2.2 Dynamic soil-structure-interaction

The dynamic soil-structure interaction or SSI is a phenomenon in which the movement of the soil during an earthquake is influenced by the presence of the structure and vice versa. It means the displacements of the soil and of the structure can't be considered as independent from each other. It is a complex phenomenon, and its importance depends on the nature of the soil, and the characteristics of the structure and foundation.

The movement of the foundation differs from the free field due to the stiffness differences between them. The incident wave is reflected and diffracted by the foundation and thus the movement of the soil in the vicinity of the foundation, called near-field soil response is modified. Therefore, in the absence of the mass (of superstructure and foundation), the movement at the base of the structure would be different from the free field due to the difference in rigidity between the ground and the foundation. The stiffness of the foundation doesn't allow the surrounding soil to follow the movements imposed by the soil in free-field conditions. As foundation doesn't allow the surrounding soil to move in the same way as it would in free-field conditions, it results in additional stresses and deformations in the foundation. This phenomenon (difference in movement) is known as kinematic interaction ((Fig. 3a)) (Perez-Herreros, 2020).

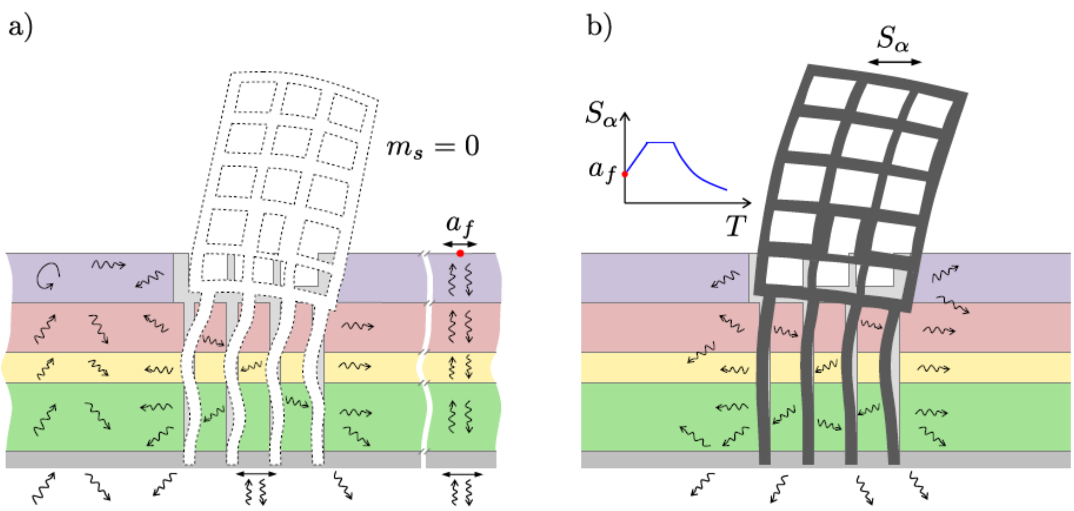

Figure 3. Illustration of (a) kinematic and (b) inertial interaction phenomena (Perez-Herreros, 2020)

Furthermore, in case of presence of superstructure, the movement induced on the foundation develops oscillations of the superstructure and thus produces inertial forces. These forces are transmitted to the foundation and consequently, the foundation and the surrounding soil experience additional dynamic forces and displacements (Fig. 3b). This phenomenon is called inertial interaction. (Perez-Herreros, 2020).

Whenever a foundation element moves against the surrounding soil, stress waves originate at the contact surface and spread outward, carrying away some of the energy transmitted by the foundation into the soil. This results in a dissipation of energy from the system which is called radiation damping. The magnitude of this damping depends mainly on the frequency of the oscillation, the geometry of the soil-foundation system, the mode of oscillation, and the stress-strain characteristics of the soil. Energy dissipation in the soil is also caused by the plasticity of the soil and possibly discontinuity conditions (uplift and/or sliding) at the foundation-soil interface. This type of damping is called hysteretic damping and is fairly frequency independent (Perez-Herreros, 2020).

It should be noted that during an earthquake, kinematic and inertial interactions act simultaneously. It is often convenient to study them separately and then superimpose their results. However, this is only valid when the behaviour of the system can be assimilated to an equivalent linear system and nonlinearities are limited. Pile foundations have been subjected to both kinematic and inertial interactions, particularly in liquifiable ground due to significant deformations and loss of strength during liquefaction (Hamada, 1992), (Ishihara, 1997). Although, it is accepted that inertial and kinematic interaction affect the dynamic behaviour of bridge pier, however, still there is no clear rule on designing against these dynamic interactions and coupling mechanism varies from case to case. Various design codes recommend different combinations of kinematic and inertial interactions; Caltrans guidelines suggest that peak pile demand should consist of 100% kinematic and 50% inertial, Chinese code assumes superimposing 100% of both, AASHTO considers only inertial force in its pseudo-static design method and Japanese design standard employs inertial force only when soil's natural period is under 0.5 sec. Other researchers have shown different combinations of kinematic and inertial forces for various cases.

This studied bridge pier structure is relatively new and dynamic soil structure interaction mechanism is one of its an explored area. The dynamic response of this pier supported over F-type and/or S-type foundation is different from the conventional piers with deep foundations and requires separate investigation to study kinematic and inertial interactions. Therefore, the following sections address several aspects of deep foundations under seismic loading and form a basis for next sections. First, post-earthquake observations of deep foundations in soft and stratified soil profiles are examined. Next, experimental studies focusing on single piles and pile groups in similar soil conditions are reviewed. Subsequently, numerical methods for analysing dynamic SSI of structures supported by deep foundations are introduced. This is followed by a review of existing studies on the seismic behavior of deep foundations, providing a comprehensive understanding of the associated phenomena and challenges. Finally, the impact of dynamic soil–structure interaction is highlighted through an analytical approach.

2.3 Post-earthquake observations of the performances of piled foundations

Numerous instances of damage to pile foundations and pile-supported structures during earthquakes have been reported in the literature. However, due to the subsurface nature of deep foundations, direct observation of damage is often limited. In most cases, post-earthquake assessments rely on visible damage in the superstructure or indirect evidence observed at the pile head, making many of these evaluations largely qualitative. As a result, the understanding of failure mechanisms is frequently inferred rather than directly measured.

Only a limited number of structures equipped with instrumentation have recorded their response during seismic events. Despite their scarcity, such case studies are particularly valuable, as they provide quantitative insights into the coupled behavior of the soil, foundation, and superstructure under dynamic loading.

In the following section, selected case studies are presented and critically examined. These examples highlight how post-earthquake observations can reveal the significant role of soil–structure interaction (SSI) in governing the response of both foundations and superstructures.

2.3.1 NHK building, 1964 Niigata earthquake

The 1964 Niigata earthquake (Mw = 7.6) caused widespread damage, much of which was attributed to liquefaction and its associated effects on pile-supported structures. The subsurface conditions in Niigata City consist predominantly of loose sand deposits extending to depths of approximately 20-230 m. Liquefaction occurring over such significant thicknesses played a critical role in the observed damage to both foundations and superstructures.

A notable example is the four-storey NHK building, which was supported by reinforced concrete piles with a diameter of 0.35 m and lengths of approximately 11-12 m (M. Hamada, 1991). Detailed investigations conducted about 20 years after the earthquake, including excavation of the foundation, revealed that the piles had sustained damage at two distinct locations: near the pile head and close to the pile tip, where a marked contrast in soil stiffness was present (Fig. 4).

The damage observed near the pile head is primarily attributed to inertial forces transmitted from the superstructure during seismic excitation. This effect was further exacerbated by the reduction in lateral soil resistance due to liquefaction, as well as by lateral ground movement associated with soil spreading. Additional contributing factors, such as second-order effects, may also have influenced the severity of damage in this region.

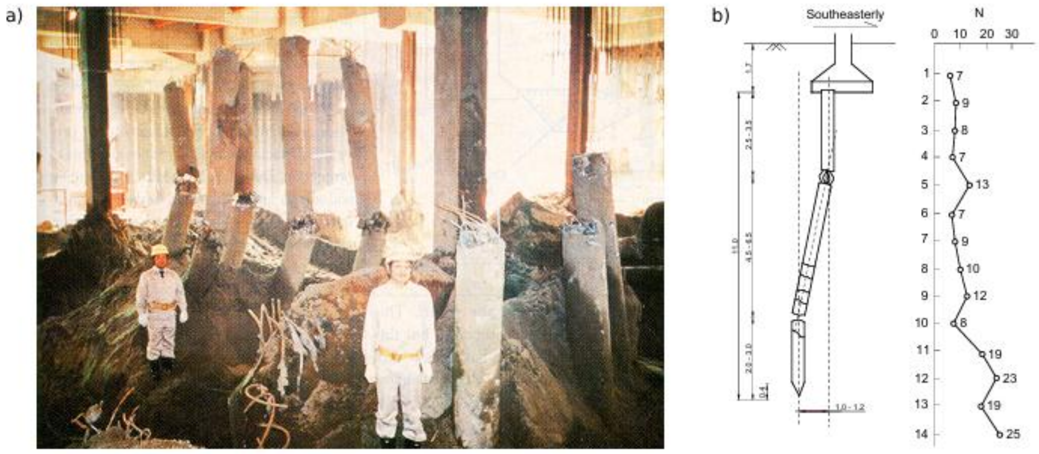

Figure 4. NHK building after 1964 Niigata earthquake: a) piles damaged by lateral spreading of the foundation soil and b) correction of pile damage and site conditions (M. Hamada, 1991)

2.3.2 Hanshin Expressway Route 3 in Kobe, 1995 Kobe Earthquake

The 1995 Kobe earthquake (Mw = 6.9) was one of the most destructive seismic events in Japan in over 60 years, resulting in more than 6,400 fatalities and widespread infrastructure damage. Nearly one-fifth of the buildings in severely affected areas were either destroyed or rendered uninhabitable.

A well-known example of structural failure is the collapse of a section of the pile-supported Hanshin Expressway (Fig. 5). The elevated structure, approximately 13 m high, consisted of 19 circular columns (3.1 m in diameter) monolithically connected to the deck and supported by groups of 16 reinforced concrete piles, each about 15 m long and 1 m in diameter.

Post-earthquake investigations identified two primary causes of failure: inadequate reinforcement detailing and reliance on elastic analysis for estimating design shear forces. At the time of construction in the 1960s, modern concepts such as ductility and capacity design had not yet been established; thus, the design was consistent with contemporary standards. However, it has been suggested that the structure would likely have survived had modern reinforcement detailing been adopted.

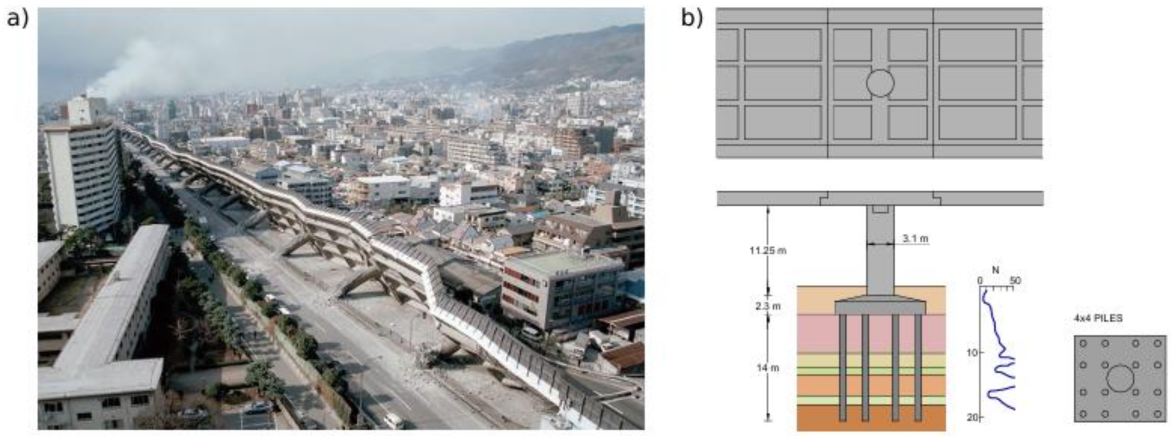

Figure 5. a) Hanshin Expressway bridge collapse after 1995 Kobe earthquake b) geometric characteristics and pile foundation (after Mylonakis et al. 2000. redrawn by Perez-Herreros, 2020)

Subsequent analyses by (Mylonakis et al. 2000) highlighted the significant influence of local soil conditions and soil-structure interaction. The authors showed that site-specific soil profiles amplified seismic waves and introduced spatial variability in both amplitude and frequency content. Furthermore, foundation flexibility led to period lengthening of approximately 30%, increasing structural demand and contributing to the collapse.

2.4 Experimental studies on the behavior of piles under seismic loading

(Perez-Herreros, 2020) conducted a dynamic centrifuge study on various configurations of pile foundation in a multi-layered soil profile under a series of earthquakes and sinusoidal base shakings. Various configurations used in dynamic testing as shown in Fig.6.

Case (a) is single pile without pile cap is used to investigate the response of structure under pure kinematic loading, case (b) studies the response of combined action kinematic and inertial action, case (c) and (d) are used to study the influence of structure slenderness on the response of pile group. It was found that the response of system depends on factors such as pile head conditions, loading type, intensity, and frequency content of input motion. It was observed that both kinematic and inertial interactions effects are important and need to be considered appropriately when pile foundations are used. Special attention should be given to kinematic interaction effects in the case of layered soil profiles with large stiffness differences between soil layers. Kinematic interactions and radiation damping are most influential to system at lower amplitudes of seismic loading, whereas inertial interaction become dominant at moderate to high level of seismic excitations.

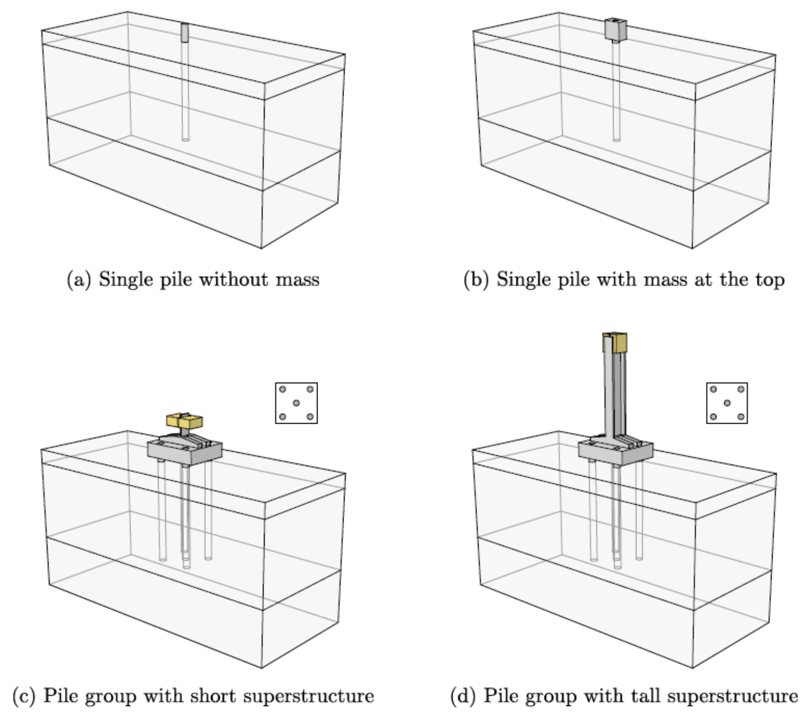

(a) Single pile without mass

(b) Single pile with mass at the top

(c) Pile group with short superstructure

(d) Pile group with tall superstructure

Figure 6. Various model configurations used in centrifuge tests (Perez-Herreros, 2020)

In the study by Hussien et al [29], the study investigated the fundamental behaviour of soil–pile group–structure interaction under seismic loading through a series of systematic centrifuge experiments conducted on dry dense sand, serving as a baseline for future studies involving liquefaction. Seven centrifuge model tests, including free-field, single-pile, and 3 × 3 grouped-pile configurations supporting single- and two-degree-of-freedom structures, were performed at 40 g using air-pluviated sand deposits. Each model was subjected to at least twelve sinusoidal base excitations with a constant acceleration amplitude of 1.5 m/s^2 and frequencies ranging from 0.5 to 12 Hz, and the results were presented in dimensionless form to cover a wide excitation range. The experiments revealed that pile-head motion is governed by two characteristic frequencies: an effective natural frequency at which motion is amplified and a pseudo-natural frequency at which pile-head response is significantly de-amplified relative to free-field motion, suggesting a potential design frequency to minimize pile demand. For free-head grouped piles, strong kinematic interaction occurred when excitation frequencies approached the ground's fundamental frequency, leading to large bending moments and pronounced pile-to-pile variation, with the center pile experiencing the highest demand. In contrast, for grouped piles supporting structures, inertial interaction dominated as excitation frequencies approached the coupled soil–pile–structure natural frequency, resulting in the largest bending moments in corner piles and the smallest in center piles. The findings emphasize the importance of accounting for both kinematic and inertial interactions in seismic pile design and highlight the need for further experimental studies under more complex conditions, particularly involving soil liquefaction, where interaction mechanisms may differ.

(Tokimatsu et. al, 2005) performed shaking table tests on a series of soil-pile-structures in dry or liquifiable sand to investigate the effects of inertial and kinematic forces as shown in Fig. 7. The results show that kinematic and inertial response combinedly effect the response of structures for both dry and liquifiable sand. It is also found that if the natural period of the superstructure is less than that of the ground the ground displacement tends to be in phase with the inertial force from the superstructure and increases the shear force transmitted to the pile head. Otherwise, the ground displacement tends to be out of phase with the inertial force, restraining the pile stress from increasing.

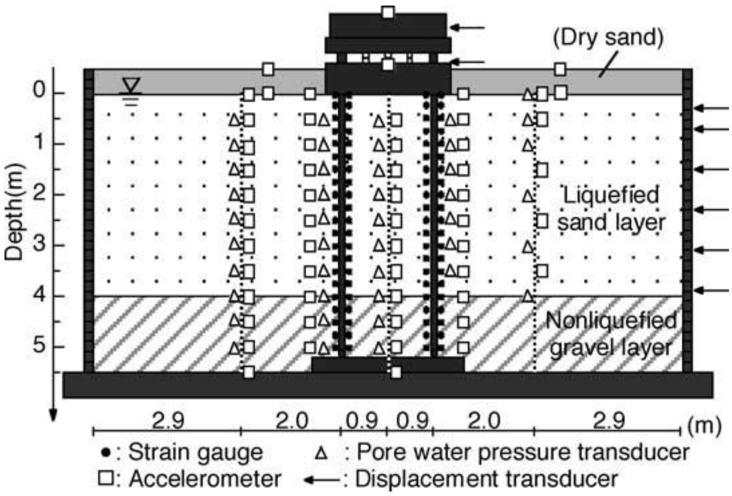

Figure 7. Soil-pile-structure model layout (Tokimatsu et. al, 2005)

(Shutong et. al., 2020) conducted a shaking table test and developed a numerical simulation procedure to study the influence of SSI on a multi-story frame structure embedded in soft soil as shown in Fig. 8. The results show that SSI reduces the dynamic response of structure as compared to as compared to case of rigid foundation. Kinematic interactions are very significant when the frequency of superstructure is close to soil and reduced impact when soil is stiffer.

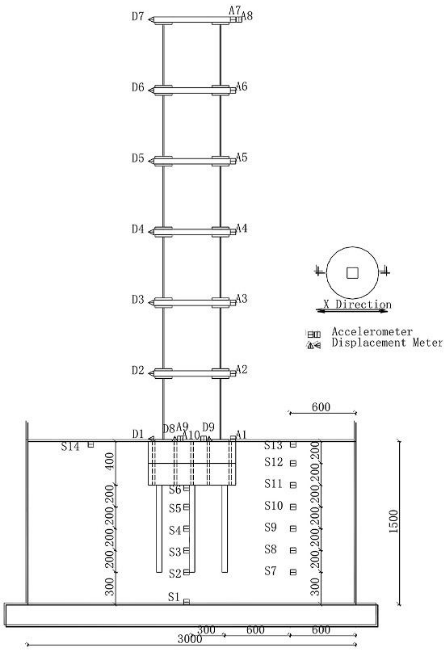

Figure 8. Model of frame structure embedded in soft soil and arrangement of measuring points (Shutong et. al., 2020)

(Toyooka et. al., 2012) carried out an analytical study on various structures including bridge pier constructed over a pile foundation in a good condition soil. Japanese code mandates inertial action only, if frequency of a layered soil profile is more than 2Hz (good condition soil). He found that kinematic action can't necessarily be negligible for foundation response particularly when superstructure inertia force is relatively small.

(K. Yamshita and J. Hamada, 2023), they employed seismic records from isolated (IS) and non-isolated (NI) piled-raft buildings with a Deep Mixing Wall (DMW) grid on soft soil during the 2011 Tohoku earthquake, the study examined the relative roles of kinematic and inertial forces on pile behavior. In the IS building, kinematic effects dominated pile-head bending moments because base isolation significantly reduced superstructure acceleration and mass effects. In contrast, in the NI building, kinematic forces and superstructure inertia contributed comparably to maximum bending moments, while raft inertia was significant in both cases.

Incremental axial forces near the pile head in the IS building were influenced by both kinematic and inertial effects, whereas in the NI building they were governed mainly by superstructure inertia, particularly in the transverse direction. Inelastic settlement and load-transfer behavior occurred in both systems during strong shaking, attributed mainly to residual pile settlement. For the IS building, residual settlement of perimeter piles was linked to raft rotation induced by kinematic effects and passive earth pressure; for the NI building, it was primarily caused by superstructure inertia and overturning moment. The ratio of the soil–pile–structure natural period to the ground predominant period (T_s/T_g) was found to strongly control the interaction of kinematic and inertial forces, influencing pile-head bending moments as well as settlement and load-transfer mechanisms. Finally, in the NI piled-raft system, most superstructure inertia was resisted by base friction on the raft, resulting in relatively small bending moments near the pile head.

2.5 Numerical methods for dynamic soil-structure interaction analysis of piled foundations

The dynamic response of structures supported by deep foundations involves complex soil–structure interaction (SSI). Traditional seismic design methods are typically conservative and based on linear elastic assumptions [43], neglecting the potential for energy dissipation through nonlinear foundation behavior. These simplifications were historically due to limited understanding and computational capabilities.

With advances in experimental research, numerical methods, and modern design approaches [44], these limitations are gradually diminishing. Although nonlinear analysis is not yet common in routine design, current codes such as Eurocode 8 [45] recognize the importance of SSI and nonlinear effects, particularly under strong seismic loading, encouraging the development of more realistic design methods. In the following sections, we have presented a few such methods which are being employed as numerical methods for computation of soil-pile response.

2.5.1 Direct method

In the direct method, the entire soil–foundation–structure system is modeled and analyzed simultaneously in a single step, typically using the finite element method (FEM). This approach allows detailed representation of soil–structure interaction (SSI), including nonlinear behavior such as material inelasticity, foundation uplift, and sliding. For pile foundations, it can directly capture pile–soil–pile interaction and the influence of loading frequency and intensity.

Despite its accuracy, the direct method has several limitations. The mesh size must be sufficiently fine to capture wave propagation, especially at high frequencies, which significantly increases computational cost. Artificial boundaries are required to simulate infinite soil domains, but they only approximate wave absorption in time-domain analysis. In addition, model boundaries must be placed far from the structure to minimize wave reflection effects.

The complexity of the analysis increases further when nonlinear behavior of soil, structure, and their interface is considered. Accurate calibration of constitutive models requires high-quality material data, and the solution typically involves iterative procedures such as the Newton–Raphson method, leading to increased computational time. As a result, the direct method is generally used for detailed analysis and research applications rather than routine design.

The governing equations are based on dynamic equilibrium, incorporating mass, damping, and stiffness, with ground motion as input. To discretize the soil domain, three numerical approaches are commonly used: FEM, finite difference method (FDM), and boundary element method (BEM).

FEM is the most widely used technique due to its flexibility in modeling complex geometries and nonlinear behavior, although it is computationally demanding. FDM is often more efficient, as it avoids assembling global matrices and updates equations at each time step. In contrast, BEM discretizes only the boundaries, reducing computational effort and naturally handling infinite domains. However, BEM is less suitable for heterogeneous soils and nonlinear problems, making FEM the preferred approach for advanced SSI analysis.

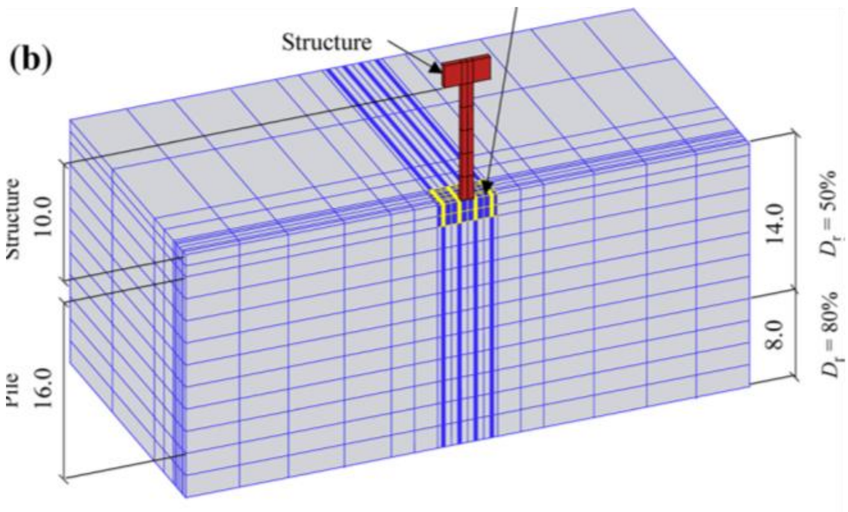

Figure 9. Finite element simulation model for pile group (Wang et al. 2017)

(Wang et. al., 2017) performed 3D FEM simulations to determine the influence of SSI on pile bending moment for pile groups and single pile with and without pile cap in liquifiable soil. Fig. 9 shows FE model of pile group configuration. It included dynamic and static analysis to determine the dominant action. Parametric studies by varying the mass and soil stiffness were also performed to discover the role of kinematic and inertial interactions. It was observed that kinematic interaction has a dominant role for pile foundations (single and pile groups) having their pile heads rotation restricted by pile cap while inertial interaction is more influential for pile heads with no pile cap.

2.5.2 Winkler type methods:

Several studies have investigated pile modeling using Winkler-type approaches. These methods idealize the soil–pile system as a series of independent horizontal layers, where each pile segment interacts with a corresponding soil layer assumed to be homogeneous and infinite. A key assumption is that the response of each layer is independent of adjacent layers.

Winkler-type models can generally be classified into two main categories. The first is based on dynamic p–y curve formulations, while the second uses discrete rheological elements to represent near-field soil behavior. Under low loading conditions, simplified linear rheological models are often sufficient. However, under strong loading, nonlinear soil behavior and interface effects—such as gapping, sliding, and friction—become important. These are typically modeled using nonlinear springs, dashpots, or contact elements, or through phenomenological interface models.

The main advantage of Winkler-type approaches is their simplicity and consistency with traditional static pile analysis methods. They are usually formulated in the time domain, making them suitable for dynamic analysis, and their computational cost remains relatively low since soil behavior is concentrated at the pile–soil interface. However, nowadays, a few pseudostatic analysis methods have also been proposed.

Despite these advantages, Winkler-type models have several limitations. They generally neglect group effects (pile-soil-pile interaction), ignore coupling between soil layers, and do not account for interaction between different loading directions. Most applications focus on single-pile response, with group effects included only through simplified interaction factors. Additionally, it can be difficult to relate model parameters to standard geotechnical soil properties, requiring careful calibration and interpretation.

2.5.2.1 Continuum based dynamic analysis method

(Chiou et al. 2020) proposed a unified analytical framework to evaluate the seismic response of pile-supported structures by simultaneously considering inertial and kinematic interaction effects. They developed a coupled model by integrating a shear beam representation of ground response with a beam-on-Winkler foundation (BWF) model for the pile-structure system, allowing both effects to be incorporated using a single input motion.

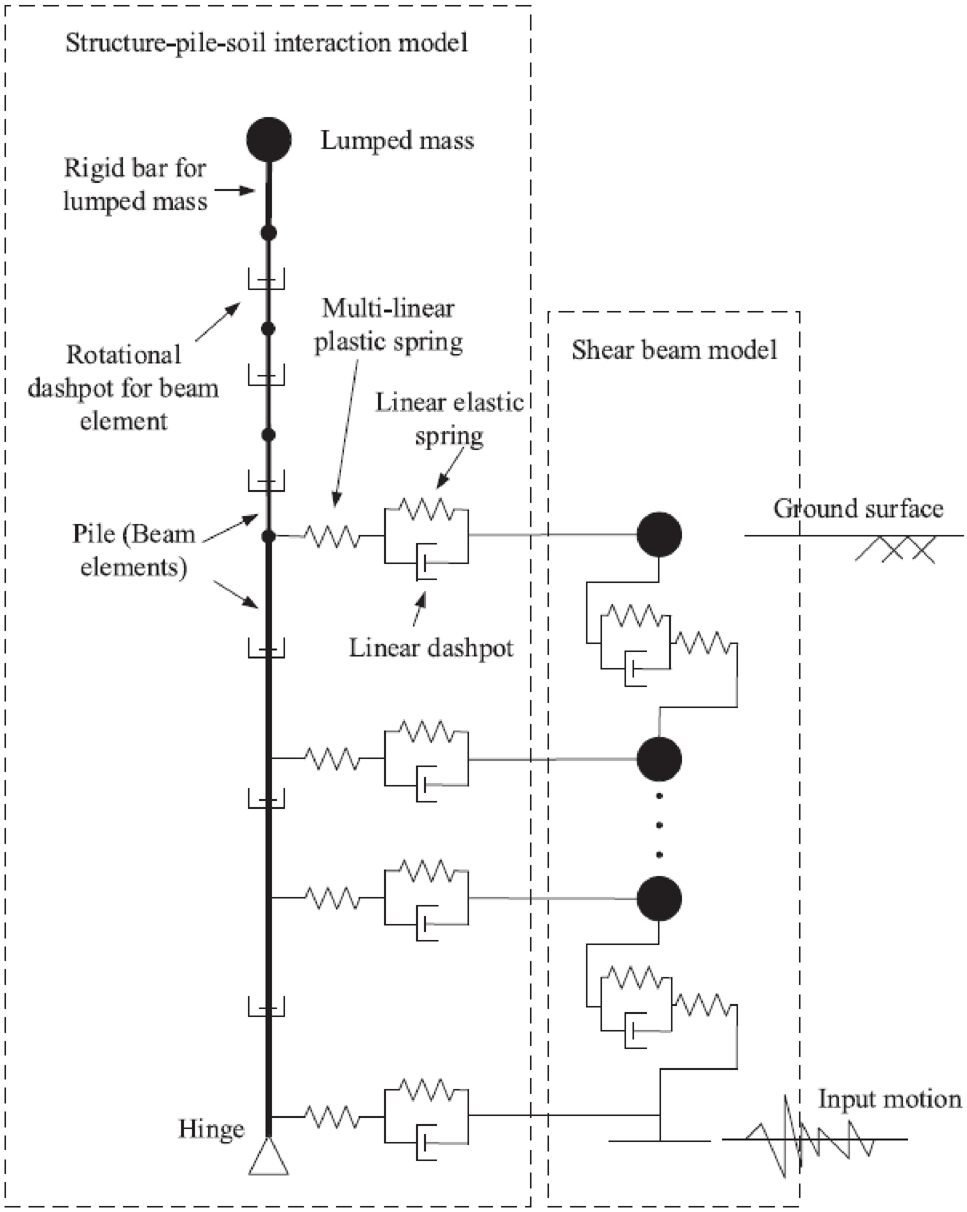

Figure 10.Combined structure-pile-soil interaction and ground response analysis model (Chiou et al. 2020).

The proposed method was validated using centrifuge shaking table tests on pile-supported systems embedded in dense sand. Both linear and nonlinear soil behaviours were considered, with nonlinear response modeled using hyperbolic constitutive relationships and hysteretic damping formulations. The results showed that the combined model can accurately reproduce structural acceleration and pile bending responses observed in experiments.

A key finding of the study is that kinematic interaction plays a significant role in the seismic response, even in relatively stiff soil conditions. Neglecting ground movement leads to underestimation of structural acceleration and pile demand. The relative contributions of inertial and kinematic effects were found to depend strongly on excitation frequency, amplitude, and the fundamental frequencies of the soil–structure system. In particular, near resonance conditions, soil nonlinearity and phase differences between inertial and kinematic components significantly influence the overall response. The study highlights the importance of considering both interaction mechanisms simultaneously for reliable seismic analysis and design of pile-supported structures.

2.5.4.2 Pseudostatic analysis methods:

Pseudostatic methods are widely used in seismic design as a simplified alternative to dynamic analysis, where earthquake effects are represented by equivalent static forces and displacements. These approaches offer computational efficiency and practical applicability but often simplify or neglect the coupled interaction between soil, pile, and structure, particularly the combined effects of inertial and kinematic loading.

To address these limitations, Chiou et al. (2022) proposed an advanced pseudostatic framework for extended pile foundations that explicitly incorporates both interaction mechanisms. In this approach, inertial loading is modeled as an equivalent static force applied at the pile head, while kinematic loading is introduced through ground displacement profiles imposed on pile–soil interaction springs. The method employs the capacity spectrum method to evaluate structural acceleration using a weighted ground motion that accounts for contributions from different soil depths. The combined effects of inertial and kinematic loading are further captured through frequency-dependent participation factors, which consider their phase relationship. Further detail on this method is also added in chapter 5 of this document.

The results demonstrate that the proposed method can reasonably reproduce dynamic response characteristics while significantly reducing computational effort. It was observed that inertial effects dominate near the pile head, whereas kinematic effects become more significant at greater depths. Furthermore, the interaction between the two mechanisms is strongly influenced by excitation frequency, with phase differences leading to either amplification or reduction of the overall response. The study highlights the importance of incorporating both mechanisms in simplified design approaches for more reliable prediction of pile behavior under seismic loading.

2.6 Chapter summary:

Under seismic loading, both kinematic and inertial interaction mechanisms develop simultaneously and contribute to the overall response of pile-supported systems. These two types of interaction differ fundamentally in their nature and in the way they influence pile behavior. In the case of pile-head loading associated with inertial interaction, the soil essentially acts as a passive resisting medium. Conversely, during seismic events, the soil motion itself imposes deformations and loads on the pile, giving rise to kinematic interaction driven by free-field soil displacements.

To properly interpret the seismic response of piles, it is therefore essential to assess whether one of these interaction mechanisms dominates, or whether significant coupling between the two occurs under specific conditions. Therefore, building an understanding of kinematic and interactions role, combinations are pivotal in unveiling the SSI mechanism of our bridge pier structure with F- and S-type of foundation.

2.7 Objectives of study:

- Reproduction analysis of experimental test results (Isobe et al, 2016) for
    - Clarification of the damage control response mechanism in F- and S-type structure
    - Identification of conditions under which S-type structure is advantageous
    - Response analysis of both structures under multiple input frequencies and a design seismic motion
- Explanation of dynamic soil-structure inetraction mechanism in both structure – response evaluation in terms of kinematic and inertial interactions
- Exploration and development of simplified analysis methods – determination of kinematic interaction factors and performance evaluation of design code-based method

CHAPTER 3. SEISMIC PERFORMANCE EVALUATION USING THREE-DIMENSIONAL ELASTO-PLASTIC FINITE ELEMENT ANALYSIS

3.1 INTRODUCTION

With the pier being a key member that must safely transfer superstructure loads to the foundation, minimizing damage to the pier, especially during seismic events, is of concern to researchers and engineers. The present study introduces a ductile, lightweight, and cost-effective pier composed of multiple steel pipes integrated by shear links. Specifically, the pier consists of four prefabricated steel pipes, combined with shear links at three different levels along the pier height, as shown in Fig. 11. The steel pipes (columns) are the main members of the load-resistant assembly; they are primarily employed to resist the vertical loads, namely, the dead and live loads. The shear links (panels), on the other hand, are made of low-yield-strength steel and have hysteretic energy dissipation properties; they are employed to resist the lateral loads arising from earthquake motion. During an earthquake, damage is intentionally directed so as to concentrate at the shear links, allowing the steel pipes to maintain their strength in accordance with the damage control design concept for bridge piers (Morishita et al., 2000; Hino et al., 2001; Marwan et al., 2002). The inherent seismic resistance of the shear panels limits the damage to the bridge during seismic events, enabling its continued use by emergency and passenger vehicles during crises.

Figure 11. Bridge column integrated by multiple steel pipes and multiple shear panels interconnecting the pipes for practical use

A comparative study of this pier and the conventional steel pier, using numerical analyses by Kanaji et al. (2004), confirms the damage control design response of the pier structure as the shear panels absorb energy and mitigate any possible damage to the steel pipes. Additionally, it demonstrates the reduced response displacement at the pier top in comparison to a conventional pier. Shinohara et al. (2012a) performed a series of numerical studies, consisting of pushover and dynamic analyses, to clarify the cause–effect relationship between the characteristic period of this pier and the response of the spectrum property of the seismic wave. Drawing from the findings of their study, design standards for bridge piers integrated with multiple steel pipes were established for the first time (Hanshin Expressway Co., Ltd., 2020). Given the validation of the damage control design and its superiority over conventional steel piers, the steel pipe combined pier has already been implemented in practical applications (Shinohara et al., 2012b).

Our research group proposes a directly-connected pile foundation with steel pipes to rationalize the foundation structure for this type of pier footing. Its structural feasibility is examined by comparing its behaviour with that of a conventional pier footing under earthquake loading (Isobe et al., 2010; Shinohara et al., 2013; Isobe et al., 2015; Isobe et al., 2016; Isobe et al., 2017). Based on the seismic energy absorption of the steel pipe pier columns, the direct connection of the pier pipes to the piles is seen to redistribute the loads of the superstructure, thereby reducing the concentration of stress at the joints and allowing for the direct transmission of loads to the piles. This design will lead to a decrease in the time and cost of the construction, and will enable the use of pile foundations in confined spaces. Shaking table tests, with pier and foundation models at a scale of 1:20, were conducted in prior studies (Isobe et al., 2015; Isobe et al., 2016; Isobe et al., 2017) to verify the advantages of the design. The structure based on the design demonstrated an outstanding seismic performance against excitations with a frequency of 2 Hz. However, assessing a structure's performance solely under a single excitation frequency is insufficient for extrapolating its response to real earthquake events.

In the present study, therefore, a three-dimensional elastoplastic dynamic finite element analysis is conducted to develop a numerical simulation method for the experimental results and to elucidate the effect of these excitation conditions. The validity of the reproduction analysis method is confirmed, and the dynamic response characteristics of the proposed structure are clarified through various analysis models, namely, static, cyclic, and seismic. Both footing and footingless types of structures are subjected to Level 2 seismic motion (in accordance with the guidelines of Hanshin Expressway) in dry sand to evaluate their responses to a real earthquake event. Furthermore, the influence of the input motion frequency on both types of structures is investigated through a parametric study by varying the input excitation frequency from 0.1 to 10 Hz. Moreover, the dynamic soil-structure interaction of the proposed structure, which considers both inertial and kinematic interactions, is briefly examined based on the results of the numerical simulation.

3.2 OUTLINE OF SHAKING TABLE MODEL EXPERIMENT

3.2.1 Experiment modes

The schematics of the specimens used in the shaking table test experiment are shown in Fig. 12. The specimens were reduced to models 1:20 in size. Assuming a ramp bridge on an urban highway, and referring to Shinohara et al. (2013), single-column piers were created considering the similarity rule (Iai, 1988). Each pier was composed of four steel pipes. The horizontal connecting members (called shear links) between the steel pipes were set at the three levels shown in Fig. 12. A shear panel, having hysteretic damping characteristics, was set at the central part of each shear link, as shown in Fig. 11. Based on the findings of the previous experimental studies by Kanaji et al. (2004), Shinohara et al. (2012a), and Shinohara (2014), a vertical stiffener was installed on each shear link having an aspect ratio (the ratio of the height to length at the central part of the shear link web) equivalent to one, to reinforce the two ends of each shear link. This was done to ensure that the shear deformation would progress steadily and that the shear links would effectively perform as a hysteretic damper. The ratio of the plate width to the thickness of the governing plate buckling was 0.48, like that in the cyclic loading tests on the columns (Kanaji et al., 2004; Shinohara et al., 2012a).

In this series of model tests, the footing type of structure (abbreviated as F) had eight steel piles to support the pier via the footing, while the footingless type of structure (abbreviated as S) had four directly-connected piles to support the pier, which is the same number as that of the pier pipes. The piles were installed with a centre-to-centre spacing of 2.5 times the pile diameter. For the S-type, an I-shaped underground beam was welded to the base of the pier pipes (the pile heads), instead of a footing, in a similar way to the case with shear panels, to avoid excessive displacement of the piles, especially around the pile heads. To connect the pier pipes to the foundation piles, the pier pipes were inserted 20 mm into the foundation piles. Any gaps between the members were filled with the same material as that used for the underground beam, and then they were welded together to ensure the alignment of the steel pipe centres and to maintain a welding thickness at least equal to that of the base steel plate. As a safety precaution in the experiment, the lower end of each pile was welded to the base steel plate, which was then bolted to the bottom of the soil tank. Therefore, the tip of each pile was completely fixed.

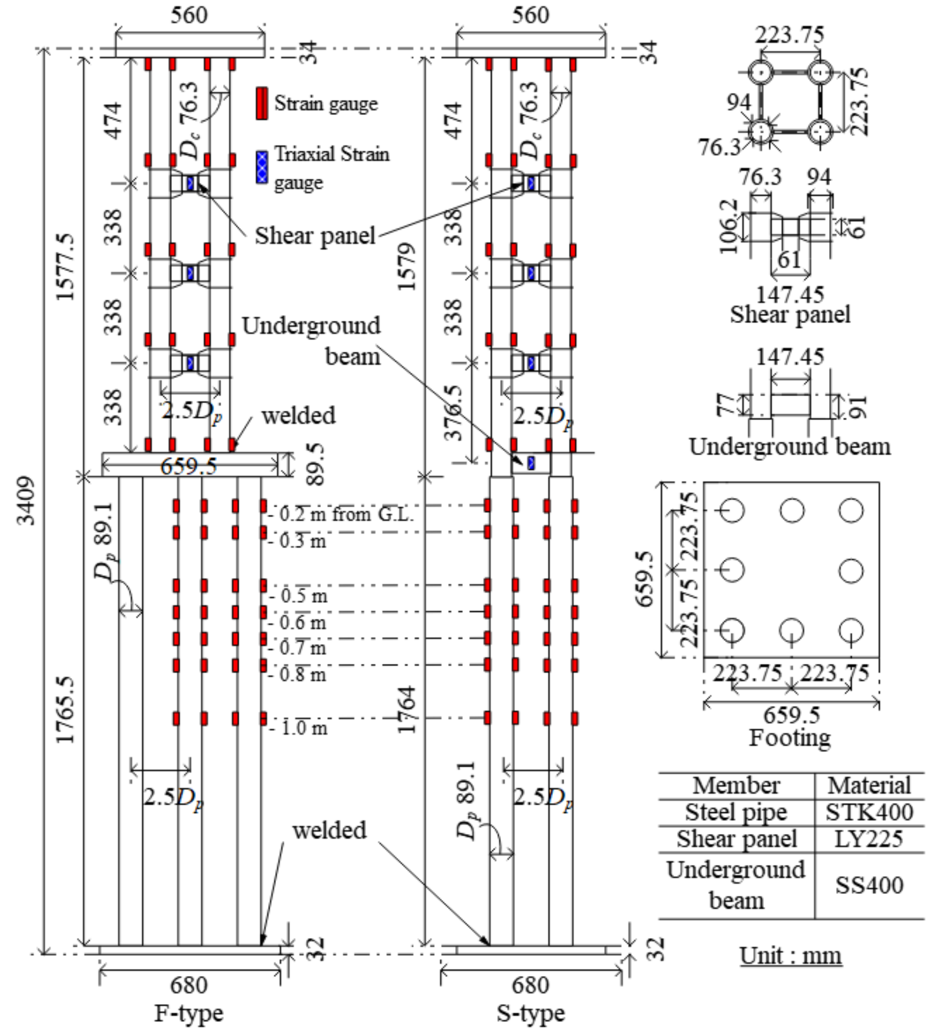

Member	Material
Steel pipe	STK400
Shear panel	LY225
Underground beam	SS400

Figure 12. Specimens and the locations of the strain gauges in the experiment (After Isobe et al., 2016)

To emulate the superstructure, a weight of 52.6 kN, having dimensions of 1586 mm x 1586 mm x 265 mm, was bolted to the upper part of each model ground (see Fig. 13). The F-type model had a steel block footing with a weight of 2.2 kN and dimensions of 659.5 mm x 659.5 mm x 89.5 mm. It was welded to the pier columns and foundation piles. The properties of the structural materials used for the specimens are shown in Table 1. It should be noted that the combined weight of the superstructure and footing does not conform to the similarity rule due to limitations in the shaking table's vibration capacity and the requirement to maintain a semi-infinite pile length. For this reason, its susceptibility to resonance has been thoroughly assessed in Section 4.2.

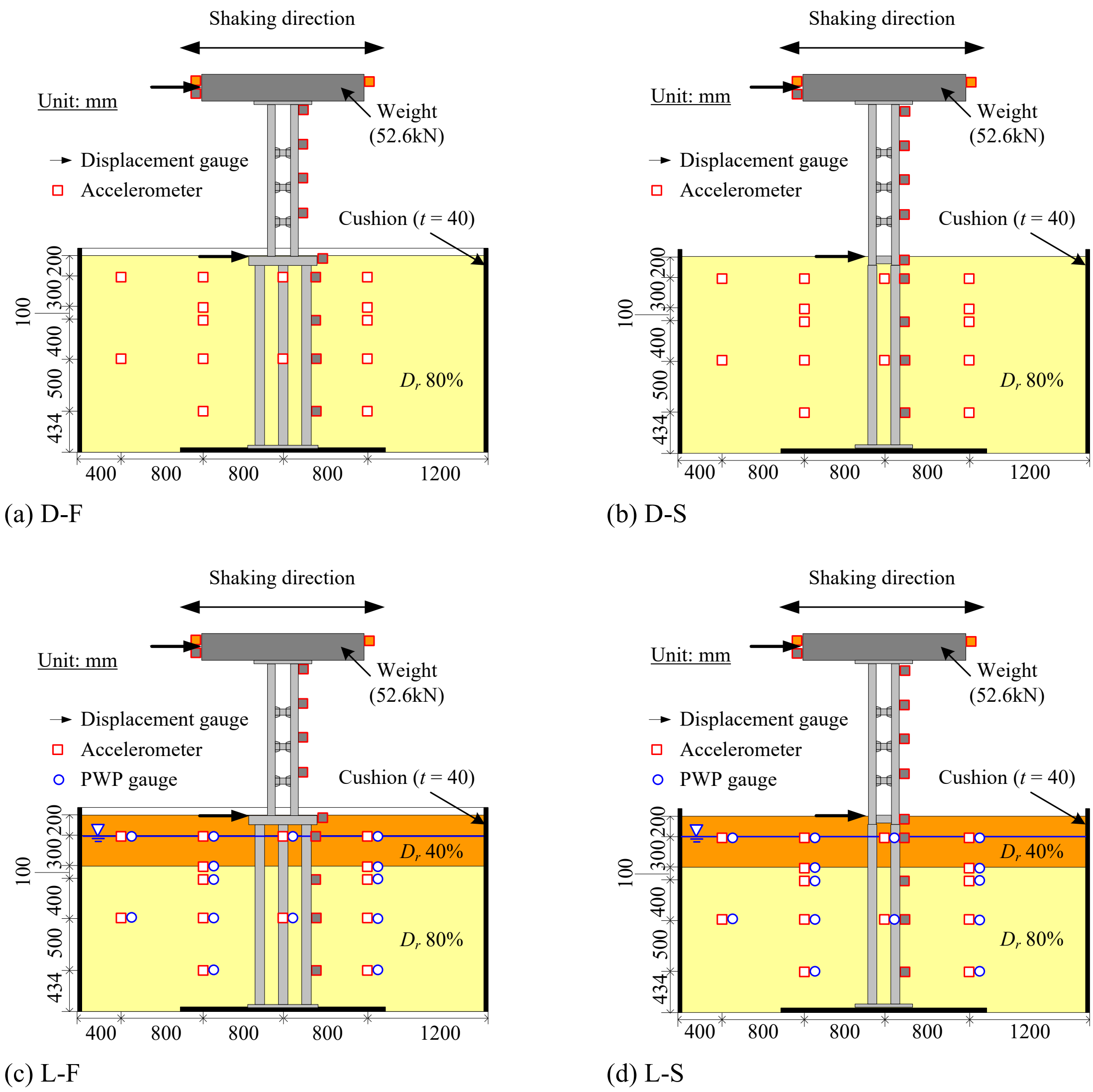

Figure 13. Model grounds along with measurement devices and their locations (After Isobe et al., 2016)

Table 1. Properties of the structural materials

Part	Standard	Size [mm]	Thickness [mm]	Yield stress [N/mm^2]
Pier (Column)	STK400	ϕ 76.3	2.8	406
Pile	STK400	ϕ 89.1	2.8	404
Shear panel	LY225	61 × 61	1.1	236
Underground beam	SS400	77 × 147	1.6	345

3.2.2 Model grounds

Each model ground used in the experiment was prepared in a rigid soil tank that was 4.0 m in length, 1.0 m in width, and 2.0 m in depth. Two types of soil grounds were prepared: dry sand (abbreviated as D) and liquefiable sand (abbreviated as L). Fig. 13 shows the different ground conditions for the F- and S-type models embedded in the D- and L-grounds set in separate soil tanks.

The L-ground was prepared using air and water pluviation methods. Dry sand, with a relative density

(Dr) of 80%, was poured into the tank to a height of 1434 mm, followed by the injection of water to raise the level to a height of 1734 mm and to create a liquefiable soil layer with a relative density of 40% using water pluviation. In addition, a 200-mm-thick layer of dry topsoil was created by air pluviation to prevent spillage of the liquifiable soil. The D-ground, with a relative density of 80%, was prepared similarly as one layer using air pluviation. The ground surface was set at a height of 1934 mm from the bottom plate for both the L- and D-grounds, aligning it with the upper surface of the footing in the F-type model and the underground beam in the S-type model. The sand was Tohoku silica sand #6 (soil grain density G_s: 2.63 Mg/m^3, maximum void ratio e_{max}: 0.878, minimum void ratio e_{min}: 0.551, and average grain diameter D_{50}: 0.34 mm).

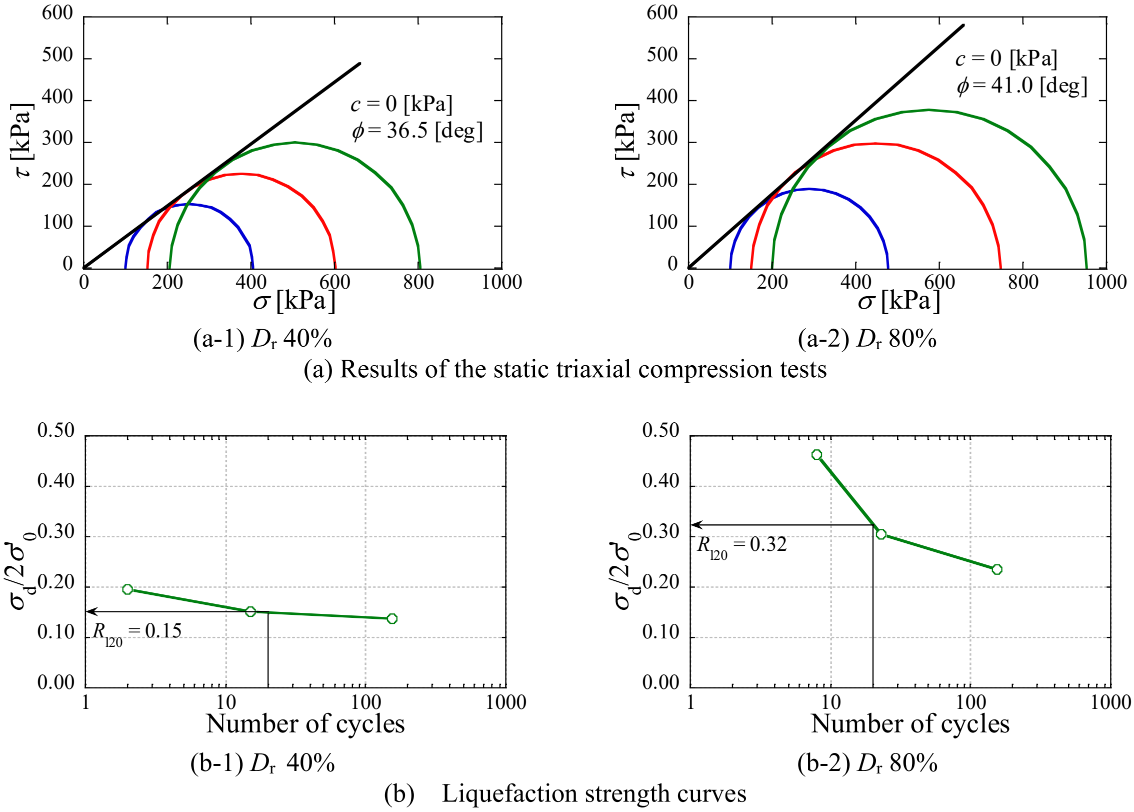

Figure 14. Results of the static and cyclic triaxial compression tests performed on the model ground specimens (After Isobe et al., 2016)

Fig. 14 shows the results of the static and cyclic triaxial compression tests performed on specimens prepared with the same relative density as that for the model grounds. From the figure, it is seen that the shear resistance angles are 36.5° (*Dr* 40%) and 41.0° (*Dr* 80%). The liquefaction strength curve values are 0.15 (*Dr* 40%) and 0.32 (*Dr* 80%) following the JGS standards which define the liquefaction strength ratio as the stress ratio for 20 cycles of loading based on Ishihara et al. (1992) and Matsuo et al. (2000).

A 40-mm-thick rubber sheet (Young's modulus *E*: 0.05 GPa, Poisson's ratio □□: 0.49, and density □□: 0.07 Mg /cm^3) was installed on the surfaces of the soil tank to mitigate the influence of the rigid soil tank (Beziar et al., 2018; Lombardi et al., 2015).

3.2.3 Excitation conditions

Table 2 provides details of the experimental cases, each conducted in a separate rigid soil tank. Two tanks were simultaneously vibrated longitudinally, one with the S-type model and the other with the F-type model embedded in the D-ground. Later, both the F-type and S-type models were simultaneously excited in the L-ground using the Public Works Research Institute's three-dimensional large shaking table.

Table 2. Experimental cases

	Footing type (F-type)	Footingless type (S-type)
Dry sand (D-ground)	D-F	D-S
Liquefiable sand (L-ground)	L-F	L-S

Table 3. Excitation procedure

Type of ground	Excitation step	Maximum input acceleration [m/s^2]	
		Target value	Measured value
Dry sand	1st	0.5	0.62
	2nd	1.0	0.94
	3rd	1.5	1.45
	4th	2.0	2.01
	5th	2.5	2.47
	6th	3.0	3.07
	7th	3.5	3.63
	8th	5.0	5.25
Liquefiable sand	1st	2.0	1.92

The input wave was a tapered sine wave applied for 10 seconds with a cycle of 0.5 seconds (frequency: 2 Hz). The input acceleration was increased in increments of 0.5 m/s^2 from 0.5 to 5 m/s^2 for the D-ground models. For the L-ground models, acceleration was applied once at 2.0 m/s^2. The input steps of the excitation procedure are detailed in Table 3. As shown in Figs. 12 and 13, the measurement include the strain, acceleration, displacement of structural elements, and the pore water pressure of the ground.

3.3 OUTLINE OF THE NUMERICAL ANALYSIS METHOD

In this study, we performed numerical analyses based on the infinitesimal deformation theory using the soil-water coupled three-dimensional elastoplastic dynamic finite element analysis (FEM) program named DBLEAVES (Ye et al., 2007) for the above-mentioned shaking table test experiment.

3.3.1 Modelling the structures and grounds

In the analysis, the model elements and structures were created based on the results of the previous research by Isobe et al. (2010). The steel pipe columns and underground beam were modelled as a bilinear beam element. The shear panels were modelled as bilinear beam elements with three bilinear spring elements attached at the centre of the beam elements in the x, y, and z directions. Simple diagrams of the modelling are provided in Fig. 15(a).

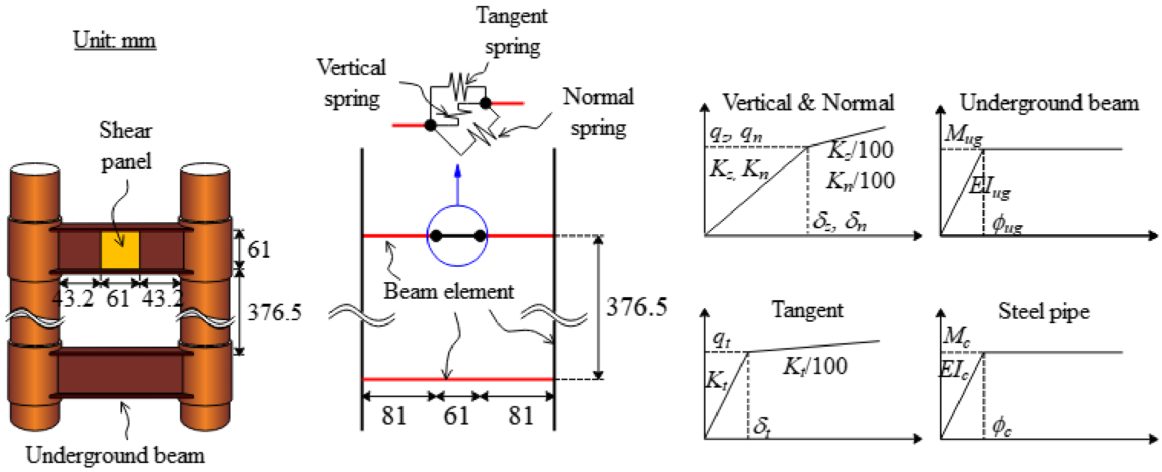

(a) Modelling of the bridge pier consisting of multiple steel pipes

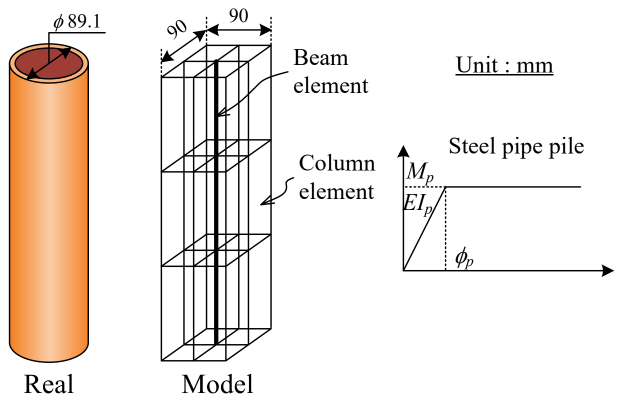

(b) Modelling of a steel pipe pile (Hybrid element)

Figure 15. Modelling of the bridge pier consisting of multiple steel pipes and steel pipe piles

The hybrid element proposed by Zhang et al. (2000), Zhang and Kimura (2002), and Zhang et al. (2007) was employed to model each steel pipe pile, as shown in Fig. 15(b). It compensates for the weakness of the beam elements, having no volume, in simulating the interaction between the ground and the piles. When using hybrid elements, it is important to determine the shares of Young's modulus for the beam and column elements. The share of flexural rigidity (*EI*) is determined as 90% for the beam elements and 10% for the column elements, based on Zhang et al. (2000), after considering the deformation characteristics of the piles and the relative rigidity between the column elements of the piles and the ground. Additionally, considering the volume of the column elements, the densities of the beam and column elements were adjusted so as to be equivalent to the mass of the piles. The parameters of the bridge pier specimens, comprising multiple steel pipes and steel pipe piles, are shown in Table 4.

Table 4. Parameters of the bridge pier specimens

(a) Bridge pier consisting of multiple steel pipes (non-linear beam element and non-linear spring element)

Model	Item	Properties
Bilinear beam element	Cross-sectional rigidity [kN]	1.29×10^5
	Flexural rigidity [kN*m^2]	8.74×10^1
	Fully plastic moment [kN*m]	6.13
	Damping constant	0.01
	Density [Mg/m^3]	7.87
Bilinear spring element	Vertical/Normal direction spring constant [kN/m]	7.22×10^4
	Vertical/Normal direction yield displacement [m]	1.16×10^{-4}
	Tangent direction spring constant [kN/m]	3.02×10^5
	Tangent direction yield displacement [m]	4.27×10^{-5}

(b) Piles (hybrid elements)

Model	Item	Properties
Bilinear beam element	Cross-sectional rigidity [kN]	1.52×10^5
	Flexural rigidity [kN*m^2]	1.27×10^2
	Fully plastic moment [kN*m]	8.41
	Damping constant	0.01
	Density [Mg/m^3]	0.69
Column element	Cross-sectional rigidity [kN]	2.18×10^{-2}
	Flexural rigidity [kN*m^2]	1.41×10^1
	Poisson's ratio	0.30
	Damping constant	0.01
	Density [Mg/m^3]	0.69

The Cyclic Mobility model developed by Zhang et al. (2007), which incorporates the concepts of subloading and superloading as described by Hashiguchi and Ueno (1977) and Asaoka et al. (2000), was used as the constitutive model. Notable features of this model are: a yield surface with a fixed C.S.L in the yield space (**Eq. (1)**), incorporation of stress-induced anisotropy and its evolution rule (**Eq. (2)**), an evolution rule for overconsolidation (**Eq. (3)**) influenced by the stress-induced anisotropy, and the evolution rule for the structure (**Eq. (4)**). Moreover, it employs the associated flow rule for simplicity (**Eq. (8)**). **Fig. 6** gives a conceptual diagram of the Cyclic Mobility Model, while Table 5 details the soil parameters used in the analysis.

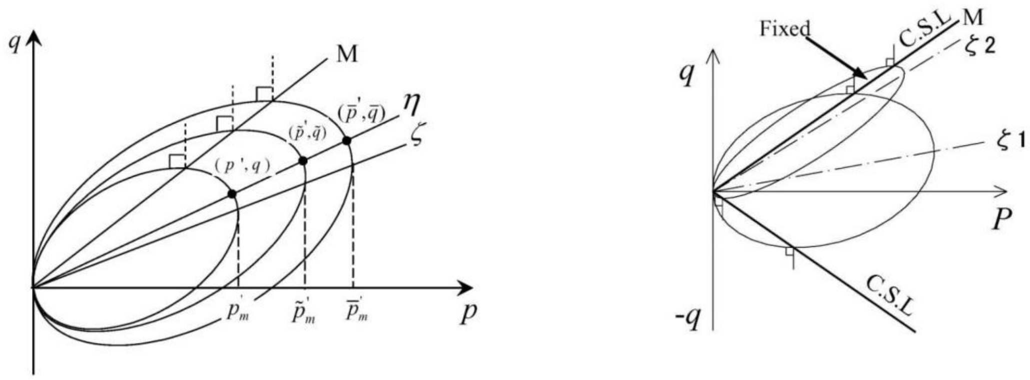

Figure 16. Conceptual diagram of the Cyclic Mobility Model (After Zhang et al., 2007)

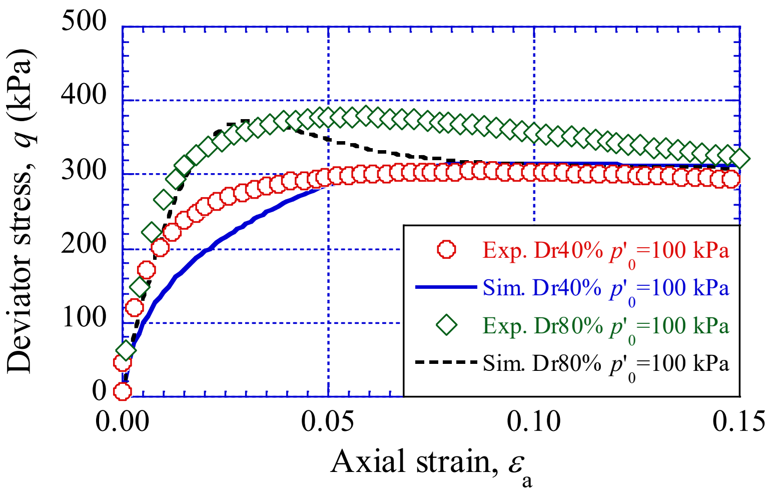

Figure 17. Results of the drained static triaxial tests and simulation

In determining the ground parameters, the above-mentioned static and cyclic triaxial test results, namely, the stress ratio in the critical state, R_f, compression index λ, swelling index κ, and void ratio N at the reference pressure (p = 98 kPa), are derived from the isotropic consolidation test results. Additional parameters were determined through a simulation of the triaxial consolidation tests, as shown in Fig. 17.

In the shaking table tests, the influence of the smaller confining pressure than that in the triaxial tests was adjusted by changing the initial overconsolidation ratio to $1/R_0$.

$$f = MD\ln\frac{p'}{p'_0} + MD\ln\frac{M^2-\zeta^2+\eta^{*2}}{M^2-\zeta^2} + MD\ln R^* - MD\ln R - \int_0^t J\mathrm{tr}\boldsymbol{D}^p d\tau = 0 \tag{1}$$

$$\dot{\boldsymbol{\beta}} = \lambda\frac{JM\sqrt{6}b_r(b_l\mathrm{M}-\zeta)\hat{\boldsymbol{\eta}}}{(M^2-\zeta^2+\eta^{*2})p'} \tag{2}$$

$$\begin{aligned}\dot{R} &= -J\frac{m}{D}\left\{\frac{(p'/p'_0)^2}{(p'/p'_0)^2+1}\right\}\ln R\,\|\boldsymbol{D}^p\| + \frac{R}{MD}\frac{\eta}{M}\frac{\partial f}{\partial\boldsymbol{\beta}}\cdot\dot{\boldsymbol{\beta}} \\ &= d\lambda\frac{-mJM\ln R\sqrt{6\eta^{*2}+\frac{1}{3}(M^2-\zeta^2)^2}}{(M^2-\zeta^2+\eta^{*2})p'}\left\{\frac{(p'/p'_0)^2}{(p'/p'_0)^2+1}\right\} + \frac{R}{MD}\frac{\eta}{M}\frac{\partial f}{\partial\boldsymbol{\beta}}\cdot\dot{\boldsymbol{\beta}}\end{aligned} \tag{3}$$

$$\dot{R^*} = J\frac{a}{\mathrm{D}}R^*(1-R^*)\sqrt{\frac{2}{3}}\|\boldsymbol{D}_s^p\| = \lambda\frac{2JMaR^*(1-R^*)\eta^*}{(M^2-\zeta^2+\eta^{*2})p'} \tag{4}$$

where a is the degradation parameter of the structure, which controls the collapse rate of the structure, m is the degradation parameter of the over-consolidation state controlling the rate of the loss of over-consolidation, b_r is an evolution parameter of anisotropy used to control the developing rate of stress-induced anisotropy when the soil is subjected to shearing or compression, and b_l is a limitation parameter used to avoid the singularity in **Eq. (1)** at the point $\zeta = M$; 0.95 is used for the value of b_l throughout this paper.

Table 5. Soil parameters (Cyclic mobility model)

Item		D_r 80%	D_r 40 %
Compression index	λ	0.028	
Swelling index	κ	0.005	
Stress ratio in the critical state	M	3.92	
Poisson's ratio	v	0.30	
Void ratio at 98 kPa	N	0.66	
Overconsolidation parameter	m	0.31	
Soil structural parameter	a or m*	0.65	
Anisotropic parameter	b_r	0.10	
Initial void ratio	e_0	0.63	0.76
Initial soil structural ratio	R^*_0	0.80	
Initial overconsolidation ratio at 9.8 kPa	$1/R_0$	73.4	1.00
Inherent anisotropy	ζ_0	0.30	
Damping constant	h	0.04	
Dry (in water) weight per unit volume [kN/m^3]	γ_d (γ')	15.8 (10.2)	- (9.50)

The other variables included in **Eqs. (1)** through **(4)** are defined as follows:

$$\eta^* = \sqrt{\tfrac{3}{2}\hat{\boldsymbol{\eta}}\cdot\hat{\boldsymbol{\eta}}}, \hat{\boldsymbol{\eta}} = \boldsymbol{\eta} - \boldsymbol{\beta}, \boldsymbol{\eta} = \tfrac{\boldsymbol{S}}{p'}, \boldsymbol{S} = \boldsymbol{T}' + p'\boldsymbol{I}, p' = -\tfrac{1}{3}\mathrm{tr}\boldsymbol{T}', \zeta = \sqrt{\tfrac{3}{2}\boldsymbol{\beta}\cdot\boldsymbol{\beta}}, \eta = \sqrt{\tfrac{3}{2}\boldsymbol{\eta}\cdot\boldsymbol{\eta}} \tag{5}$$

where $\boldsymbol{S}$ is the deviatoric stress tensor, $\boldsymbol{\beta}$ is the anisotropic stress tensor, and $\boldsymbol{T'}$ is the Cauchy effective stress tensor. J is the Jacobian determination of deformation gradient tensor $\boldsymbol{F}$, and D is the dilatancy parameter which can be expressed by λ and κ, as follows:

$$D = \frac{\lambda - \kappa}{M(1 + e_0)} \tag{6}$$

$\boldsymbol{D}^p$ denotes the plastic component of stretching $\boldsymbol{D}$ which is assumed to be positive in tension; it is related to the plastic volumetric strain rate.

$$\varepsilon_v^p = -\int_0^t J\mathrm{tr}\boldsymbol{D}^p\, d\tau \tag{7}$$

The following associated flow rule is employed in the model:

$$\boldsymbol{D}^p = d\lambda \frac{\partial f}{\partial \boldsymbol{T}'} \tag{8}$$

The consistency equation for the subloading yield surface can then be given as

$$\frac{\partial f}{\partial \boldsymbol{T}'}\cdot\dot{\boldsymbol{T}}' + \frac{\partial f}{\partial \boldsymbol{\beta}}\cdot\dot{\boldsymbol{\beta}} + MD\frac{\dot{R}^*}{R^*} - MD\frac{\dot{R}}{R} - J\mathrm{tr}\boldsymbol{D}^p = 0 \tag{9}$$

3.3.2 Analysis conditions

The analysis domain was set as the half-sectional domain shown in Fig. 18 in consideration of the symmetry of the structures and the loads used in the tests. The number of nodes was 15423, and the number of elements was 13464. For the boundary conditions, the nodes on the bottom surface were fixed in all directions, while the side surfaces were supported by rollers in the vertical direction. The cushioning material, installed to diminish the influence of the boundaries, was modelled as a solid element. The influence of the cushioning material will be discussed in the Appendix.

The analysis utilized a proportional type of initial stiffness for the viscous damping model. Natural frequencies for the D-F and D-S types were calculated using the waveforms at the pier top during the free vibration time using the Ricker wavelet (Ricker, 1945), which has a minute acceleration amplitude. The damping constants of the ground and the structure were set to 4% and 1%, respectively. Under these analysis conditions, the natural frequencies were calculated as 2.78 Hz for D-F and 1.86 Hz for D-S, which roughly agree with the experimental values of 2.70 Hz for D-F and 1.84 Hz for D-S. Similarly, a

Ricker wavelet analysis was performed using dry soil only in the soil box. The soil surface response measured at the centre of the soil box indicated a natural frequency of 8 Hz for the soil. The time increment in the analysis was 0.005 seconds, and the Newmark-□□method was used for the time integration.

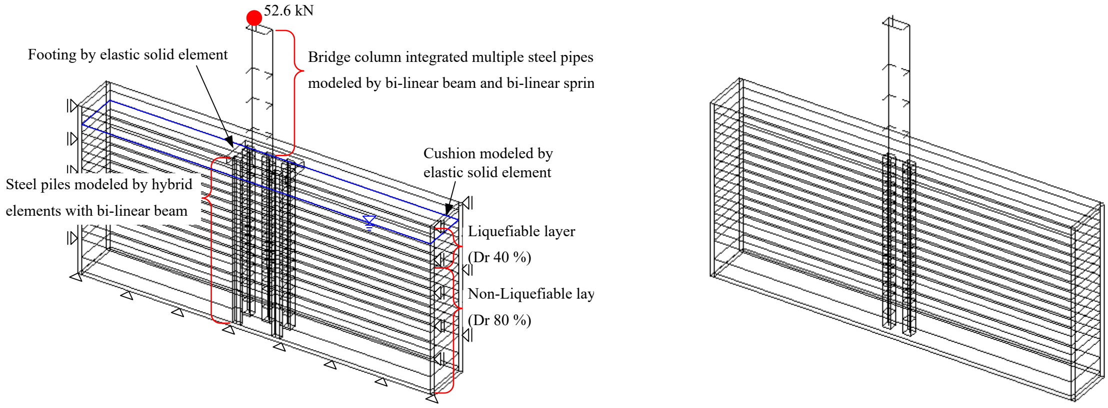

(a) Footing type (L-F)   (b) Footingless type

Figure 18. Analysis mesh used in the reproduction analysis

The dead load of the superstructure was simply modelled as a mass point of 5.36 x 10^3 kg (to be exact, it was 2.68 x 10^3 kg because of the half-sectional domain). The differences in the superstructure inertial force and pile bending moment between a point mass modelling and a solid mass modelling are almost negligible, as will be shown in the Appendix for both the F- and S-type structures.

3.3.3 Analysis cases

3.3.3.1 Cyclic loading

(a) Reproduction analysis

We conducted a reproduction analysis through a numerical simulation of the shaking table tests to assess the seismic performance of a bridge pier constructed using F- and S-type foundations. The selected cases for the numerical simulation included the first to fourth and eighth input excitations on a dry sand ground, as well as the first input excitation on a liquefiable ground. Throughout the simulation, we varied only the amplitude of the input cyclic wave for numerical stability, and did not consider the influence of the previous motions on the stress and strain histories. However, the findings presented in Section 4.1 confirm that the influence of the previous motions on the stress and strain histories was minimal compared to the impact of the variations in amplitude.

(b) Parametric study

In the parametric study, we adjusted the input frequency from 0.1 Hz to 10 Hz, and the acceleration amplitude from 0.5 m/s² to 5.0 m/s². These adjustments were made to ensure that the shear panels experienced plastic deformation during the ground motion.

3.3.3.2 Seismic loading

Additionally, we employed Level-2 input seismic motion as specified in the Guidelines for Seismic Design of Cut and Cover Tunnels published by Hanshin Expressway Co., Ltd. The amplitude and time axis of the waves recorded at a depth of 83 meters beneath Port Island during the Hyogo-ken Nanbu Earthquake were adjusted to match the scale of the model tests. This waveform encompasses a range in frequencies with predominant components close to 2 Hz and a maximum acceleration magnitude of 6.0 m/s². However, as the model does not perfectly satisfy the similarity law of weight and the associated natural frequency (Isobe et al., 2016), the time axis was further adjusted in various cases to ensure that the dominant frequency of the irregular waves would ccomprehensively cover the natural frequencies of both structure types. This loading simulation was carried out for both types of structures, namely, those with footings and those without footings, under dry sand conditions, using the same Finite Element Method (FEM) model as in the previously mentioned simulations.

3.3.3.3 Static loading

In the static loading analysis, a pushover analysis was conducted to assess the structure's response. In other words, a horizontal force equivalent to the inertial force was applied statically at the pier top for both D-F and D-S structures, employing the same FE model as that utilized in the preceding simulations.

3.4 RESULTS OF REPRODUCTION ANALYSIS AND DISCUSSION

3.4.1 Dry sand ground cases

Fig. 19 depicts the relationship between the inertial force and the lateral displacement at the pier top under dry sand conditions, considering various sets of input excitations ranging from the first to the fourth and the eighth input accelerations. The figure showcases both the experimental and simulated outcomes for the D-F and D-S structures. However, as a precautionary measure, the tests for D-F were halted due to excessive strain observed at the pier base during the third input excitation. Consequently, the response of D-F to the remaining excitations was derived through the numerical simulations only.

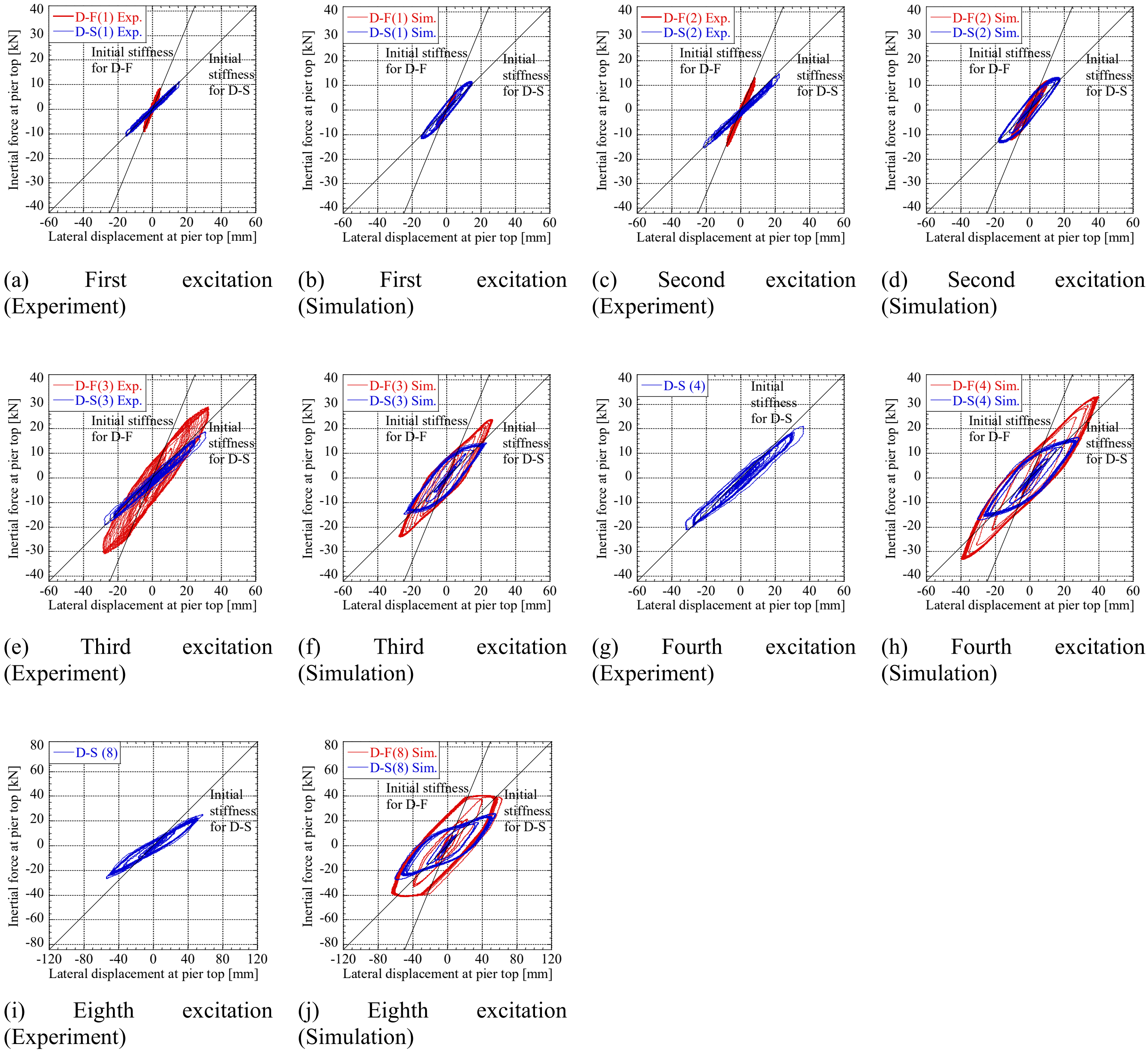

(a) First excitation (Experiment)

(b) First excitation (Simulation)

(c) Second excitation (Experiment)

(d) Second excitation (Simulation)

(e) Third excitation (Experiment)

(f) Third excitation (Simulation)

(g) Fourth excitation (Experiment)

(h) Fourth excitation (Simulation)

(i) Eighth excitation (Experiment)

(j) Eighth excitation (Simulation)

Figure 19. Comparison of the experimental and simulation results for the relationship between the inertial force and the lateral displacement at the pier top

The inertial force was calculated as the product of the response acceleration observed at the pier top and the mass corresponding to the weight of the superstructure. The comparison in the figure between the experimental and the numerical simulation results indicates that the numerical simulations tended to underestimate both the inertial force and the lateral displacement at the pier top. Specifically, in the case of D-F, only the initial stiffness was marginally underestimated, while in the case of D-S, both the initial stiffness and the hysteresis loop were slightly overestimated. This overestimation may be attributed to simplifications made in the model, such as representing the superstructure weight as a point mass, modelling piles as hybrid members, and treating shear panels as springs. Although the differences caused by these individual simplifications are minor, their combined effect might explain the quantitative discrepancies observed in the numerical simulation results. Despite these discrepancies, the peak values for the inertial force and pier top displacement are nearly perfectly simulated from the first to the eighth steps.

Based on these findings, Fig. 20 presents skeleton curves illustrating the relationship between the maximum inertial force and the lateral displacement at the pier top. The skeleton curves obtained from the experiment are seen to have been effectively reproduced through the reproduction simulation and static pushover analysis. The results indicate that the inertial force and pier top displacement in D-F gradually increase until the second excitation input, and then exhibit exponential growth thereafter. In the third step, these response values for D-F exceed those for D-S, and continue to do so in subsequent steps. Although no experimental results for D-F were available for comparison after the third acceleration input, the simulation results indicate that the inertial force reaches a plateau at approximately 36 kN, and that the displacement increases sharply, consistent with the pushover analysis results. In the case of D-S, the skeleton curve is almost accurately reproduced, and the increments in the inertial force and pier top displacement are gradual until the eighth step. The suppression of the decrease in rigidity in D-S is also reproduced in the 4th and subsequent steps.

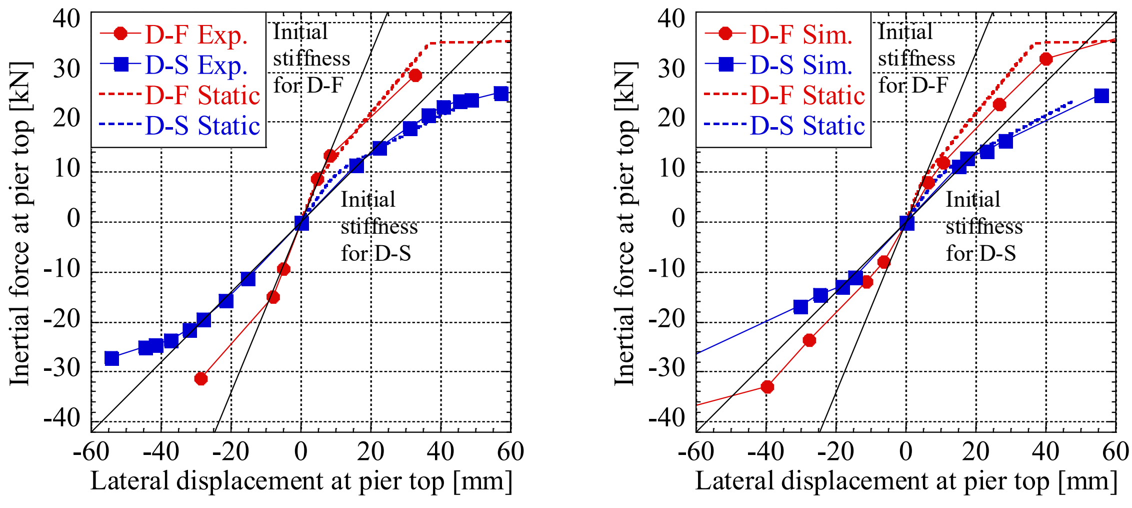

(a) Experiment and static simulation results (b) Cyclic and static simulation results

Figure 20. Comparison of the experimental and simulation results for the relationship between the maximum inertia force and the maximum lateral displacement at the pier top

Fig. 21 illustrates the relationship between the inertial force at the pier top and the shear strain of the upper shear panel. Despite a tendency for the analysis results to overestimate the shear strain in both structures as the excitation input increases, the behaviour of each structure is qualitatively reproduced with sufficient accuracy for understanding the mechanism. In the first and second steps, D-S generates a larger shear strain than D-F, consistent with the observations in Figs. 19 and 20. Only D-S exceeds the yield strain in the first step, while D-F exceeds the yield strain after the second step. Subsequently, D-F exhibits larger shear strain than D-S in the third step. These findings highlight a strong correlation between the yielding of the shear panels and the response of the pier top. In D-F, the stiffness of the entire structure decreased significantly after the yielding of the shear panels, leading to a sharp increase in the inertial force and lateral displacement of the pier top. In contrast, in D-S, the decrease in stiffness of the entire structure, due to the yielding of the shear panels, was relatively small compared to that of D-F.

To strengthen our understanding, a numerical simulation is performed with shear panels modelled as perfectly elastic springs and compared against an elastoplastic panel case for D-F and D-S under the third excitation step. Figs. 22(a) and (b) show that, in the case of perfectly elastic springs, the lateral displacement and inertial force at the pier top are significantly decreased. This is because the shear panels just reach their yield strain and do not perform their intended role as an energy dissipator, whereas the lateral displacement at the pier top undergoes drastic amplification after the plastic deformation of the shear panels. This suggests that excessive deformation of the shear panels could modify the flexural stiffness along the pier columns, potentially lowering the structure's natural frequency to closer to 2 Hz and amplifying its response. In the case of D-S, an opposite trend is observed. By modelling the shear panels as perfectly elastic springs, the lateral displacement and inertia force at the pier top are increased significantly. A contrasting consequence is shown for the shear panels just reaching their yield strain and not performing their intended role as an energy dissipator. This leads to the finding that the plasticization of the shear panels becomes beneficial as it brings the natural frequency of the structure away from the input motion frequency in the given case. This indicates that the relationship between excitation frequency and structure frequency plays a key role in determining the response of a structure. A comparison of the rest of the response variables is provided in Table 6.

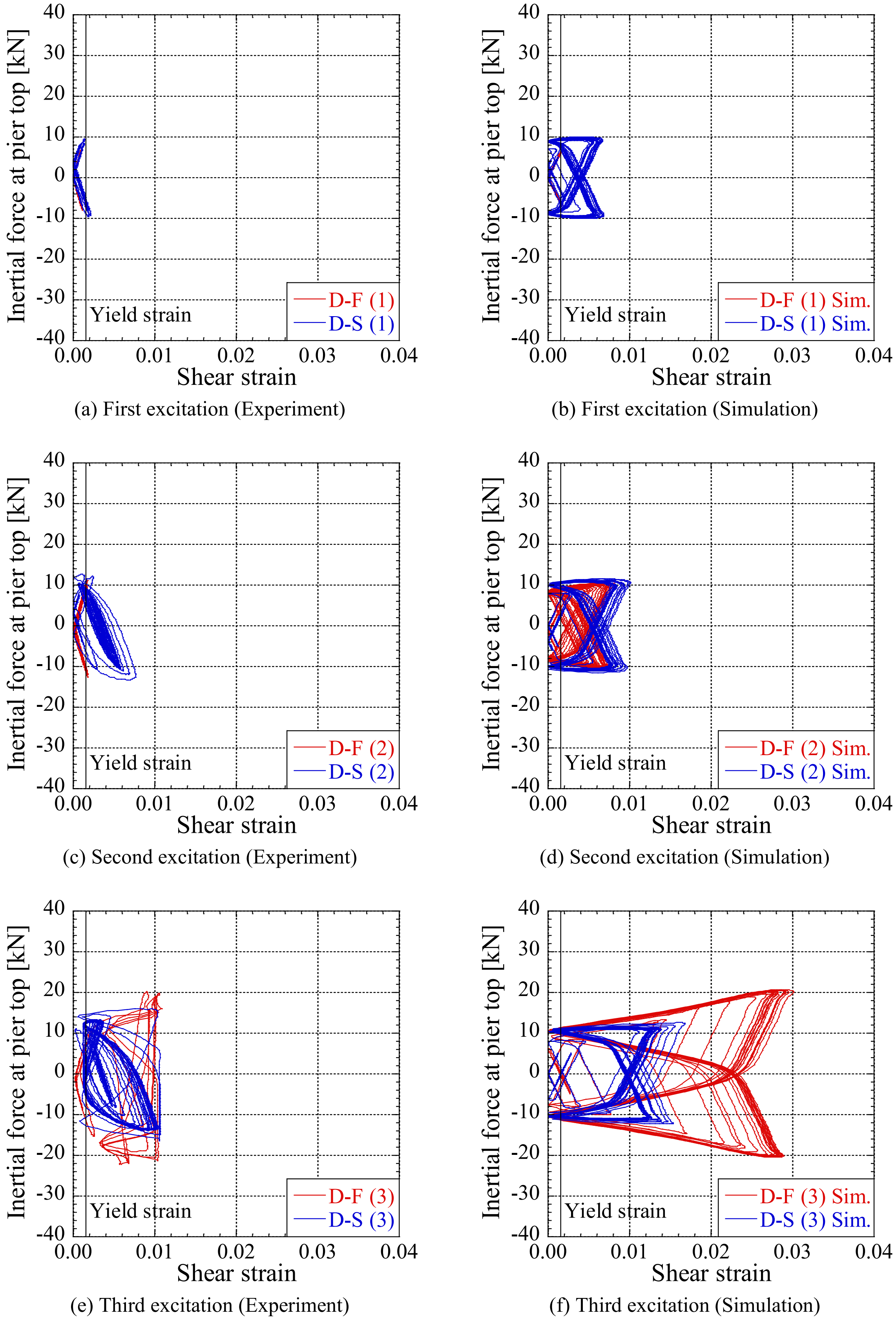

(a) First excitation (Experiment)
(b) First excitation (Simulation)
(c) Second excitation (Experiment)
(d) Second excitation (Simulation)
(e) Third excitation (Experiment)
(f) Third excitation (Simulation)

Figure 21. Relationship between the inertial force at the pier top and the shear strain in the upper shear panel

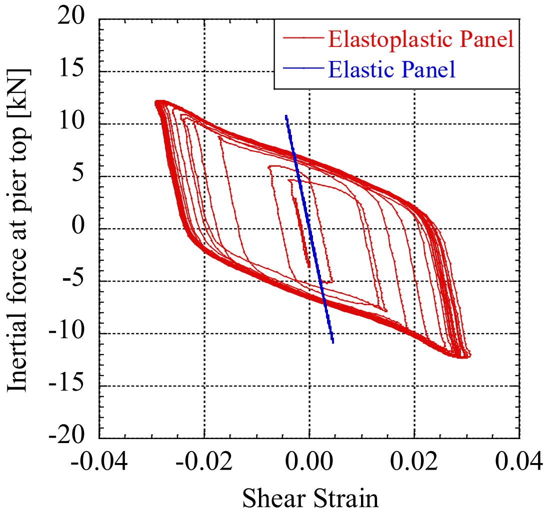

(a) Inertia force vs shear strain for D-F (3)

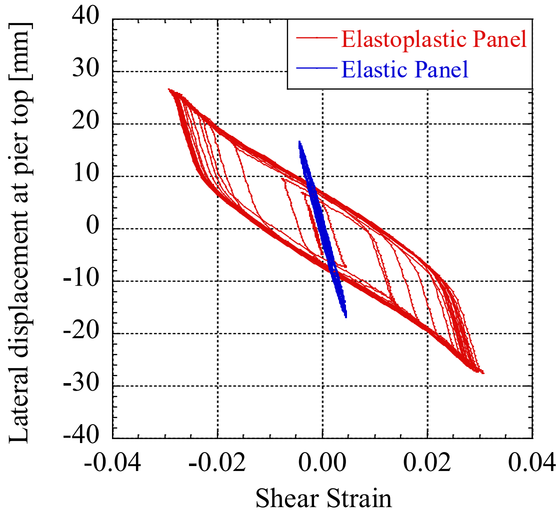

(b) Lateral displacement at pier top vs shear strain for D-F (3)

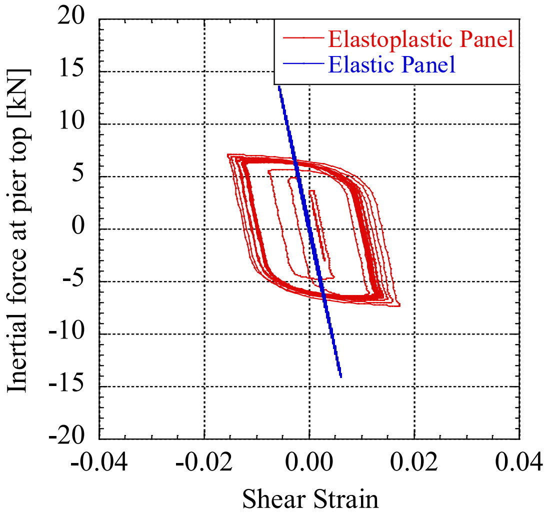

(c) Inertia force vs shear strain for D-S (3)

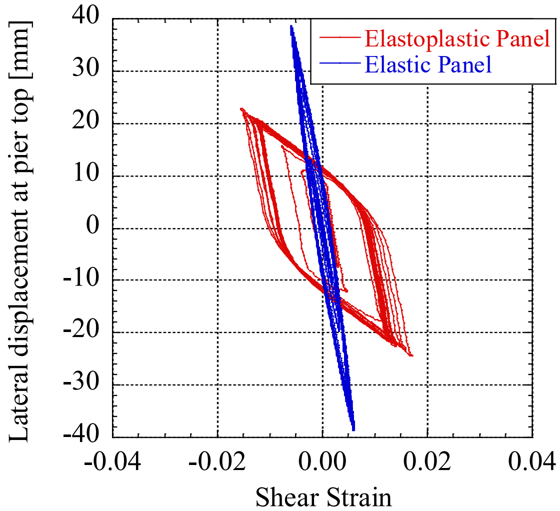

(d) Lateral displacement at pier top vs shear strain for D-S (3)

Figure 22. Responses of the superstructure against shear strain for elastoplastic (EP) and elastic shear panels (E) under the third excitation step

Table 6. Comparison of the response parameters for the F- and S-type structures under elastic and elastoplastic shear panels corresponding to the third excitation step

Structure type (Shear panel modelling)	A_{PT} [m/s^2]	Mc [kN*m]	D_{PT} [mm]	S	A_{PH} [m/s^2]	M_P [kN*m]	D_{PH} [mm]	Q [kN]
D-F (EP)	4.56	2.86	27.5	0.0306	3.44	0.90	8.75	5.27
D-F (E)	3.99	1.12	16.8	0.0045	2.72	0.86	8.32	5.12
D-S (EP)	2.79	1.02	24.5	0.0171	2.54	0.97	9.04	3.54
D-S (E)	5.38	1.58	38.7	0.0060	3.17	1.44	19.6	6.82

A_{PT}: pier top acceleration, Mc: pier base moment, D_{PT}: pier top displacement, S: shear strain of the upper panel, A_{PH}: pile head acceleration, M_P: pile head moment, D_{PH}: pile head displacement, and Q: pile head shear force

Focussing on the response characteristics and deformation mechanism of the structure and the ground, the third excitation results were selected, as the magnitude and nature of the relationship between the maximum pier top acceleration and the lateral acceleration is contrary to the first and second excitation cases.

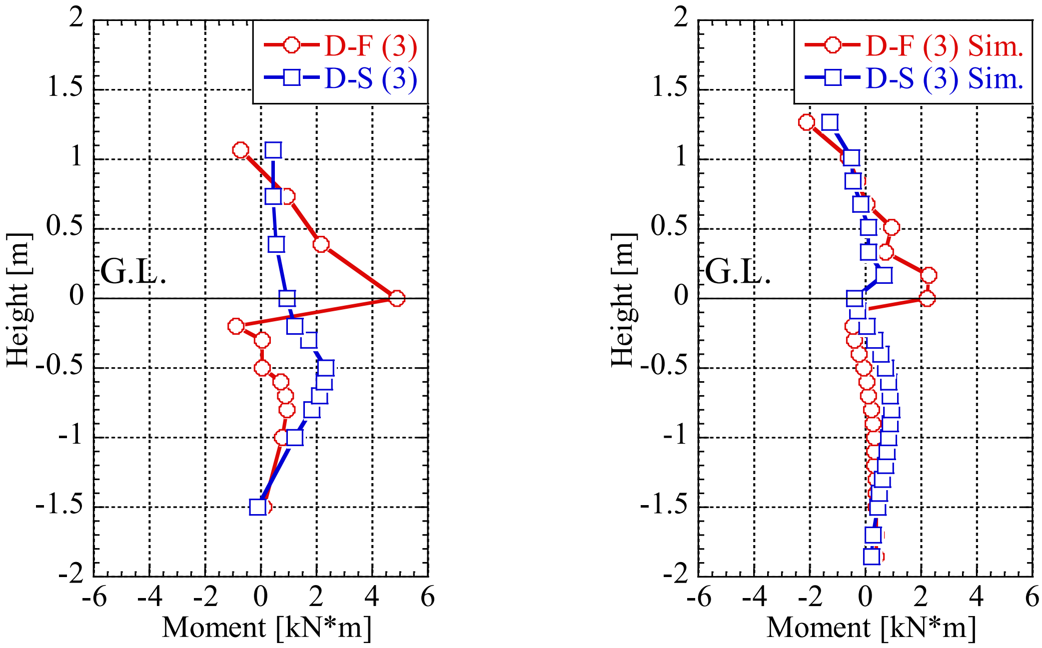

(a) Third input (Experiment) (b) Third input (Simulation)

Figure 23. Distributions of the bending moments generated in the piles and pier when the maximum lateral displacement occurs at the pier top

Figs. 23 and 24 illustrate the longitudinal distributions of the bending moments and lateral displacement of the piles and the pier, respectively, at the point when the maximum lateral displacement occurs at the top of the pier. The lateral displacement of the piles and the pier is derived through a second-order integration of the values measured using accelerometers installed on both the piles and the pier, as depicted in Fig. 13. The bending moments of the piles are computed using strain gauges installed along their lengths. In Fig. 23, the trends in the bending moments at both the column base and the piles were effectively reproduced. D-F exhibits a greater bending moment at the column base, while D-S demonstrates a greater bending moment at the piles. Moreover, the bending moments at the pile tips tend to converge.

Fig. 24 demonstrates that the analysis satisfactorily captures the trends in displacement and shear deformation of both structures. The F-type exhibits a greater displacement at the pier top and tends to show increased shear deformation at the pier, whereas the S-type exhibits similar pile head displacement to the F-type, probably due to the slight overestimation of the stiffness in the simulation. The behaviour of the pier and the piles align with the characteristics of the shear panels discussed earlier. The reduced pile head deflection in D-F may be attributed to the variance in foundation stiffness, where a group of eight piles and pile caps possesses greater stiffness than the 2 x 2 piles directly connected to the columns in D-S.

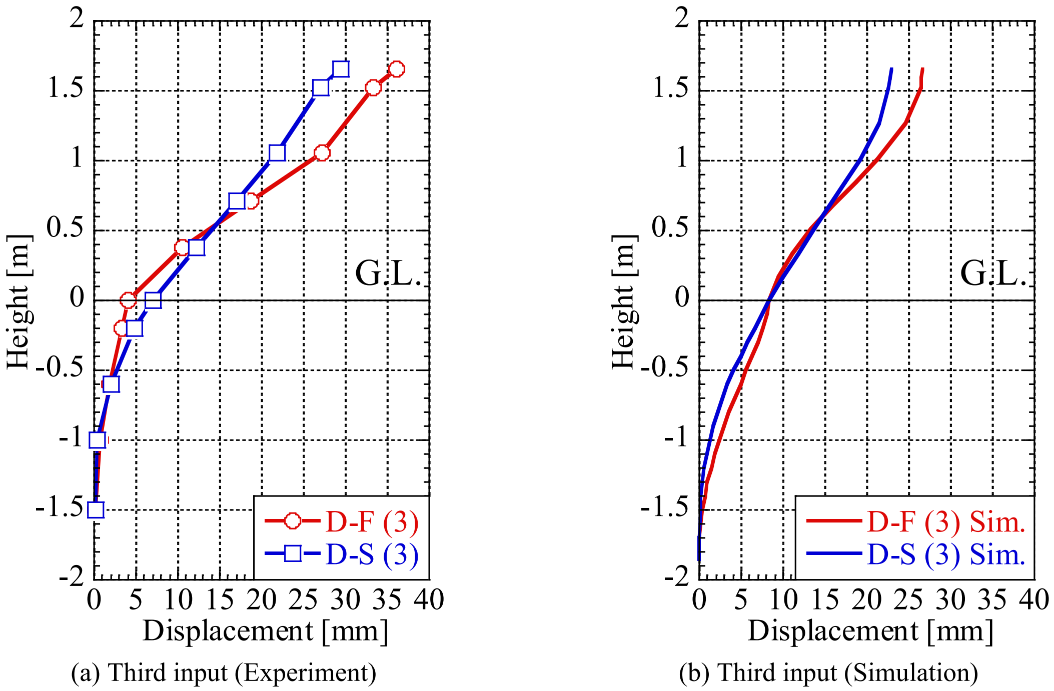

Figure 24. Distributions of the lateral displacement of the piles and pier when the maximum lateral displacement occurs at the pier top

The decrease in stiffness in the D-F structure, after the yielding of the shear panels, leads to significant acceleration and an increase in lateral displacement at the pier top, while the D-S structure mitigates the displacement effectively due to the minor decrease in stiffness. However, it is possible that these observed effects are influenced by the unusual condition of the excitation occurring between the natural frequencies of the two structures. The experiment does not clarify the relationship among the structure's natural frequency, input wave frequency, and impact of the decrease in stiffness on the natural frequency of the structure. Thus, in the next section, the seismic performance will be evaluated against the varied frequency sine and random waves to address these gaps in knowledge.

3.4.2 Results with L2 seismic input

Fig. 25 displays the time history of the input acceleration waveform and the Fourier spectrum of the random input acceleration waveform for bedrock whose predominant frequency components are 1.59 Hz and 2.07 Hz. Subsequent response analysis results for the random wave are depicted in subfigures Figs. 26 (a) to (d). Fig. 26(a) presents a comparison of the inertial force and lateral displacement at the pier top. The relationship between the inertial force at the pier top and the shear strain in the upper shear panel is illustrated in Fig. 26(b). Fig. 26(c) shows the distribution of bending moments in the piles and the pier when the maximum lateral displacement occurs at the pier top, while Fig. 26(d) shows the distribution of lateral displacement of the piles and the pier under the same conditions.

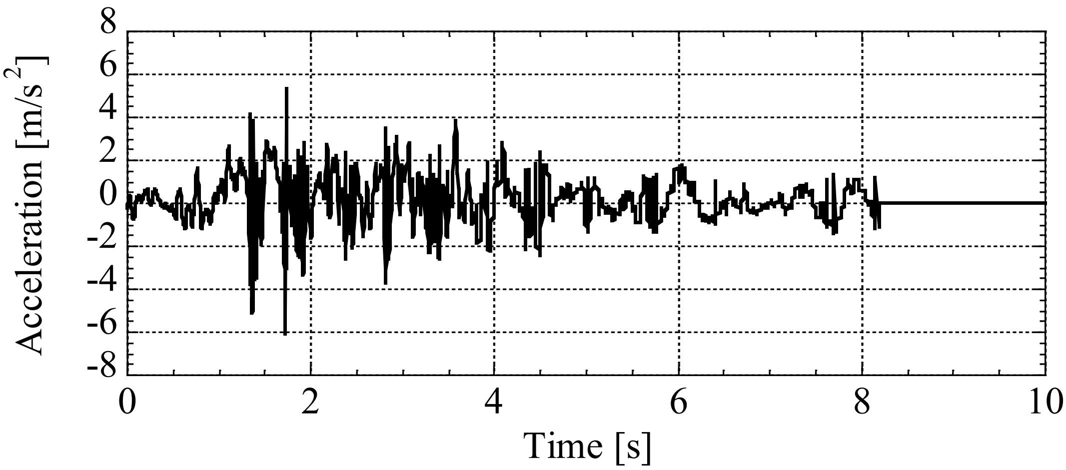

(a) Time history of the input acceleration waveform

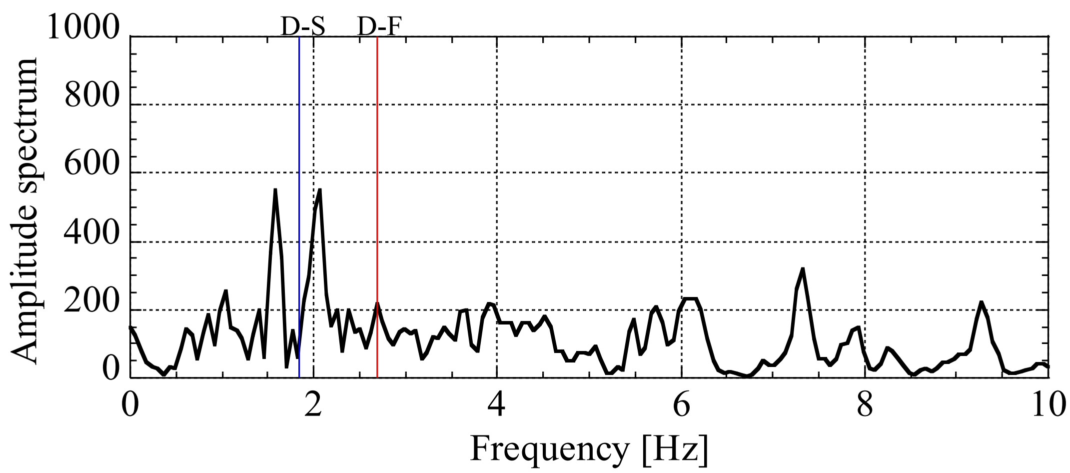

(b) Fourier spectrum of the input acceleration waveform

Figure 25. Level-2 input seismic motion specified in the Guidelines for Aseismic Design for Cut and Cover Tunnels published by Hanshin Expressway Co., Ltd.

It is noteworthy that similar trends were observed for the sine wave previously described. The response values for each structural member are provided in Table 7. Although the maximum response acceleration (A_{PT}) and maximum lateral displacement at the pier top (D_{PT}), moment at the pier base (M_C), and maximum shear strain in the shear panels (S) are larger for D-F compared to D-S, these values did not reach those for the fully plastic moment (8.41 kN*m) of the pier columns in D-F. The amplification of the response after the yielding of the shear panels could be the reason behind the larger values observed in D-F. Similarly, while the maximum lateral displacement of the pile heads (D_{PH}) and maximum bending moment of the piles (M_P) are larger in D-S than D-F, these values also did not reach the fully plastic moment. The lower stiffness of the substructure in D-S would make the piles deform significantly, thereby resulting in larger bending moments. In summary, the superstructure response amplifications in D-S are significantly reduced compared to D-F, making it a favourable option against the L2 input motion used in this analysis despite the relatively large pile head deflection.

To address the similarity rule for susceptibility to resonance, we conducted an additional analysis on the relationship between the predominant frequency of the seismic motion and the natural frequency of the structure. By varying the L2 input motion's predominant frequency from 1.2 Hz to 4.85 Hz (adjusting the time step from 0.006 to 0.0015 seconds), while holding Arias Intensity (Arias, 1970) constant, it was found that the D-F and D-S response trends remained consistent with the original case (0.004 seconds), as shown in Fig. 27. The predominant components of those additional L2 inputs thoroughly consider the ranges in natural frequency of both D-F and D-S types.

As the predominant frequency decreased to 1.2 Hz, the D-S responses increasingly exceeded those of D-F, particularly in pier top displacement, pile bending moment, and pile head displacement, aligning with the reduced natural frequency of D-S after shear panel yielding. The unique behaviour at 1.85 Hz corresponds to its proximity to the reduced natural frequency of D-F. Although the weight similarity rule was not fully met, our findings indicate that this discrepancy did not significantly impact the relative structural responses.

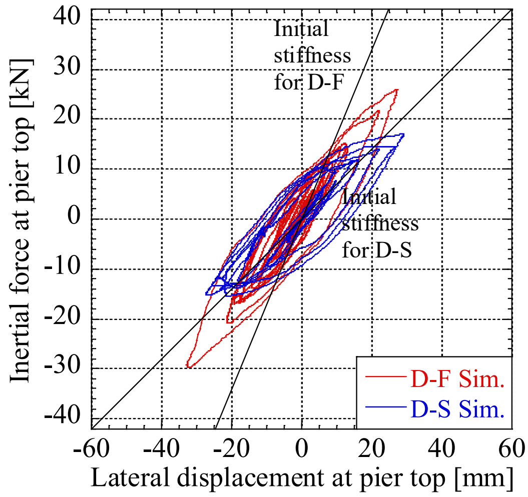

(a) Inertial force at the pier top vs lateral displacement at the pier top

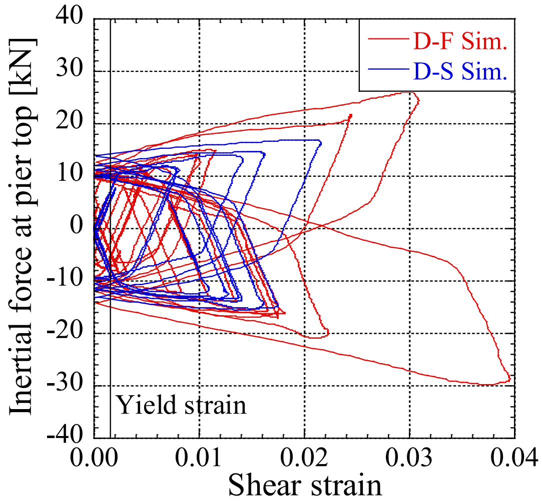

(b) Inertial force at the pier top vs shear strain in the upper shear panel

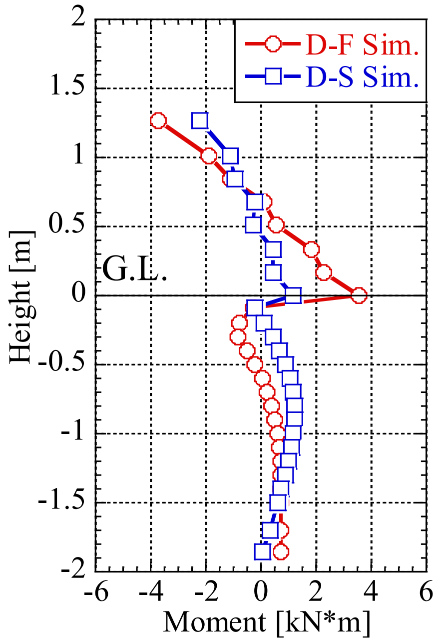

(c) Bending moments of the pier and piles

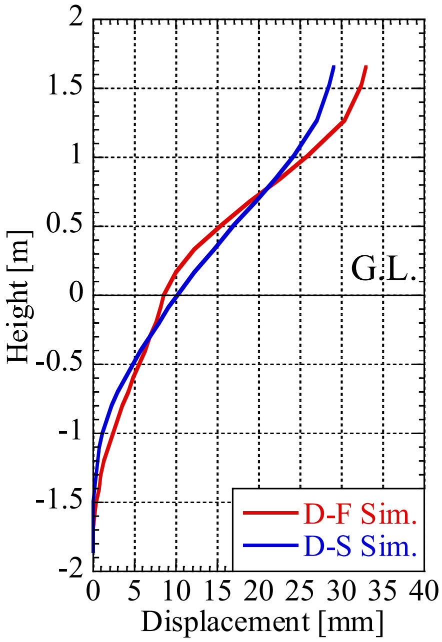

(d) Lateral displacement of the pier and piles

Figure 26. Response analysis results against Level-2 seismic motion

Table 7. Comparison of the response values for each member against Level-2 seismic motion

Part	Item	D-F	D-S
Pier	Maximum response acceleration at the pier top, A_{PT} [m/s^2]	5.61	3.24
	Maximum horizontal deformation at the pier top, D_{PT} [mm]	32.9	29.0
	Moment at the base, M_C [kN*m] Ratio to the fully plastic moment	3.54 0.58	1.17 0.19
Panel	Maximum shear strain, S Ratio to the yield shear strain	0.039 21.19	0.022 12.20
Pile	Maximum horizontal deformation at the pile top, D_{PH} [mm]	8.55	11.5
	Maximum bending moment, M_P [kN*m] Ratio to the fully plastic moment	0.94 0.10	1.23 0.13

3.4.3 Results with varying input frequencies

Figs. 27(a) to (i) present radar charts displaying the ratios of the response values for each member of the D-S type compared to those of the D-F type across different frequencies of the input sine wave.

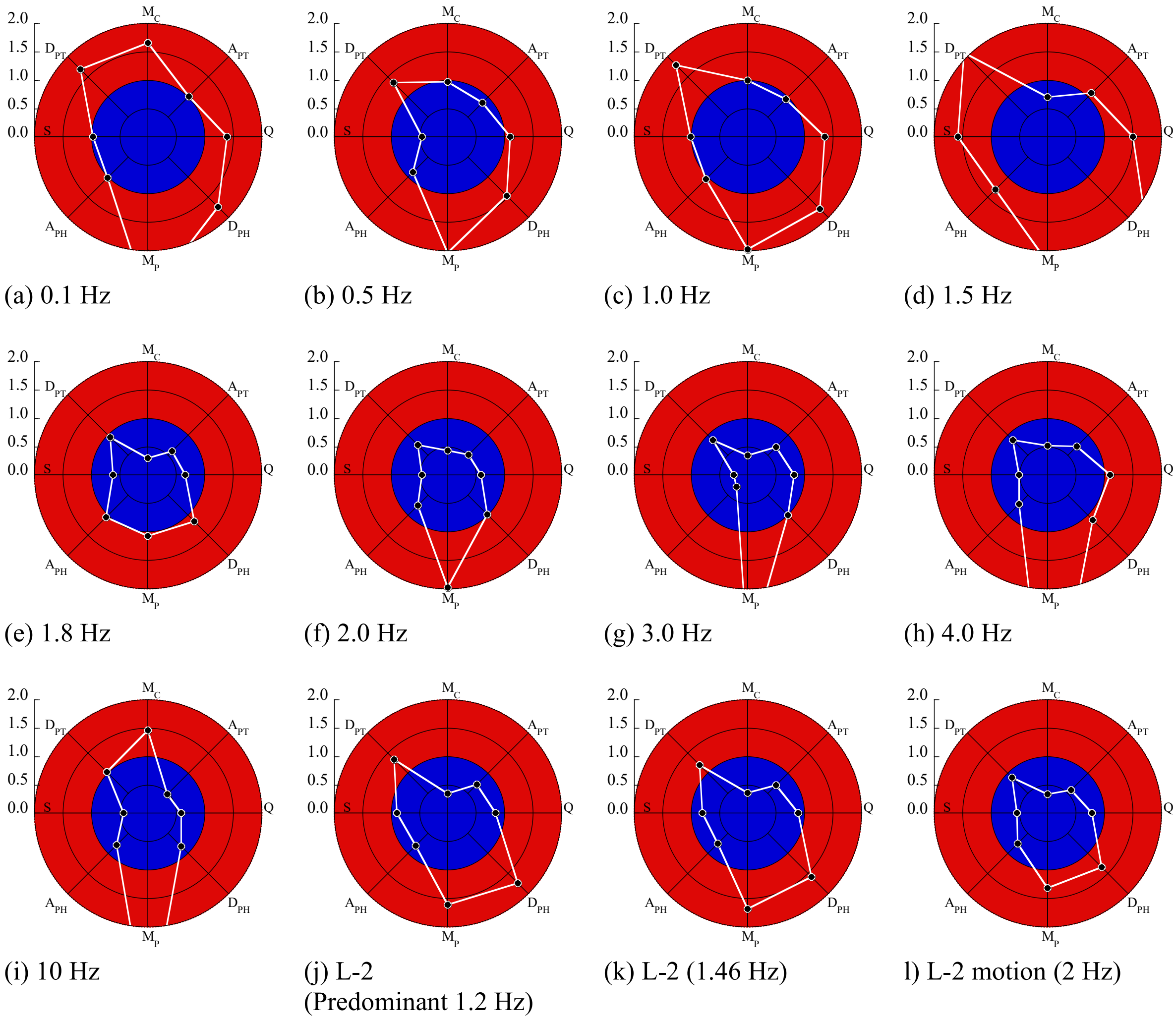

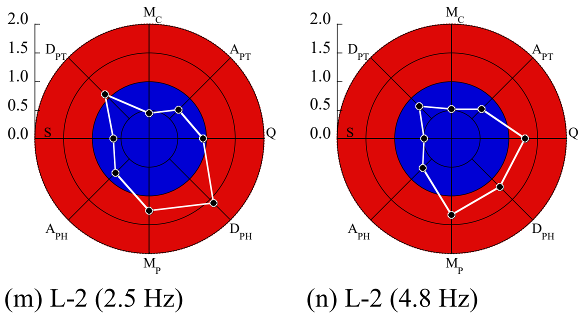

$\boldsymbol{S}$: maximum shear strain of a panel, $\boldsymbol{D_{PT}}$: maximum displacement at the pier top, $\boldsymbol{M_C}$: bending moment at the pier base, $\boldsymbol{A_{PT}}$: maximum acceleration at the pier top, $\boldsymbol{Q}$: shear force at the pile head, $\boldsymbol{D_{PH}}$: maximum pile head displacement, $\boldsymbol{M_P}$: maximum pile bending moment, and $\boldsymbol{A_{PH}}$: maximum pile head acceleration.

Figure 27. Comparison of the results of the response analysis against the input waves with various frequencies (D-S/D-F)

The charts suggest that lower input wave frequencies result in smaller response values for the footing type, whereas higher input wave frequencies lead to smaller response values for the footingless type.

Furthermore, in Fig. 28, it is evident that the shear strain remains minimal until 1 Hz for both D-F and D-S. However, a notable increase in shear strain occurs at 1.5 Hz for D-S and 1.8 Hz for D-F. The lower response values of the superstructure in D-F (Fig. 27) at lower frequencies can be attributed to the insufficient shear strain of the panels, which fails to alter the stiffness and amplify the structure's response. Additionally, the proximity of the input frequency to the system frequency governs the system's response, resulting in the amplification of the inertial force (Beziar et al., 2018). It is presumed that the yielding of the panels reduces the system frequency closer to 1.5 Hz for D-S and 2 Hz for D-F, leading to resonance phenomena and significantly larger amplifications in the structure.

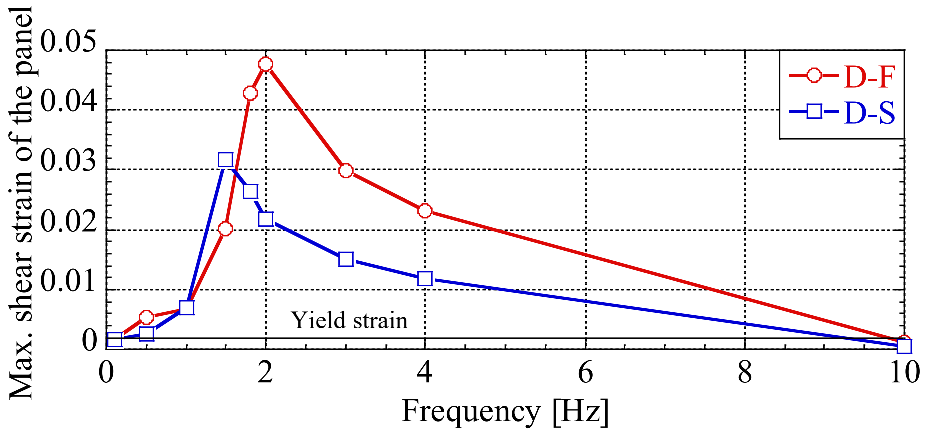

Figure 28. Variation in the maximum shear strain of the panels against the input frequencies

Likewise, Fig. 29 presents the lateral displacement profiles of the piles and the pier across various input motion frequencies. The profile at 1 Hz reveals a relatively substantial lateral deformation of both the piles and the pier in D-S type compared to D-F. At 2 Hz, the lateral deformation increases in both structures, particularly at the pier top, where the displacement exceeds three times its value at 1 Hz for the D-F type. This increase is directly related to the substantial shear strain of the panels, as depicted in Fig. 28. At 4 Hz, the same tendency as 2 Hz is observed, but the amounts of displacement at the pier top and the pile head at 4 Hz are less than those at 2 Hz. At 10 Hz, the magnitude of the lateral displacements is further reduced and the deformation pattern exhibits slight changes. The shear deformation of the pier is notably minimal compared to that of the piles, indicating less influence of the inertial action. Conversely, the additional reduction in pile head deformation could be attributed to the heightened kinematic action of the soil as the ground deformation becomes excessive near its natural frequency (8 Hz). Consequently, the pier structure exhibits a secondary mode, as noted by Hussien et al. (2015).

Despite the favourable soil conditions, according to the Japanese design code, both kinematic and inertial interactions appear to influence the soil response, as noted by Toyooka et al. (2012). Furthermore, supporting evidence for the observed response is found in the findings of Murono et al. (2000), Tokimatsu et al. (2005), and subsequent studies, suggesting that, when a superstructure's frequency is lower than that of the ground, the ground displacement tends to be out of phase with the inertial force, and vice versa.

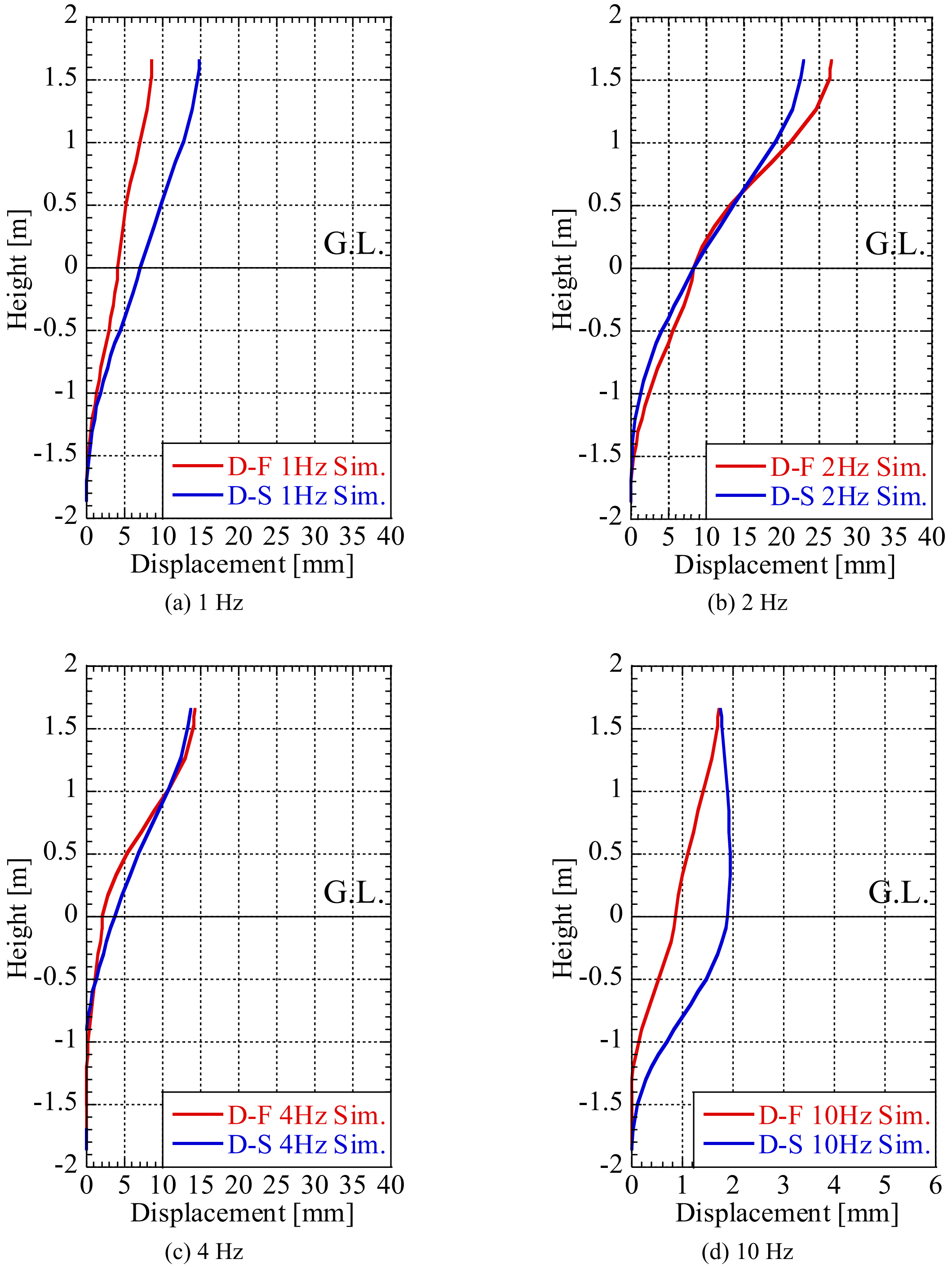

Figure 29. Lateral displacement profiles of the pier and piles against various frequencies of input motion

3.4.4 Liquefiable ground cases

Fig. 30 presents a comparison of the time histories of the excess pore water pressure ratio (EPWPR) of the ground between the experimental and the analytical results. The EPWPR at G.L. -0.2 m indicates a liquifiable layer, while that at G.L. -0.6 m indicates a non-liquifiable layer. In both L-F and L-S, the soil reaches liquefaction at approximately 5 seconds, which is consistent for both the experimental and simulation analyses. The natural periods of the L-F and L-S models after liquefaction were determined as 0.481 sec and 0.683 sec, respectively, based on observations of the free vibration phase immediately after the main shaking during experiments (Isobe et al., 2016). The numerical simulation estimated these periods as 0.45 sec and 0.60 sec for L-F and L-S, respectively, which are slightly underestimated but reasonable given the simplifications and assumptions applied here.

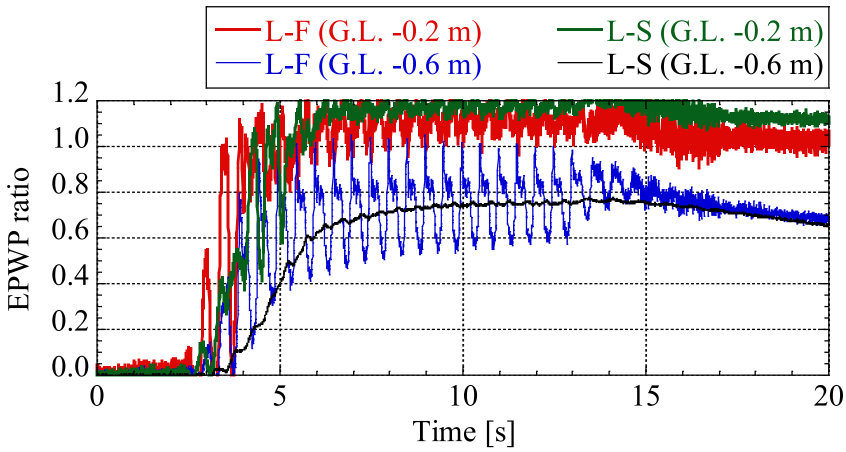

(a) Experimental results

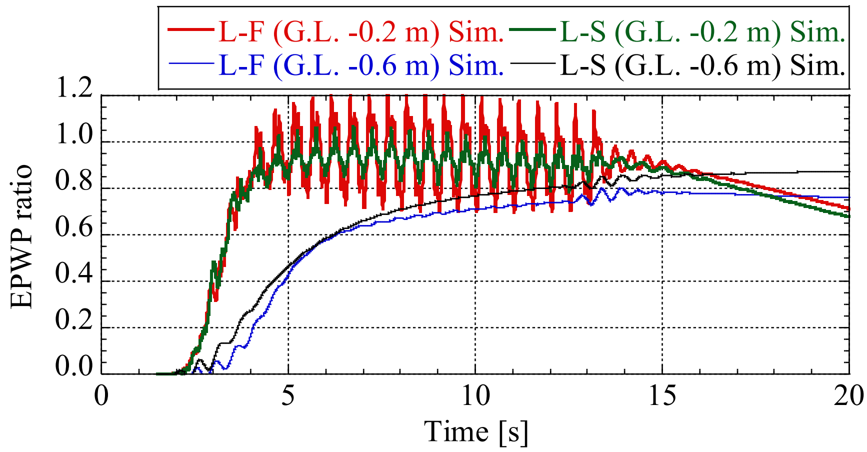

(b) Simulation results

Figure 30. Comparison of the time histories of the excess pore water pressure ratio of the ground for the experimental and simulation results

Fig. 31 illustrates the relationship between the inertial force and the lateral displacement of the pier top and compares the simulated responses with the experimental observations. Similar to the cases with the D-ground, the analysis tends to overestimate the initial stiffness and hysteresis loop of the L-S, but accurately reproduces the hysteresis loop of the L-F. Furthermore, the tendencies for the larger maximum acceleration and maximum lateral displacement in L-F than in L-S are successfully reproduced, aligning with the experimental results.

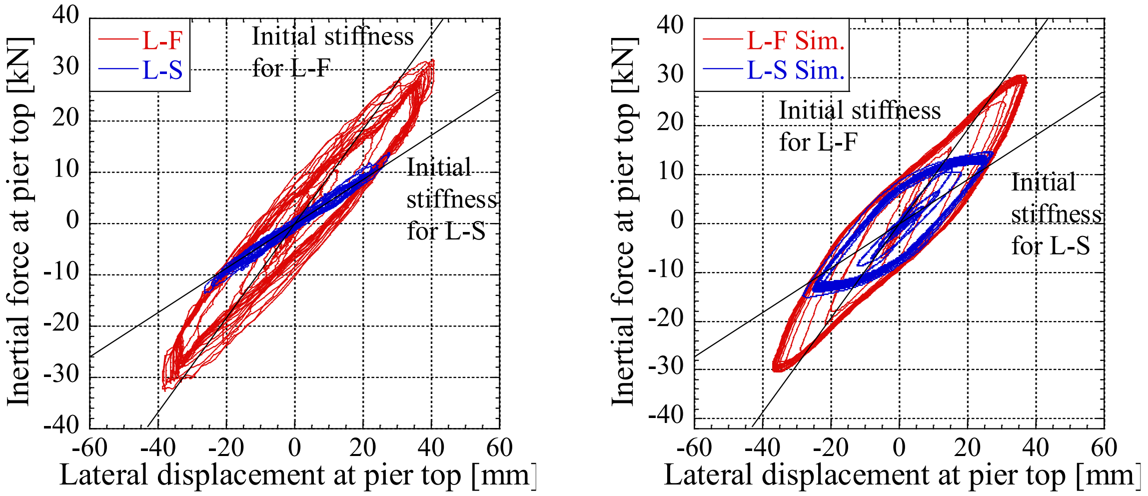

(a) Experiment results (b) Simulation results

Figure 31. Comparison of the experimental and simulation results for the relationship between the inertial force and the lateral displacement at the pier top for the case with liquefiable sand

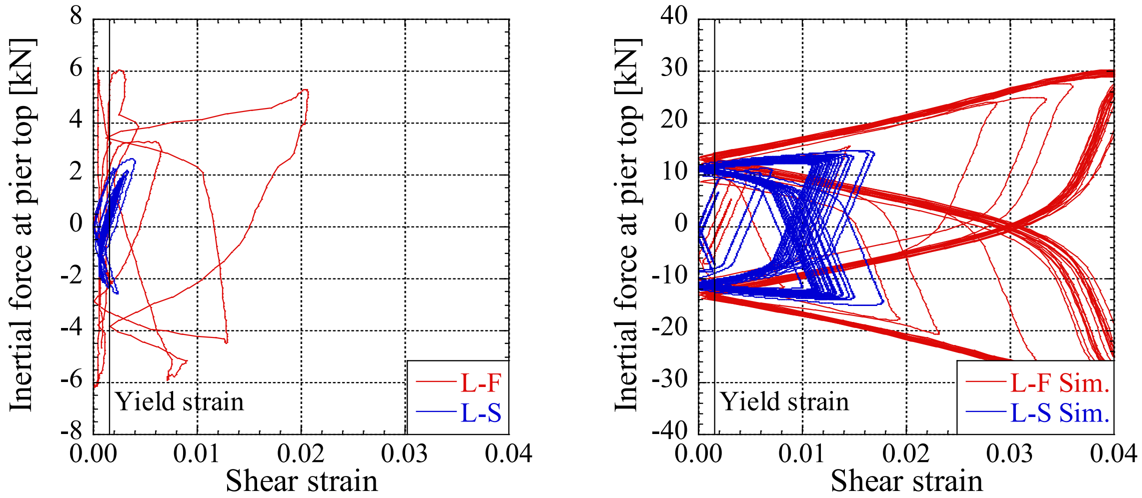

(a) Experiment results (b) Simulation results

Figure 32. Relationship between the inertial force at the pier top and the shear strain in the upper shear panel for the case with liquefiable sand

Fig. 32 displays the relationship between the inertial force at the pier top and the shear strain in the upper shear panel. Similar to the D-ground case, the reproduction analysis slightly overestimates the shear strain in both structures, with a more pronounced tendency in L-F. Although measured strain values in the large strain region of the experiment were unavailable, due to the detachment of the strain gauges on the shear panels after out-of-plane deformation, the analysis successfully replicated the trend of the shear strain values to exceed the yield strain in both cases, with larger shear strain being observed in L-F than in L-S.

Figs. 33 and 34 depict the longitudinal distributions of the bending moments and lateral displacement, respectively, in the piles and the pier, at the occurrence of the maximum lateral displacement at the pier top. The bending moment in the pier base is larger for L-F compared to L-S, while the moment in the piles is larger for L-S than for L-F. Additionally, the bending moment tends to converge at the pile tip similar to the experimental case where the pile tips are fixed. However, there is a slight difference that is probably due to an imperfect modelling of the relative stiffness between the piles and the ground in the deeper sections of the model. The analysis successfully captures the observed tendencies in the bending moment distribution in the piles and the pier, the nearly equivalent levels of lateral displacement values at the pile heads for both L-F and L-S, a larger displacement at the pier top for L-F, and a tendency for L-F to exhibit larger shear deformation in the column than L-S.

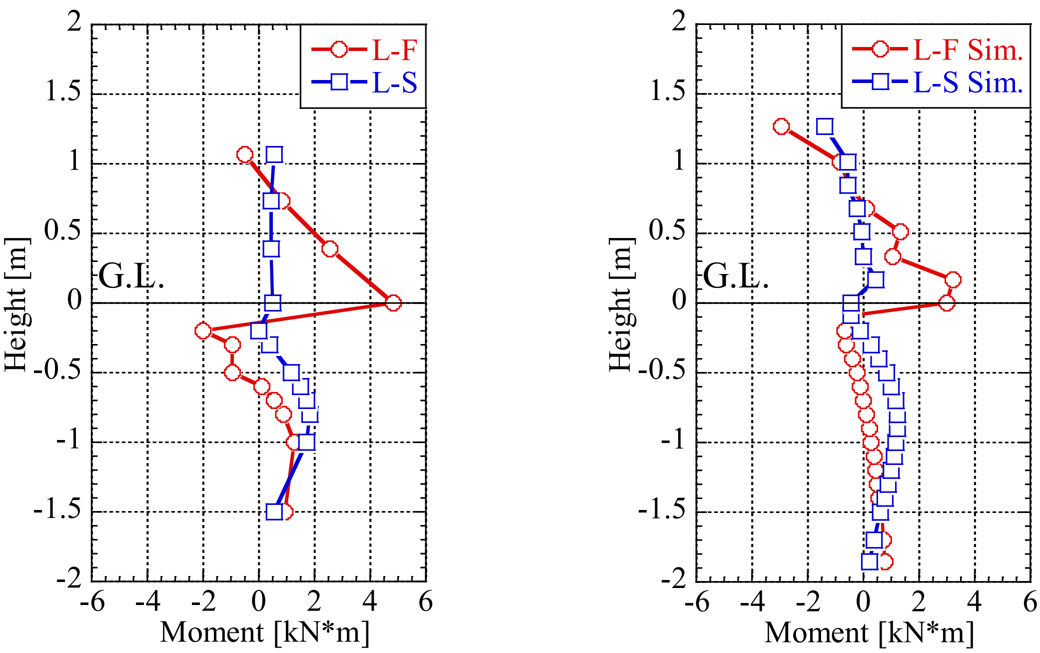

(a) Experiment results (b) Simulation results

Figure 33. Distributions of the bending moments generated in the piles and pier when the maximum lateral displacement occurs at the pier top for the case with liquefiable sand

Unlike the D-ground cases, the displacement at the pile heads for L-F is larger than that for L-S. This difference can be attributed to several factors. One factor is the excessive response displacement of the unsaturated surface layer above the liquefied ground, which may lead to increased subgrade reaction forces around the pile heads. Another factor is that the liquefaction-induced reduction in the subgrade reaction forces beneath the piles could contribute to the increased pile head deformation under the influence of the inertial force of the footing. This hypothesis is supported by studies indicating that liquefaction decreases the lateral resistance provided by the surrounding soil, leading to increased pile flexibility (Wilson et al., 2000; Rollins et al., 2005). Studying the role of the subgrade reaction force as kinematic action may further corroborate these findings in the next section.

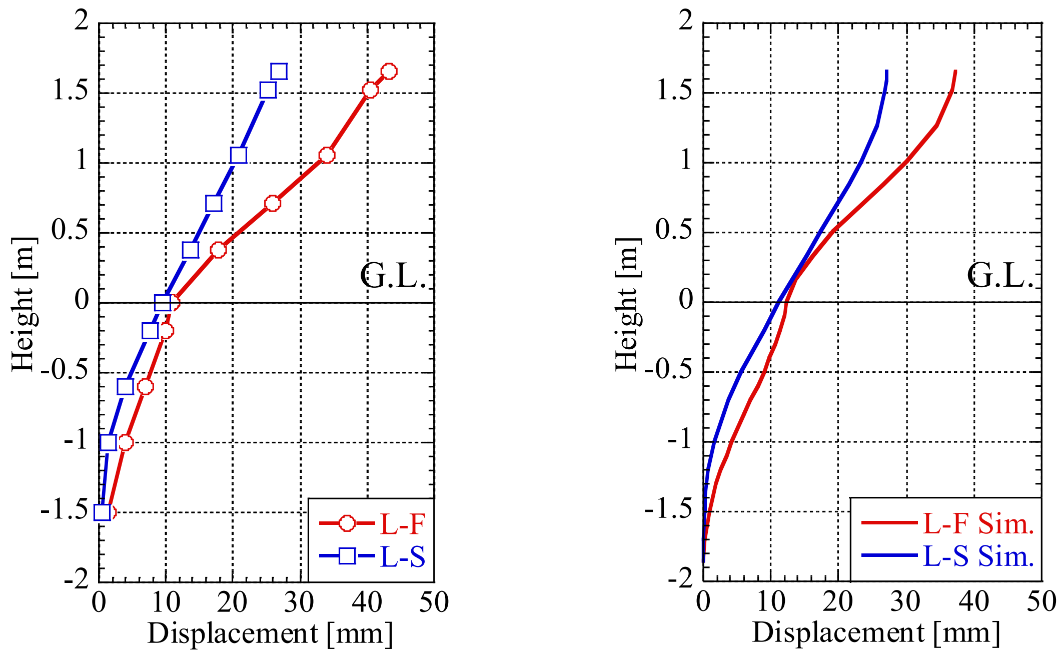

(a) Experiment results (b) Simulation results

Figure 34. Distributions of the lateral displacement in the piles and pier when the maximum lateral displacement occurs at the pier top for the case with liquefiable sand

3.4.5 Kinematic interaction

Kinematic interaction refers to the effects of relative displacement and velocity between the soil and the structure during dynamic loading, such as earthquakes. It plays a crucial role in influencing the behaviour and response of structures, particularly piles and foundations, subjected to seismic forces. Wang et al. (2017) noted that pile deformation is influenced by both kinematic and inertial actions in liquifiable sand. Fig. 35 illustrates the relationships between the inertial force and the pile head shear, and between the inertial force and the earth pressure, during the fourth excitation. Earth pressure is calculated as the difference between the inertial force and the net pile head shear, following the approach of Tokimatsu et al. (2005). It shows that, for D-S, the inertial force exceeds the shear force at the pile heads, suggesting that the surrounding ground provides a supporting mechanism, with the earth pressure causing a decrease in the pile bending moments and shear forces. In contrast, for D-F, the earth pressure tends to be out of phase with the inertial force, causing most of the inertial force to transfer directly to shear force. While earth pressure occasionally acts as a supporting force, its magnitude is relatively low.

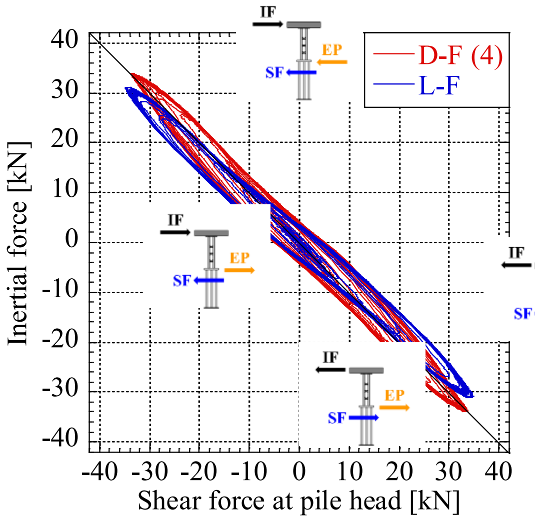

(a) Inertial force vs Shear force at the pile heads for D-F (4) and L-F

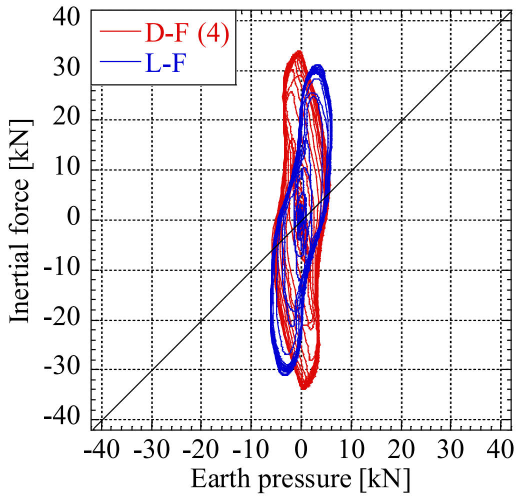

(b) Inertial force vs Earth pressure for D-F (4) and L-F

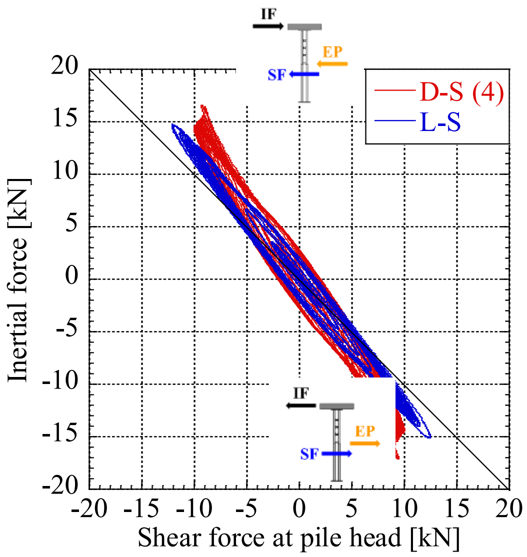

(c) Inertial force vs Shear force at the pile heads for D-S (4) and L-S

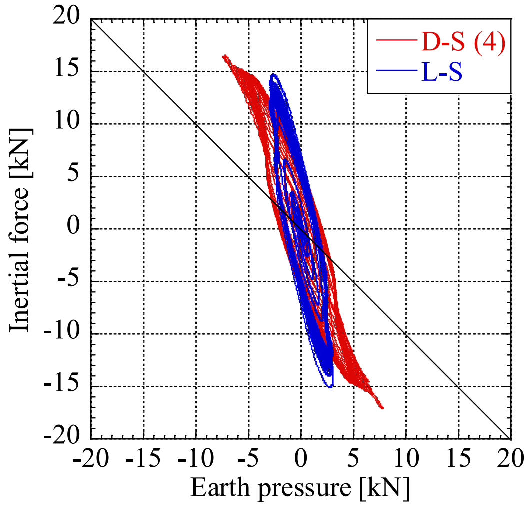

(d) Inertial force vs Earth pressure for D-S (4) and L-S

Figure 35. Relationships between the inertia force and the shear force at the pile head and between the inertial force and the earth pressure for D-F (4), D-S (4), L-F and L-S

In the case of the L-S type, the earth pressure counteracts the inertial force, thereby reducing the shear force transmitted at the pile heads. However, the magnitude of the earth pressure force is reduced by 62% compared to the D-S type. On the other hand, the earth pressure is in alignment with the inertial force, thereby increasing the pile head shear force for L-F. Earth pressure and inertia force are not exactly in the same phase; however, they have a greater tendency to act in the same direction. When the earth pressure acting as kinematic force aligns with the inertial force, it acts as additional force on the structure, making it an unconventional and critical case.

Although the kinematic forces in L-F and D-F are similar in magnitude, their impact appears more pronounced in liquefiable grounds for several reasons. Firstly, the pile head deformation in L-F exceeds that in D-F. Secondly, the inertial force in L-F is slightly lower than that in D-F and, importantly, the earth pressure in L-F acts in the same direction as the inertial force. Kinematic force may not serve as a supporting force when aligned with the inertial force, depending on the relationship between the natural frequency of the structure and the input motion. Conversely, studies by Kaynia et al. (1996) and Hussien et al. (2015) suggest that when a structure's natural frequency is lower than that of the ground, the kinematic interaction can be the primary contributor to the seismic force in the piles, particularly when the excitation frequency does not closely match the natural frequency of the coupled soil-pile-structure system (fSSI).

For F-type structures, the input seismic excitation falls within a relatively narrow band of the soil-pile-structure system's natural frequency compared to S-type structures, meaning that the inertial interaction generally prevails. Based on the above discussion, it is evident that the earth pressure acting as a kinematic force on the footing block, aligned with the inertial force, amplifies the pile head deformation more in L-F than in L-S.

Overall, the S-type structures demonstrate the potential for an improved seismic performance, while leveraging the stiffness and damping of the underground beam and under the favourable influence of the kinematic action in the soil. It should be noted that this discussion provides a preliminary overview of kinematic forces in F- and S-type structures under the specified conditions, without extensively examining the relationship between the natural frequency of the structure and ground excitation. A detailed analysis of the influence of the inertial and kinematic interactions on the structural response will be addressed in a next chapter.

3.5 Chapter summary:

- The numerical simulation reproduces the shaking table results with sufficient accuracy both qualitatively and quantitatively for dry and liquifiable sand cases.
- It is learnt that F type notes lower response values at lower excitation steps-thereby performing better. It effectively utilizes the hysteretic damping function of the shear panel. However, in instances where a significant strain leads to out-of-plane deformation in the shear panel, a sharp reduction in the overall structure's stiffness and response amplification is observed.
- S type tends to have better performance at higher excitation steps. S-type maintains the hysteretic damping function of the shear panel for a relatively long period by leveraging the strength of the underground beam, and gradual reduction in the overall structure's stiffness.
- Sharp stiffness reduction happens after shear panels plastic deformations in F-type structure. This in relationship with input excitation frequency is determined as an important factor in controlling the response amplifications of both structures.
- The advantage of the S-type over the F-type is also found in L2 seismic motion, however, it also depends on the relationship between the natural frequency of the structure and the input wave frequency.

CHAPTER APPENDIX

To examine the influence of cushioning material on a structure, a numerical simulation without cushioning material was performed and compared against a simulation model with cushioning material for case D-F. Under seismic excitation of 2 m/s^2, the soil element near the boundary was seen to exhibit a uniform stress-strain pattern for the model with cushioning material, mirroring the real ground conditions. However, an erratic stress-strain pattern was recorded in the cushion-less case, and significant shear stress was observed near the boundary due to the rigid confinement of the soil box (Fig. A1(a)). Consequently, the rationale for incorporating cushioning material was validated. Nevertheless, even in instances without cushioning material, neither the pile heads nor the superstructure exhibited any substantial influence in their response (Fig. A1(b)). Consequently, the contribution of a rigid soil tank to structural deformation appears to be relatively insignificant.

The wide top weight used in the experiment (Fig. 3) implies significant rotational inertia, which could affect the pier structure's response. However, a comparison of the responses with a solid element superstructure to a point mass model for cases L-F and D-S showed negligible differences (Figs. A2 and A3). Thus, a point mass approach was adopted for reproducing the proposed structure's analysis.

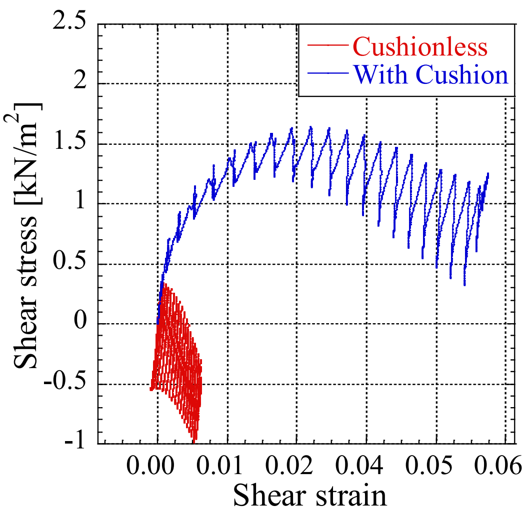

(a) Shear stress - shear strain relationship of the soil element near the boundary

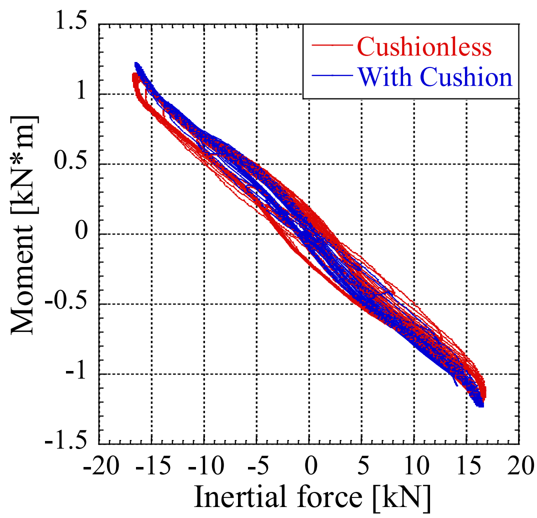

(b) Bending moments of the pile heads and inertial force of the superstructure

Figure A1. Comparison of the soil and structure's responses with and without cushion

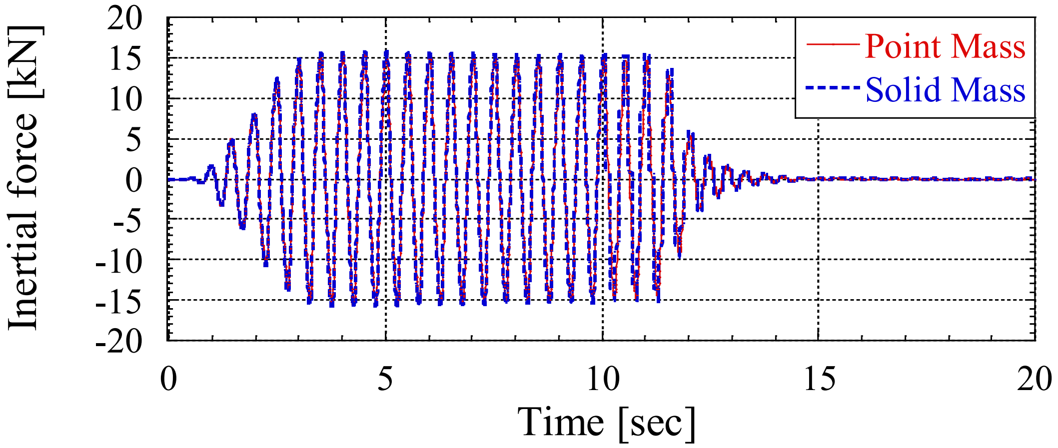

(a) Superstructure inertial force

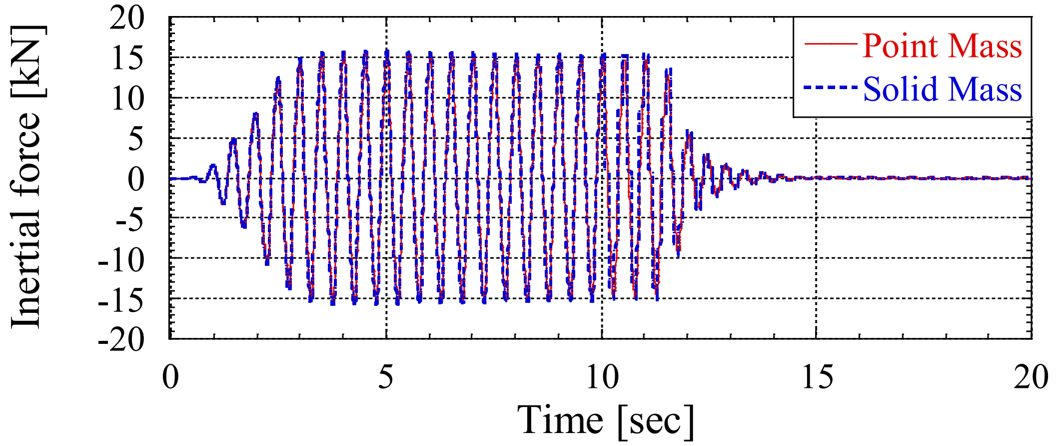

(b) Pile head bending moment

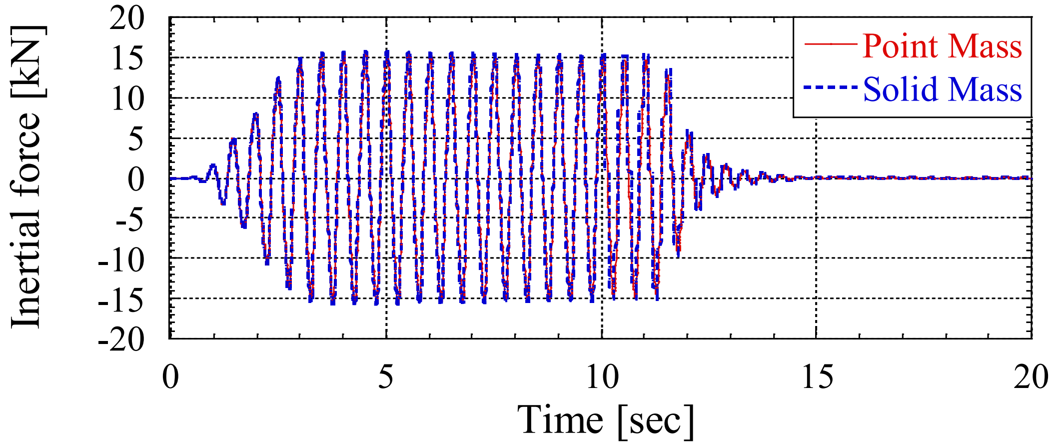

(c) Pile head displacement

Figure A2. Comparison of the superstructure and the pile head responses for the point mass and solid mass superstructure case (L-F)

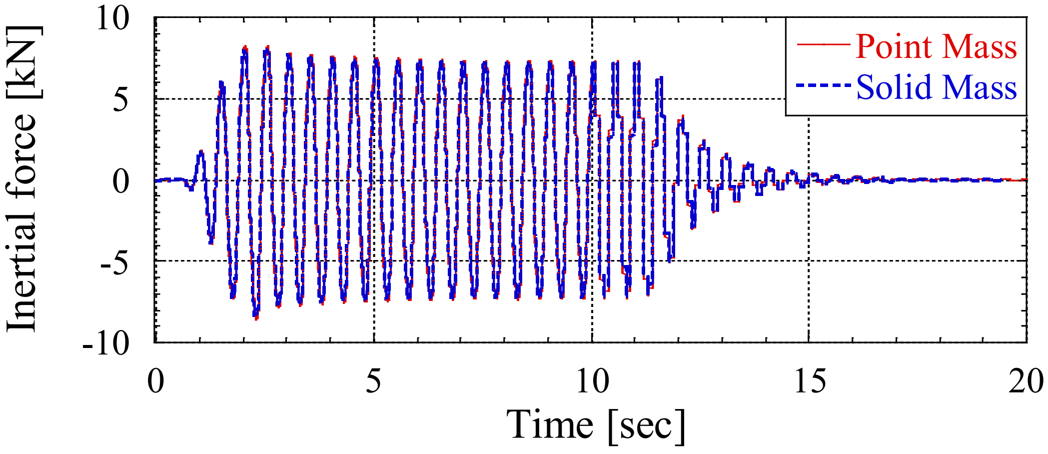

(a) Superstructure inertia force

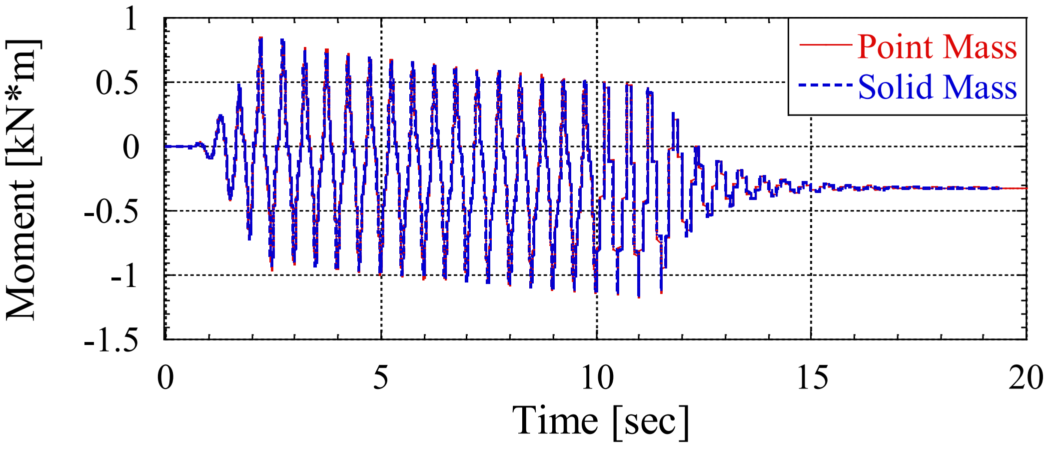

(a) Pile head bending moment

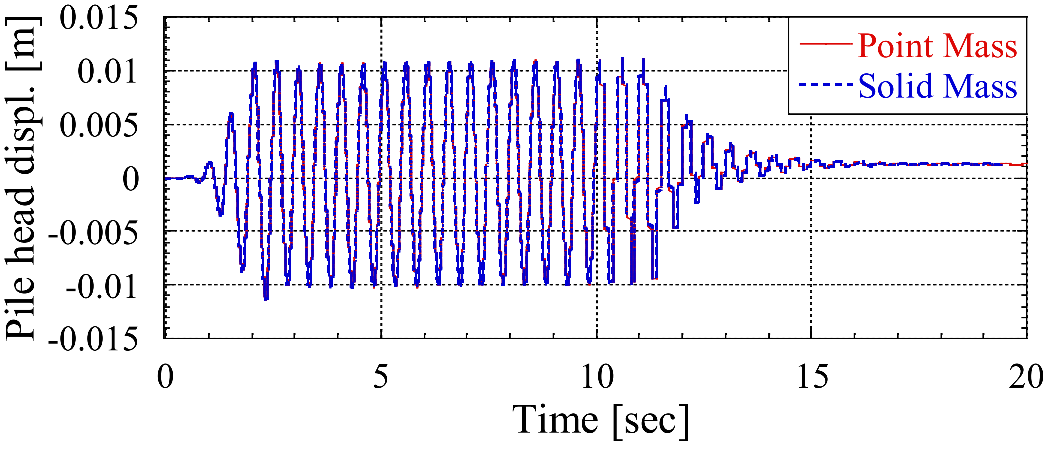

(a) Pile head displacement

Figure A3. Comparison of the superstructure and the pile head responses for the point mass and solid mass superstructure case (D-S)

CHAPTER 4. DYNAMIC FREQUENCY-DEPENDENT SOIL-PILE-STRUCTURE INTERACTION

4.1 INTRODUCTION

This chapter investigates the soil-structure interaction behaviour of the proposed smart bridge pier system under dynamic excitation, with particular emphasis on how inertia and kinematic forces influence different foundation configurations. The numerical model established in the previous chapter is now applied to study the SSI in four representative cases i.e. D-F, D-S, LF and L-S corresponding to fourth excitation step. The dynamic response is interpreted through comparisons of time-domain histories, kinematic–inertial coupling, earth pressure development, pile bending moment formation, and deformation mechanisms. To further isolate the physical sources of pile demand, two additional numerical experiments are performed for each of the above four cases: one in which the superstructure is removed to quantify pure kinematic action of the soil, and another in which the surrounding soil is removed so that the piles and pier respond solely to inertial excitation. Finally, a frequency-domain phase analysis is carried out to identify whether the pile response is governed predominantly by the motion of the superstructure, the far-field soil, or a combination of both.

4.2 Footing type with dry sand (D-F)

4.2.1Time history analysis:

The time history response of key parameters for the D-F case is presented in Fig. 36 under a sinusoidal input motion with a frequency of 2 Hz and a peak acceleration of 2 m/s². The pier-top and pile-head accelerations are amplified by approximately 3.4 and 1.73 times the input motion, respectively, and remain nearly in phase with each other, with a slight lag relative to the input. The pile displacement also follows the phase of the pier-top response, indicating strong structural control, whereas a clear phase difference is observed between the pile and the surrounding soil displacement, suggesting limited kinematic influence. The evolution of pile bending moment closely follows the inertial force at the pier top, and the magnitude of earth pressure remains relatively small in comparison. Overall, these observations indicate that the pile response in the D-F case is predominantly governed by inertial interaction, with only a minor contribution from kinematic effects.

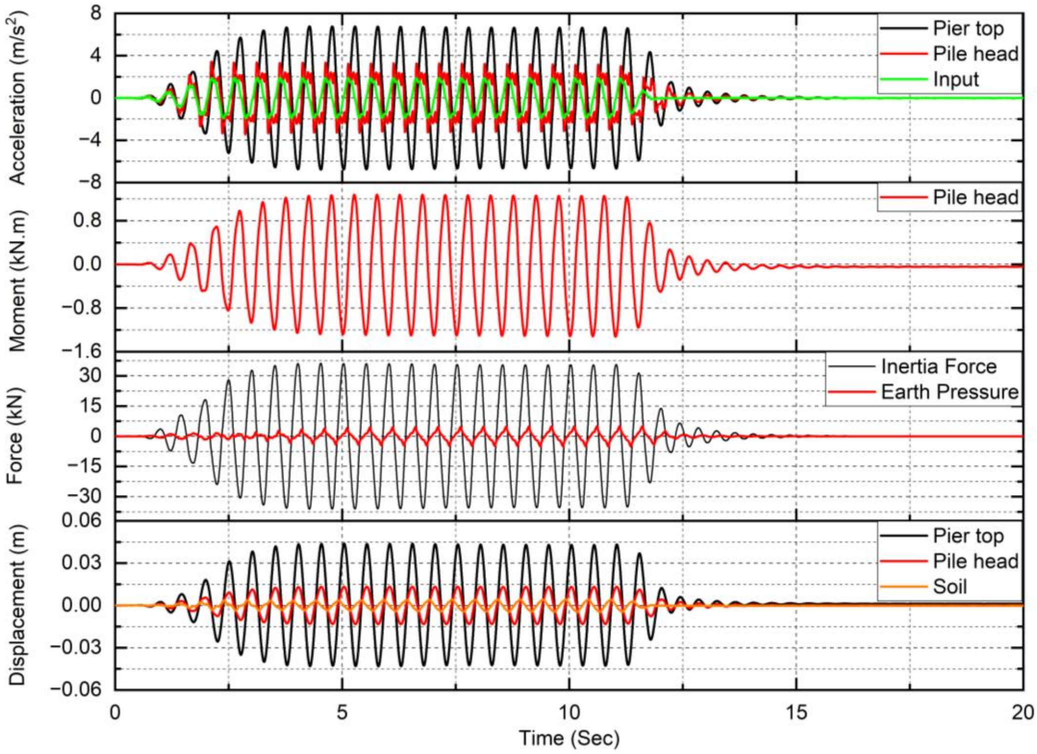

Figure 36. Evolution of various response parameters along the course of excitation for DF type

4.2.2 Pile bending moment:

Figure 37 presents the bending moment and deformation profiles of the pile and surrounding ground at key instants, including maximum pile bending moment, maximum inertial force, and maximum ground displacement. At the instant of maximum pile bending moment, the peak value occurs near the pile head at approximately 1.5 kN·m, with a corresponding pile deformation of about 13 mm. A comparison of inertial force and earth pressure indicates that the contribution of kinematic interaction is minimal at this stage, as earth pressure remains significantly lower than inertia. A similar bending moment and deformation profile is observed at the instant of maximum inertial force, confirming the dominant role of inertia. In contrast, at the instant of maximum surface ground displacement, both inertial force and earth pressure are reduced and act in opposite directions, resulting in a significant decrease in pile response, with bending moment and deformation reduced by approximately 70% and 85%, respectively, consistent with a reduction of about 78% in inertial force. Despite larger ground deformation compared to pile displacement, the limited influence of soil suggests a phase difference between soil and pile motion, with soil response lagging behind the pile. This phase mismatch explains the weak kinematic contribution and will be examined further through phase difference and interaction decomposition in the subsequent sections.

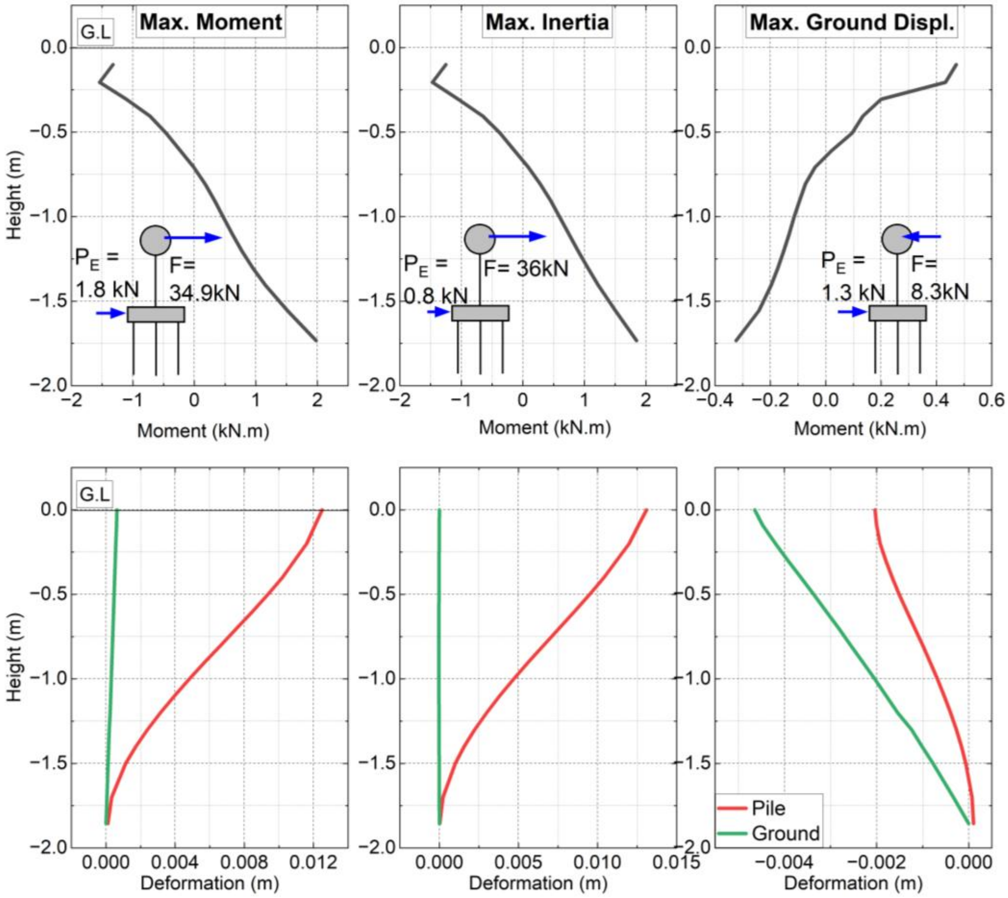

Figure 37. Pile bending moment and deformation profiles at various instances

4.2.3 Inertial vs kinematic interactions:

The results presented in the previous sections correspond to the response of the D-F system under the combined effects of inertial and kinematic interactions. To better understand the contribution of each mechanism, additional numerical simulations are performed to isolate these effects. In the first case (DFNS), the superstructure mass and pier are removed, leaving only the pile–foundation system embedded in the soil. The resulting response represents pure kinematic interaction induced by ground deformation. This case serves as a reference for evaluating the extent to which pile bending in the full system is driven directly by soil movement.

In the second case (F-type), the surrounding soil is removed while retaining the superstructure and column. In this configuration, the system responds to input excitation without soil restraint, representing pure inertial action. The resulting bending moment and acceleration responses provide a reference for quantifying inertial contribution in isolation. Together, these two simplified models enable decomposition of the total pile response into kinematic and inertial components, allowing clear identification of the governing interaction mechanism. The schematics of these simulation cases are shown in Fig. 38.

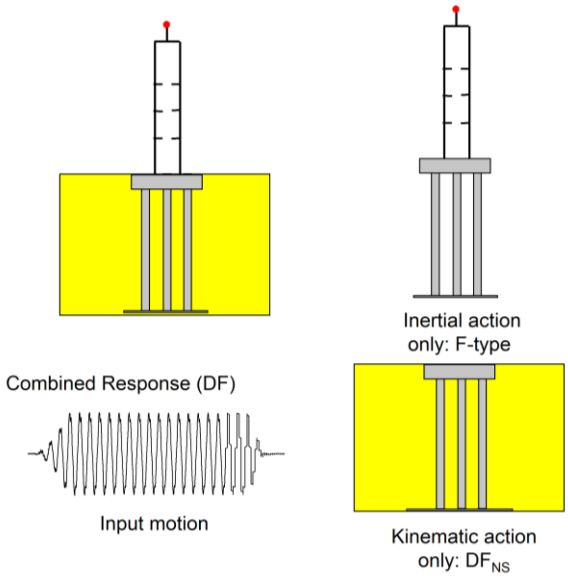

Figure 38. Various analysis types conducted to determine the role of kinematic and inertial interactions

Before proceeding towards the comparison of pile moment and deformations profile from various cases, we have first carried phase analysis to get a firsthand view of the expected role of inertial and kinematic interactions.

4.2.3.1 Qualitative comparison of inertial and kinematic interactions:

The dynamic response of soil–pile–structure systems depend not only on the amplitudes of vibration but also on the timing relationship between motions of the superstructure, the pile, and the surrounding soil. Since phase determines whether components move together or in opposition, frequency-domain phase analysis provides a direct means to distinguish inertia-controlled behaviour from soil-controlled (kinematic) behaviour. Acceleration time histories are obtained at the pier top, at multiple depths along the pile, and in the surrounding soil at corresponding elevations. Each signal is transformed into the frequency domain, and its dominant frequency is identified as the frequency at which the amplitude spectrum reached its maximum. This dominant frequency characterizes the principal oscillatory component of the response at that location and allows a consistent comparison across soil, pile, and inertial motions.

The phase of each signal is computed from its Fourier transform, and the phase difference between pairs of signals is evaluated at a particular dominant frequency. Two sets of comparisons are performed. The first examined the phase difference (PD) between the pier top inertial acceleration and acceleration at different pile depths determined at the dominant frequency of inertial acceleration. The second comparison involved phase difference of soil–pile acceleration pairs at each depth corresponding to the dominant frequency of soil.

Let $x(t)$and $y(t)$denote acceleration time histories recorded at different locations in the system (e.g., pier top vs. pile, or pile vs. soil). Their Fourier transforms are computed as

$$X(\omega) = \int x(t)e^{-i\omega t}\, dt, Y(\omega) = \int y(t)e^{-i\omega t}\, dt.$$

Each transform is expressed in polar form,

$$X(\omega) = \mid X(\omega) \mid e^{i\phi_x(\omega)}, Y(\omega) = \mid Y(\omega) \mid e^{i\phi_y(\omega)},$$

where $\mid X \mid$and $\mid Y \mid$are amplitude spectra, and ϕ_x, $\phi_y$are phase angles.

The dominant frequency of signal $x(t)$is determined from the maximum amplitude of its spectrum:

$$f_d = \frac{1}{2\pi}[\arg \max_{\omega} \mid X(\omega) \mid]$$

The phase difference between two signals at frequency ω is

$$\Delta\phi(\omega) = \phi_y(\omega) - \phi_x(\omega),$$

evaluated in this study at the dominant frequency of each signal pair. A positive phase difference indicates that $y(t)$ lags $x(t)$; a negative value implies that it leads.

For pier–pile phase evaluation,

$$x(t) = \text{pier top acceleration}, y(t) = \text{pile acceleration at depth } z,$$

and the resulting phase difference helps describe qualitative role of inertial force in pile response. A positive phase difference indicates that pile follows the pier top inertia force and vice versa.

For soil–pile phase evaluation,

$$x(t) = \text{pile acceleration depth z}, y(t) = \text{soil acceleration at depth } z,$$

and the phase relationship reflects the role of kinematic force in pile response. A positive phase difference indicates that soil lags behind pile implying a reduced role of kinematic forces, whereas a negative phase difference implies that pile follows the soil which enhances the role of kinematic force.

By combining these two types of phase comparisons, the analysis distinguishes where the pile response is governed primarily by inertial loading from the superstructure, where it is controlled by soil deformation, and where it is influenced by both.

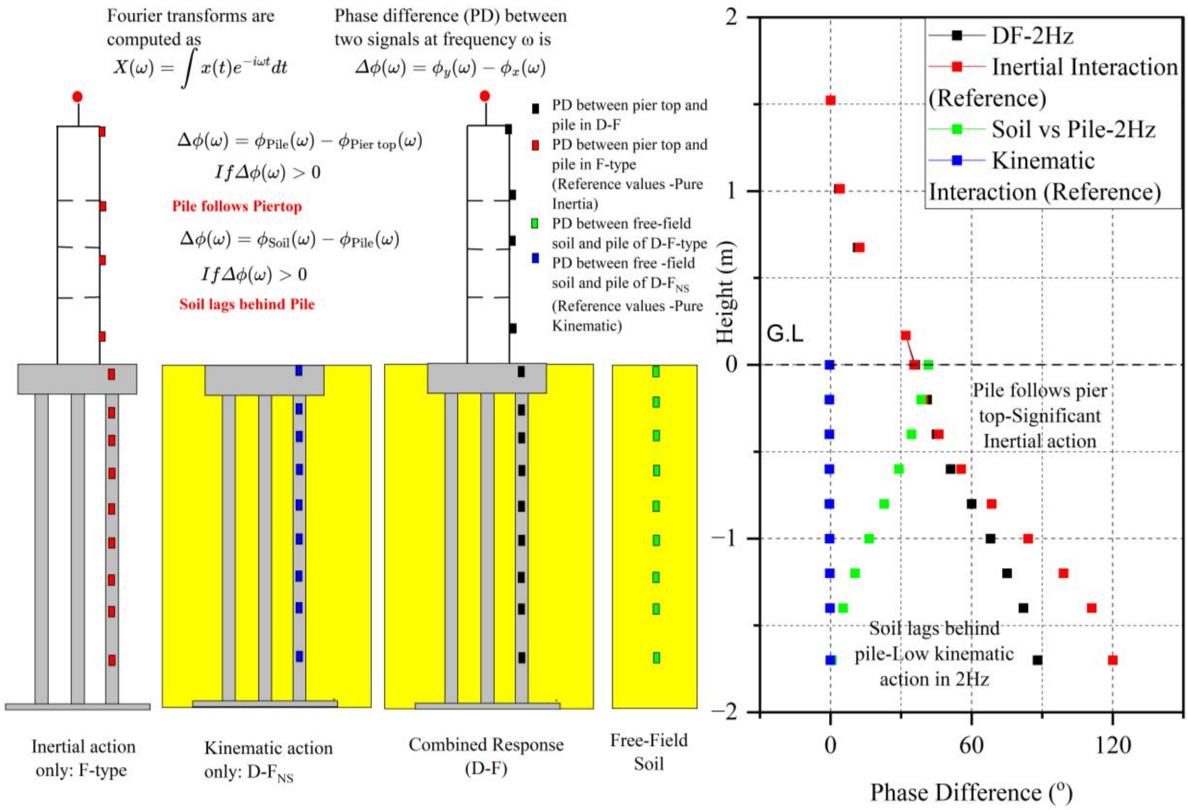

Figure 39. Phase difference calculation between pier top and pile, and soil and pile for DF type

Figure 39 illustrates the locations along the pier and pile where phase differences (PD) are evaluated with respect to the pier top for the D-F case, along with the corresponding soil depths (green boxes) used for kinematic assessment. The reference phase differences for inertial interaction are obtained from the F-type configuration, while those for kinematic interaction are derived from the DFNS case based on the phase relationship between free-field soil and pile response. The results indicate that the PD between the pier top and pile in the D-F case remains positive and closely matches the inertial reference case, confirming that the pile response follows the motion of the superstructure and is primarily governed by inertial interaction. In contrast, the PD between soil and pile in the D-F case is positive and opposite in trend to the kinematic reference case, where the phase difference is negative under pure kinematic loading. This suggests that soil motion lags behind the pile response and therefore contributes minimally to pile demand. Minor differences in PD observed in the lower portion of the pile between D-F and F-type cases can be attributed to soil influence and partial fixity at the pile base. Overall, the phase analysis confirms that inertial interaction dominates the pile response in the D-F system, with limited kinematic contribution.

4.2.3.2 Quantitative comparison of inertial and kinematic interactions:

To quantify the relative contributions of inertial and kinematic interactions in the D-F case, the responses from the F-type (inertial-only) and DFNS (kinematic-only) simulations are compared under the same sinusoidal input. The pile deformation and bending moment obtained from the combined analysis (D-F) lie between those from the F-type and DFNS cases. In addition, the pier displacement and bending moment responses in D-F closely match those of the F-type analysis, indicating a dominant influence of inertial forces. The isolated pile deformation due to inertial loading is approximately 1.5 times that of the combined response, whereas the kinematic contribution is only about 0.2 times. Similarly, the pile moment profile in the upper half shows strong agreement between D-F and F-type results, while in the lower half, the response lies between the inertial-only and kinematic-only cases, indicating a relatively greater kinematic contribution at depth.

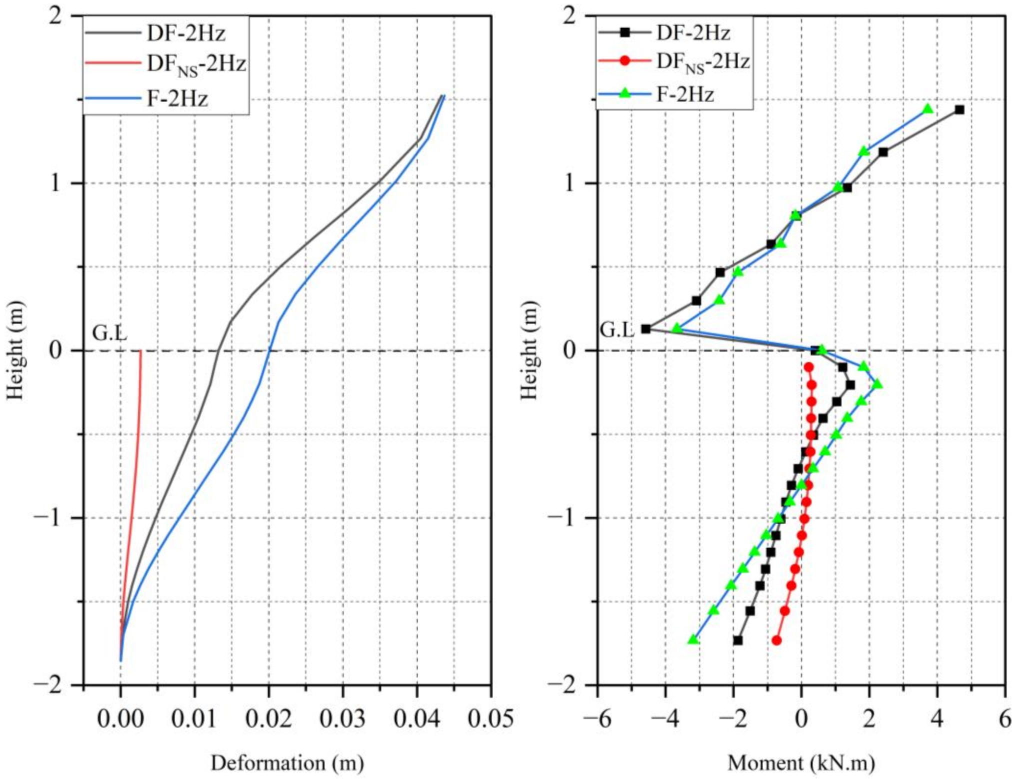

Figure 40. A comparison of isolated pile deformation and moment of kinematic and inertial interactions against the combined response in DF

Quantitatively, the kinematic interaction alone produces a pile head moment of approximately 0.18 times the combined response, whereas inertial interaction produces about 1.58 times the same value. This confirms that the pile response in the D-F case is primarily governed by inertial forces, with only a limited contribution from kinematic effects. The ratio of inertial to kinematic pile head moment is approximately 7, highlighting the dominant role of inertia. This behavior is attributed to the proximity of the input motion frequency to the natural frequency of the D-F system, which amplifies inertial response while limiting kinematic influence. The effect of frequency on these interaction mechanisms is further examined in the subsequent sections.

4.2.4 Parametric study on variation of input motion frequency:

After establishing the SSI mechanisms under the baseline excitation of 2 Hz and 200 gal, the chapter extends the investigation through a systematic parametric study in which the input frequency of the applied sinusoidal motion is varied. The purpose of this study is to clarify how the frequency content of excitation controls the balance between inertia-dominated and kinematic-dominated response in the smart bridge pier system and its supporting soil.

4.2.4.1 Input motion:

The parametric study begins by producing sinusoidal input waves with frequencies ranging from 1 Hz to 10 Hz. To ensure that comparisons across frequencies remain fair, the total energy associated with each ground motion is kept constant by adjusting the amplitude of acceleration. Arias intensity is adopted as the energy metric, and all input waves are scaled to a uniform reference value of about 270m/sec.

Arias Intensity represents the cumulative seismic energy of an input excitation transmitted to soil-structure system. It was proposed by Arias (1970) and accounts for both the amplitude and duration of shaking which makes it more suitable than instantaneous parameters like PGA when dealing with soil non-linearity and cumulative structural demands. It is defined as follows:

$$I_A = \frac{\pi}{2g}\int_0^T a^2(t)\,dt$$

where $a(t)$ represents the acceleration time history, g is acceleration due to gravity, and $T$is the input motion duration. The integration of the squared acceleration over time captures the total input energy delivered to the system.

A uniform Arias intensity ensures that all sinusoidal input waves—from 1 to 10 Hz—carry the same energy content. By scaling each wave to a constant Arias intensity, differences in response can be attributed solely to the effect of input frequency, not energy variation. Therefore, the acceleration amplitude is varied, the number of loading cycles is fixed at twenty for all cases, while the time step of the excitation is changed to achieve the intended frequency. Table. 8 presents the generated input waves and their Arias intensities is included to demonstrate equivalence of energy content across the entire frequency range.

Table 8. Excitation characteristics of various input motions

Input frequency (Hz)	**Number of cycles**	**Acceleration amplitude (m/sec^2)**	**Arias Intensity (m/sec)**
1	20	1.36	270
2	20	2.0	268
4	20	2.84	270
6	20	3.48	271
8	20	4.04	273
10	20	4.50	271

4.2.4.2 Phase Difference:

Phase difference (PD) is used as an indicator to identify the relative contributions of inertial and kinematic interactions to pile response. The PD between acceleration time histories of the pier top and various points along the pier and pile indicates whether the pile follows the superstructure response along its depth. Similarly, the PD between pile and free-field soil reflects the lag or lead of soil motion relative to the pile. Reference values for inertial interaction are obtained from the F-type configuration, while kinematic interaction is assessed through comparison with the DF_{NS} case.

Figure 41 presents the variation of PD along the height of the pier–pile system for different input frequencies listed in Table 8. For the 1 Hz case, the PD between pier top and pile is positive and consistent with the inertial reference, indicating that the pile follows the superstructure response. The PD between soil and pile is also positive and close to zero, suggesting that soil motion lags slightly and contributes minimally. A similar trend is observed at 2 Hz, where the pile response remains dominated by inertial interaction, with the pier top leading both pile and soil responses.

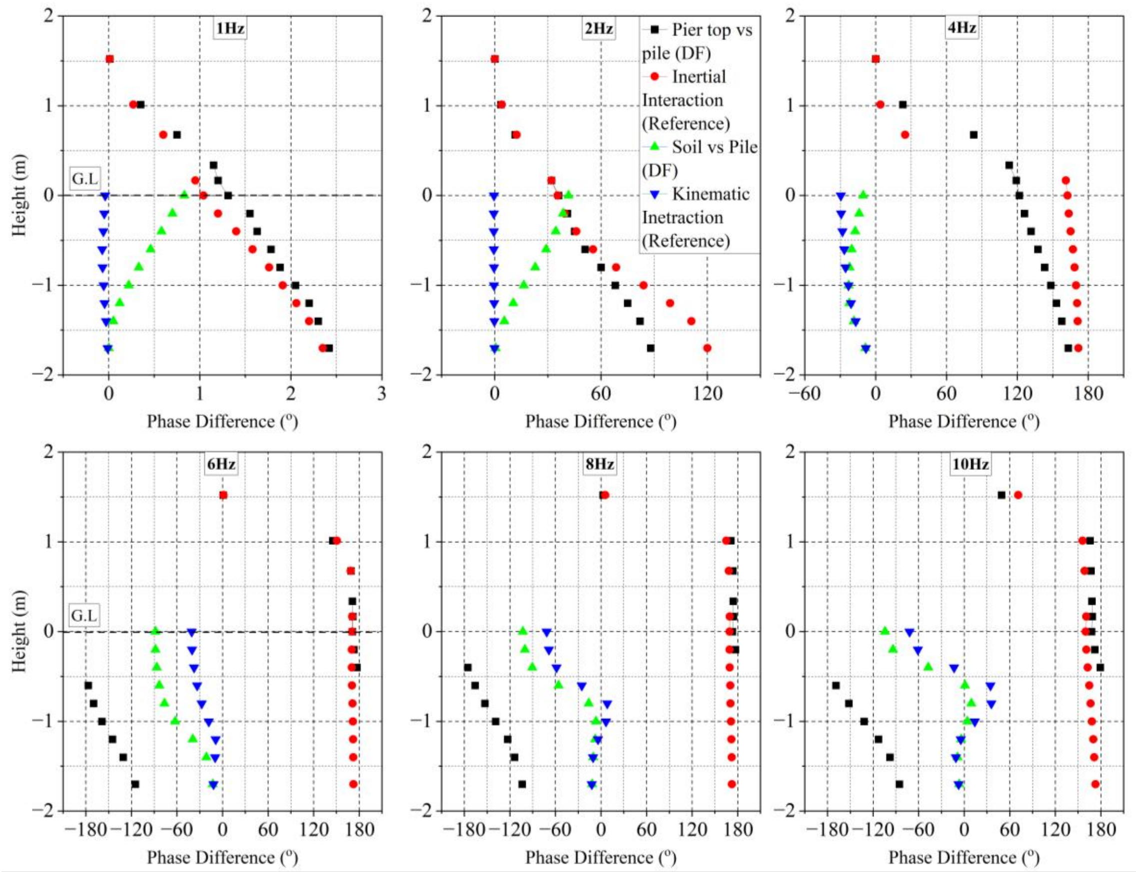

Figure 41. Phase difference between pier vs pile and pile vs free-field soil under various frequencies for DF-type structures

At 4 Hz, the response exhibits mixed behavior. The PD between soil and pile becomes negative and aligns with the kinematic reference case, indicating that the pile begins to follow soil motion. However, the PD between pier top and pile remains positive and consistent with the inertial reference, demonstrating that both inertial and kinematic interactions contribute significantly to the response.

For higher frequencies (6–10 Hz), the PD indicates that soil motion leads the pile response, while the influence of inertial interaction becomes limited. The pile follows both soil and structural motion, but the influence of the pier top is confined to the upper portion of the pile. This "inertial influence zone," defined by positive PD between pier and pile, extends to a depth of approximately 0.4 m at 6 Hz and reduces to about 0.2 m for 8 Hz and higher frequencies. Below this zone, the pile response is governed primarily by kinematic interaction.

To determine the direction of action of inertial and kinematic loadings, the phase difference of pier top and soil acceleration response (averaged over its depth) is determined by the following relationship:

$$\Delta\phi_{soil-pier}(\omega) = \phi_{pile-pier}(\omega) + \phi_{soil-pile}(\omega)$$

Therefore, table 9 listing the phase difference between soil (kinematic action) and pier acceleration (inertial action) is obtained. A positive phase difference values indicates a lead mechanism soil kinematic action compared to inertial action and vice versa applies for negative phase difference values. It indicates that a lead mechanism is observed in for 1-4Hz and a lag mechanism for 6-10Hz. To generalize the findings, frequencies range (1-10Hz) has been divided into three frequency ranges, namely low (1-2Hz), medium (4-6Hz) and high (8-10Hz). It is evident that soil tends to lead and matches its direction with the pier top response at low to medium frequency range. However, it tends to shift direction and turns against the pier top inertial action at medium to high frequency range (6-10Hz) as well. The directions could be understood using the animations placed alongside table 9.

Table 9. List of soil-pile phase differences for various input frequency cases

Input Freq. (Hz)	PD = Soil-Pier	Soil Response	Directions	Animations
1	2.30	Lead	Similar	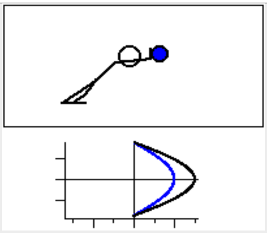
2	82.80	Lead	Similar	
4	124.90	Lead	Similar	
6	-103.90	Lag	Opposite	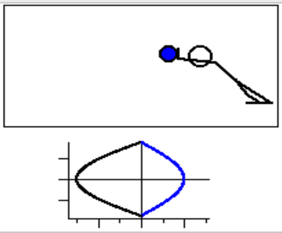
8	-114.10	Lag	Opposite	
10	-53.50	Lag	Opposite	

In summary, phase difference analysis provides a clear framework for interpreting the governing interaction mechanisms as well as clarifies their directions. The results indicate that inertial interaction dominates at lower frequencies (1–2 Hz) in similar direction with kinematic action, kinematic interaction governs at higher frequencies (6–10 Hz) in opposite direction to inertial interaction, and both mechanisms contribute significantly at intermediate frequencies (e.g., 4 Hz).

4.2.4.3 Moment and Deformation:

Fig. 42 shows the pier and pile moment distribution curves maximum bending moment measured in the pile for cases corresponding to inertia force only (F-type), kinematic force only (DF_{NS}) and under the combined action (D-F). The results are shown from left to right in the increasing order of input motion frequency.

First, the kinematic force only cases (DF_{NS}) are analysed and compared against each other. Secondly, the inertia force only cases (F-type) are compared against each other. Finally, the cases (D-F) which are under the combined action of inertial and kinematic force are discussed and compared against the respective F-type and DF_{NS} to reveal the respective impact of inertial and kinematic forces.

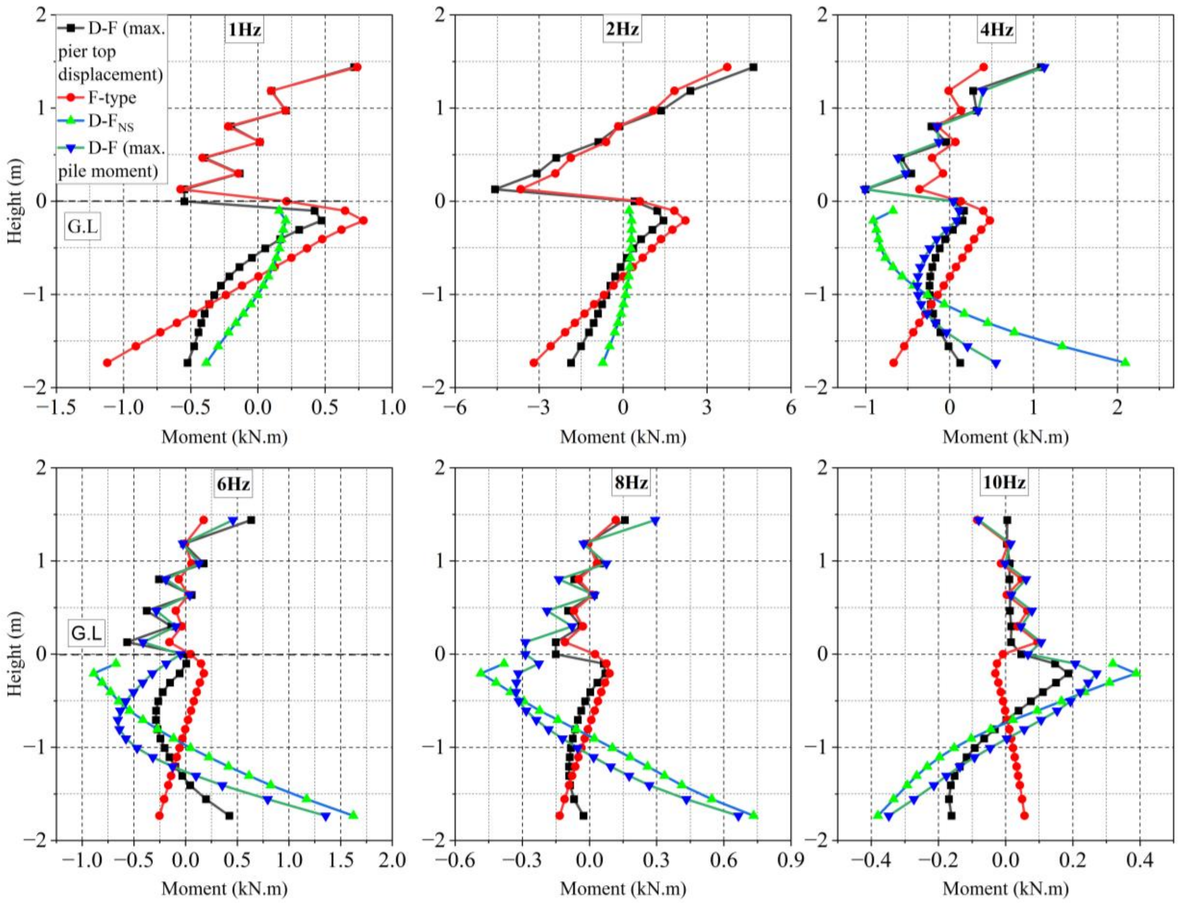

Figure 42. A comparison of pile bending from various cases (D-F, F-type and DF_{NS}) at various frequencies.

4.2.4.3.1 Kinematic interaction:

The shapes of pile bending moment profiles are approximately similar in all cases with maximum bending moment values observed in the pile are close to pile head and are presented in Fig. 43 for various cases. Although the values of pile moment near the pile tip are sometimes larger than the those near pile head, however, due to the reasons mentioned in the previous chapter pertaining to poor capability of the numerical model near pile tip, the values are not considered for comparison as maximum values. The maximum pile head moment is 0.91 kN.m across different frequencies and is observed at 4Hz. It should be noted that yield moment and plastic moment capacity of the pile section are about 6.14 kN.m and

8.41 kN.m approximately. This shows the importance of considering kinematic interaction effects while designing pile foundations in a relatively good condition soil since kinematic moment could represent 15% of pile yield moment.

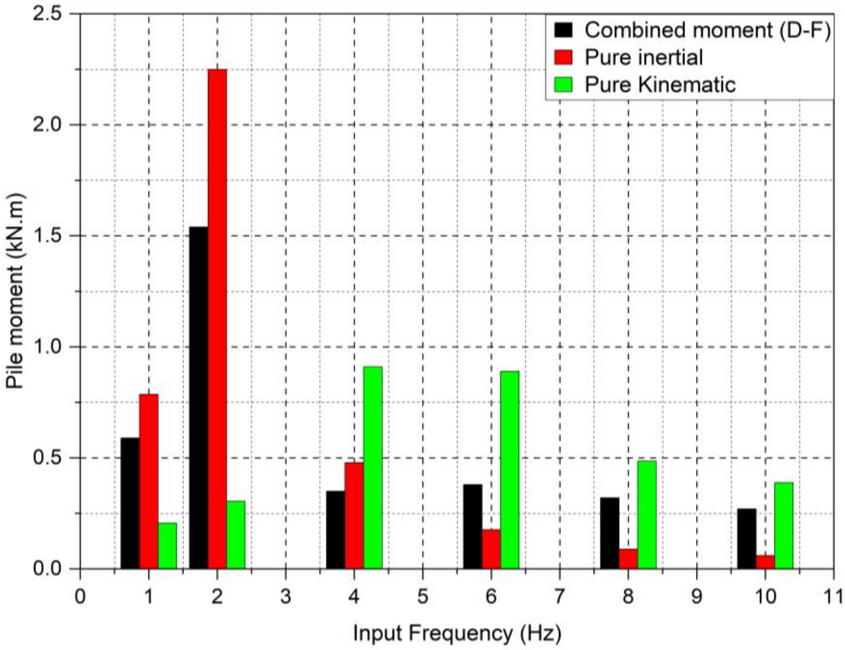

Figure 43. Maximum bending moment values near the pile head

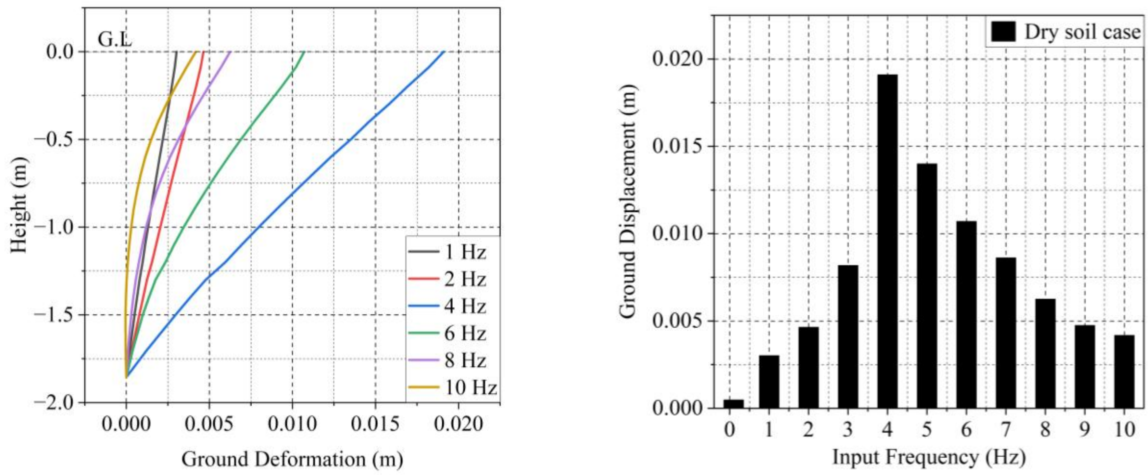

a) Ground deformation profile

b) Maximum value of ground deformation

Figure 44. Comparison of ground deformation of dry soil under various input excitations

Moreover, the reason behind maximum moment at 4Hz could be attributed to the fact that natural frequency of soil is about 6Hz and that of DF_{NS} configuration is about 6.5Hz. Therefore, while the input frequency is in the vicinity of those natural frequencies, kinematic effects are amplified. Moreover, it is also expected that response frequency of soil decays and decreases closer to 4Hz during shaking and this would cause the maximum pile moment at that frequency. This could also be confirmed by comparing the free-field soil deformation profiles at various frequencies that maximum surface ground deformation happens at 4Hz as shows in Fig. 44.

4.2.4.3.2 Inertial Interaction:

Bending moment profiles pertaining to F-type case are almost similar across various frequencies as shows in Fig. 42. It is a one-degree curve under inertial loading only and having no influence of a distributed kinematic load on the pile. The maximum inertial pile head bending moment across various frequencies is 2.25 kN.m and is observed at input frequency case of 2Hz as indicated in Fig. 43. This is because it is in close band of response frequency of F-type structure which leads to amplification of inertial acceleration and hence pile moment. Moreover, it represents about 37% of the yield moment capacity of pile section. This not only highlights the individual but relative importance of inertial interaction in the design of pile foundations.

4.2.4.3.3 Kinematic and Inertial Interactions:

The bending moment profiles for the D-F case, representing the combined effects of inertial and kinematic interactions, are shown in Fig. 42. A comparison across different input frequencies reveals notable differences in both the shape of the moment distribution and the timing of peak response. At lower frequencies (1–4 Hz), the instant of maximum pier-top displacement closely corresponds to the maximum pile head moment. In contrast, at higher frequencies (6–10 Hz), this correspondence no longer holds, and the maximum pile moment occurs at a different instant. Accordingly, additional moment profiles are presented for these cases at the instant of maximum pile head moment. Since maximum pier-top displacement coincides with peak inertial force, the close agreement at lower frequencies indicates inertial dominance, whereas the reduced moment values at higher frequencies highlight the diminishing influence of inertia.

Across all cases, the maximum pile moment is observed at 2 Hz, which is close to the dominant frequency of both F-type and D-F configurations, suggesting resonance at the pier top. At 1–2 Hz, the pile moment profile exhibits a smooth, single-curvature shape similar to that of the inertial-only case. Although the F-type response shows slightly higher moment values, the kinematic contribution remains limited, with the kinematic-only moment reaching approximately 19% of the combined response. This confirms that inertial interaction governs pile response at lower frequencies, consistent with phase difference results indicating that the pile follows the pier-top motion while soil response lags.

At 4 Hz, the response reflects a transition in behavior. The moment profile deviates from the single-curvature shape and exhibits characteristics of both inertial and kinematic interactions, with the upper portion aligning more closely with inertial response and the lower portion with kinematic response. Although the kinematic-only pile head moment reaches its maximum value of 0.91 kN·m at this frequency, the corresponding combined response is reduced to about 0.35 kN·m (approximately 38%), indicating significant counteraction by inertial effects. This demonstrates that both mechanisms contribute substantially at intermediate frequencies.

At higher frequencies (6–10 Hz), the pile moment profile in the D-F case increasingly resembles the kinematic response. At 6 Hz, inertial interaction contributes approximately 50% of the combined pile head moment, while the kinematic-only response is about three times larger, indicating strong counteraction between the two mechanisms. This interaction is depth-dependent: inertial effects are primarily confined to the upper portion of the pile (approximately 0.4 m from the pile head), while kinematic interaction dominates at greater depths. As frequency increases further (8–10 Hz), the inertial influence becomes limited to the immediate vicinity of the pile head, with the kinematic mechanism governing the overall pile response. This trend is consistent with phase difference analysis, which shows a progressive reduction in the depth of the inertial influence zone.

Figure 45 illustrates the deformation envelopes of the pier column and foundation piles for different configurations across various input excitation frequencies. A comparison of deformation profiles reveals notable differences in magnitude, shape, and pile head response at the instant of maximum pile bending moment. Since this instant does not always coincide with peak pier-top displacement, additional deformation profiles are presented for cases corresponding to the maximum pile head moment.

Across all frequencies, the maximum pier-top and pile deformations are observed at 2 Hz, which is close to the dominant frequency of both F-type and D-F configurations, indicating resonance effects. At lower frequencies (1–2 Hz), the pile deformation profile exhibits a smooth, single-curvature shape similar to the inertial-only case. Although the deformation values in the inertial-only case are slightly higher than those in the D-F case, the kinematic contribution remains limited, with the kinematic-only deformation reaching approximately 20% of the combined response. This confirms the dominant role of inertial interaction at lower frequencies.

At intermediate frequencies, both inertial and kinematic effects contribute significantly. Although the overall deformation magnitudes are relatively close, the deformation gradient differs, being steeper in the pier and milder along the pile. Inertial interaction alone produces a pile head deformation of approximately 0.0042 m, while kinematic interaction produces about 0.00734 m in the opposite direction. Their combined effect results in a significantly reduced net deformation at the pile head, indicating strong counteraction between the two mechanisms.

frequencies.

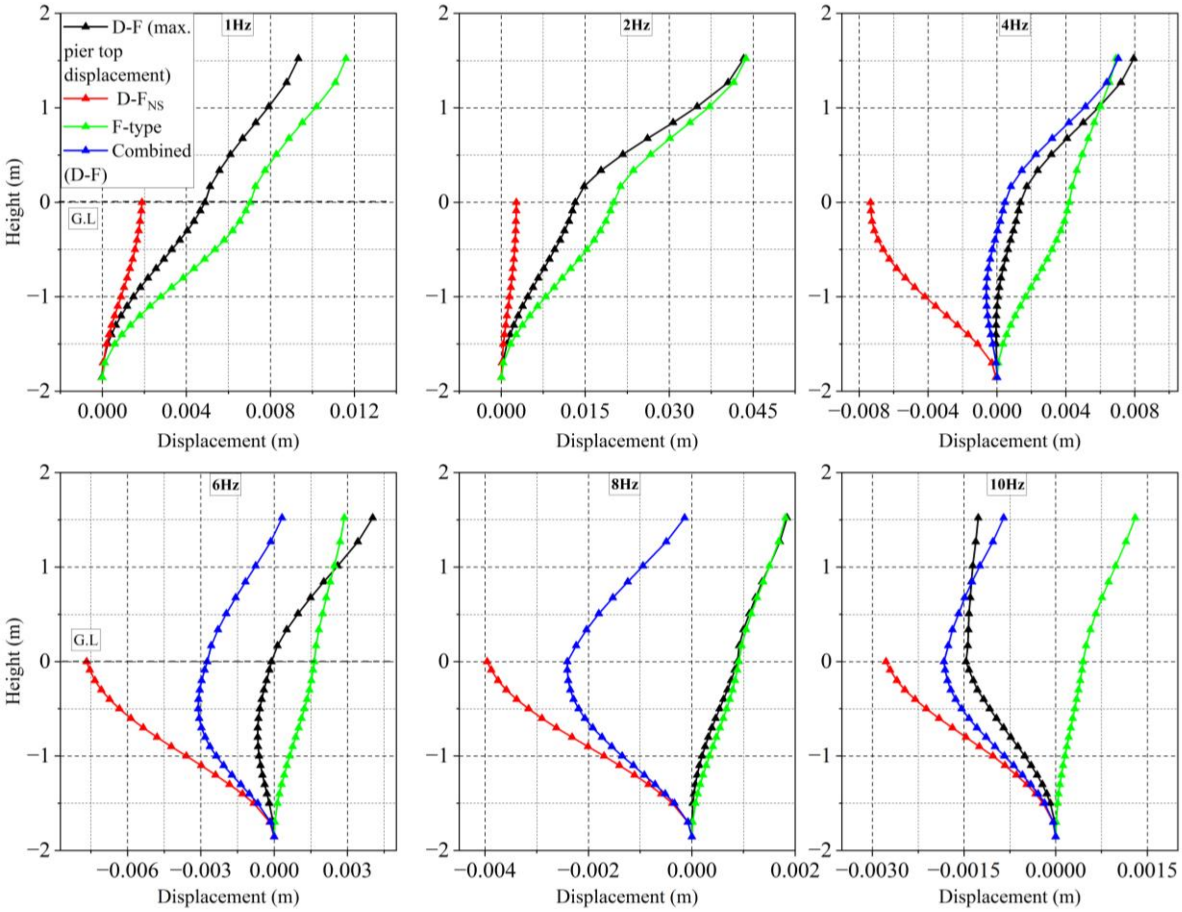

Figure 45. A comparison of pile deformation from various cases (D-F, F-type and DFNS) at various frequencies.

At higher frequencies (6–10 Hz), the deformation profile corresponding to maximum pile moment increasingly resembles the kinematic response. At 6 Hz, the inertial contribution produces a maximum pier-top deformation of only 0.00287 m, which is about 6.5% of the value at 2 Hz, indicating a reduced influence of inertia. As a result, inertial interaction primarily affects the pier and upper portion of the pile, while deformation in the lower part is governed by kinematic interaction. At 8–10 Hz, inertial influence is limited to the immediate vicinity of the pile head, and kinematic interaction dominates the overall pile deformation.

In summary, the observed deformation patterns are consistent with the bending moment results and phase difference analysis, confirming a frequency-dependent transition in the governing interaction mechanism. Inertial interaction dominates near the structural natural frequency, while kinematic interaction governs near the soil natural frequency, with both mechanisms contributing at intermediate

4.3 Footingless type with dry sand (D-S)

4.3.1 Time history analysis:

The time evolution of various response variables against an input sinusoidal wave of 2Hz and maximum amplitude of 2m/sec^2 are shown in Fig. 46. The pier top and pile head acceleration are approximately equally amplified by about 1.6 and 1.5 times the input acceleration respectively. Both are in almost phase with each other but slightly lag the input acceleration. Similarly, the pile head displacement is in phase with pier top, however, it has a clear phase difference with soil displacement. The evolution of pile bending to its maximum value is somewhat similar to inertia force at the pier top. Moreover, the value of earth pressure is generally in the range of 30-40% of the inertia force and is in opposite phase. This may enhance the contribution of kinematic action towards pile response. However, it should also be noted that the area of action of earth pressure is relatively low as compared to D-F type. Therefore, DS_{NS} analysis would be used to quantify the contribution of kinematic interaction.

4.3.2 Pile bending moment and deformations:

Figure 47 presents the bending moment and deformation profiles of the pile and surrounding ground at key instants, including maximum pile bending moment, maximum inertial force, and maximum ground displacement. At the instant of maximum pile bending moment, the peak value occurs at a depth of approximately 1.15 m with a magnitude of 1.318 kN·m, while the corresponding pile deformation reaches about 12 mm. The earth pressure at this stage is approximately 43% of the inertial force, indicating a notable contribution of kinematic interaction. A similar bending moment and deformation profile is observed at the instant of maximum inertial force, confirming the dominant role of inertia. In contrast, at the instant of maximum surface ground displacement, both inertial force and earth pressure are significantly lower and act in the same direction, resulting in reduced pile response, with bending moment and deformation decreasing to about 38% and 50% of their peak values, respectively, while inertia reduces to approximately 22% of its maximum. Despite large ground deformation, the relatively low earth pressure suggests a phase difference between soil displacement and the resulting soil–pile interaction force. This indicates a state where soil displacement toward the pile is at its maximum, while the pile response lags, and peak earth pressure develops only when the pile moves further into the soil. Furthermore, pile deformation in all cases follows the direction of inertial force, with a pronounced deformation gradient near the upper portion of the pile, suggesting that kinematic interaction either acts in the same direction as inertia or has a limited opposing effect. These observations highlight the importance of phase relationships in understanding kinematic contributions, which will be further examined through decomposition of inertial and kinematic interactions in the subsequent section.

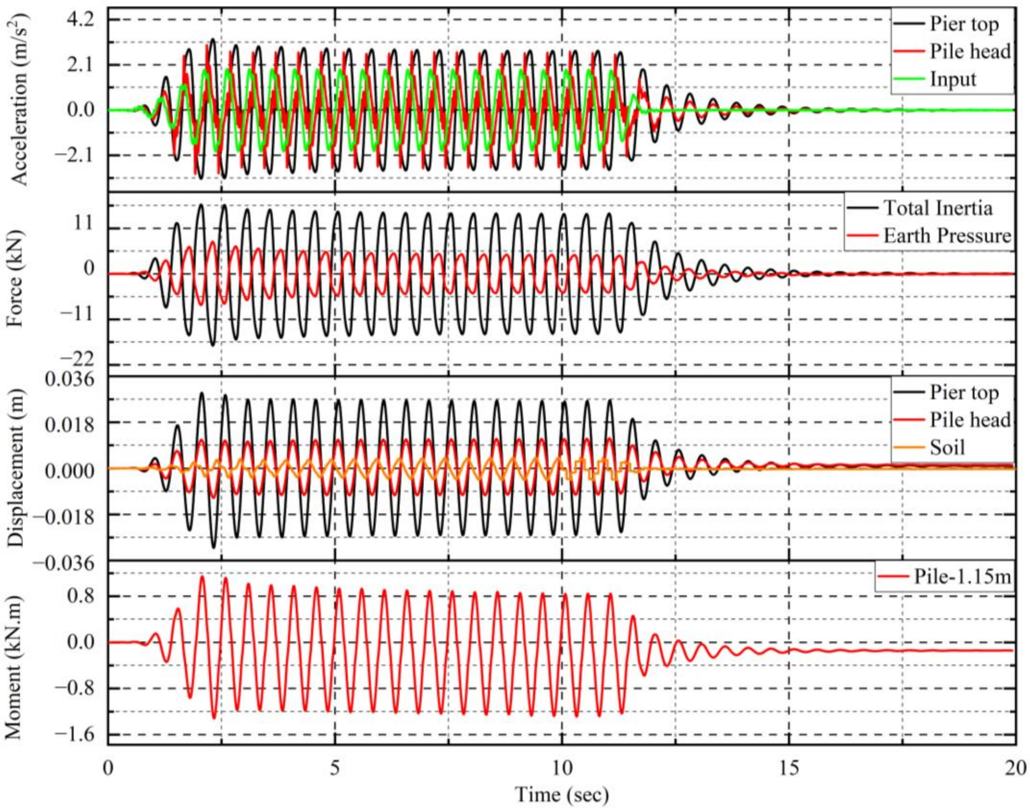

Figure 46. Time evolution of various response parameters for D-S type

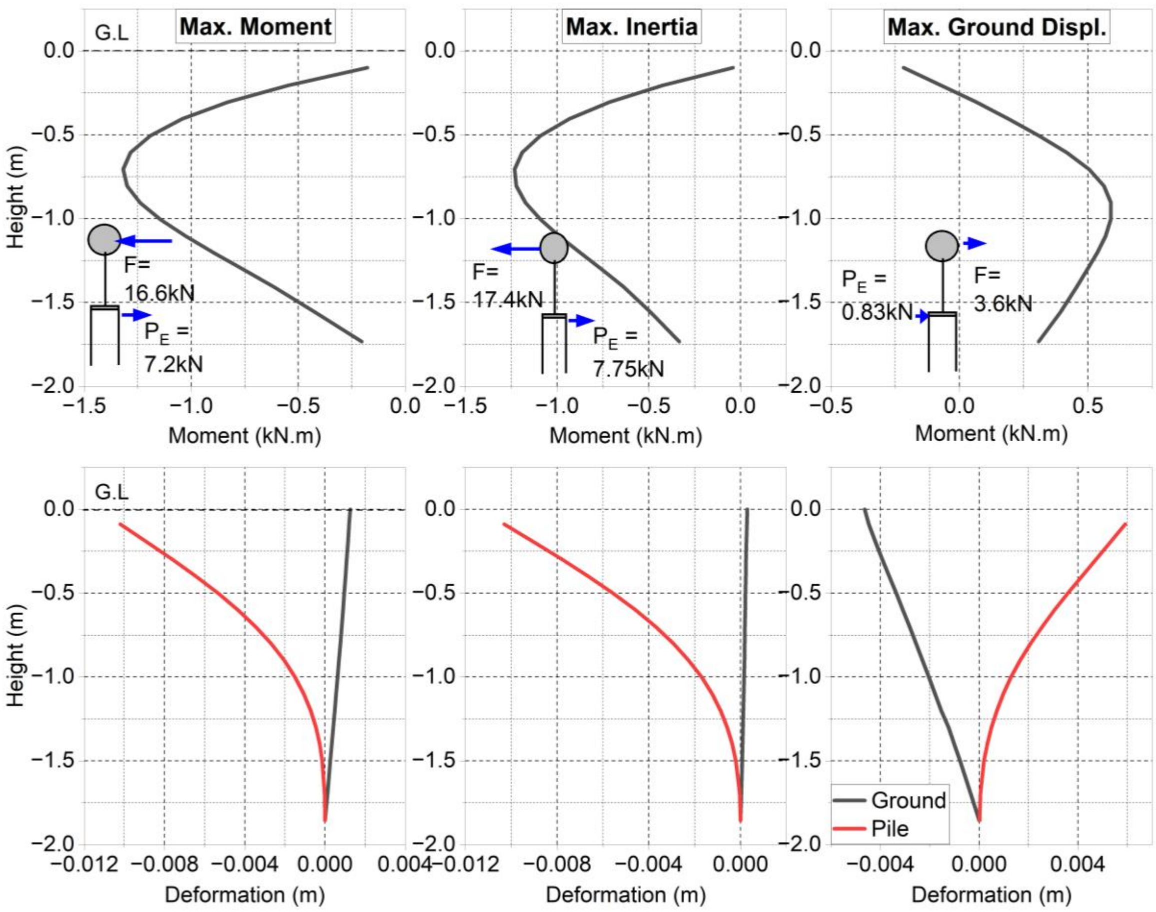

Figure 47. Bending moment and deformation envelopes of piles and ground at key instances

Figure 48 illustrates the locations along the pier and pile where phase differences (PD) are evaluated with respect to the pier top for the D-S case, along with the corresponding soil depths (green boxes) used for assessing kinematic interaction. The reference phase differences representing inertial-only behavior are obtained from the S-type configuration and shown as red dots, while the phase difference between free-field soil and pile in the D-S_{NS} case serves as the reference for pure kinematic interaction. The results indicate that the PD between the pier top and pile remains positive in the D-S case, implying that the pile response follows the motion of the superstructure. Furthermore, the PD values along the depth are consistent with those of the inertial reference case, highlighting the dominant influence of pier-top acceleration. In contrast, the PD between soil and pile is also positive, indicating that soil motion lags behind the pile and therefore contributes minimally to kinematic loading. Although the reference kinematic PD is slightly negative and close to zero, the observed phase relationship in the D-S case is qualitatively opposite to that of the pure kinematic condition. This confirms that the pile response in the D-S system is predominantly governed by inertial interaction.

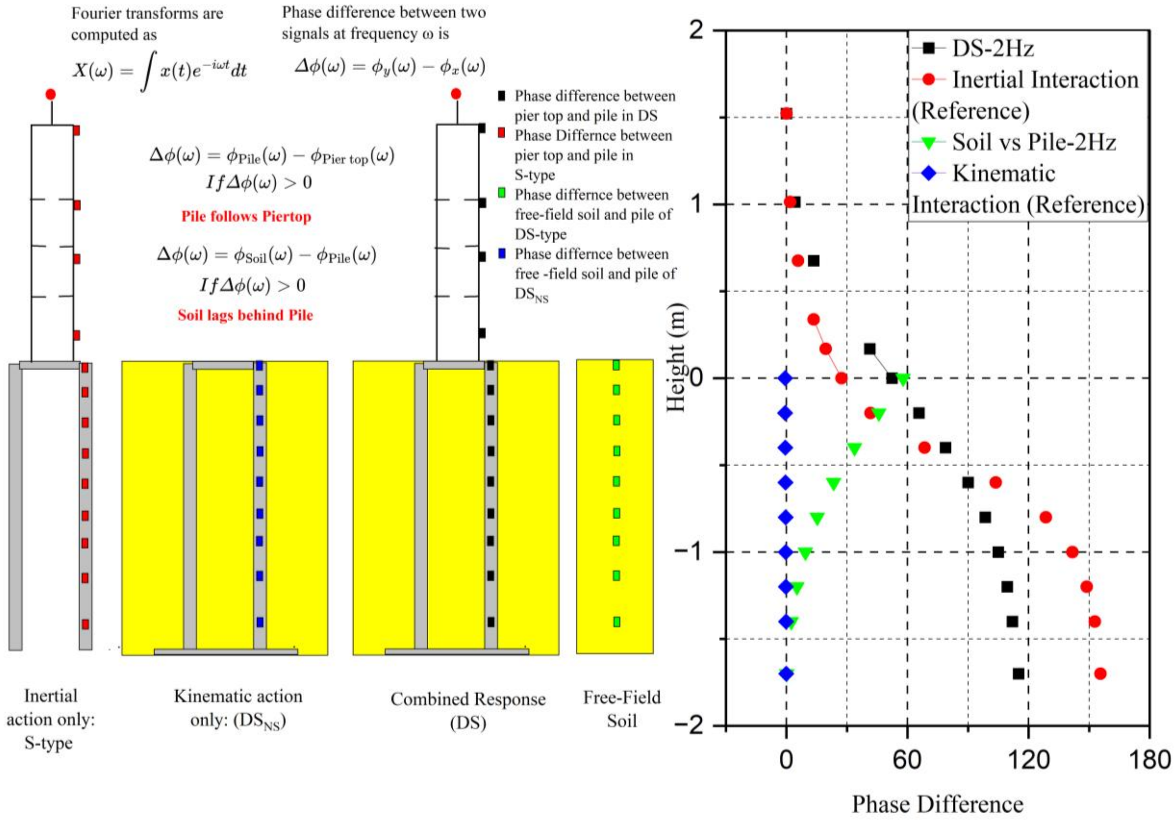

Figure 48. Phase difference calculation between pier top and pile, and soil and pile for DS type

4.3.3 Quantitative comparison of inertial and kinematic interactions:

To quantify the relative contributions of inertial and kinematic interactions in the D-S case, the responses from the S-type (inertial-only) and DSNS (kinematic-only) simulations are compared under the same sinusoidal input. Similar to the D-F case, the pile deformation in D-S lies between the inertial-only and kinematic-only responses. However, unlike D-F, the pier displacement and bending moment in D-S are slightly larger than those of the S-type configuration. This can be attributed to the closer proximity of the input frequency (2 Hz) to the natural frequency of the D-S system (1.8 Hz), which enhances inertial amplification compared to the S-type system. The isolated pile deformation due to inertial loading is approximately 1.4 times the combined response, while the kinematic contribution is about 0.27 times. A comparison of pile moment profiles shows that, similar to D-F, the upper portion of the pile is governed by inertial interaction, whereas the lower portion exhibits a stronger influence of kinematic interaction.

Quantitatively, the kinematic-only case produces a maximum pile moment of about 0.29 kN·m near the ground surface, while the inertial-only case results in a pile head moment of approximately 1.5 kN·m.

In contrast to D-F, where the maximum moment occurs near the pile head, the peak pile moment in D-S is located at a depth of approximately 0.7 m below the ground surface. This shift is attributed to the combined effects of soil confinement and the restraining action of the underground beam, which reduce bending demand at the pile head. Although the locations of maximum moment differ among D-S, S-type, and DSNS cases, the relative contributions remain consistent: kinematic interaction produces about 0.22 times, and inertial interaction about 1.15 times, the combined response. The ratio of inertial to kinematic contribution is approximately 5.2, indicating that inertial interaction still governs the pile response in D-S, though to a lesser extent than in D-F. This highlights a relatively increased role of kinematic interaction in the D-S system. As observed in the D-F case, the balance between these mechanisms is strongly dependent on input frequency, which is further examined in the subsequent sections.

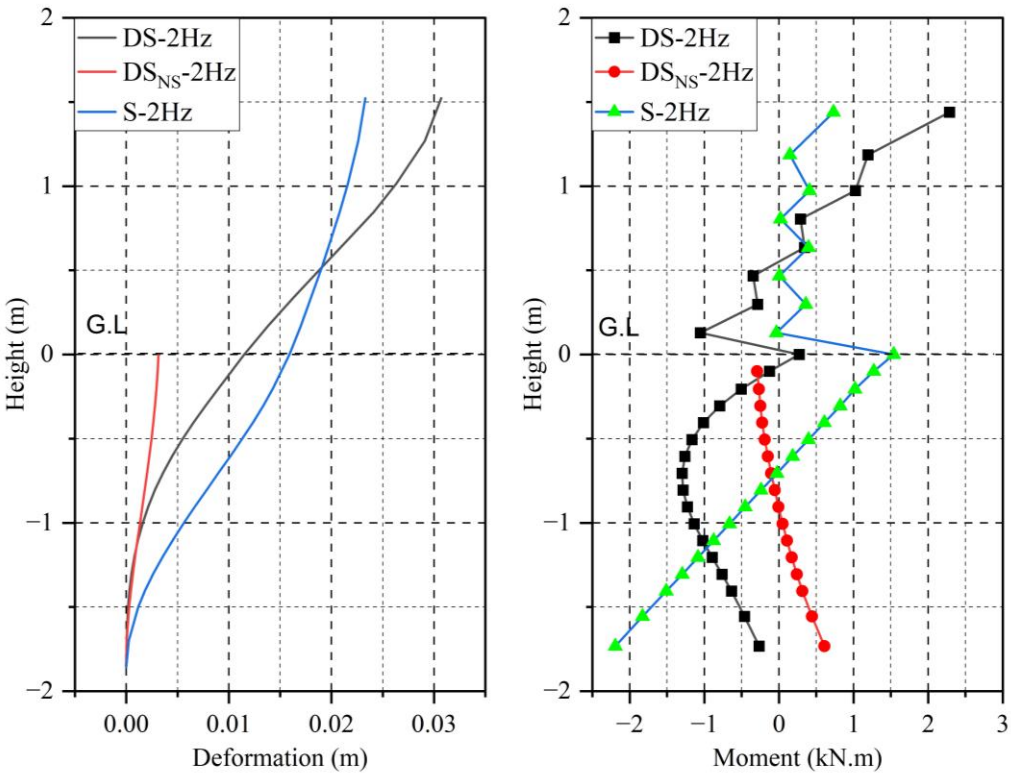

Figure 49. A comparison of isolated pile deformation and moment of kinematic and inertial interactions against the combined response in DS

4.3.4 Parametric study on variation of input motion frequency:

After establishing the SSI mechanisms under the baseline excitation of 2 Hz and 200 gal, the chapter extends the investigation through a systematic parametric study in which the input frequency of the applied sinusoidal motion is varied while maintaining a constant Arias intensity. It decouples the kinematic and inertial interactions through phase difference analysis and comprehending the moment and deformation envelopes of pile and pier obtained from various analysis configurations.

4.3.4.1 Phase Difference:

Phase difference (PD) is used as an indicator to identify the relative contributions of inertial and kinematic interactions to pile response. The PD between acceleration time histories of the pier top and various points along the pier and pile (shown by black boxes in Fig. 50) indicates whether the pile follows the superstructure response along its depth. The PD between pile and free-field soil (green dots) represents the lag or lead of soil motion relative to the pile. Reference values for inertial interaction are obtained from the S-type configuration (red dots), while the PD between free-field soil and pile in the DSNS case (blue dots) serves as the reference for kinematic interaction.

Figure 50 presents the variation of PD along the height of the pier–pile system for different input frequencies listed in Table 8. These results provide the basis for evaluating the relative dominance of inertial and kinematic interactions in the D-S system across the frequency range.

The phase difference profiles are analyzed starting from the 1 Hz case. The PD between pier top and pile remains positive and closely matches the inertial reference (S-type), indicating that the pile follows the superstructure response. In contrast, the PD between soil and pile is positive, whereas the kinematic reference case shows slightly negative values, indicating that soil motion lags behind the pile and contributes minimally. A similar trend is observed at 2 Hz, where the pier top leads both pile and soil responses, confirming the dominance of inertial interaction. This behavior is consistent with the D-F case, although the influence of kinematic interaction is slightly more pronounced in D-S.

At 4 Hz, the response exhibits transitional behavior similar to that observed in the D-F case. The pile–soil PD becomes negative and aligns with the kinematic reference, indicating that the pile begins to follow soil motion. However, the pier-top–pile PD remains positive and consistent with inertial interaction up to a depth of approximately 0.7 m, beyond which it deviates from the inertial reference. This suggests that both inertial and kinematic interactions contribute significantly, with inertia governing the upper portion of the pile and kinematic effects dominating at greater depths.

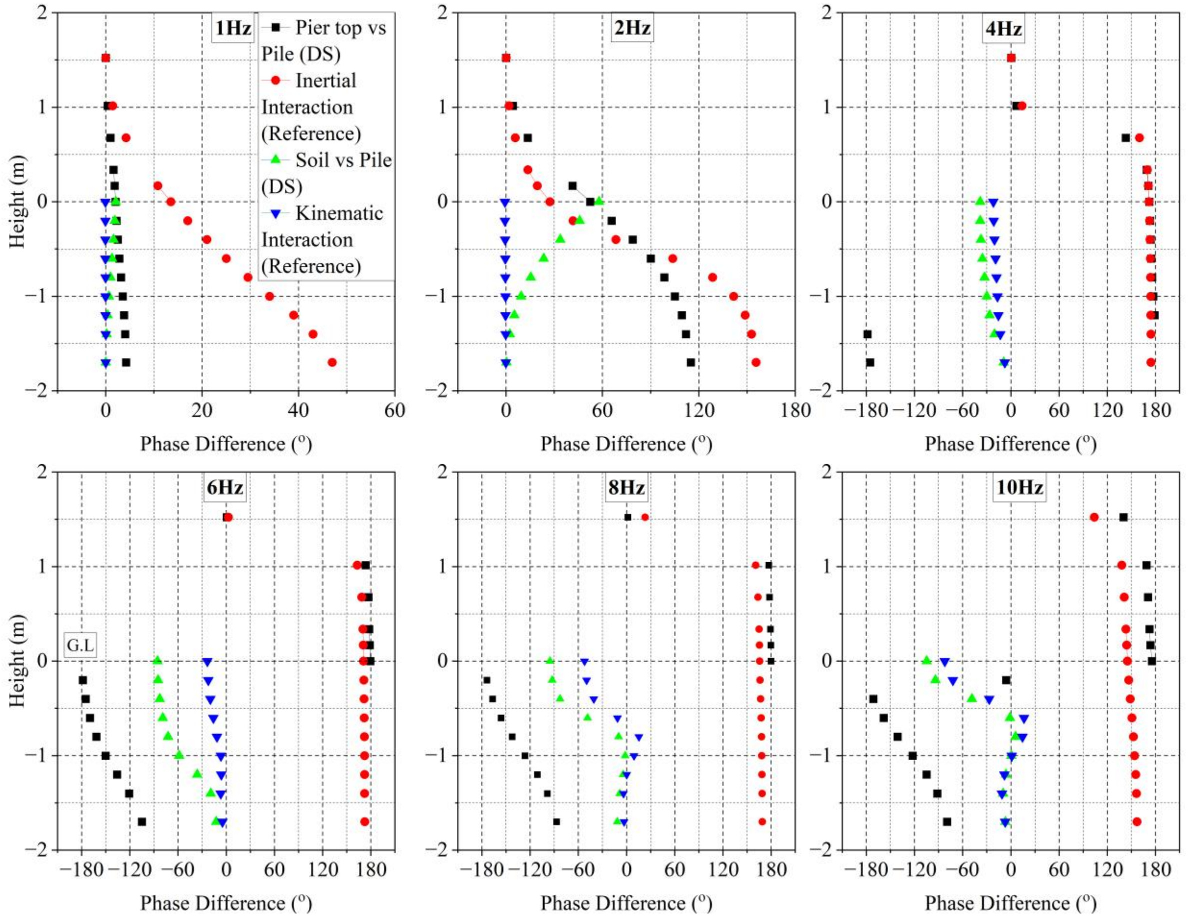

Figure 50. Phase difference between pier vs pile and pile vs free-field soil under various frequencies for DS-type structures

For higher frequencies (6–10 Hz), the PD indicates that soil motion leads the pile response, while the contribution of inertial interaction becomes increasingly limited. The pile follows both soil and structural motion, but the influence of the pier top is confined to a shallow "inertial influence zone" near the ground surface. This zone extends to about 0.2 m at 6 Hz and reduces to nearly zero for 8–10 Hz, indicating that kinematic interaction governs the pile response over most of its length. Compared to the D-F case, this transition occurs more rapidly in the D-S system, highlighting the relatively stronger role of kinematic interaction.

The values of soil-pier phase difference for D-S, L-F and L-S cases are presented at the end of this chapter as concluding summary. However, it is found that inertial and kinematic actions are found to have similar directions at low frequencies (1-2Hz) and opposite directions at medium to high frequencies (4-10Hz) for all D-F, D-S, L-F and L-S cases.

In summary, phase difference analysis confirms a frequency-dependent transition in the governing interaction mechanism. Inertial interaction dominates at lower frequencies (1–2 Hz), kinematic interaction governs at higher frequencies (6–10 Hz), and both mechanisms contribute significantly at intermediate frequencies (e.g., 4 Hz). Compared to the D-F case, the D-S system exhibits an earlier and more pronounced shift toward kinematic dominance.

4.3.4.2 Moment and Deformation profiles:

Fig. 51 shows the pier and pile moment distribution curves maximum bending moment measured in the pile for cases corresponding to inertia force only (S-type), kinematic force only (DS_{NS}) and under the combined action (D-S). The results are shown from left to right in the increasing order of input motion frequency.

First, the kinematic force only cases (DS_{NS}) are analysed and compared against each other. Secondly, the inertia force only cases (S-type) are compared against each other. Finally, the cases (D-S) which are under the combined action of inertial and kinematic force are discussed and compared against the respective S-type and DF_{NS} to reveal the impact of inertial and kinematic forces.

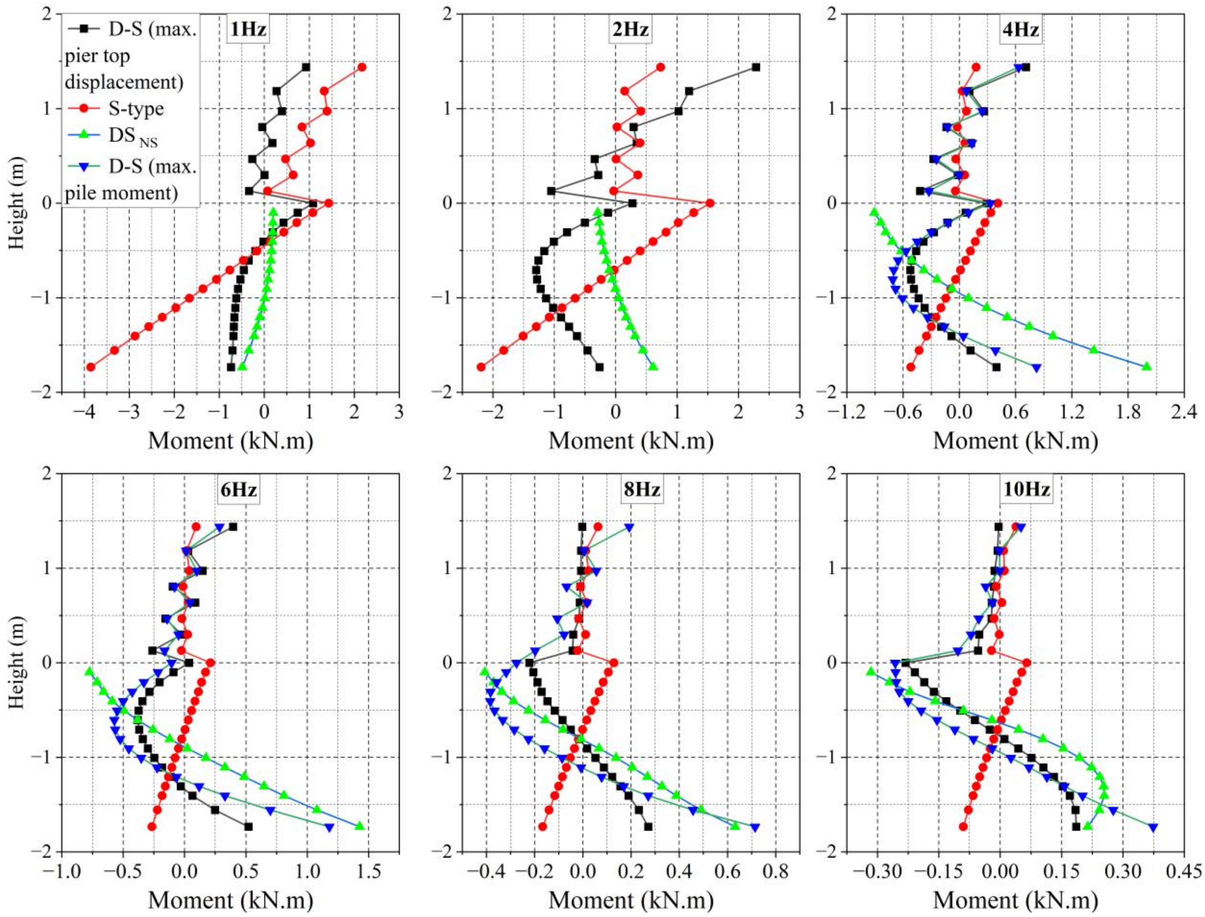

Figure 51. A comparison of pile bending from various cases (D-S, S-type and DS_{NS}) at various frequencies.

4.3.4.2.1 Kinematic interaction:

The pile bending moment profiles for the D-S case are shown in Fig. 52. The overall shape of the profiles remains similar across different frequencies, with maximum bending moments generally occurring near the pile head. Although higher values are occasionally observed near the pile tip, these are not considered for comparison due to known limitations of the numerical model in that region, as discussed previously. The maximum pile head moment is approximately 0.90 kN·m, occurring at 4 Hz, followed by the 6 Hz case. This value corresponds to about 15% of the pile yield moment.

The peak moment at 4 Hz can be attributed to the proximity of the input frequency to the natural frequencies of the soil (≈6 Hz) and the DSNS configuration (≈6.3 Hz), leading to amplification of kinematic interaction. Additionally, the effective response frequency of the soil may decrease during shaking, shifting closer to 4 Hz and further enhancing pile demand. This behavior is supported by free-field soil deformation profiles (Fig. 44), which show maximum surface ground deformation at 4 Hz. These observations are consistent with earlier findings, indicating that kinematic interaction becomes dominant when the input frequency approaches the natural frequency of the soil.

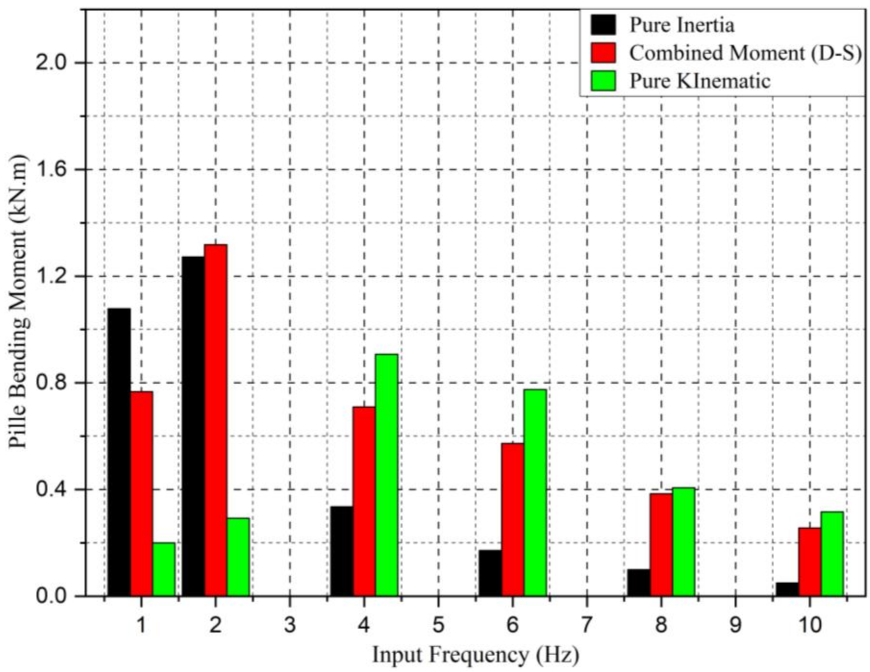

Figure 52. Maximum values of pile moment in S-type configuration

4.3.4.2.2 Inertial Interaction:

Bending moment profiles pertaining to S-type case are almost similar across various frequencies as shows in Fig. 52. It is a one-degree curve under inertial loading only without the influence of a distributed kinematic load on the pile. The maximum inertial pile head bending moment across various frequencies is 1.99 kN.m and is observed at input frequency case of 1Hz as indicated in Fig. 52. This is because it is in close band of response frequency of S-type structure which leads to amplification of inertial acceleration and hence pile moment. Moreover, it represents about 32% of the yield moment capacity of pile section. This not only highlights the individual but relative importance of inertial interaction in the design of pile foundations.

4.3.4.2.3 Kinematic and Inertial Interactions:

The bending moment profiles for the D-S case, representing the combined effects of inertial and kinematic interactions, are shown in Fig. 51. A comparison across different input frequencies reveals variations in both the shape of the moment distribution and the timing of peak response. At lower frequencies (1–4 Hz), the instant of maximum pier-top displacement closely corresponds to the maximum pile moment, indicating strong inertial control. In contrast, at higher frequencies (6–10 Hz), this correspondence weakens, and the maximum pile moment occurs at a different instant. Consequently, additional moment profiles are presented for these cases at the instant of maximum pile moment. The reduced agreement at higher frequencies reflects the diminishing influence of inertial interaction. Compared to the D-F case, however, the difference between these two instants is less pronounced in D-S, which can be attributed to the lower stiffness of the D-S foundation system, leading to relatively larger pile moments even at the instant of maximum pier-top displacement.

Across all frequencies, the maximum pile moment in D-S is observed at 2 Hz, which is close to the dominant frequency of the system, indicating resonance effects. At 1–2 Hz, the pile moment distribution near the head resembles that of the inertial-only (S-type) case. However, the inertial-only response is 40% and 18% higher than the D-S response at 1 Hz and 2 Hz, respectively, indicating a non-negligible kinematic contribution. The kinematic-only case (DSNS) produces moment profiles that qualitatively match the lower portion of the pile but contribute only about 20–22% of the combined response. These observations confirm that inertial interaction dominates at lower frequencies, consistent with phase difference results showing that the pile follows the superstructure while soil response lags.

At 4 Hz, the response exhibits a clear transition. The pile moment profile deviates from the inertial shape even in the upper region and aligns more closely with the kinematic profile in the lower portion. The maximum kinematic pile head moment (0.90 kN·m) exceeds the inertial value (0.41 kN·m), while the combined response (0.71 kN·m) lies between the two. This indicates that kinematic interaction becomes significant and partially counteracted by inertia. Notably, inertial interaction reduces the kinematic response by only about 12%, highlighting the increasing dominance of kinematic effects, particularly below a depth of approximately 1.15 m. This interpretation is consistent with phase difference analysis, which indicates combined interaction near the pile head and kinematic dominance at greater depths.

At higher frequencies (6–10 Hz), the pile moment profile in D-S increasingly approaches the kinematic envelope. At 6 Hz, inertial interaction contributes approximately 38% of the combined pile head moment, while the kinematic-only response is about 1.35 times larger, indicating strong counteraction between the two mechanisms. However, this inertial influence is limited to the upper portion of the pile. The depth of the inertial influence zone, identified from phase difference analysis, is approximately 0.2 m from the pile head (corresponding to about 1.7 m in Fig. 41), and reduces further to about 0.1 m at 8–10 Hz. Below this zone, kinematic interaction fully governs the pile response. These results confirm a more rapid transition toward kinematic dominance in the D-S system compared to the D-F case.

Figure 53 illustrates the deformation envelopes of the pier column and foundation piles for different configurations across various input excitation frequencies. A comparison of deformation profiles shows clear variations in magnitude, shape, and pile head response at the instants of maximum pile bending moment and peak pier-top displacement.

Across all cases, the maximum pier-top and pile deformations in the D-S system occur at 2 Hz, which is close to its dominant frequency, indicating resonance effects. At this frequency, the pile deformation profile closely resembles that of the inertial-only (S-type) case, particularly near the pile head. However, the deformation values in the inertial-only case are slightly larger than those in the D-S case, indicating a counteracting influence of kinematic interaction. The kinematic-only response produces deformation profiles that differ from the combined case and contributes only about 26–27% of the pile head deformation in D-S. Conversely, the pile head deformation in the D-S case is significantly lower than that of the inertial-only case, reflecting reduced inertial amplification due to the difference in system frequencies. This behavior highlights that inertial interaction dominates when the input frequency is close to the structural natural frequency (1–2 Hz), while kinematic effects play a secondary but non-negligible role.

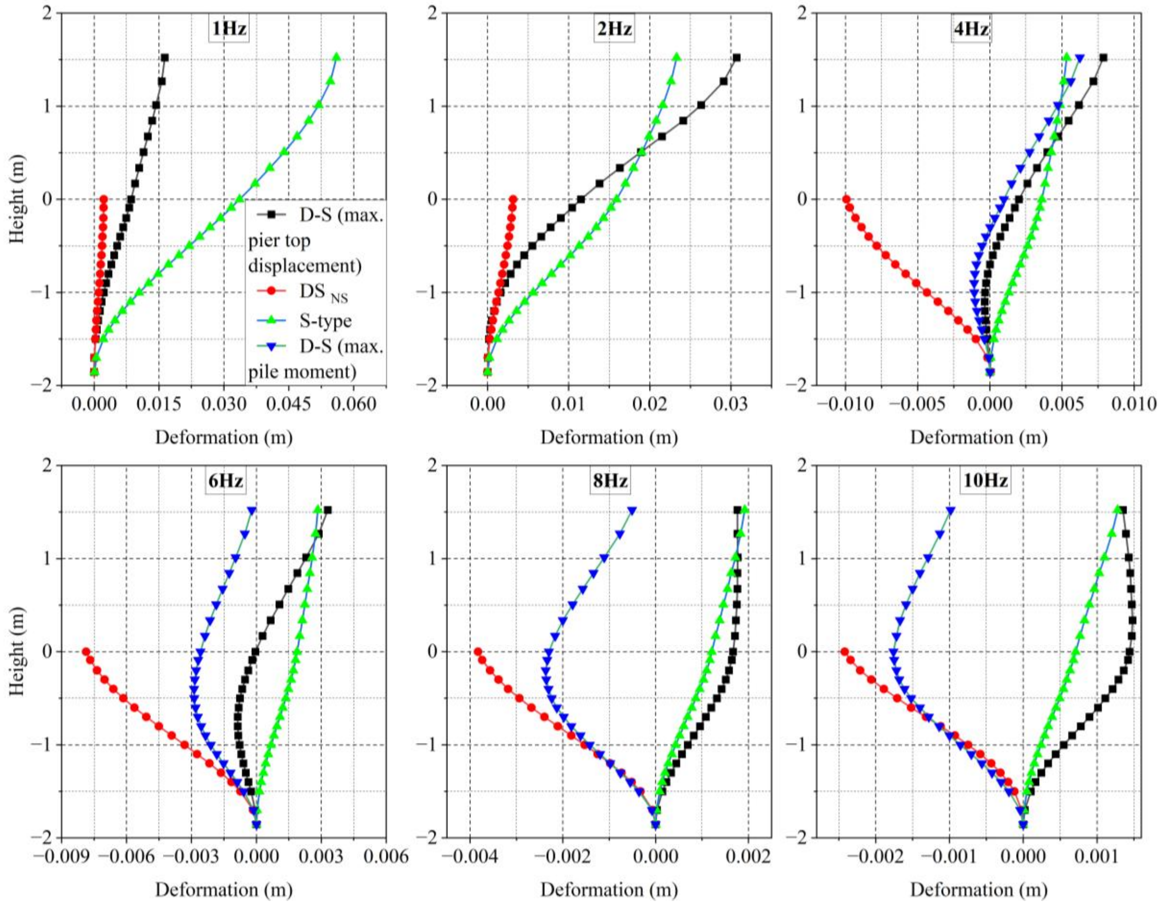

Figure 53. A comparison of pile deformation from various cases (D-S, S-type and DS_{NS}) at various frequencies.

At 4 Hz, the deformation profile of the D-S system reflects a transition in behavior. The overall shape partially resembles that of the inertial-only (S-type) case, particularly at the pier top, where displacement values are similar. However, the deformation gradient is relatively mild along the pile and steeper in the pier, indicating a redistribution of deformation. The inertial-only case produces a pile head deformation of approximately 0.0053 m, while the kinematic-only case produces about 0.00994 m in the opposite direction. Their combined effect reduces the pile head deformation in the D-S case to approximately 0.002 m, with near-zero or slightly negative deformation at greater depths. This strong counteraction indicates that kinematic interaction plays a significant role in governing pile response at this frequency. At higher frequencies (6–10 Hz), the deformation profile corresponding to maximum pile moment in the D-S case increasingly approaches the kinematic response. At 6 Hz, inertial interaction produces a maximum pier-top deformation of approximately 0.00287 m, which is only about 5% of the value observed at 1 Hz, indicating a substantial reduction in inertial influence. As a result, inertial effects are confined to the pier and the upper portion of the pile, while deformation in the lower part follows the direction of kinematic loading. At 8–10 Hz, the influence of inertia becomes negligible and is limited to the immediate vicinity of the pile head, with kinematic interaction fully governing the deformation response.

In summary, the deformation behavior is consistent with the trends observed in bending moment and phase difference analyses. The results confirm that the system response is strongly dependent on the frequency content of the input motion. Inertial interaction dominates when the input frequency is close to the structural natural frequency, whereas kinematic interaction governs when the input frequency approaches the natural frequency of the soil. At intermediate frequencies, both mechanisms contribute significantly through interaction and counteraction effects.

4.4 Footing type with dry sand (L-F)

4.4.1 Time history analysis:

Let's start with a time history analysis of various response variables as shown in Fig. 54. Input motion is a sinusoidal wave of 2Hz and maximum amplitude of 2m/sec^2. The pier top and pile head acceleration are amplified by about 3.1 and 2.0 times the input acceleration. Both are in phase with each other but slightly lag the input acceleration. Similarly, the pile displacement is in phase with pier top, however, it has a clear phase difference with soil displacement (and tends to lag soil-check with PD values). The evolution of pile bending to its maximum value is similar to inertia force at the pier top and unlike the soil surface displacement. Moreover, the value of earth pressure is quite low compared to inertia force. Therefore, the time history analysis of these parameters suggest that inertia force could be a major contributor of the pile response.

4.4.2 Pile bending moment:

Figure 55 shows the bending moment and deformation profiles of pile and ground at various instances such as maximum pile bending moment, maximum inertial force and maximum ground displacement. At the instant of maximum pile bending moment, the pile moment near the head reaches to 1.95 kN.m and pile deformation also reaches close to its maximum value of 17mm. Inertia force is about of six times of earth pressure and both act in the same directions.

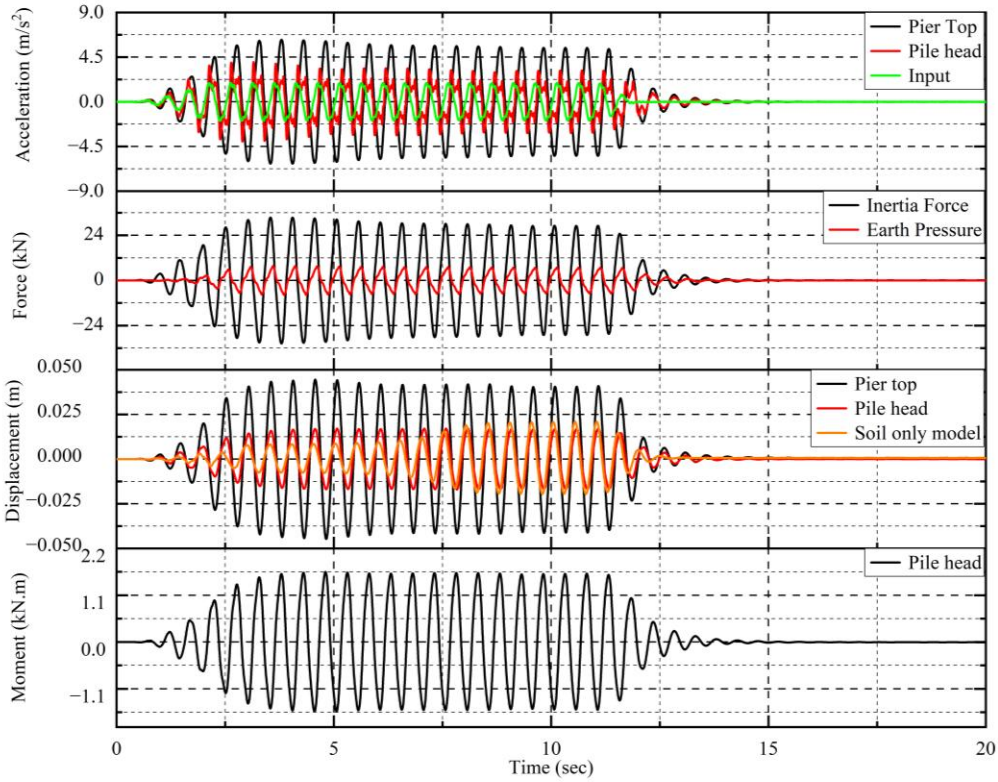

Figure 54. Evolution of various response parameters along the course of excitation for L-F type

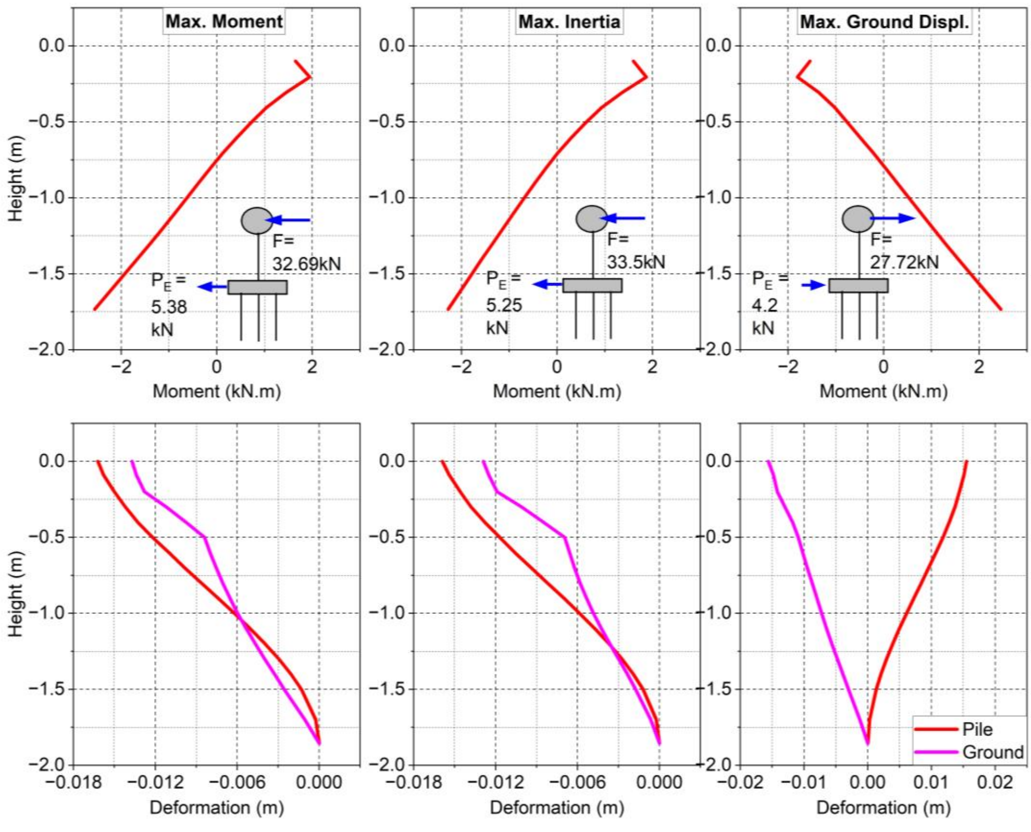

Figure 55. Pile bending moment and deformation profiles at various instances

The instant of maximum inertia force produces a similar bending moment and deformation profile of pile and a similar relationship of inertia and earth pressure force. Whereas the instant of maximum of surface soil deformation notes a 20% and 15% reduction in value of earth pressure and inertia force respectively and consequently, the pile bending moment as well as deformation is reduced by about 7% and 4% respectively against the instant of maximum pile moment. This value of earth pressure is just 0.55 time of the maximum value contrary to the expectation of a maximum value. However, since this value of earth pressure represents a net value based on the earth pressure acting at the rear and front face, the relationship of ground surface displacement and net earth pressure force at pile head is not straightforward. Although the maximum moment profile has a closer similarity with that of maximum inertia force, however, the major qualitative as well quantitative roles of inertial and kinematic aren't well defined. Therefore, we will determine the phase difference as well as the contribution of inertial and kinematic action in the upcoming sections.

4.4.3 Qualitative comparison of inertial and kinematic interactions:

Fig. 56 shows all points of piles and pier against which the phase difference with respect to pier top is determined in LF type. It also shows the corresponding depths of soil against pile for phase difference calculations as green boxes. Moreover, the phase difference of pier top and various points along the depth are determined for F-type structure to visualize the effect of inertia force only and to serves as reference for inertial interactions. Similarly, the reference for kinematic interaction is established by determining the phase difference of free-field soil and pile of LF_{NS} analysis. The results on the right side indicate that phase difference between pier top and pile in LF is positive and similar to the reference inertial interaction case, indicating that pile would follow the pier top response. This highlights the dominant role of pier top acceleration in the response of pile. Moreover, the PD of soil and pile in L-F is positive and opposite to the reference kinematic interaction case. In the reference kinematic interaction case pile responds under soil displacement loading and the pile-soil phase difference is on the negative side. This mismatch of soil-pile PD against reference kinematic PD indicates that pile response is not dominated by kinematic action of soil. (It implies that soil lags and fails to exert significant kinematic demand on pile in LF type.) Consequently, it is determined that inertial interaction primarily cause pile response with limited contribution of kinematic interaction. The differences in PD for LF and F-type in the lower part of pile are due to soil action and partially due to the fixity of piles to baseplate.

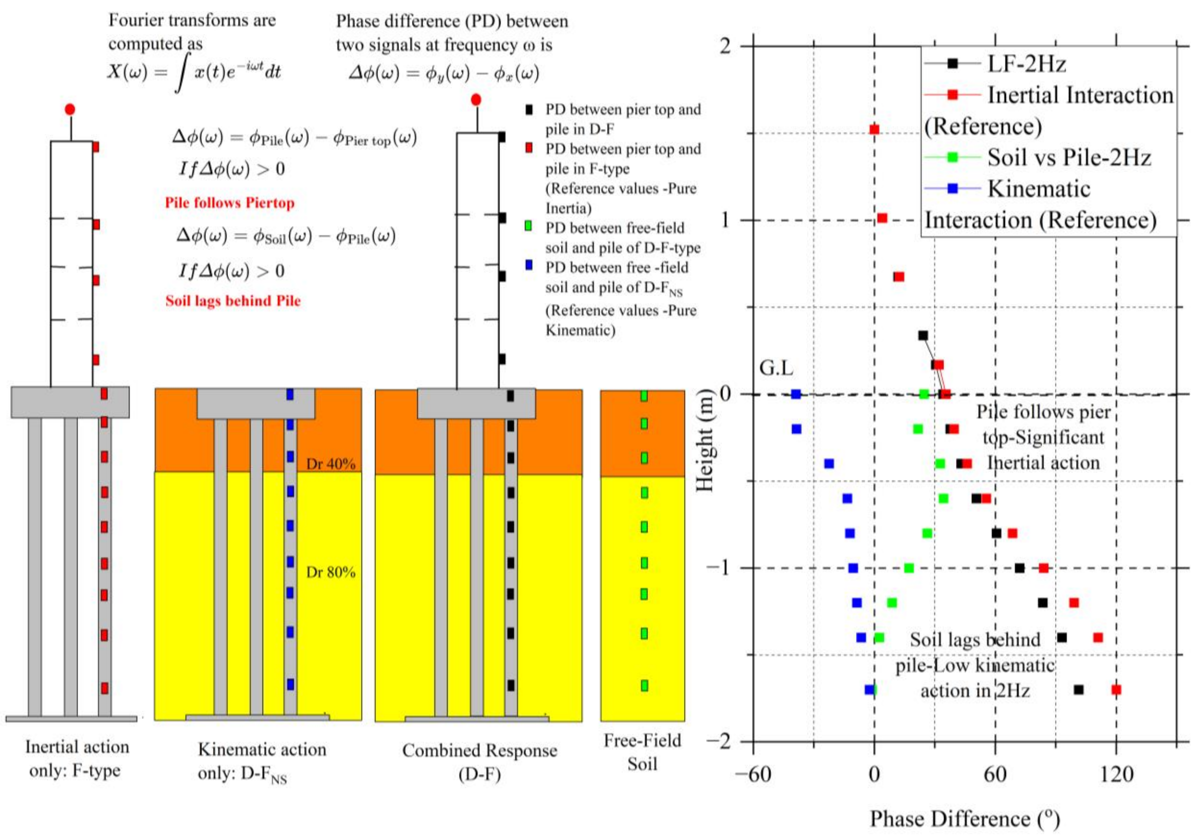

Figure 56. Phase difference calculation between pier top and pile, and soil and pile for L-F type

4.4.4 Qualitative and quantitative comparison of inertial and kinematic interactions:

To determine the quantitative role of inertial and kinematic interaction in DF type, we will look at the analysis results of F-type and LF_{NS} simulations subjected to the same sinusoidal input as LF. Pile deformation as well as bending moment values obtained from LF are similar to F-type analysis, suggesting a dominant role of inertial force. Isolated pile deformations caused by inertial force and kinematic force are about 1.2 times and 0.15 times the values of combined analysis (LF) respectively. Similarly, a comparison of pile moment profiles indicates a good match between F-type analysis and LF-type across it depth.

Quantitatively the kinematic action alone produces a pile head moment of just 0.16 times and inertial action produces about 1.2 times the value from the combined analysis. This confirms that role of kinematic action is limited and it is inertial action which controls the response of piles in LF type. Moreover, ratio of pile head moment due to inertia and that due to kinematic action is about 7.4 indicating a head-to-head comparison of individual interactions. The reason behind such amplified values due to inertial action and lower values due kinematic action are proximity of input wave frequency against the natural frequency of LF type structure and soil. This relationship is further studied in the upcoming sections by varying the input motion frequency.

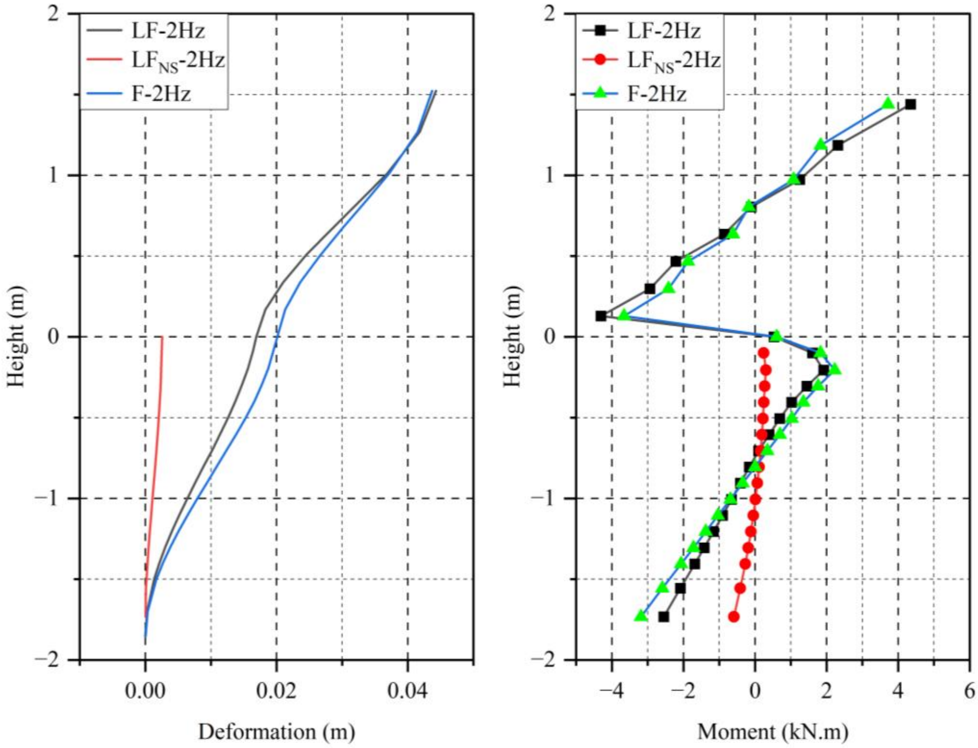

Figure 57. A comparison of isolated pile deformation and moment of kinematic and inertial interactions against the combined response in L-F

4.4.4.1 Phase Difference:

Phase difference is used as an indicator to identity the potential contribution of inertial and kinematic actions towards pile. The phase difference between acceleration time histories of pier top and various points along the pier and pile as indicated in Fig. 58, by black box, determines whether pile follows the pier top in entirety or up to a certain depth. The phase difference between pile and free-field soil indicates the lag or lead of soil response against the pile by green dots. Moreover, the phase difference between pier top and pile for F-type structure only case is also determined to provide reference values in case of inertial interaction only, by red dots. Finally, the PD of free-field soil and pile in LF_{NS} is shown as blue dots and serve as a reference for kinematic interaction only.

Fig. 48 indicates the phase difference variation along the height of pier structure with foundation for input frequencies as listed in Table 8.

Let's start analysing the profiles, staring from 1Hz case. The phase difference values between pier top and piles are positive and similar for both F-type and L-F indicating that pile follows the pier top response (inertial interaction). The phase difference between soil and pile at various depths is positive indicating that soil lags behind the pile response, though the values are close to zero. Therefore, it is anticipated that inertial force at pier top would dominate the response of pile with a limited contribution from kinematic soil displacement. In case of 2Hz, the phase difference of pier top and pile is positive and similar for both F-type and L-F, indicating a lead of pier top acceleration against the pile. Whereas, the soil lags behind pile as indicated by a positive phase difference between pile and soil, as per the nomenclature explained previously.

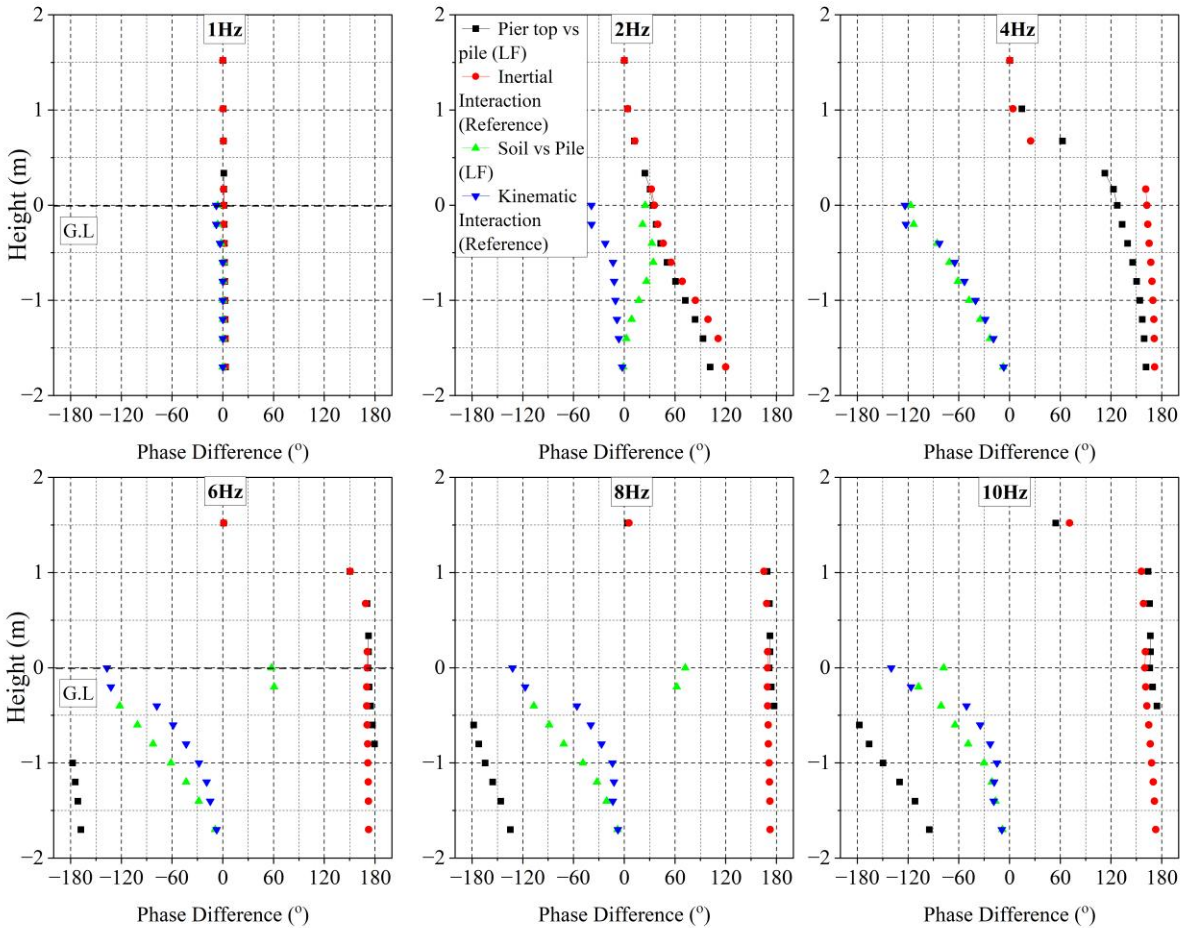

Figure 58. Phase difference between pier vs pile and pile vs free-field soil under various frequencies for LF-type structures

The 4Hz case is quite interesting as the values of phase difference between and soil and pile turn negative and match the reference kinematic interaction case indicating the pile follows the directions of soil. However, the piertop-pile phase difference in L-F is also positive and similar to reference inertial interaction. This indicates that pile responds under the combined action of inertial and kinematic interactions.

The cases corresponding to 6, 8 and 10Hz also indicate that soil leads the pile motion with a limited contribution from pier top inertia. Pile follows both pier top inertia as well as soil loading, however, the influence zone of pier top is restricted to upper part of pile as pile follows soil load only below that zone. The influence zone is pier top in pile section is marked from ground surface up to which phase difference between pier and pile is positive. The depth of this zone is 1m for 6Hz which the reduces to 0.6m for 8Hz and onwards cases. Therefore, it is anticipated that kinematic action of soil would dominate the pile response with limited contributions coming from inertial action particularly below the influence zone of pier top.

The values of soil-pier phase difference for D-S, L-F and L-S cases are presented at the end of this chapter as concluding summary. However, it is found that inertial and kinematic actions are found to have similar directions at low frequencies (1-2Hz) and opposite directions at medium to high frequencies (4-10Hz) for all D-F, D-S, L-F and L-S cases.

In summary, phase difference helps us decode and provides a perspective in the pile response against the inertial and kinematic actions. It has indicated that inertial action controls the pile response at lower frequencies such a 1-2Hz, kinematic action controls at higher frequencies such as 6-10Hz, whereas middle frequencies such as 4Hz case would have significant role of both actions.

4.4.4.2 Moment and Deformation:

Fig. 59 shows the pier and pile moment distribution curves corresponding to maximum bending moment measured in the pile for cases corresponding to inertia force only (F-type), kinematic force only (LF_{NS}) and under the combined action (L-F). The results are shown from left to right in the increasing order of input motion frequency.

First, the kinematic force only cases (LF_{NS}) are analysed and compared against each other. Secondly, the inertia force only cases (F-type) are compared against each other. Finally, the cases (L-F) which are under the combined action of inertial and kinematic force are discussed and compared against the respective F-type and LF_{NS} to reveal the respective impact of inertial and kinematic forces.

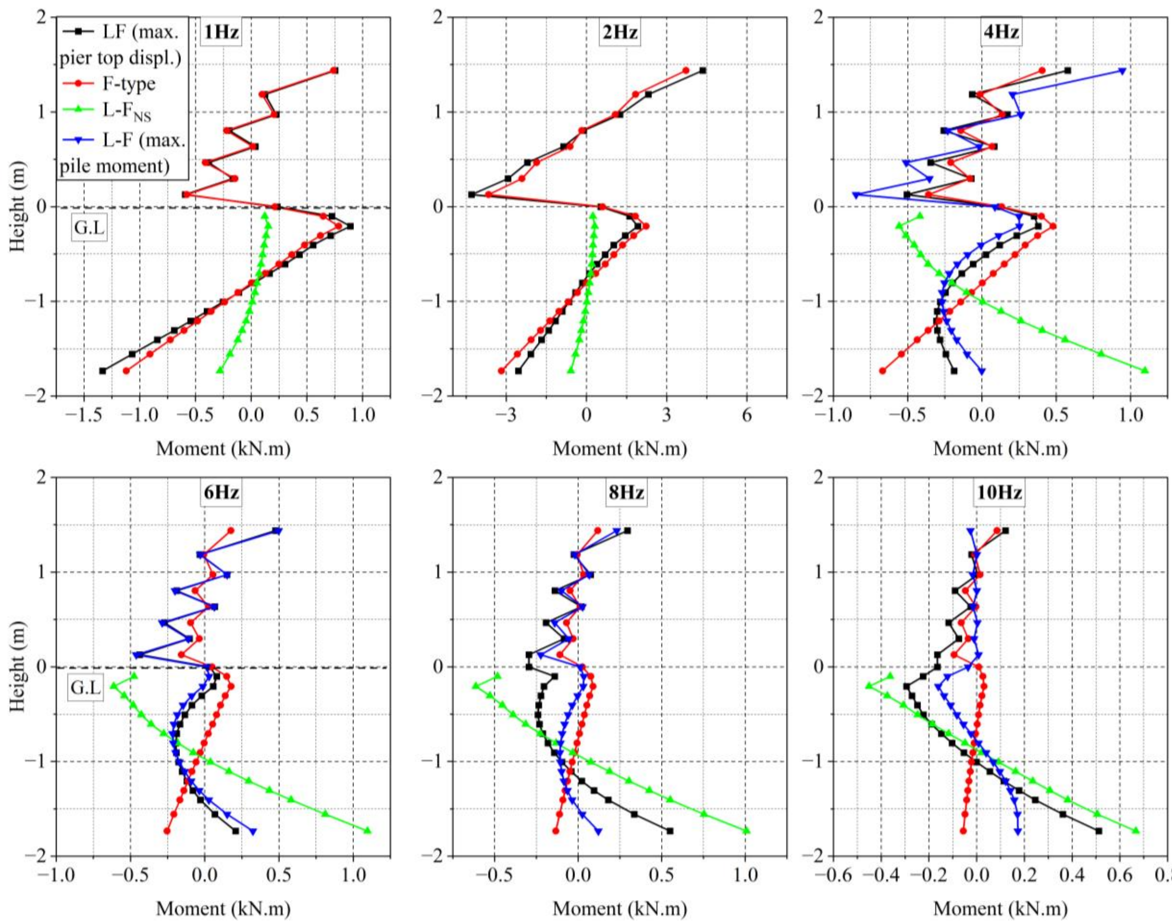

Figure 59. A comparison of pile bending from various cases (L-F, F-type and L-F_{NS}) at various frequencies.

4.4.4.2.1 Kinematic interaction:

The shapes of pile bending moment profiles are approximately similar in all cases with maximum bending moment values observed in the pile are close to pile head and are presented in Fig. 60 for various cases. Although the values of pile moment near the pile tip are sometimes larger than the those near pile head, however, due to the reasons mentioned in the previous chapter pertaining to poor capability of the numerical model near pile tip, the values are not considered for comparison as maximum values. The maximum pile head moment is 0.61 kN.m across different frequencies and is observed at 6Hz. It should be noted that yield moment and plastic moment capacity of the pile section are about 6.14 kN.m and 8.41 kN.m approximately. This shows the importance of considering kinematic interaction effects while designing pile foundations a soil profile containing liquifiable layer near the pile head since kinematic moment could represent 10% of pile yield moment.

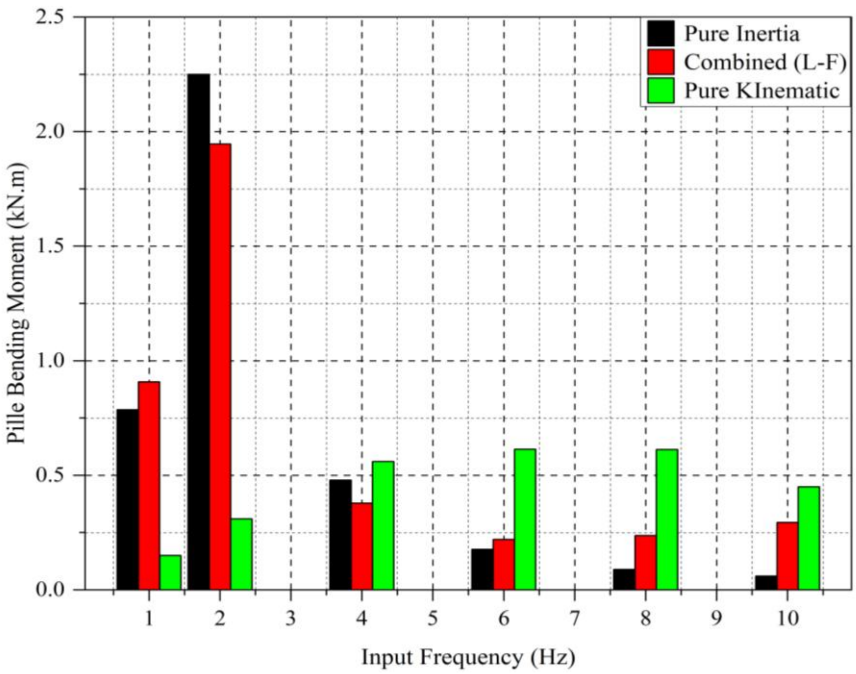

Figure 60. Maximum bending moment values near the pile head

Moreover, a comparison of ground deformation profiles for L-type ground is shown in Fig. 61. It indicates that a uniform maxima is not observed for surface and deeper soil layers especially near the interface at 0.5m depth. Across all frequencies, max. surface displacement is observed in case of 2Hz which is then followed 4Hz. It is because the predominant frequency of surface soil (Dr 40%) is about 4.2Hz which is expected to fall closer to 2Hz after liquefaction and cause displacement amplifications. However, the large ground deformations in dense sand layers at this frequency is unexpected and unexplainable at the moment. The predominant frequency of deeper dense soil (Dr 80%) is about 6Hz and is probably expected to fall to 4Hz since EPWPR doesn't reach 1 to cause full liquefaction. Therefore, a relatively larger value of displacement is observed at the interface for 4Hz case and is followed by 6Hz.

Moreover, the reason behind maximum moment at 6Hz could be attributed to the fact that natural frequency of soil is about 5.5Hz and that of LF_{NS} configuration is about 6Hz. Therefore, while the input frequency is in the vicinity of those natural frequencies, kinematic effects are amplified. Moreover, it is also expected that response frequency of soil decays and decreases closer to 4Hz during shaking and this would cause the maximum pile moment at that frequency. This could also be confirmed by comparing the free-field soil deformation profiles at various frequencies that maximum surface ground deformation happens at 4Hz as shows in Fig. 61.

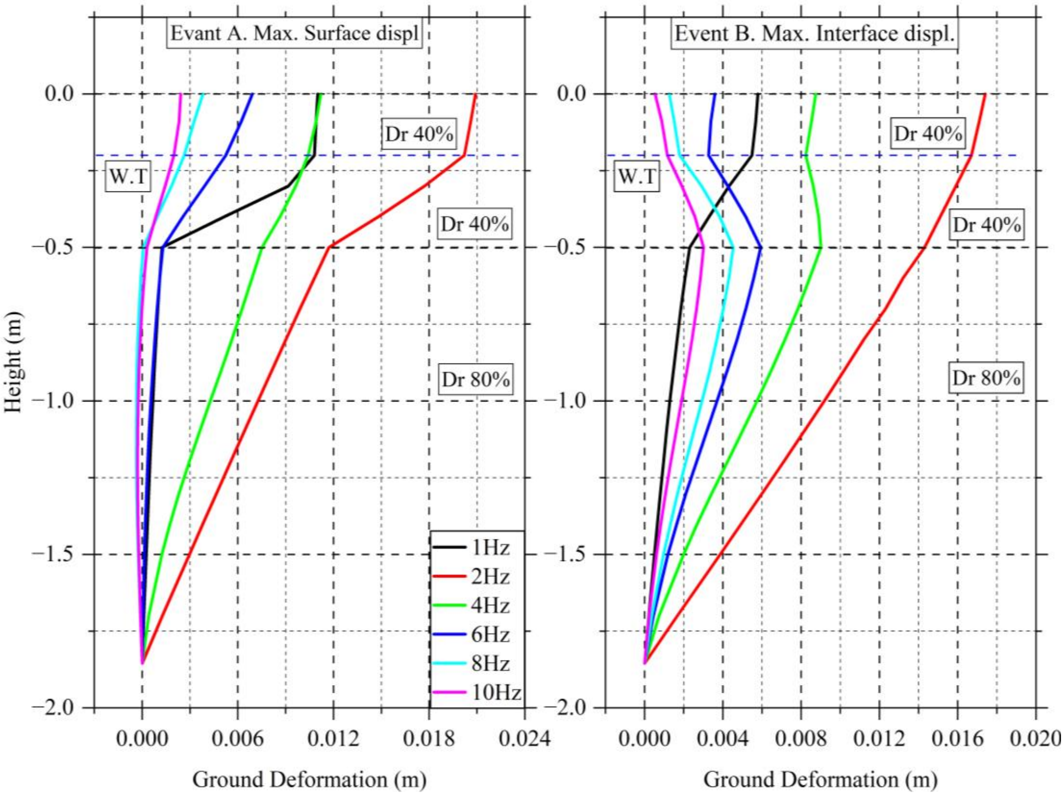

a. Soil deformation profile at the instant of maximum surface and maximum interface displacement

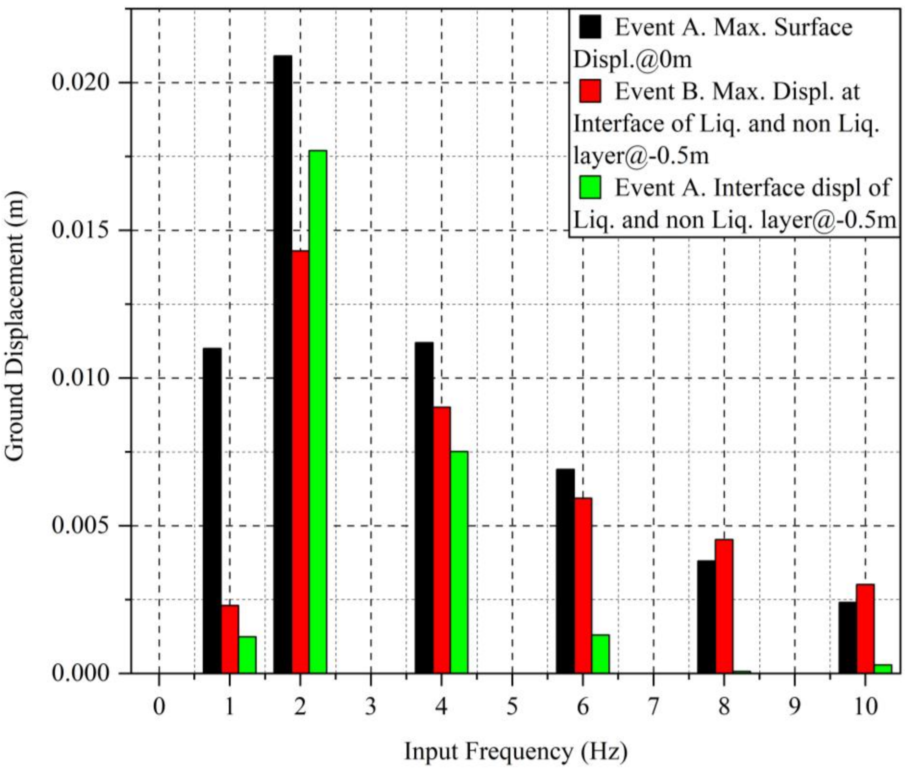

b. Comparison of soil deformation at the surface and interface of liquifiable and non-liquifiable layers

Figure 61. Comparison of ground deformation of dry soil under various input excitations

4.4.4.2.2 Inertial Interaction:

Bending moment profiles pertaining to F-type case are almost similar across various frequencies as shows in Fig. 59. It is a one-degree curve under inertial loading only and having no influence of a distributed kinematic load on the pile. The maximum inertial pile head bending moment across various frequencies is 2.25 kN.m and is observed at input frequency case of 2Hz as indicated in Fig. 60. This is because it is in close band of response frequency of F-type structure which leads to amplification of inertial acceleration and hence pile moment. Moreover, it represents about 37% of the yield moment capacity of pile section. This not only highlights the individual but relative importance of inertial interaction in the design of pile foundations.

4.4.4.2.3 Kinematic and Inertial Interactions:

Bending moment profiles pertaining to L-F type correspond to the combined action of kinematic and inertial interactions and are also shown in Fig. 59. A comparison of pile moment profiles across various inputs shows notable differences such as the shape and instant of maximum pile bending moment. At lower frequencies (1-6Hz), the instant of pier top displacement would produce a moment which is very close to maximum pile head moment. However, at higher input frequencies (8-10Hz), the instant of pier top displacement does not correspond to maximum pile moment. Therefore, bending moment curves corresponding to the instant of maximum pile moment are plotted. The fact that maximum pier top displacement is observed when inertia force is maximum indicates that inertial interaction controls pile response at 1-6Hz. However, the contribution of inertial interaction is greatly reduced at higher frequencies (8-10Hz) as shown by lower values in moment curves at the instant of maximum pier top displacement.

A comparison of bending moment curves across various frequencies indicates that maximum moment is observed at 2Hz case. This is in close vicinity of dominant frequency of F-type and L-F type configuration and a possible resonance at pier top explains large values of pile moment. Moreover, the shape of pile moment distribution at 1-2Hz is close to a one-degree curve as observed in F-type case. The values of pile moment in F-type are slightly larger than those of L-F type indicating that kinematic action does have a certain contribution at 2Hz. Kinematic interaction produces a moment profile which does not really match with that of L-F type; however, its maximum pile head moment represents 16% of corresponding pile moment in L-F. This highlights the dominant role of inertial interaction at lower frequencies. Previously, phase difference investigation also confirmed that pile follows the pier top response, whereas soil lags behind the pile at 1-2Hz cases limiting its influence on pile response.

At 4Hz, the shape of pile moment is no longer a one-degree curve and only partially matches with moment profile of inertial interaction in the upper part and with that of kinematic interaction in the lower part of pile. Moreover, similar moment curves are observed at the instant of maximum pier top displacement and maximum pile moment highlighting the significant role of inertial action. The maximum pile moment is 0.38 kN.m which is sandwiched between kinematic pile head moment of 0.56 kN.m and inertial moment of 0.48 kN.m. A similar phenomenon is also observed at 6Hz and the moment diagrams alone are not sufficient to identify the dominant of inertial or kinematic action and therefore requires an investigation of deformed shapes. However, based on moment values, it is safe to say that pile response in D-F is significantly influenced by both inertial and kinematic action. Phase difference of pile against pier top and soil also indicated that pile follows both interaction up to 1m for 6Hz and throughout height for 4Hz.

At 8-10, the shape as well as value of pile moment in L-F type gets closer to kinematic moment envelopes. At 8Hz, the inertial interaction would represent less than 50% of the pile head moment observed in L-F type, although kinematic pile head moment is approximately 3 times of that in L-F type. This indicates that inertial action counteracts the kinematic action up to a height of 0.7m, below which pile moment diagram tends to match closely with kinematic moment. The phase difference analysis also identified the influence zone of inertial action as 0.5m. which is pretty closer to 0.7m. At 10Hz, the influence of inertial action is only limited to pile head and kinematic action completely dominates the pile moment value.

Fig. 62 illustrates the deformation envelopes of the pier column as well as foundation piles for different configurations across various input excitation frequencies. A comparison of deformation profiles across various inputs shows notable differences in magnitude, shape and pile head deformation at instant of maximum pile bending moment. Since the instant of maximum pile moment is not always at the instant of peak pier top displacement, additional deformation curves are presented for those cases corresponding to the instant of maximum pile head moment.

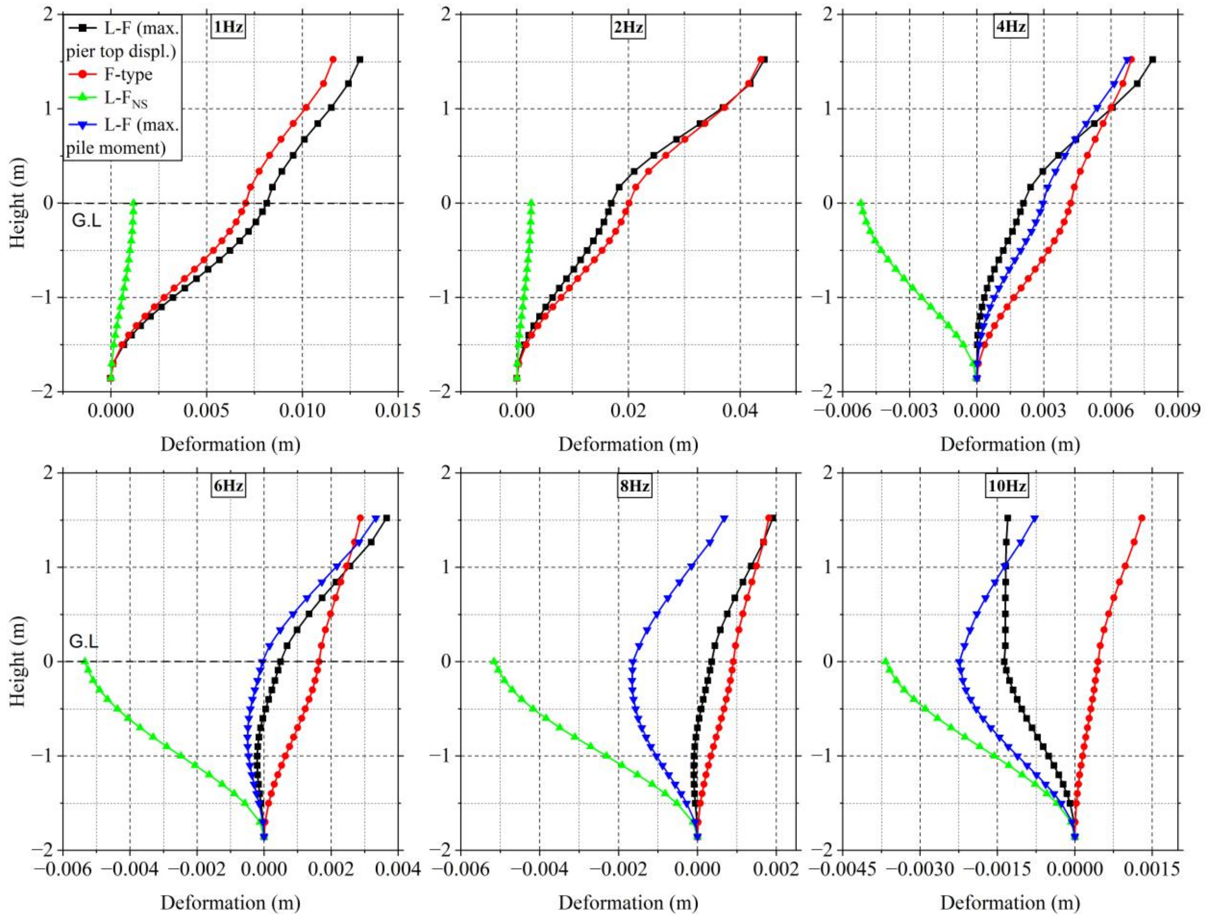

Figure 62.. A comparison of pile deformation from various cases (L-F, F-type and L-F$_{NS}$)

A comparison of deformation curves across various frequencies indicates that maximum pier top as well pile deformation is observed at 2Hz case which is in close vicinity of dominant frequency of F-type and L-F type configuration. Moreover, the shape of pile deformation distribution at 1-2Hz is close to a one-degree curve as observed in pure inertia (F-type) case. The deformation values of in pure inertia case are slightly larger than those of L-F type suggesting that kinematic action does have a certain contribution at 2Hz. Kinematic interaction produces a deformation profile which does not quite match with that of L-F type; however, its maximum pile head deformation represents 15% of corresponding deformation in L-F. This highlights the dominant role of inertial interaction at lower frequencies.

At 4Hz, the deformed shapes of LF-type at both instances (pier top displacement as well maximum pile moment) partially match with that of F-type and pier top displacement values are quite close. It is such that deformation gradient in pile is quite mild, however, it is quite steeper in pier. Inertial action alone would produce pile head deformation of about 0.0042m and that of kinematic action is 0.00519m acting in opposite direction. This bring down the pile head deformation in LF-type to 0.00296m when pile moment is maximum. This indicates that pile response in L-F is controlled by inertial action with significant role of kinematic action. A similar phenomenon is also observed for 6Hz case, where the kinematic displacement of pile reaches its peak value of 0.00535m and further increase it significance thereby decreasing the contribution gap against the inertial action.

At higher frequencies, the shape as well as value of pile deformation, corresponding to maximum pile moment in L-F type, gets closer to kinematic moment envelope as the frequency increases to 8-10Hz. At 8Hz, the inertia action produces a maximum pier top deformation of 0.00181m which is just 6.5% of the value observed at 2Hz. Such a reduced value of inertial interaction control the response of pier top and upper part of the pile only since pile deformation below that are in opposite directions to that of pier top and follows the direction of kinematic action. Similarly, at 10Hz, the influence of inertial action is further reduced to pier and pile displacement in L-F type tends to match displacement corresponding to pure kinematic action.

In summary, the mechanism of soil structure interaction explained in terms of inertial and kinematic interaction is consistent in both moment as well as deformation envelopes and well backed by phase differences analysis as well. It is confirmed that the response of the system in terms of maximum bending moment and deformation depends on frequency content of input motion. At frequencies in the vicinity of response frequency of structure, the inertial interactions prevail. Similarly, kinematic interactions are significantly high and control the response of piles in the vicinity of response frequency of soil.

4.5 Footingless type with Liquifiable sand (L-S)

4.5.1 Time history analysis:

The time evolution of various response variables against an input sinusoidal wave of 2Hz and maximum amplitude of $2m/sec^2$ are shown in Fig. 63. The pier top and pile head acceleration are approximately equally amplified by about 1.35 and 1.5 times the input acceleration respectively. Both are in almost phase with each other, but slightly lag the input acceleration. (At time pile head acceleration also tends to lead pier top). Similarly, the pile head displacement is in phase with pier top, however, it has a slight phase difference with soil displacement which tends to lead pile displacement at the start and then becomes in same phase. The evolution of pile bending to its maximum value is somewhat similar to inertia force at the pier top as well as earth pressure. Moreover, the value of earth pressure is generally in the range of 22-30% of the inertia force and is in same phase. This may enhance the contribution of kinematic action towards pile response. However, it should also be noted that the area of action of earth pressure is relatively low as compared to L-F type. Therefore, LS_{NS} analysis would be used to quantify the contribution of kinematic interaction.

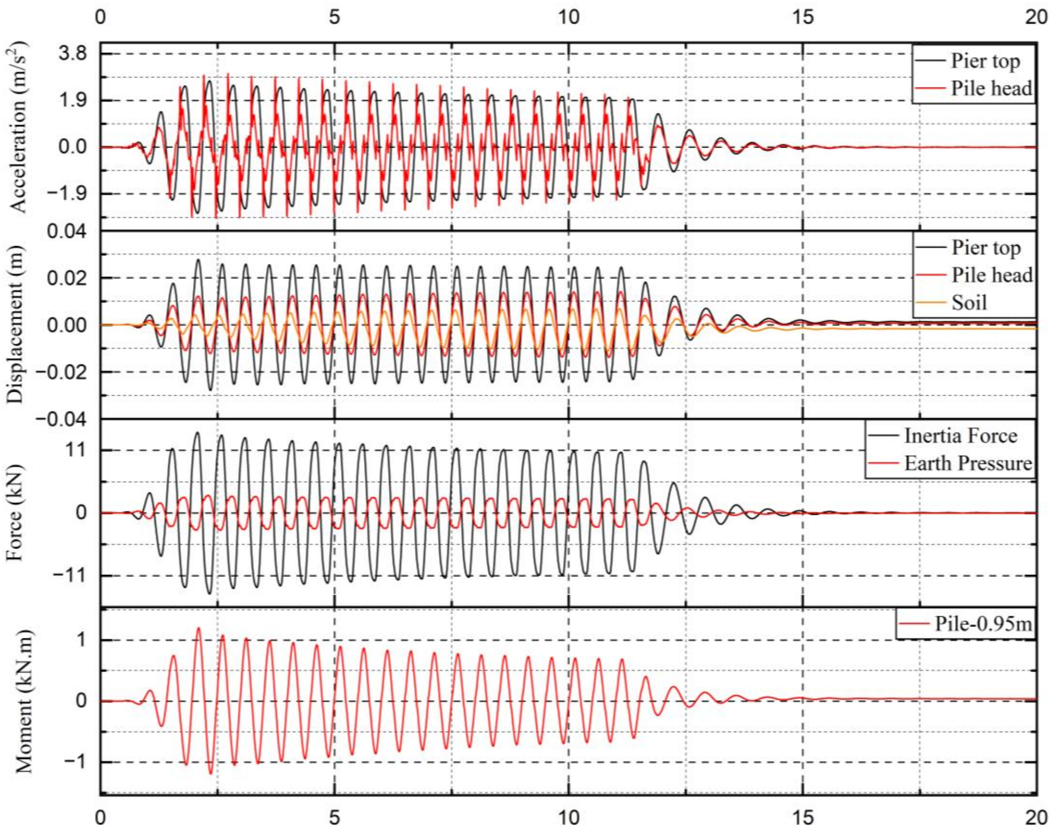

Figure 63. Time evolution of various response parameters for L-S type

4.5.2 Pile bending moment and deformations:

Figure 64 shows the bending moment and deformation profiles of pile and ground at various instances such as maximum pile bending moment, maximum inertial force and maximum ground displacement. At the instant of maximum pile bending moment, the pile moment at about 0.95m is maximum with a value of 1.2 kN.m and pile deformation also reaches close to its maxima and attains 85% of it. Comparison of earth pressure against the inertia force indicates that it is about 35% of inertia force in the same direction thereby increasing the contribution of kinematic action. The instant of maximum inertia force produces a similar bending moment and deformation profile of pile as well as soil. Whereas the instant of maximum of surface soil deformation notes a 50% reduction of earth pressure as well as 31% inertia force with both acting in same directions. However, the pile bending moment at pile head increases more than two-fold and deformation is reduced to about 71% of its maximum value. It also suggests a possibility of large confinement reduction near the pile head due to high EPWPR at that instant. It represents such a state when soil has displaced at its maximum towards pile, however, due to reduction in confinement and stiffness, its influence on pile deformation is reduced. Since ground deformation is quite higher than other cases, a lower value of earth pressure indicates that phase difference exists between soil displacement and earth pressure force itself. This suggests the need of phase difference analysis between soil and pile to help clarify the role of kinematic interaction. Moreover, pile deformation in all cases follows the direction of inertia force and its deformation gradient is quite mild especially in the upper part suggesting either kinematic interaction acts in the same direction as inertia or its contribution is quite low if it is in opposition of inertial interaction. In the next section, we will also decouple the pile response against inertial and kinematic interactions.

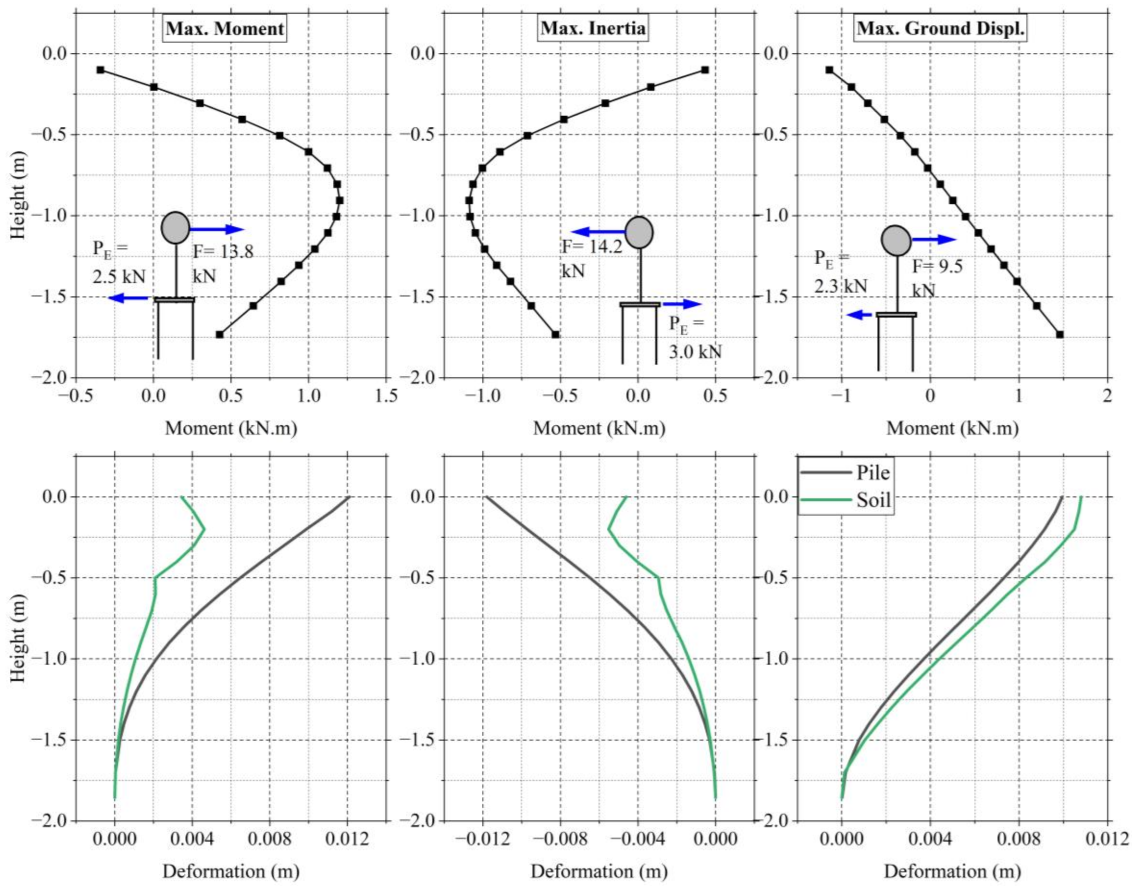

Figure 64. Bending moment and deformation envelopes of piles and ground at key instances

Fig. 65 shows all points of piles and pier against which the phase difference with respect to pier top is determined in LS type. It also shows the corresponding depths of soil against pile for kinematic phase difference calculations as green boxes. Moreover, the reference phase difference of pier top and various points along the depth are determined for S-type structure to visualize the effect of inertia force only-shown as red dots. The phase difference of free field soil and pile in LS_{NS} case serves as the reference for kinematic interaction only. The results on the right side indicate that phase difference between pier top and pile is positive in S-type, establishing a reference case where pile follow the pier top response. A comparison of the PD between S-type and L-S indicates nearly same values for various points along pier and pile. This highlights the dominant role of pier top acceleration in the response of pile. Moreover, the PD of soil and pile is positive which implies that soil lags and fails to exert significant kinematic demand on pile. The reference PD of soil and pile is negative value although nearly zero for non-liquified layers. However, since the pile's response is qualitatively opposite to pile-soil PD of the reference kinematic interaction case, it is interpretable that pile response in LS type is dominated by inertial interaction.

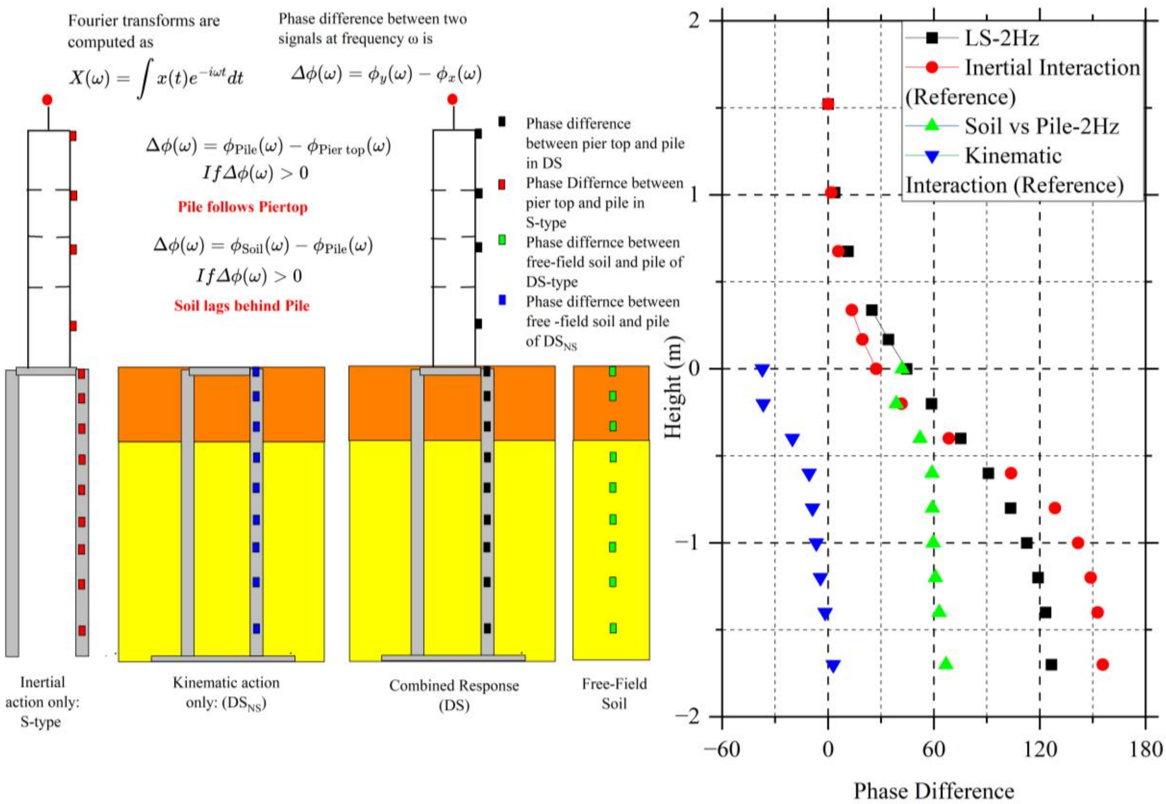

Figure 65. Phase difference calculation between pier top and pile, and soil and pile for L-S type

4.5.3 Quantitative comparison of inertial and kinematic interactions:

To determine the quantitative role of inertial and kinematic interaction in LS type, we will look at the analysis results of S-type and LS_{NS} simulations subjected to the same sinusoidal input as LS. Pile deformation values obtained from LS are sandwiched between S-type (inertial force only) and LS_{NS}

(kinematic force only). Moreover, the pier displacement and bending moment values also match to a certain extent, however, the values in LS are slightly larger than those of S-type. This is due to fact that input excitation frequency (2Hz) is in the relatively close proximity of dominant frequency of LS type (1.8Hz) as compared to 1Hz in S-type and this leads to enhanced inertial force in LS-type. Isolated pile deformations caused by inertial force and kinematic force are about 1.3 times and 0.49 times the values of combined analysis (LS) respectively. Similarly, a comparison of pile moment profiles indicates a better match between S-type analysis and LS-type in the upper half of pile in qualitative terms only. In the lower half of pile, the pile moment values are inclined towards LS_{NS} type suggesting a significant role of kinematic action as well.

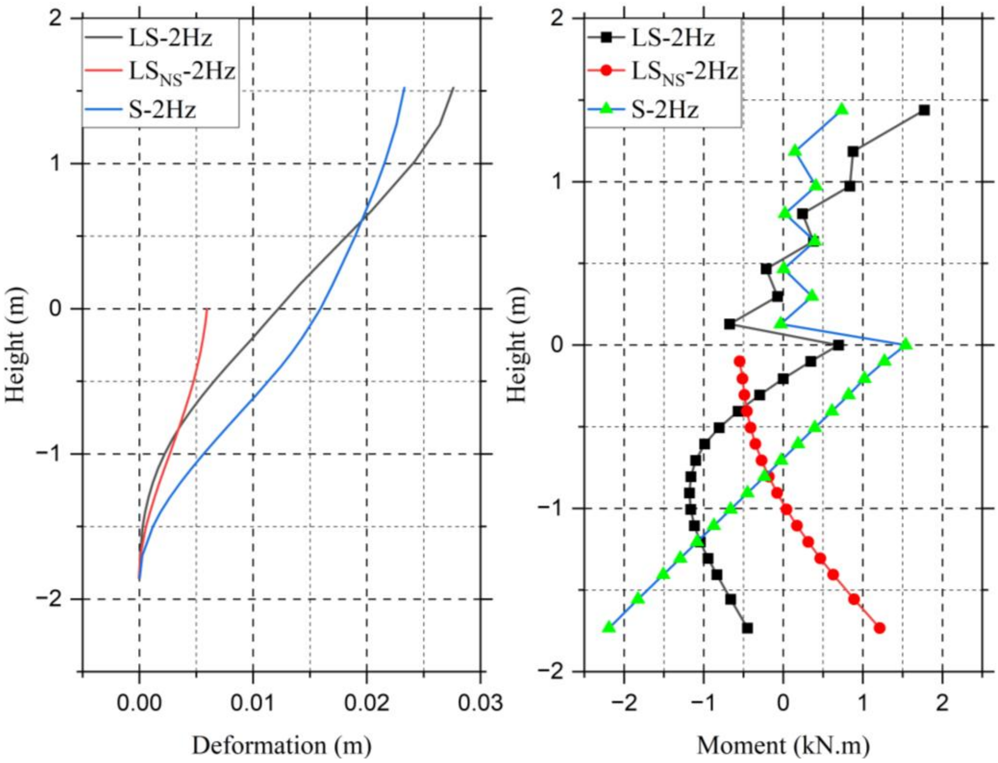

Figure 66. A comparison of isolated pile deformation and moment of kinematic and inertial interactions against the combined response in L-S

Quantitatively the kinematic action alone produces a maximum pile moment of about 0.55 kN.m near the ground surface. Similarly, the inertial force alone produces a maximum pile head moment of about 1.5 kN.m. However, the location of maximum pile moment (1.18 kN.m) in LS type is at 0.9m below the ground surface courtesy of soil confinement and underground beam restraining the bending strain at pile head. Although the location of maximum pile moment isn't same across LS, S-type and LS_{NS} analysis, however, kinematic interaction yields about 0.45 times and inertial action produces about 1.27 times the value observed in LS. This confirms that role of kinematic action is limited and it is inertial action which controls the response of piles in LS type in quantitative terms as well. Moreover, ratio of pile head moment due to inertia and that due to kinematic action is about 2.8 indicating a head-to-head comparison of individual interactions. However, the relationship of kinematic and inertial interactions is highly dependent on input excitation frequency content and therefore it is further studied by varying the input motion frequency.

4.5.4 Qualitative Comparison

4.5.4.1 Phase Difference:

Phase difference is used as an indicator to identity the potential contribution of inertial and kinematic actions towards pile. The phase difference between acceleration time histories of pier top and various points along the pier and pile as indicated in Fig. 67, by black box, determines whether pile follows the pier top in entirety or up to a certain depth. The phase difference between pile and free-field soil indicates the lag or lead of soil response against the pile by green dots. Moreover, the phase difference between pier top and pile for S-type structure only case is also determined to provide reference values in case of inertial interaction only, by red dots. Finally, the PD of free-field soil and pile in LS_{NS} is shown as blue dots and serve as a reference for kinematic interaction only.

Let’s start analysing the profiles, staring from 1Hz case. The phase difference values between pier top and piles are positive and similar for both S-type and L-S type indicating that pile follows the pier top response (inertial interaction). The phase difference between soil and pile at various depths is positive, whereas the soil-pile PD in reference kinematic interaction case is on the negative side, though the values are close to zero. This indicates the soil lag and reduced influence on pile response in L-S type. Therefore, it is inferred that inertial force at pier top would dominate the response of pile with a limited contribution from kinematic soil displacement. In case of 2Hz, the phase difference of pier top and pile is positive and similar for both S-type and L-S, indicating a lead of pier top acceleration against the pile. Whereas, soil lags pile response as indicated by a positive phase difference opposite to what is observed in reference kinematic interaction case, as explained previously.

The 4Hz case is quite interesting (alike L-F 4Hz) as the pile-soil phase difference turns negative and match the reference kinematic interaction case indicating that pile follows the directions of soil (with an exception of unsaturated soil layer data points). However, the piertop-pile phase difference in L-S is also positive until the pile tip and exactly similar to reference inertial interaction. This indicates that pile responds under the combined action of inertial and kinematic interactions throughout pile length, however inertia action might dominate since pier top-pile PD exactly matches the reference inertial interaction values.

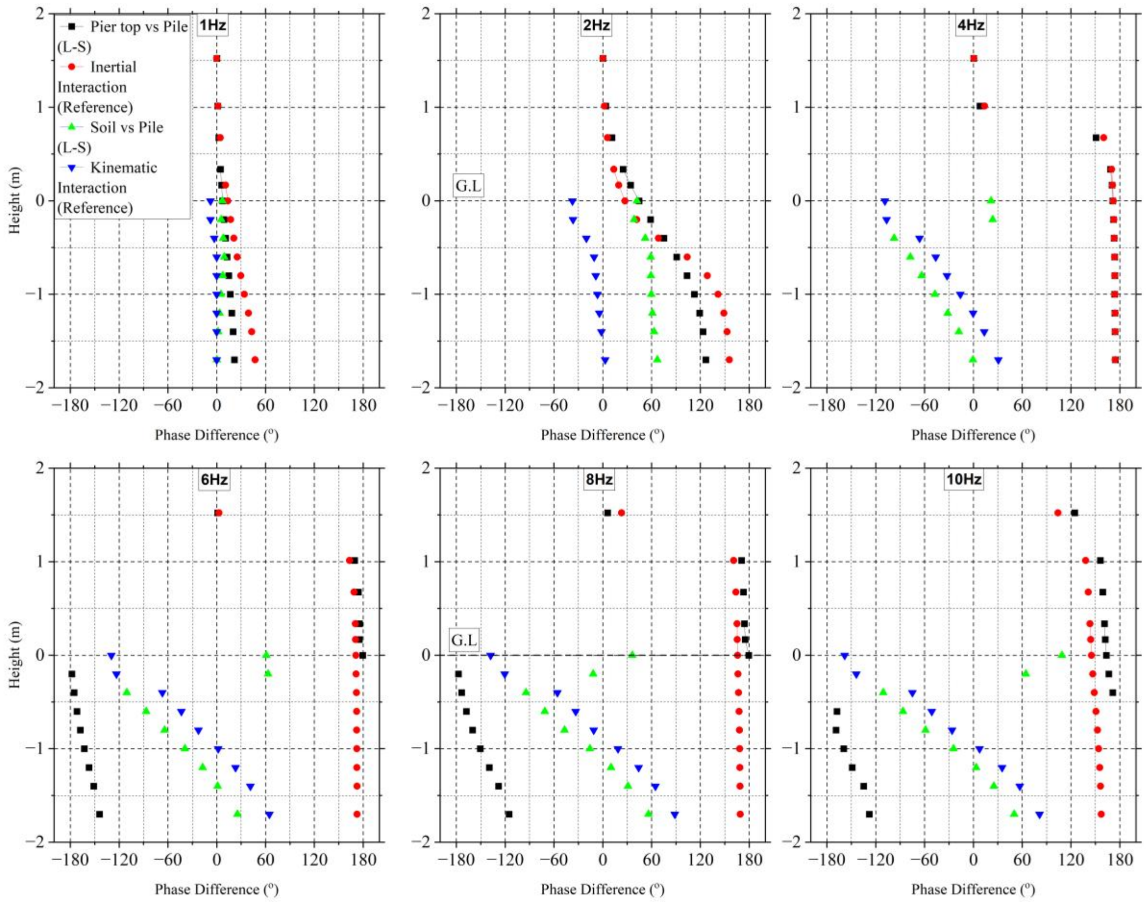

Figure 67. Phase difference between pier vs pile and pile vs free-field soil under various frequencies for LS-type structures

The cases corresponding to 6, 8 and 10Hz also indicate that soil leads the pile motion with a limited contribution from pier top inertia. Pile follows both pier top inertia as well as soil loading, however, the influence zone of pier top is restricted to upper part of pile as pile follows soil load only below that zone. The influence zone of pier top inertia in pile section is marked from ground surface up to which phase difference between pier and pile is positive. The depth of this zone is 0.2m for 6-8Hz which slightly increases to 0.4m for 10Hz case. Therefore, it is anticipated that kinematic action of soil would dominate the pile response with limited contributions of inertial action particularly below the influence zone of pier top for 6-10Hz.

The values of soil-pier phase difference for D-S, L-F and L-S cases are presented at the end of this chapter as concluding summary. However, it is found that inertial and kinematic actions are found to have similar directions at low frequencies (1-2Hz) and opposite directions at medium to high frequencies (4-10Hz) for all D-F, D-S, L-F and L-S cases.

In summary, phase difference helps decode the pile response against the inertial and kinematic actions. It has indicated that inertial action controls the pile response at lower frequencies such a 1-2Hz, kinematic action controls at higher frequencies such as 6-10Hz, whereas middle frequencies such as 4Hz case would have significant role of both actions.

4.5.3.1 Moment and Deformation profiles:

Fig. 68 shows the pier and pile moment distribution curves maximum bending moment measured in the pile for cases corresponding to inertia force only (S-type), kinematic force only (LS_{NS}) and under the combined action (L-S). The results are shown from left to right in the increasing order of input motion frequency.

First, the kinematic force only cases (LS_{NS}) are analysed and compared against each other. Secondly, the inertia force only cases (S-type) are compared against each other. Finally, the cases (L-S) which are under the combined action of inertial and kinematic force are discussed and compared against the respective S-type and LS_{NS} to reveal the impact of inertial and kinematic forces.

4.5.3.1.1 Kinematic interaction:

The shapes of pile bending moment profiles are approximately similar in all cases with maximum bending moment values observed in the pile are close to pile head and are presented in Fig. 69 for various cases. Although the values of pile moment near the pile tip are sometimes larger than the those near pile head, however, due to the reasons mentioned in the previous chapter pertaining to poor capability of the numerical model near pile tip, the values are not considered for comparison as maximum values. The maximum pile head moment is 0.57 kN.m across different frequencies and is observed at 4Hz, representing 9% of pile yield moment, and is followed by 2Hz case.

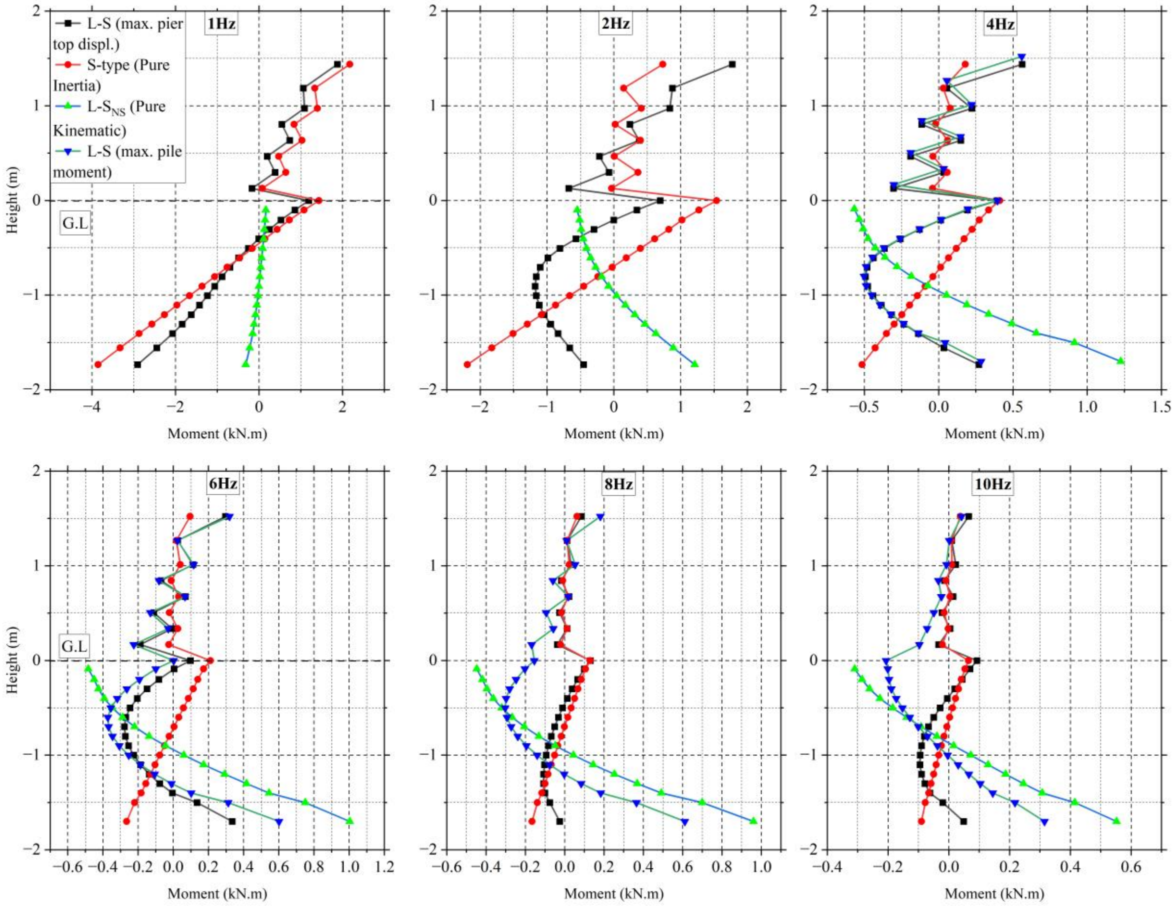

Figure 68. A comparison of pile bending from various cases (L-S, S-type and LS_{NS}) at various frequencies.

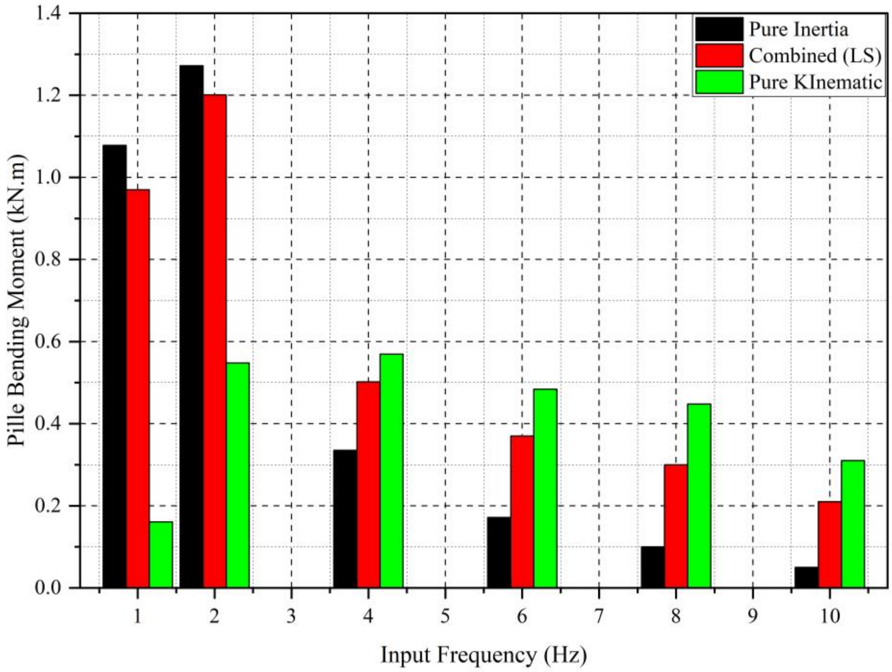

Figure 69. Maximum values of pile moment in S-type configuration

Moreover, the reason behind maximum moment at 4Hz could be attributed to the fact that natural frequency of soil is about 5.95Hz and that of LS_{NS} configuration is about 6.3Hz. Therefore, while the input frequency is in the vicinity of those natural frequencies, kinematic effects are amplified. Moreover, it is also expected that response frequency of soil decays and decreases closer to 4Hz during shaking after an increase in EPWPR and this would cause the maximum pile moment at that frequency. Since it is followed a kinematic moment maximum at 2Hz, this suggest that soil natural frequency decays even further below 4Hz due to liquefaction. This could also be confirmed by comparing the free-field soil deformation profiles at various frequencies that maximum surface ground deformation happens at 2Hz and followed by 4Hz as shows in Fig. 61.

4.5.3.1.2 Inertial Interaction:

Bending moment profiles pertaining to S-type case are almost similar across various frequencies as shows in Fig. 68. It is a one-degree curve under inertial loading only without the influence of a distributed kinematic load on the pile. The maximum inertial pile head bending moment across various frequencies is 1.27 kN.m and is observed at input frequency case of 2Hz as indicated in Fig. 69. This is because it is in close band of response frequency of S-type structure which leads to amplification of inertial acceleration and hence pile moment. Moreover, it represents about 20% of the yield moment capacity of pile section. This not only highlights the individual but relative importance of inertial interaction in the design of pile foundations.

4.5.3.1.3 Kinematic and Inertial Interactions:

Bending moment profiles pertaining to L-S type correspond to the combined action of kinematic and inertial interactions and are also shown in Fig. 68. A comparison of pile moment profiles across various inputs shows slight differences such as the shape and instant of maximum pile bending moment. At lower frequencies (1-2Hz), as well as at intermediate frequencies of 4-6Hz, the instant of pier top displacement would produce a moment which is very close to maximum pile moment. However, at higher input frequencies (8-10Hz), the instant of pier top displacement does not correspond to maximum pile moment. Therefore, additional bending moment curves are presented for those cases corresponding to the instant of maximum pile moment. The fact that maximum pier top displacement is observed when inertia force is maximum indicates that inertial interaction directly controls pile response at lower frequencies. However, the contribution of inertial interaction is greatly reduced at higher frequencies as shown by lower values in moment curves at the instant of maximum pier top displacement. (It is also noted that difference in moment values at the instances of max. pier top displacement and max. pile moment is not as large as it was observed in the corresponding L-F type cases at higher frequencies (6-10Hz). This is due to the lower stiffness of LS type foundation which leads to enlarged pile moments at instance of maximum pier top displacement.

A comparison of bending moment curves across various frequencies indicates that maximum moment is observed at 2Hz case. This is in close vicinity of dominant frequency of L-S type configuration and a possible resonance at pier top explains large values of pile moment. Moreover, the shape of pile moment distribution at 1-2Hz follows S-type case near the pile head. The values of pile moment in S-type are 11% and 6% larger than those of L-S type at 1Hz and 2Hz, respectively, indicating that kinematic action might have a limited contribution. Kinematic interaction analysis (LS_{NS}) produces a moment profile which matches with that of L-S type qualitatively in the lower part; however, its maximum pile head moment represents only 19% of corresponding pile moment in L-S at 1Hz which rises to 45% at 2Hz. This highlights the dominant role of inertial interaction at lower frequencies. Previously, phase difference investigation also confirmed that pile follows the pier top response, whereas soil lags behind the pile at 1-2Hz cases limiting its influence on pile response.

At 4Hz, the shape of pile moment no longer matches with moment profile of inertial interaction even in the upper part, however, it matches with that of kinematic interaction in the lower part of pile. The maximum value of kinematic pile head moment is 0.57 kN.m and that of inertial moment is 0.33 kN.m. The maximum moment in L-S type is 0.50 kN.m which is 12% lower than kinematic value but 34% higher than the inertial value. This not only confirms the reduced influence of inertial interaction but the counteractive influence of kinematic interaction. The significance of kinematic interaction could be assessed through the fact that inertial influence counteracts the maximum kinematic pile moment by merely 12%. Therefore, it is safe to say that pile response in L-S is significantly influenced by kinematic action. Moreover, since instant of maximum pile moment and maximum pier top displacement tend to coincide with each other, it indicates a special relationship between inertia force and soil earth pressure such that inertia force remains close to its maxima, however, earth pressure doesn't achieve maxima here as both counteract each other. Or probably if both reach maxima, earth pressure maxima effect is way higher than inertia force. Phase difference of pile against pier top and soil indicated that pile is under both interactions in the upper part, however, kinematic interaction dominates in the lower part. Similar tendency has been observed at 6Hz, with kinematic action contribution slightly increasing over inertia force.

At higher frequencies (8-10Hz), the shape as well as value of pile moment in L-S type gets closer to kinematic moment envelope. At 8Hz, the inertial interaction would represent about 40% of the pile head moment observed in L-S type, although kinematic pile head moment is approximately 1.5 times of that in L-S type. This indicates that inertial action counteracts and reduces the kinematic action up to 54% near the pile head. At lower heights, hight kinematic action completely dominates the pile moment values. The phase difference analysis identified the influence zone of inertial action and depth of this zone from the pile head was determined as 0.2m. At 10Hz, the influence of inertial action is only limited to pile head and kinematic action completely dominates the pile moment value. Phase difference analysis also indicated that depth of inertial influence zone is about 0.4m.

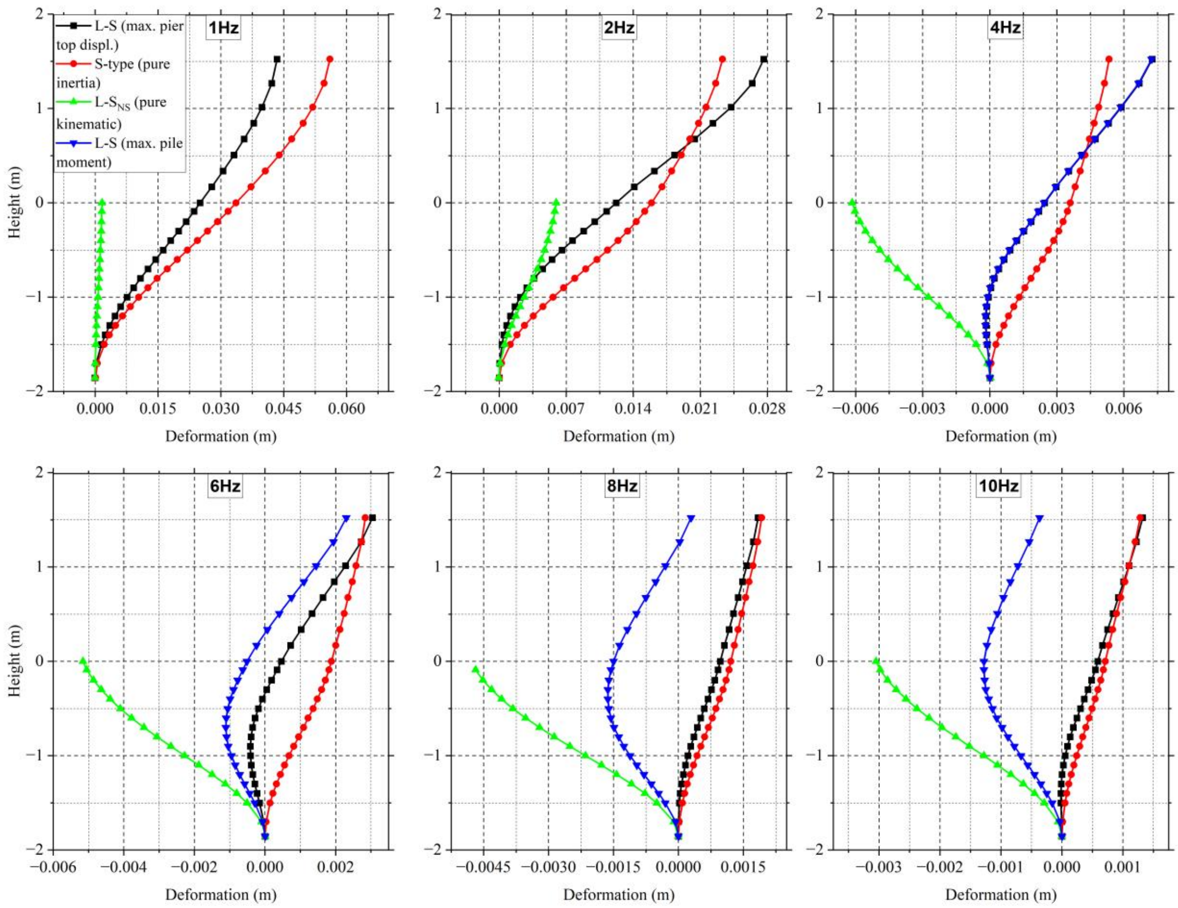

Figure 70. A comparison of pile deformation from various cases (L-S, S-type and L-S$_{NS}$) at various frequencies.

Fig. 70 illustrates the deformation envelopes of the pier column as well as foundation piles for different configurations across various input excitation frequencies. A comparison of deformation profiles across various inputs shows notable differences in magnitude, shape and pile head deformation at the instant of maximum pile bending moment and peak pier top displacement. A comparison of deformation curves across various frequencies indicates that maximum pier top as well pile deformation is observed at 1Hz case which is in close vicinity of reduced dominant frequency of L-S type configuration probably after shear panel yielding is combined with liquefaction induced soil frequency decrease. Moreover, the shape of pile deformation distribution at 1Hz is close the one observed in pure inertia (S-type) case although, deformation values in pure inertia case are 1.3 times of L-S type at the pile head level indicating the influence of kinematic action and relationship of input and structure frequency. At 2Hz, pile head deformation in pure inertia case exceeds the coupled L-S case by 30%, however pier top deformation is 16% lower than the corresponding value in L-S. Kinematic interaction produces a deformation profile which tends to match with the corresponding values of L-S for about half of its length, however, it is close to 48% of the value at pile head. This indicates a slightly enhanced role of kinematic interaction which is still dominated by inertial interactions.

At 4Hz, the deformed shape of LS-type partially matches with that of S-type as only pier top displacement values are quite close. It is such that deformation in pile is close to zero in the bottom half of pile, however, it is mildly positive in the upper part of pile following the pier deformation. Inertial action alone would produce pile head deformation of about 0.0036m and that of kinematic action is 0.00616m acting in opposite direction. This brings down the pile head deformation in LS-type to just 0.00243mm in the direction of pier top. This indicates that pile head response in L-S is dominated by inertia force (due to its longer moment arm), however, it is significantly influenced by kinematic interaction as well.

At higher frequencies, the shape as well as value of pile deformation, corresponding to maximum pile moment in L-S type, gets closer to kinematic moment envelope as the frequency increases from 6Hz to 10Hz. At 6Hz, the inertia action produces a maximum pier top deformation of 0.00284m which is just 5% of the value observed at 1Hz. Such a reduced value of inertial interaction control the response of pier top and upper part of the pile only since pile deformation below that are in opposite directions to that of pier top and follows the direction of kinematic action. At 8-10Hz, the influence of inertial action is only limited to pier and pile head, and kinematic action completely dominates the pile deformation value.

4.6 Chapter summary

In summary, the mechanism of soil structure interaction explained in terms of inertial and kinematic interaction is consistent in both moment as well as deformation envelopes and well backed by phase differences analysis as well. It is confirmed that the response of the system in terms of maximum bending moment and deformation depends on frequency content of input motion. At frequencies in the vicinity of response frequency of structure, the inertial interactions prevail. Similarly, kinematic interactions are significantly high and control the response of piles in the vicinity of response frequency of soil.

More, it indicates that inertia force and soil kinematic displacement tend to be in same direction at low frequencies (1-2Hz) At medium to high frequencies (4-10Hz), the directions tend to be opposite as shown in Fig. 71 and Table 10.

Table 10. List of phase difference values across various frequencies for D-S, L-F and L-S configurations

Input Freq. (Hz)	PD = Soil-Pier (D-S)	PD = Soil-Pier (L-F)	PD = Soil-Pier (L-S)	Soil Response	Direction
1	4.13	3.54	19.80	Lead	Similar
2	113.50	82.52	150.60	Lead	Similar
4	67.03	85.00	141.10	Lead	Similar
6	-172.20	-16.24	-144.20	Lag	Opposite
8	-137.80	-74.77	-126.80	Lag	Opposite
10	-107.30	-86.42	-48.49	Lag	Opposite

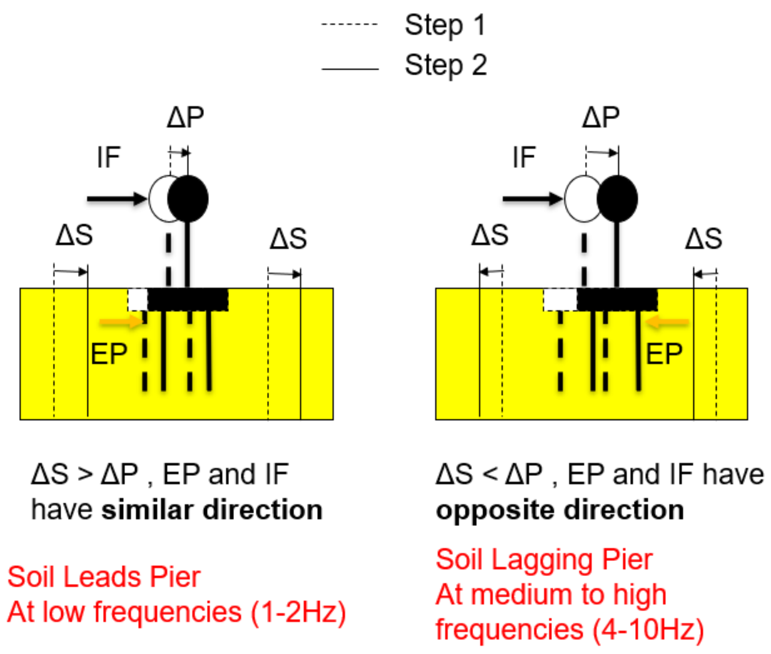

Figure 71. Summarization of the direction of kinematic and inertial loadings

CHAPTER 5: SIMPLIFIED STATIC ANALYSIS FRAMEWORK

5.1 Introduction:

Piles are subjected to both inertial loading, arising from the superstructure above the foundation level, and kinematic loading induced by soil deformation during dynamic excitation. A direct and rigorous approach to evaluate pile response under the combined influence of these loadings is through dynamic analysis using three-dimensional finite element modeling (3D FEM), which employs a continuum representation of the soil–pile–structure system (Shrestha et al. 2019).

An alternative dynamic analysis approach is the beam-on-Winkler foundation (BWF) model, which is comparatively simpler and widely used in practice. However, incorporating ground deformation effects within the BWF framework remains challenging. This is because it requires a prior ground response analysis to obtain soil deformation time histories at various depths, which are then applied as input motions along the length of the soil–pile–structure model (Rahmani et al. 2018). Consequently, dynamic analysis methods—whether continuum-based or Winkler-type—are generally considered computationally demanding and time intensive.

To address these limitations, pseudostatic approaches (Luo et al. 2002; Chiou et al. 2020) have been developed as mechanistically informed and computationally efficient alternatives. In these methods, the pile–superstructure system is typically idealized as a single-degree-of-freedom (SDOF) system. The ground response analysis is first conducted to obtain the maximum soil displacement profile, which is used to represent kinematic loading. In parallel, inertial loading is estimated using the ground surface acceleration together with the natural frequency of the soil–pile–structure system to determine the maximum structural acceleration.

Luo et al. (2002) proposed a pseudostatic framework that explicitly accounts for both kinematic and inertial loading. However, since these two load components generally exhibit a phase difference under dynamic conditions, their contributions cannot be simply superimposed. To address this, contribution factors for inertial and kinematic loading are introduced based on the relationship between the structural and ground natural periods. This concept has been incorporated into the Japanese design code for railway structures for the seismic design of pile foundations.

In the present study, the philosophy of the Japanese design code is adopted and further refined based on the mechanistic understanding of kinematic and inertial interactions developed in the previous chapter. First, the conventional pseudostatic analysis procedure as defined in the Japanese design code is outlined. This is followed by the introduction of a proposed FEM-based hybrid pseudostatic analysis methodology. In addition, the interaction factors specified in the Japanese design code are evaluated within this framework to assess their accuracy in predicting the dynamic response of the pier–pile system, and corresponding modifications are proposed to enhance the effectiveness of the approach.

5.2 Japanese Railway Design Method (RTRI, 2012)

The Japanese Railway Design Method adopts a conventional soil-pile-structure interaction modeling approach as introduced by (Chiou et. al 2022] is indicated in the Fig. 72. It indicates that piles being modeled as beam elements and soil as springs elements. These soil-pile springs are combined with dashpots to emulate the damping of system. Moreover, the p-y relationship between soil and pile is simulated by a hyperbolic curve as expressed by **Eq. (10).**

$$p = \frac{k_h(z)\, D_y}{1 + \frac{k_h D_y}{p_u} y} \tag{10}$$

Where p accounts for soil reaction, y for displacement of soil-pile interaction springs, $k_h(z)$ as the horizontal subgrade reaction coefficient at depth z, and $p_u$as the ultimate soil capacity. Moreover, the horizontal subgrade is generally related to elastic modulus of soil and is given as **Eq. (11)** for laterally loaded piles.

$$k_h = \frac{\eta E_{max}}{D} = \frac{2\eta G_{max}\,(1+v)}{D} \tag{11}$$

Where D is the pile diameter, E_{max} is the peak elastic modulus, v is the Poison's ratio and η is a modification factor whose values varies between 0.45 to 1.2 based on characteristics of soil-pile structure system (Yoshida et al. 1972) and (Broms BB, 1964).

The ultimate soil capacity (p_u) is based on the American Petroleum Institute (API, 2000) approach for a *p–y* curve of sandy soil using the following **Eqs. (12-14).**

$$p_u = \min(p_{us}\,, p_{ud}) \tag{12}$$

$$p_{us} = (C_1 z + C_2 z)\gamma' z \tag{13}$$

$$p_{ud} = C_3 . D . \gamma' z \tag{14}$$

Where p_{us} and p_{ud} are the ultimate soil capacities of soil at shallow and deeper heights. γ' is the effective unit weight of the soil; and C_1, C_2, and C_3 are the empirical constants that depend on the soil friction angleϕ'.

The force-displacement relations of soil springs could be established using coefficient of subgrade reaction **Eq. (11)** and the and spacing of soil-pile inetraction springs. Moreover, since soil-pile interactions are a parallel combination of springs and dashpots, the hysteretic behavior of spring-dashpots system is established using the Masing model. The damping coefficient of dashpot is determined as follows:

$$C = 6\omega^{-1/4}.\rho_s.V_s^{5/4}.D^{3/4}.s + \frac{2\xi_s}{K_h} \quad (15)$$

Where Vs is the shear wave velocity of soil, K_h represents the stiffness of soil-pile inetraction springs and s is their spacing. The value of K_h is determined as follows:

$$K_h = k_h.s \quad (16)$$

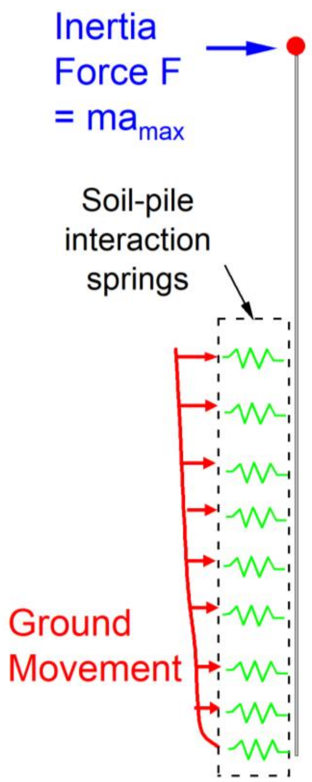

Figure 72. Pseudostatic pushover model (Redrawn after J.-S. Chiou et al. 2022)

Based on this approach, the seismic response of pile foundation is evaluated by combining the inertia force and ground displacement as a simultaneous loading based on their phase difference. The combination has been determined to vary over time and the design method focuses on the two critical instants:

i. A dominant inertia force case (or the instant of maximum inertia force)

ii. A dominant ground displacement case (or the instant of maximum ground displacement).

Therefore, the total loading on the soil-pile-structure system could be expressed using **Eqs. (17-18)**.

$$R_t = 1.0 \; x \; R_a + v \; x \; f(z) \tag{17}$$

$$R_t = v \; x \; R_a + 1.0 \; x \; f(z) \tag{18}$$

Where R_t is the total seismic load, R_a is the inertia force and $f(z)$ is the ground displacement loading. Moreover, v is the interaction factor and its value is given by the relationship of natural period of structure and ground indicated in Fig. 72 or give by the following expressions:

Upper-bound value v_U:

$v_U = 1.0$ $(\alpha \leq 0.75)$

$v_U = -2.0\alpha + 2.5$ $(0.75 < \alpha \leq 1.10)$

$v_U = 0.3$ $(1.10 \leq \alpha)$

Lower-bound value v_L:

$v_L = 0.0$ $(\alpha \leq 0.75)$

$v_L = -2.0\alpha + 1.5$ $(0.75 < \alpha \leq 1.10)$

$v_L = -0.7$ $(1.10 \leq \alpha)$

Where $\alpha = \frac{T_s}{Tg/\alpha_g}$

a. Analytical expression for interaction factors

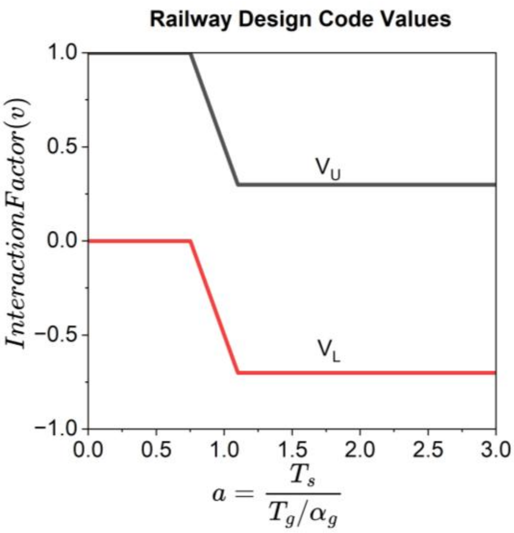

b. Graphical expression of interaction factors

Figure 73. Interaction factor for combining inertia force and kinematic loading

Where v_U is the upper bound and $v_L$is the lower bound of inetraction factor. The parameter α, accounts for the relationship of natural period structure (Ts), natural period of ground (Tg) and the stiffness reduction factor α_g due to excessive strains during dynamic excitations. The value of stiffness reduction is highly dependent on the soil non-linearity which is directly influenced by the amplitude of excitation. Therefore, it is taken as 0.7 for L1 and 0.5 for L2 earthquakes or equivalent excitations.

Based on these factors, the **Eq. (17-18)** could be rewritten as:

$$R_t = 1.0\ x\ R_a + v_U\ x\ f(z) \tag{19}$$
$$R_t = 1.0\ x\ R_a + v_L\ x\ f(z) \tag{20}$$
$$R_t = v_U\ x\ R_a + 1.0\ x\ f(z) \tag{21}$$
$$R_t = v_L\ x\ R_a + 1.0\ x\ f(z) \tag{22}$$

This shows the instant of maximum inertia force is either supported (**Eq. 19**) or counteracted (**Eq. 20**) by a reduced value of maximum ground displacement. Similarly, the instant of maximum soil displacement is either supported (**Eq. 21**) by a reduced value of inertia force or counteracted by it (**Eq. 22**). Consequently, the one which exerts maximum demand onto pile foundation is chosen as a governing equation.

5.3 Hybrid pseudostatic analysis method

In this study, the Japanese Railway Design method is implemented as a hybrid pseudostatic framework in which a three-dimensional finite element (FEM) model is employed in place of the conventional beam–spring representation for modeling soil–pile–structure interaction. The FEM model used here is identical to that adopted for the dynamic analyses presented in Chapters 3 and 4.

The primary rationale for employing the FEM approach lies in its ability to inherently capture soil–structure interaction without requiring explicit definition of modeling components such as soil and structural damping, p–y curves, or spring stiffness parameters, which are essential in conventional beam–spring methods. As a result, several time-consuming modeling steps are eliminated.

Furthermore, inertial and kinematic loadings are applied in a static pushover analysis format within DBLEAVES, significantly reducing the computational complexity and analysis time associated with fully dynamic simulations. On average, the computation time is reduced by approximately 75% for the F-type configuration and 93% for the S-type configuration.

Figure 74 presents an overview of the differences between the conventional pseudostatic analysis model and the proposed FEM-based hybrid pseudostatic model. The primary distinction lies in the application of kinematic loading, which in the proposed method is applied through solid finite elements, whereas in the conventional model it is introduced via soil–pile interaction springs. A second key difference arises from the use of solid elements, where kinematic loading can only be applied at the model boundaries, since its application within the domain leads to tensile stresses that may interrupt the continuation of the analysis in the numerical solver. These differences necessitate the introduction of a calibration factor to ensure comparability of kinematic interaction factors between the two approaches. The calibration factor is defined as the ratio of the kinematic interaction factor obtained from the proposed FEM method to that recommended by the Japanese design code, and has been evaluated for each case as presented in the following sections.

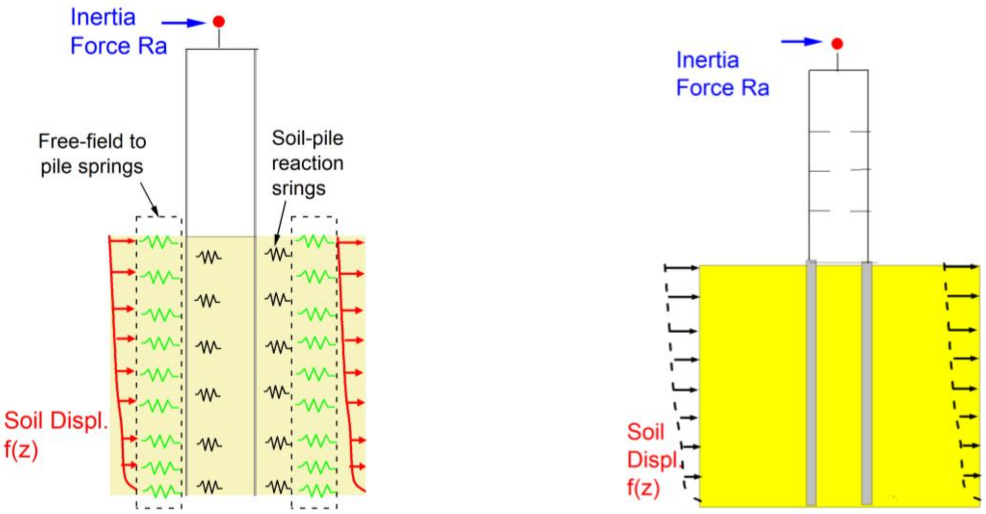

a. Conventional pseudostatic analysis model

b. FEM based hybrid pseudostatic analysis model

Figure 74. Comparison of conventional pseudostatic analysis modeling against FEM based hybrid pseudostatic analysis model.

5.3.1 Determination of inertia force

Determination of inertia force is a major factor in affecting the efficiency of pseudostatic methods. Researchers have proposed various methods to determine this and one of them is response spectrum method. In this method, maximum ground surface acceleration is determined and them multiplied with an amplification factor to determine the superstructural acceleration. However, there's no consensus on which depth of soil should be used as a reference for ground acceleration to be multiplied with amplification factor. The ground motion at a single depth may not completely represent the contribution of other excitation depths resulting in a under or overestimation of superstructure acceleration. Moreover, the acceleration spectrum method is generally applicable for a linearly elastic system with a fixed system period and damping ratio; however, when the system is nonlinear, the method must be further modified to account for the nonlinear effect of the system. Numerous methods have been proposed to account for this effect, such as the capacity spectrum method (CSM), ductility reduction factor method, and inelastic response spectrum method (Tanaka and Sakai, 2024), (Veletsos and Newmark, 1960) and (Villanueva, 1980).

The results of our dynamic analysis already incorporate all these factors and resultantly the value of superstructure accelerations determined could be considered sufficient. Therefore, the peak values of superstructure acceleration multiplied with mass provides values of inertial loading.

5.3.2 Determination of soil displacement profile

In accordance with (Chiou et al. 2022) (Dezi F et al. 2010), the ground deformation profile is obtained at the instant of maximum ground surface displacement for dry soil. At first a 3D FEM model of soil is prepared having same dimensions, soil properties and boundary conditions as it is D-F or D-S type configurations.

5.3.3 Dry Sand Cases (D-F and D-S)

To perform pseudostatic analysis for dry sand cases, both the inertial force and the ground deformation profile are required, which are obtained from dynamic analysis. Figure 75a shows the maximum surface ground deformation profiles derived from dynamic analysis for various input frequency cases, which are used as kinematic loading applied to the soil–pile system together with the inertial force at the pier top for both D–F and D–S configurations. Similarly, Figure 75b presents the inertial force values at the pier top as well as at the footing level (for D–F), as obtained from dynamic analysis.

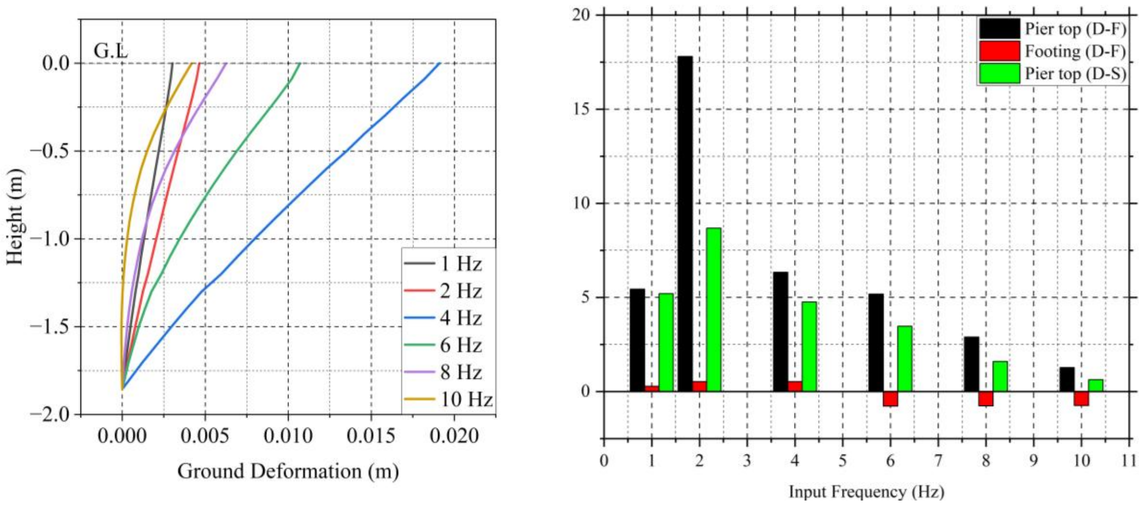

a. Maximum ground surface displacement profile

b. Maximum inertia force values at pier top and footing level

Figure 75. Inertial and kinematic loadings for hybrid pseudostatic analysis of D-F and D-S type configurations.

These loading are applied simultaneously which employing the interaction factors given by RTRI (2012) guidelines. Based on Fig. 73, the values of inetraction factors requires to input Tg = 0.158sec, Ts = 0.5sec (F-type) and Ts = 0.87sec (S-type) and α_g= 0.5 as various excitations corresponds to L2 input motion. This determines the inetraction factors such as V_U = 0.3 and V_L = -0.7 and following load combinations as indicated in **Eqs. (23-26).**

$$R_t = 1.0\ x\ R_a - 0.7\ x\ f(z) \tag{23}$$

$$R_t = 1.0\ x\ R_a + 0.3\ x\ f(z) \tag{24}$$

$$R_t = 0.3\ x\ R_a + 1.0\ x\ f(z) \tag{25}$$

$$R_t = -0.7\ x\ R_a + 1.0\ x\ f(z) \tag{26}$$

Figure 76 presents the moment and deformation profiles of the pier–pile system in D–F configurations obtained using the hybrid pseudostatic method while employing the interaction factors given by the RTRI (2012) guidelines. Based on previous discussions, the cases are categorized into low (1–2 Hz), intermediate (4–6 Hz), and high (8–10 Hz) frequency ranges. At low frequencies, comparison with dynamic analysis is carried out using four different combinations of inertial and kinematic loading. It is observed that the inertia-dominated combination with loading direction consistent with kinematic action (**Eq. 24**) reproduces the dynamic response with the best accuracy. In contrast, the kinematic-dominated combinations (**Eqs. 25–26)** significantly underestimate both pier and pile responses. Although the inertia-dominated combination in **Eq. 23** provides a reasonable estimate of the pier response, the opposing kinematic loading counteracts pile head deformation, resulting in large deviations in pile moment and deformation compared with dynamic analysis results.

The results corresponding to intermediate frequencies (4–6 Hz) show improved agreement of moment and deformation profiles when inertia dominates and kinematic loading is applied in the opposite direction. However, the kinematic interaction factor of 0.7 in Eq. 14 leads to excessive pile moment and deformation, causing large discrepancies in both pile and pier responses relative to dynamic analysis. Similarly, kinematic-dominated combinations **(Eqs. 25–26)** overestimate the pile response, while the inertia-dominated combination with loading in the same direction **(Eq. 24)** also overpredicts pile moment and deformation. Nevertheless, **Eq. 23** can be considered a suitable reference case, and improved accuracy can be achieved by refining the kinematic interaction factor.

In the case of 6 Hz, the moment and deformation profiles corresponding to opposite directions of inertial and kinematic loading are presented. Consistent with the previous observations, **Eq. 23** reproduces the dynamic response with comparatively good accuracy. Therefore, a similar approach involving modification of the kinematic interaction factor has been adopted.

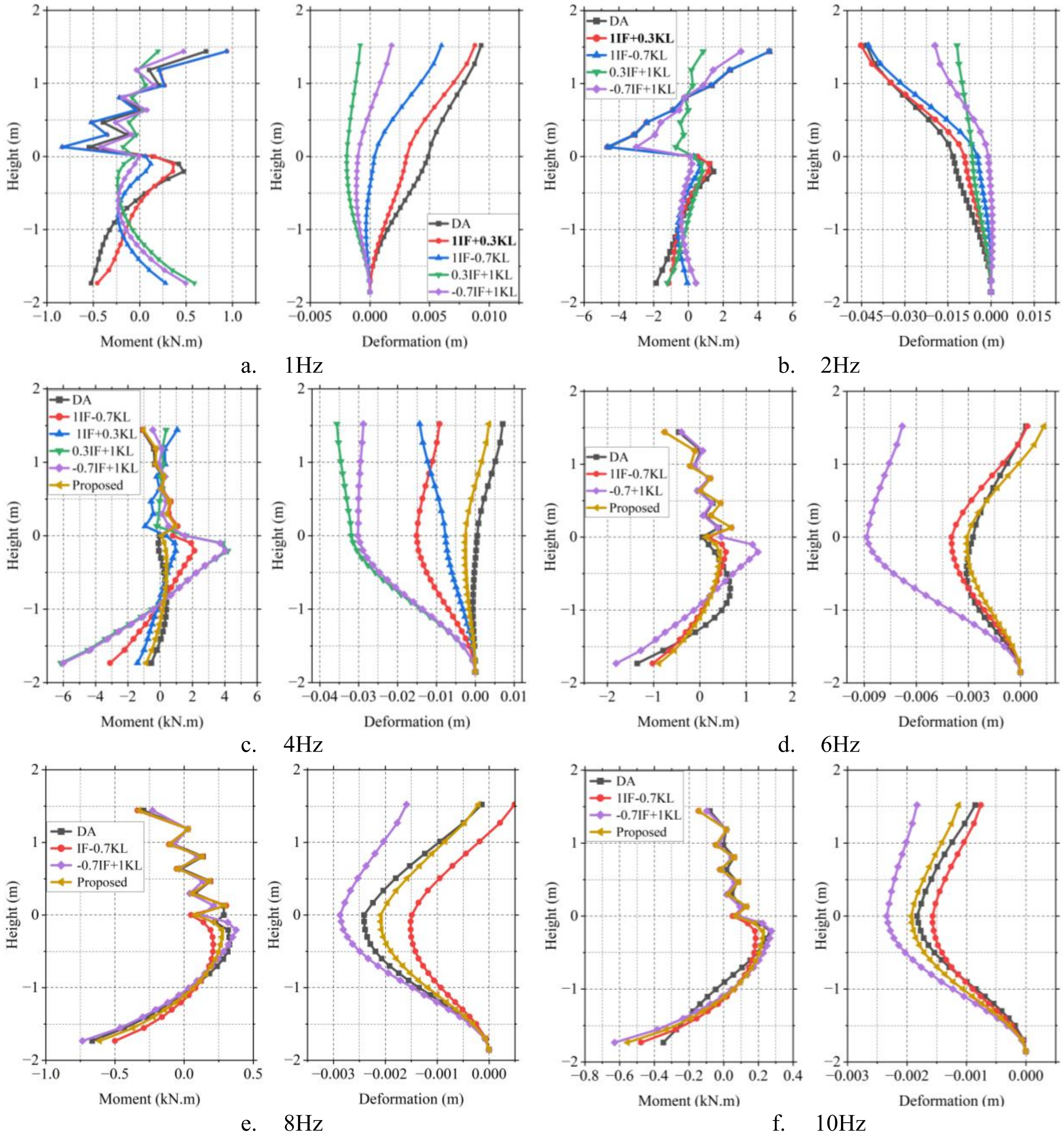

Figure 76. Moment and deformation profiles of pier and pile for D-F configuration

At higher frequencies (8–10 Hz), the inertial and kinematic loadings remain in opposite directions, and the dynamic analysis results are bounded between the combinations given by **Eqs. 23** and **26**. This indicates that the inertia-dominated combination with a kinematic interaction factor of 0.7 tends to underestimate the response, whereas the kinematic-dominated combination with a factor of 1 tends to overestimate the dynamic response. Therefore, consistent with the previous cases, a slight adjustment of the kinematic interaction factor in **Eq. 23** is introduced, which improves the accuracy of the proposed method.

Table 11. presents those combination values of inetraction factors which provide better results of static analysis method against the dynamic ones. It lists the kinematic inetraction factors as b instead of *v* in RTRI method. It highlights a calibrated kinematic factor as b' which is then directly compared against the RTRI kinematic factor v.

Table 11. List of RTRI (2012) and proposed inertial and kinematic factors for D-F and D-S configurations

Design Combination $R_t = a \text{ x } R_a + \text{b}' \text{ x } f(z)$									
	Railway Design Method (Eq. 14-15)		**Proposed Values**				**Railway Design Method (Eq. 17)**		
Input Freq.	Inertia Factor a	Kinematic factor v	Inertia Factor a	Kinematic Factor b (D-F)	Calibrated Kinematic Factor $b' = b/2.33$ (D-F)	Calibrated Kinematic Factor b' (D-S)	Inertia Factor a	Kinematic Factor b (D-F)	Kinematic Factor $b' = b/2.33$ (D-F)
1	1	0.3	1	0.7	0.3	0.30			
2	1	0.3	1	0.7	0.3	0.30			
4	1	-0.7	1	-0.7	-0.3	-0.30			
6	1	-0.7	1	-1.5	-0.64	-0.40			
8	1	-0.7	1	-2.0	-0.86	-0.60	0.7	-2.33	-1
10	1	-0.7	1	-2.0	-0.86	-0.70	0.7	-2.33	-1

5.3.3.1 Calibration factor

Based on the differences in modeling approaches adopted in the hybrid pseudostatic method, a calibration factor is required to enable direct comparison with the interaction factor values recommended by RTRI. Typically, calibration of FEM-based methods is performed by applying a horizontal load at the pile head, and the calibration factor is obtained through back-analysis of the bending moment distribution such that the maximum bending moment predicted by the conventional soil–pile model matches that from the FEM analysis. In the present study, the kinematic interaction factor (b) is determined using the proposed FEM-based pseudostatic method such that the resulting moment profile closely reproduces that obtained from dynamic analysis. This value of b is then compared with the value proposed by RTRI to derive the calibration factor. The calibration is carried out for low-frequency cases (1–2 Hz), as these correspond to large pile head deformations.

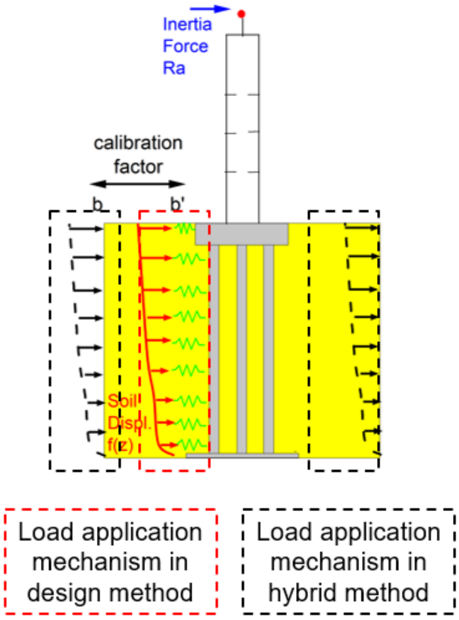

Figure 77. Calibration of kinematic loading factor in hybrid method

$$\text{Calibration factor} = \frac{\text{FEM determined value of kinematic inetraction factor}}{\text{RTRI proposed value of kinematic fcator}} = \frac{0.7}{0.3} = 2.33$$

Table 11 lists the calibrated values of the kinematic interaction factor proposed based on the hybrid method and compares them with the RTRI (2012) recommended values. The results indicate that the calibrated kinematic factors are equal to or lower than the corresponding RTRI values for low to intermediate frequencies (1–6 Hz). At higher frequencies, the proposed kinematic factors are slightly higher than those used in inertia-dominated combinations (Eqs. 23–24) but remain lower than those associated with kinematic load-dominated combinations (Eqs. 25–26). This confirms both the applicability and the conservative nature of the Japanese Design Standards.

For the D–S type structure, similar results have been obtained, and the corresponding kinematic interaction factors are listed in Table 1. These values are equal to or lower than those specified in the Japanese Railway Design Standards, further confirming the conservative applicability of the code. In addition, the kinematic factors for the D–S configuration are lower than those for the D–F configuration, highlighting the relatively reduced influence of kinematic loading due to the smaller interaction area between the soil and piles.

5.3.4 Liquifiable soil cases (L-F and L-S):

The applicability of the hybrid method is further evaluated for liquefiable soil configurations by adopting the same procedure to obtain inertial forces and kinematic displacement profiles. Figure 78 shows the corresponding inertial forces applied at the pier top and the ground deformation profiles at the model boundaries. It is observed that the instance of maximum displacement in the surface soil layers does not coincide with that in the deeper layers, particularly at the interface between loose and dense sand. The loose layers follow the maximum displacement of the surface layer, whereas the dense layers follow the maximum displacement at approximately 0.5 m below the surface, i.e., at the interface. Accordingly, two deformation profiles are defined: Event A (maximum surface displacement) and Event B (maximum interface displacement).

Since only one deformation profile can be used as kinematic loading, the selection is made based on the comparison of soil deformation at the surface and interface levels, as shown in Figure 51b. At lower frequencies, both the surface displacement and interface displacement corresponding to Event A are quantitatively higher than those of Event B. In contrast, at higher frequencies, the interface displacement of Event B exceeds the corresponding values of Event A. Therefore, Profile A is adopted as kinematic loading for lower frequencies (1–2 Hz), whereas Profile B is used for intermediate to higher frequencies (4–10 Hz).

Note that although, for intermediate frequencies (4–6 Hz), the surface displacement of Event A remains higher than the interface displacement of Event B, similar to the case for 1–2 Hz, Profile A was also initially considered as kinematic loading. However, it was found to have a comparatively smaller influence on the pile response.

5.3.4.1 Excess Pore Water Pressure Ratio (EPWPR):

Since water table is located just 0.2m below the surface, it poses risk of high EPWPR and liquefaction in the saturated soil layers. Previously, it has been learned that loose sand, in fact, undergoes liquefaction as well. Therefore, it has been deemed necessary to study the EPWPR situation throughout soil depth.

Fig. 79 shows the EPWPR history and marks the points where maximum value of pile bending moment (BM) is observed. This value has been noted for the near surface loose sand layers located in between 1.7-1.4m as well as for deeper layers up to a depth of 0.8m. Table 12 list all these values.

Under such higher values of EPWPR, the confining effect of soil surrounding the soil is affected which in turn influences the soil-pile interaction mechanism. In conventional methods such effect is reflected in the values of shear modulus of soil being reduced after liquefaction induced stiffness degradation. In the hybrid pseudostatic method, such effect has been accounted for by using the effective unit weight of soil for initial vertical and lateral stress calculations and then reducing the horizontal stresses by an amount equivalent to EPWPR in that layer. For example, at 1Hz cases, the soil horizontal stress around pile are reduced to 10% and 50% of their values in the loose and dense sand layers respectively. This ensures that the impact of kinematic loading onto the piles is taken care of.

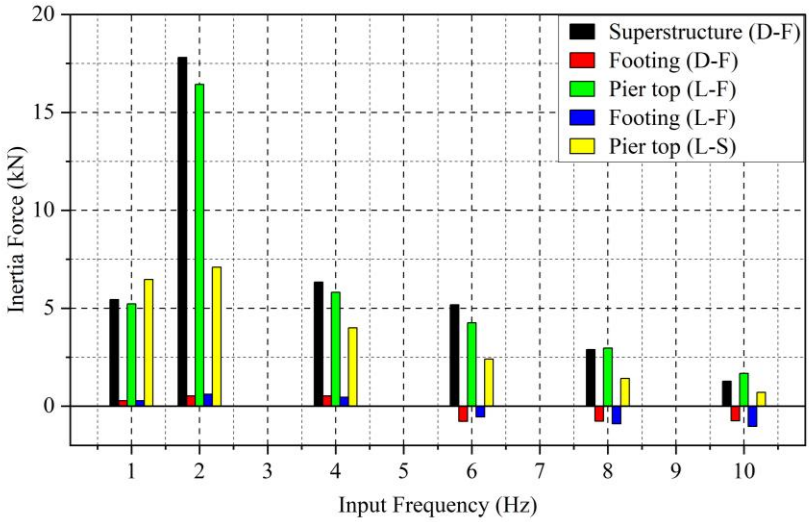

a. Inertial force at pier top and footing level

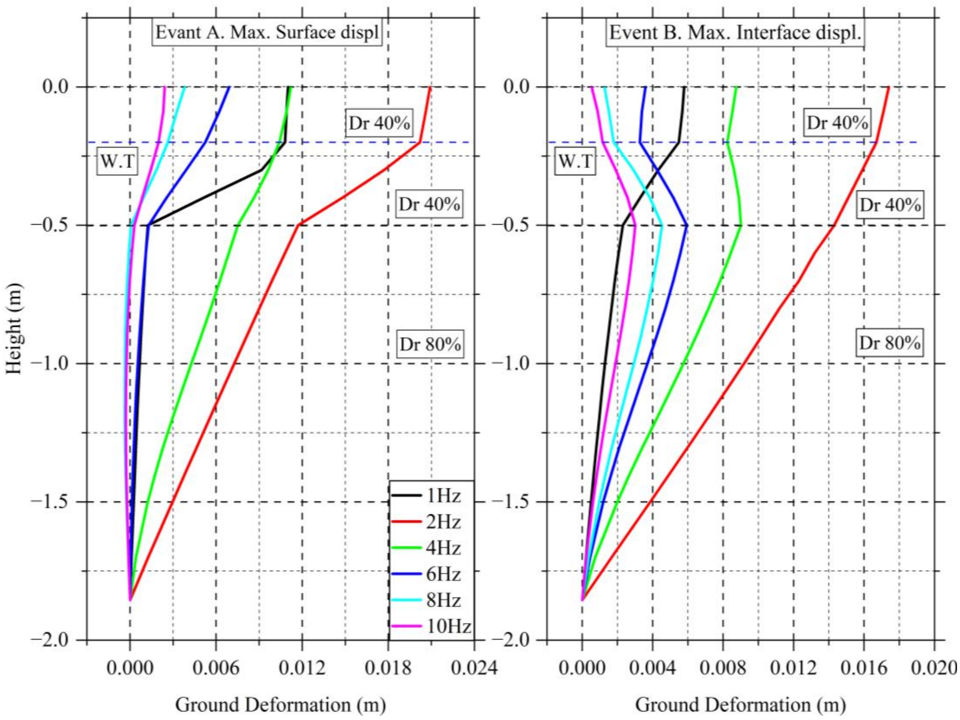

a. Ground deformation profile at the instant of maximum surface and maximum interface displacement

Figure 78. Inertia force and ground deformation profiles for liquifiable soil cases

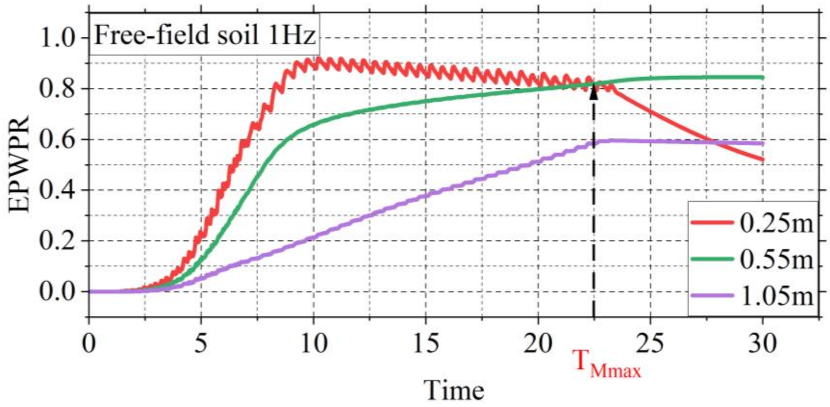

a. EPWPR history for 1Hz

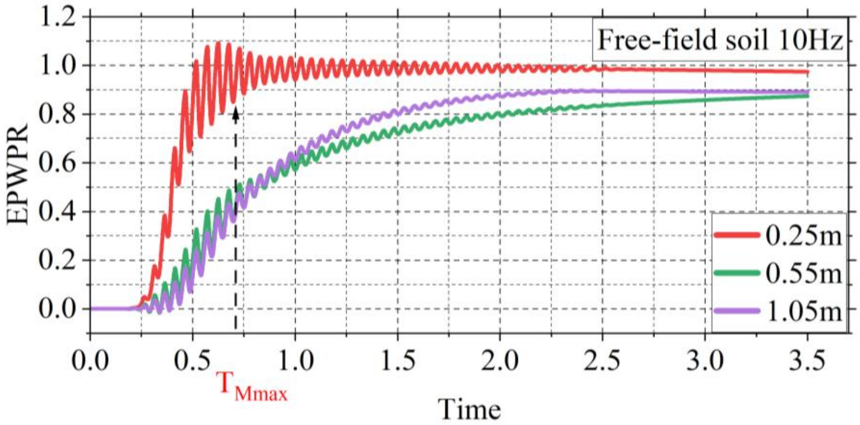

b. EPWPR history for 10Hz

Figure 79. EPWPR at the instant of maximum pile moment

Table 12. EPWPR at the instant of maximum pile moment for L-F configuration

Input Freq.	**EPWPR**	
	Liq. Soil (1.4~1.7m)	**Non. Liq. Soil (1.1~1.4m)**
1Hz	0.9	0.5
2Hz	0.9	0.5
4Hz	0.95	0.8
6Hz	0.8	0.4
8Hz	0.85	0.4
10Hz	0.85	0.4

5.3.4.2 Results:

Based on the RTRI (2012) design guidelines, the interaction factors are calculated as 0.3 and −0.7, which are essentially the same as those for dry sand cases. Accordingly, similar design combinations are applied to liquefiable soil configurations.

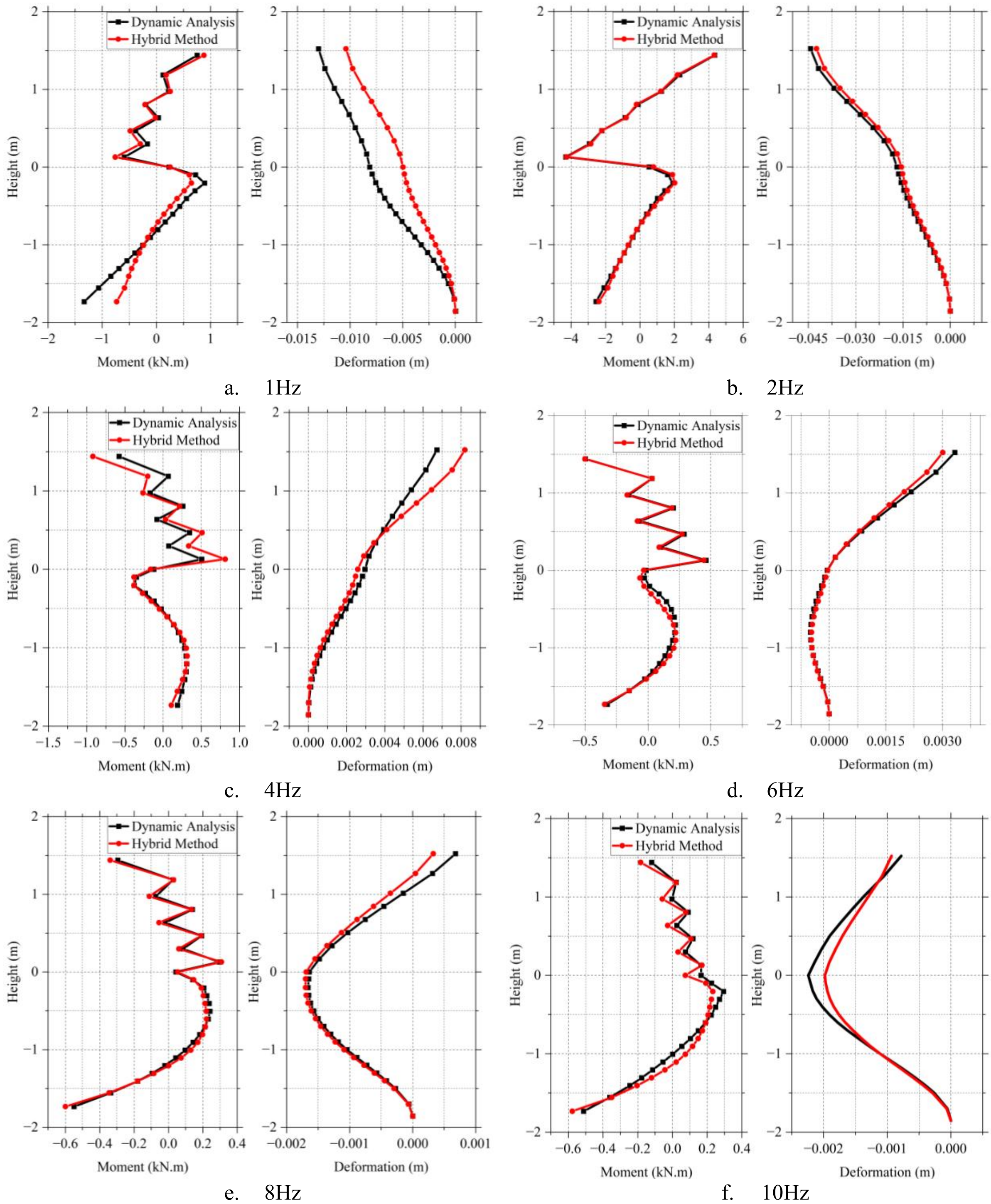

a. 1Hz b. 2Hz

c. 4Hz d. 6Hz

e. 8Hz f. 10Hz

Figure 80. Comparison of moment and deformation profiles from hybrid pseudostatic and dynamic analysis

Figure 80 presents a comparison of moment and deformation profiles obtained from the hybrid pseudostatic analysis method against those from dynamic analysis across various frequencies for the L–F configuration. The results indicate that the hybrid method reproduces the moment and deformation profiles with significantly better accuracy than in the dry sand cases. The response follows similar kinematic and inertial loading mechanisms: at lower frequencies, the inertia-dominated combination with loading direction consistent with kinematic action (**Eq. 24**) provides better agreement, whereas at intermediate to high frequencies, the kinematic loading direction becomes opposite to the inertial loading, leading to a transition from inertia-dominated (**Eq. 23**) to kinematic-dominated combinations (**Eq. 26**). However, the kinematic-dominated combination tends to overestimate the pile response, indicating the need for refinement of the kinematic interaction factor.

Table 13 lists the interaction factor combinations that provide better reproducibility of the pile dynamic response. The results indicate that the proposed calibrated kinematic factors are equivalent to the governing values of the Railway Design Method at lower frequencies. At intermediate frequencies, the proposed factors are slightly lower, whereas at higher frequencies, they are found to be slightly higher than those specified by the Railway Design Method.

Table 13. List of inertial and kinematic factors for L-F and L-S configurations

Design Combination $R_t = a \text{ x } R_a + b' \text{ x } f(z)$								
	Railway Design Method (Eq. 14-15)		**Proposed Method**			**Railway Design Method (Eq.17)**		
Input Freq.	Inertia Factor a	Kinematic factor v	Kinematic Factor **b** (L-F)	Calibrated Kinematic Factor $b' = b/3.33$ (L-F)	Calibrated Kinematic factor b' (L-S)	Inertia Factor **a**	Kinematic Factor **b**	Kinematic Factor **b'**
1	1	0.3	1	0.3	0.30			
2	1	0.3	1	0.3	-0.30			
4	1	-0.7	-0.5	-0.15	-0.36			
6	1	-0.7	-1.7	-0.51	-0.54			
8	1	-0.7	-2.7	-0.81	-0.60	0.7	-3.3	-1
10	1	-0.7	-3.4	-1.02	-0.60	0.7	-3.3	-1

In addition, the proposed kinematic factors for the L–S configuration are also presented. These values are slightly lower than those of the L–F configuration, owing to the reduced contact area for soil–pile interaction. Furthermore, the proposed kinematic factors for both L–F and L–S configurations are generally lower than the corresponding values for the D–F and D–S cases, respectively, for all frequencies except 10 Hz. The smaller values of kinematic factors indicate a reduced influence of kinematic interaction in liquefiable soil conditions. Although liquefiable soils typically exhibit larger deformation compared to dry sand layers, which would suggest a greater contribution of kinematic loading, the reduced kinematic factors imply that the effective soil loading decreases due to stiffness degradation associated with liquefaction. This also suggests that the presence of liquefiable soil layers near the surface does not significantly amplify the pile response.

It must be noted that the above findings are specific to the experimental conditions reproduced through numerical simulations, and therefore additional cases should be investigated to generalize these observations. Regarding the applicability of the Japanese Railway Design Method, its prescribed load combinations are found to be comprehensive in evaluating pier–pile response and consistently provide conservative estimates across different configurations.

5.4 Chapter Summary:

- The proposed hybrid pseudostatic method successfully reproduces the dynamic response of both types of structures in dry sand after simply applying inertial loading at pier top and soil displacement at the boundaries.
- The method made applicable to liquifiable soil cases as well, however, it required incorporation of high EPWPR based reduction in confining pressure of soil.
- The actual values of kinematic inetraction factors are determined to be within the range defined by Japanese design standards. This confirms the conservative applicability of current standards to S-type configuration.

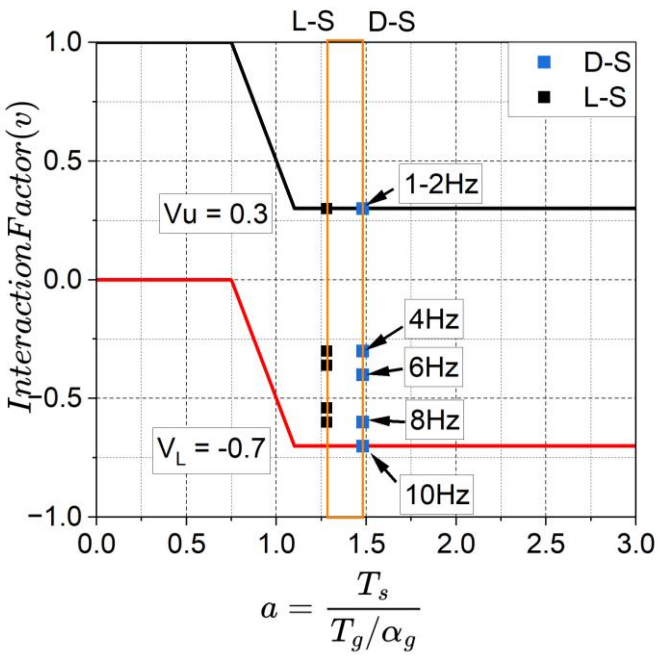

Figure 81. Comparison of kinematic factors for D-S and L-S

CHAPTER 6: CONCLUSION

In this doctoral dissertation, the behavior of bridge-pier structure with different systems has been studied under dynamic loading. It employed 3D finite element modeling simulations to reproduce the experimental results of shaking table tests. The study extends further into unveiling the dynamic soil-structure inetraction mechanism in ends with a hybrid pseudostatic analysis that has been proposed to reproduce the dynamic response of pier-pile structure. The main contributions and conclusions of the present work are summarized below:

- The numerical simulation qualitatively and quantitively reproduced the shaking table test results with sufficient accuracy.
- The simulation clarified that the preference of the S-type bridge pier over the F-type one was seen to depend on the relationship between the natural frequency of the structure and the input wave frequency. This finding therefore suggests the necessity of analysing the superstructure, substructure, foundation, and ground as one unit for dynamic analyses.
- It was found that the F-type bridge pier incorporates a mechanism that effectively utilizes the hysteretic damping function of the shear panels, resulting in the formation of a plastic hinge at the base of the pier in the final state. However, in instances where significant strain leads to out-of-plane deformation or cracks in the shear panels, due to a sharp reduction in the overall structure's stiffness, there may be a sudden increase in the inertial force and lateral displacement at the pier top. Therefore, the reduction in stiffness and the variation in natural frequency of the entire structure, due to the plastic deformation of the shear panels, should also be considered during the design phase.
- The S-type bridge pier maintains the efficacy of the hysteretic damping function of the shear panels for a relatively extended period of time by leveraging the strength of the underground beam, owing to the gradual reduction in the overall structure's stiffness.
- The numerical simulation showed that the S-type model exhibited a better performance against deformation in soft grounds, where the excessive response displacement and liquefaction of the ground are of concern, courtesy of the favourable influence of the kinematic force in the area of lower resistance. The lateral displacement of the piles in the F-type model, having a large superstructure mass-to-footing mass ratio, could be partly attributed to the heightened kinematic

action of the soil at the footing block. In real structures, with superstructure mass-to-footing mass ratios close to one, the influence of the footing's inertial force and kinematic action on the lateral displacement of the piles is expected to be enhanced.

- The dynamic simulations conducted over a range of excitation frequencies clarify the frequency-dependent roles of inertial and kinematic interactions in governing pile response. Peak inertial moment is observed at 2 Hz whereas peak kinematic moment is observed at around 4-6 Hz. This along with phase difference value and pile deformation shapes indicates that pier-pile response is dominated by inertial interaction at lower frequencies (1-2Hz). However, at intermediate frequencies (4-6Hz), the kinematic interaction also becomes quite significant and completely dominant at higher frequencies (8-10Hz).
- An FEM based hybrid pseudostatic analysis method is proposed as a fast alternative to dynamic analysis. It has shown satisfactory to high accuracy performance in estimating the critical pier-pile deformation and moment envelops. The method is based on the mechanistic understanding of soil-structure interaction mechanism that varies based on the direction inertial and kinematic loadings imposed on pier-pile structure.
- The Japanese railway design method provides reasonable estimates of response under inertial-dominated conditions but overestimates pile response when kinematic interaction tends to dominate. To address this limitation, revised values of kinematic interaction factor are proposed, offering a rational basis for improving the accuracy of dynamic pile response predictions within the Japanese Railway Design Standards.

Future work:

In this study, we have focused on a few cases and therefore generalization of these results is under limited conditions. Therefore, following ideas have been proposed to enhance the methods and findings of this study.

- Accuracy of numerical simulations could be enhanced by employing a more suitable beam-spring combination for shear panels. Currently, we have used bilinear beam-spring combination which has resulted in some discrepancies. However, in future, other types of models such R-O (Ramberg-Osgood) spring model to model the non-linear hysteretic behavior shear panels.
- Similarly, the pile response near the tip hasn’t been successfully reproduced. The vertical slope of pile deformation near the pile tip usually becomes 90^{o}, however, it remained lower than that

for all cases. This is due to improper modeling of soil stiffness surrounding pile tip and it was confirmed that an increase in soil confining stresses results in a response closer to experimental.

- Testing of new configurations to increase the existing database: such as comparing several pile spacings, different pile distributions, soil profiles (type of soil and stratigraphy) and superstructures would enhance the understanding of SSI mechanisms.
- Further investigation on the system response with different dynamic and seismic excitations is also desirable to generalize the response under a larger set of loading frequencies and intensities.
- The hybrid method focused on the reproduction of pier-pile response under sinusoidal excitations only and therefore, should be further evaluated under real seismic events or design input motions as well.
- Generalization of the adopted numerical simulation procedure for large scale structures is major goal in future which would also pave way for efficient use of the proposed hybrid pseudostatic method.

REFERENCES

[1] A. Pecker, R. Paolucci, C. Chatzigogos, A. A. Correia, and R. Figini. The role of nonlinear dynamic soil-foundation interaction on the seismic response of structures. In S. ISSMGE, editor, Second International Conference on Performance Based Design in Earthquake Geotechnical Engineering, May 2012.

[2] American Association of State Highway and Transportation Officials (AASHTO), 2014. Guide specifications for LRFD seismic bridge design. 2nd ed. Washington, DC: AASHTO

[3] American Petroleum Institute. API recommended practice for planning, designing, and constructing fixed offshore platforms-working stress design. Report RP-2A-WSD, API Publishing Services, Washington, DC; 2000

[4] Arias, A.: A measure of earthquake intensity, R. J. Hansen (Ed.), Seismic Design for Nuclear Power Plants, MIT Press, Cambridge, MA, 438–489, 1970.

[5] Asaoka, A., Nakano, M. and Noda, T.: Superloading yield surface concept for highly structured soil behavior, Soils and Foundations, 40(2), 99-110, 2000.

[6] Baziar, M., H., Rafiee, F., Azizkandi, A., S., and Lee, C., J.: Effect of super-structure frequency on the seismic behavior of pile-raft foundation using physical modelling, Soil Dynamics and Earthquake Engineering, 104, 196-209, 2018.

[7] Broms BB. Lateral resistance of piles in cohesive soil. Journal of Soil Mechanics and Foundations Division, ASCE 1964;90(2):27–63.

[8] California Department of Transportation (Caltrans), 2011. Guidelines on Foundation Loading and Deformation Due to Liquefaction Induced Lateral Spreading. Internal Policy Proposal.

[9] Chiou, J. S., Fu, Y. W., & Lee, Y. W. (2022). Pseudostatic analysis for seismic responses of extended piles considering inertial and kinematic effects. *Engineering Structures*, *252*, 113572.

[10] Chiou, J. S., Hung, W. Y., Lee, Y. T., & Young, Z. H. (2020). Combined dynamic structure-pile-soil interaction analysis considering inertial and kinematic effects. *Computers and Geotechnics*, *125*, 103671.

[11] Tanaka, N., & Sakai, K. (2024). Combination of seismic actions in seismic deformation method considering nonlinearization of ground and structure. Proceedings of the Japan Society of Civil Engineers (JSCE), 80(13), 23-13119.

[12] Dezi F, Carbonari S, Leoni G. Static equivalent method for the kinematic interaction analysis of single piles. Soil Dyn Earthquake Eng 2010;30(8):679–90.

[13] G. Mylonakis, G. Gazetas, N. Gerolymos, and I. Anastasopoulos. Recent Advances in Applied Mechanics, Honorary Volume for Professor A.N.Kounadis, N.T.U.A., chapter Detrimental Role of Soil-Structure Interaction and the Collapse of the 18-Pier Fukae Bridge in Kobe, pages 145–159. 2000.

[14] Hamada M (1992) Large ground deformations and their effects on lifelines: 1964 Niigata earthquake. Case studies of liquefaction and lifelines performance during past earthquake. Technical report NCEER-92-0001, National Centre for Earthquake Engineering Research, Buffalo

[15] Hanshin Expressway Co., Ltd.: Guidance for the design, manufacture, and erection of steel column integrated by multiple steel pipes, 2020. (in Japanese)

[16] Hashiguchi, K. and Ueno, M.: Elastoplastic constitutive laws of granular material, Constitutive Equations of Soils, Proc. 9th ICSMFE., Spec. Ses. 9 (eds. by Murayama, S. and Schofield, A. N.), Tokyo, JSSMFE, 73-82, 1977.

[17] Hino, S., Lee, J., Ohta, T., Mazda, T. and Tang, J.: Analytical study on seismic characteristics of Multi-Column Composite Bridge Piers using concrete filled tubular columns, Journal of Structural Engineering, 47A, 1423-1432, 2001. (in Japanese)

[18] Hussien, N., M., Karray, M., Tobita, T. and Iai, S.: Kinematic and inertial forces in pile foundations under seismic loading, Computers and Geotechnics, 69, 166-181, 2015.

[19] Hussien, N., M., Karray, M., Tobita, T. and Iai, S.: Kinematic and inertial forces in pile foundations under seismic loading, Computers and Geotechnics, 69, 166-181, 2015.

[20] Iai, S.: Sililitude for Shaking Table Tests on Soil-Structure-Fluid Model, Report of the Port and Harbour Research Institute, Ministry of Transport, 27(3), 3-24, 1988. (in Japanese)

[21] Ishihara K (1997) Terzaghi oration: geotechnical aspects of the 1995 Kobe earthquake. In: Proceedings of the international conference on soil mechanics and foundation engineering, Hamburg, pp 2047–2073

[22] Ishihara, K., and Yoshimine, M.: Evaluation of settlements in sand deposits following liquefaction during earthquakes, Soils and Foundations, 32(1), 173-188, 1992.

[23] Isobe, K., Kimura, M., Ohtsuka, S. and Akiyama, K.: Three-dimensional finite element analysis on

static lateral resistance characteristics of steel pipe pile foundation supporting integrated column by multiple steel pipes, Journal of Structural Engineering, 56A, 1041-1053, 2010. (in Japanese)

[24] Isobe, K., Sawamura, Y., Kimura, M. and Soga, Y.: Evaluation of seismic performance of a bridge column integrated by multiple steel pipes with directly-connected piles based on shaking table tests, Proc. of the 19th International Conference on Soil Mechanics and Engineering, 2785-2788, Seoul, Republic of Korea, 2017.

[25] Isobe, K., Sawamura, Y., Sugiyama, H., Shinohara, M., Soga, Y., Kobayashi, H. and Kimura, M.: Seismic performance of a multiple steel pipes bridge pier integrated by pile foundation without a footing using shaking table tests, Journal of Japan Society of Civil Engineers, Ser. C (Geosphere Engineering), 72(4), 327-338, 2016. (in Japanese)

[26] Isobe, K., Sugiyama, H., Shinohara, M., Kobayashi, H., Sawamura, Y., Mitsuyoshi, Y. and Kimura, M.: Shaking table test and numerical simulation on seismic performance of a bridge column integrated by multiple steel pipes with directly-connected piles, The 6th Japan-China Geotechnical Symposium, Japanese Geotechnical Society Special Publication, 1(6), 35-40, 2015.

[27] J. Lysmer. Analytical procedures in soil dynamics - state of the art. In ASCE Conference on Soil Dynamics and Earthquake Engineering, Pasadena, California, 1978.

[28] Japan Road Association: Specifications for highway bridges Part V: Seismic Design ver. 2012, 2012.

[29] Jesus Perez-Herreros. Dynamic soil-structure interaction of pile foundations: experimental and numerical study. Civil Engineering. École centrale de Nantes, 2020. English. NNT: 2020ECDN0002. tel-02972312

[30] Kanaji, H., Suzuki, H., Nonaka, T. and Magoshi, K.: Fundamental study for damage control structure of an integrated column by multi steel pipes with hysteretic damper, Journal of Structural Engineering, 50A, 559-566, 2004. (in Japanese)

[31] Kaynia, A. M. and Mahzooni, S.: Forces in pile foundations under seismic loading, Journal of Engineering Mechanics, 122(1), 46-53, 1996.

[32] Kimura, M. and Zhang, F.: Seismic evaluations of pile foundations with three different methods based on three-dimensional elastic-plastic finite element analysis, Soils and Foundations, 40(5), 113-132, 2000.

[33] Liu, J., Qiu, M., Gao, W. et al., 2010. Application Handbook for the Technical Code for Building

Pile Foundations (JGJ 94), China Architecture and Building Press, Beijing (In Chinese).

[34] Liu, S., Li, P., Zhang, W., & Lu, Z. (2020). Experimental study and numerical simulation on dynamic soil-structure interaction under earthquake excitations. Soil Dynamics and Earthquake Engineering, 138, 106333.

[35] Lombardi, D., Bhattacharya, S., Scarpa, F., Bianchi, M.: Dynamic response of a geotechnical rigid model container with absorbing boundaries, Soil Dynamics and Earthquake Engineering, 69, 46-56, 2015.

[36] Luo X, Murono Y, Nishimura A. Verifying adequacy of the seismic deformation method by using real examples of earthquake damage. Soils Dyn Earthquake Eng 2002;22(1):17–28.

[37] M. Hamada. Damage to piles by liquefaction-induced ground displacements. In Proceedings of the 3rd US Conference Lifeline Earthquake Engineering, ASCE, pages 1172–1181, Los Angeles, 1991.

[38] Marwan, N., Rafael, M. and Man-Chung, T.: Seismic Resistant Design of the Single Tower of the New San Francisco-Oakland Bay Bridge, 3rd International Suspension Bridge Operators' Conference, 2002.

[39] Matsuo, O., Okamura, M., Uzuoka, R. and Mihara, M.: Numerical analyses of the damaged dikes in the 1995 Hyogo-ken Nanbu earthquake, Pro. of the 12th World Conference on Earthquake Engineering (No. 0621), 2000.

[40] Morishita, Y., Takahisa, T., Aoki, T., Fukumoto, Y., Okamoto, T. and Matsui, E.: Experimental study on Strength and Ductility of a Rigid-Frame Steel Pier with Intermediate Cross Beam, Journal of Structural Engineering, 46A, 831-840, 2000. (in Japanese)

[41] Murono, Y. and Nishimura, A.: Evaluation of seismic force of pile foundation induced by inertial and kinematic interaction, Proc. of 12th World Conference on Earthquake Engineering (No. 1496), 2000.

[42] NAKAMURA, R., KANAJI, H., & KOSAKA, T. (2014). *Development and design of new steel pipe integrated pier with shear link*. Technical report, Technical report, Hanshin Expressway Company Limited, Osaka.

[43] NF EN 1998-5 - Eurocode 8 - Partie 5 - Fondations, ouvrages de soutènement et aspects géotechniques, sep 2005.

[44] Nikolaou, S., Mylonakis, G., Gazetas, G. and Tazoh, T.: Kinematic pile bending during

earthquakes: Analysis and field measurements, Geotechnique, 51(5), 425-440, 2001.

[45] Rahmani A, Taiebat M, Finn WDL, Ventura CE. Evaluation of p-y springs for nonlinear static and seismic soil-pile interaction analysis under lateral loading. Soil Dyn Earthquake Eng 2018;115:438–47.

[46] Railway Technical Research Institute, 2012. Design Standards for Railway Structures and Commentary (Seismic Design), Maruzen.

[47] Ricker, N.: The computation of output disturbances from amplifiers for true wavelet inputs, Geophysics, 10, 207-220, 1945.

[48] Rollins, K. M., Gerber, T. M., Lane, D., Ashford, S. A.: Lateral Resistance of a Full-Scale Pile Group in Liquefied Sand, Journal of Geotechnical and Geoenvironmental Engineering, 131(1), 115-125, 2005.

[49] Shinohara, M., Kanaji, H., Kosaka, T. and Imai, T.: Design and Construction of Highway Viaduct Supported by New Steel Pipe Integrated Pier with Shear Link, 9th German-Japanese Bridge Symposium, 2012b.

[50] Shinohara, M., Kanaji, H., Kosaka, T. and Imai, T.: Design and Construction of Highway Viaduct Supported by New Steel Pipe Integrated Pier with Shear Link, 9th German-Japanese Bridge Symposium, 2012.

[51] Shinohara, M., Kanaji, H., Oniki, K. and Kimura, M.: A proposal of a bridge column integrated by multiple steel pipes with directly-connected piles and a seismic response analysis, Journal of Japan Society of Civil Engineers, Ser. C (Geosphere Engineering), 69(3), 312-325, 2013. (in Japanese)

[52] Shinohara, M., Kanaji, H., Oniki, K. and Kimura, M.: A proposal of a bridge column integrated by multiple steel pipes with directly-connected piles and a seismic response analysis, Journal of Japan Society of Civil Engineers, Ser. C (Geosphere Engineering), 69(3), 312-325, 2013. (in Japanese)

[53] Shinohara, M., Kanaji, H., Oniki, K. and Sugiura, K.: Basic properties of an integrated column by multiple steel pipes with hysteretic shear damper, Journal of Structural Engineering, 58A, 471-483, 2012a. (in Japanese)

[54] Shinohara, M.: Evaluation of Seismic response characteristics of an integrated steel pipe pier and rationalization of its foundation structure, Doctoral Degree Thesis of Kyoto University, 9-29, 2014. (in Japanese)

[55] Shrestha S, Ravichandran N. 3d nonlinear finite element analysis of piled-raft foundation for tall wind turbines and its comparison with analytical model. J GeoEngineering 2019;14(4):259–76.

[56] Shrestha, N. R., Saitoh, M., Saha, A. K., & Goit, C. S. (2021). Frequency-and intensity-dependent impedance functions of laterally loaded single piles in cohesionless soil. Soils and Foundations, 61(1), 129-143.

[57] Tokimatsu, K., Suzuki, H. and Sato, M.: Effects of inertial and kinematic interaction on seismic behavior of pile with embedded foundation, Soil Dynamics and Earthquake Engineering, 25, 753-762, 2005.

[58] Tokimatsu, K., Suzuki, H., & Sato, M. (2005). Effects of inertial and kinematic interaction on seismic behavior of pile with embedded foundation. *Soil Dynamics and Earthquake Engineering*, *25*(7-10), 753-762.

[59] Toyooka, A., Murono, Y., Nogami, Y. and Nishimura, T.: Effect of inertial and kinematic interaction on seismic behavior of various types of structures, Quarterly Report of RTRI, 53(2), 93-101, 2012.

[60] Toyooka, A., Murono, Y., Nogami, Y. and Nishimura, T.: Effect of inertial and kinematic interaction on seismic behavior of various types of structures, Quarterly Report of RTRI, 53(2), 93-101, 2012.

[61] Veletsos AS, Newmark NM. Effect of inelastic behavior on the response of simple systems to earthquake motions. In: Proceedings of the Second World Conference on Earthquake Engineering, Japan; 2; 1960. p. 895–912.

[62] Villanueva AS. Ductility reduction factors for earthquake design. Eng Struct 1980;2 (1):52–6.

[63] Wang, R., Liu, X. and Zhang, J., M.: Numerical analysis of the seismic inertial and kinematic effects on pile bending moment in liquefiable soils. Acta Geotechnica, 12(4), 773-791, 2017.

[64] Wang, R., Liu, X. and Zhang, J., M.: Numerical analysis of the seismic inertial and kinematic effects on pile bending moment in liquefiable soils. Acta Geotechnica, 12(4), 773-791, 2017.

[65] Wilson, D.W., Boulanger, R.W., Kutter, B.L.: Observed seismic lateral resistance of liquefying sand, Journal of Geotechnical and Geoenvironmental Engineering, 126 (10), 898-906, 2000.

[66] Ye, B., Ye, G., Zhang, F. and Yashima, A.: Experiment and numerical simulation of repeated liquefaction-consolidation of sand, Soils and Foundations, 47(3), 547-558, 2007.

[67] Yoshida I, Yoshinaka R. A method to estimate modulus of horizontal subgrade reaction for a pile. Soils Found 1972;12(3):1–17.

[68] Zhang, F., and Kimura, M.: Numerical prediction of the dynamic behaviors of an RC group-pile foundation, Soils and Foundations, 42(3), 77-92, 2002.

[69] Zhang, F., Kimura, M., Nakai, T., and Hoshikawa, T.: Mechanical behavior of pile foundations subjected to cyclic lateral loading up to the ultimate state, Soils and Foundations, 40(5), 1-17, 2000.

[70] Zhang, F., Ye, B., Noda, T., Nakano, M. and Nakai, K.: Explanation of cyclic mobility of soils: Approach by stress-induced anisotropy, Soils and Foundations, 47(4), 635-648, 2007